



THE INTERACTION OF CARBON DIOXIDE WITH
AMINO ACIDS, PEPTIDES, AND HEMOGLOBIN:
A STUDY BY ^{13}C NUCLEAR MAGNETIC RESONANCE



JON STANLEY MORROW

1974

YALE



MEDICAL LIBRARY

YALE



MEDICAL LIBRARY



Digitized by the Internet Archive
in 2017 with funding from
Arcadia Fund

THE INTERACTION OF CARBON DIOXIDE WITH
AMINO ACIDS, PEPTIDES, AND HEMOGLOBIN:
A STUDY BY ^{13}C NUCLEAR MAGNETIC RESONANCE

JON STANLEY MORROW

Submitted to the Faculty of the Graduate School in partial
fulfillment of the requirements for the degree
Doctor of Philosophy in the Department of
Chemistry
Indiana University
July, 1974
Bloomington, Indiana

July 26, 1974

This is to certify that the thesis submitted by Jon S. Morrow has been accepted by the Ph.D. Advisory Committee as satisfactory in partial fulfillment of the requirements for the degree of Doctor of Philosophy.

Chairman Frank R. N. Gurd
(Research Adviser)

Adrian Alcock

EH Cordes

John P. Richards

Sid Robinson

Copyright 1974

Jon Stanley Morrow

To Lynn

ACKNOWLEDGEMENTS

It is impossible to thank adequately with a simple acknowledgement a person such as Professor Frank R. N. Gurd, just as it is impossible to describe in a few words the impact that association with such a man has on one's ideals and aspirations. Much more than an outstanding teacher, Dr. Gurd is a warm and compassionate person, a genuine and loyal friend, a person willing to give as much of himself as he expects from you. His constant and unselfish guidance will forever be a source of strength; but he will forever be warmly remembered as a genuine friend.

Special thanks also to:

Dr. Philip Keim for his assistance at various stages of this work. His wisdom, insight, hard work, and Volkswagon proved invaluable.

Richard J. Wittebort who unselfishly provided assistance in many areas of this investigation. His considerable mathematical talents were most helpful. He also must be thanked for making many of the photographs which appear herein.

Dr. Margaret Garner, William Garner, and Richard Bogart for many helpful discussions and assistance in keeping the equipment running. Richard Bogart is also to be thanked for his help with the computer programming.

Valerie Pascuzzi for her considerable technical assistance during the later stages of this work. Without Valerie, many of the experiments reported herein might not have come to fruition.

Robert Addleman and Professor Clouse for developing and patiently maintaining the outstanding NMR facilities upon which this entire study

was based. Their assistance and availability, often at inconvenient hours, is sincerely appreciated.

Professor Adam Allerhand for his assistance and advice on both the more esoteric matters of NMR theory, as well as the more practical matters such as supplying a computer program or a 3 MHz crystal.

James B. Matthew for his unselfish assistance and many helpful discussions.

Susan Crum, Betty Jurgens, and Kathy Owens for typing this manuscript.

Dr. Sid Robinson for the long term loan of his Natelson Microgasometer.

Dr. Frank Zeller for the use of his laboratory for work with the chickens.

My other colleagues in Dr. Gurd's research group for their cooperation and support throughout the course of my graduate career.

Most of all, I wish to thank Lynn, for the artwork; for the many "served in the lab" meals, for her moral support, for her supreme patience, and for her unconditional love. It is Lynn's sacrifices that to large measure insured the success of this work.

ABSTRACT

Carbon dioxide is of paramount importance in the regulation of many bodily functions. Historically, the measurement and quantitation of CO_2 interactions with peptides and proteins has been difficult, primarily due to its volatility and multiplicity of potential forms (CO_2 , H_2CO_3 , HCO_3^- , $\text{CO}_3^{=}$, and carbamate $-\overset{\text{H}}{\text{N}}-\text{COO}^-$). Most of these are observable by ^{13}C Fourier transform nuclear magnetic resonance spectroscopy. Bicarbonate and carbonate exist in fast exchange, the observed resonance being titratable between the limits of 24.4 and 32.6 ppm upfield of external CS_2 . Conversely, the chemical shift of the carbamino resonance of most amino acids, peptides, and proteins examined is invariant with pH and falls between the limits of 28.2 and 30 ppm. Its integrated area is a sensitive function of the carbamate equilibrium constant (K_c) and the amine dissociation constant (K_z). Studies on valine containing peptides and valine and cysteine amino acids suggest that significant structural reordering may result from carbamate formation.

The results on human adult deoxyhemoglobin (Ao) confirm the allosteric role of carbamate formation, but also indicate a non-carbamate CO_2 or HCO_3^- binding at pH values below neutrality. The results suggest that the β chain NH_2 -terminus binds the major portion of CO_2 at pH values below 7.8, while in carboxyhemoglobin (HbAoCO) the NH_2 -terminals of both alpha and beta chains contribute approximately equally to the observed CO_2 binding. This interpretation demands the

absence of slowly interconverting conformations in the protein; the possible invalidity of this assumption is discussed. A comparison of the carbamate linewidths in the protein solutions with theory indicates that the carbamate dissociation rates are pH dependent, and generally greater at the alpha chain NH_2 -terminus.

Preliminary studies of carbamate formation in [5-Ile] angiotensin II and [8-homolys]-vasopressin indicate that they will form carbamates to an appreciable extent under physiologic conditions of pH and carbonate levels. The suggestion is made that carbamino formation may be a quite general and functionally important phenomenon throughout biology.

TABLE OF CONTENTS

Chapter I	Introduction	
	Bohr Effect	2
	2,3-Diphosphoglycerate	4
	Carbon Dioxide	4
	^{13}C Fourier Transform Nuclear Magnetic Resonance	5
	References	7
Chapter II	Materials and Methods	
	Materials	15
	Methods	18
	Measurement of pH	18
	Measurement of Total Carbonates	18
	Dialysis Tubing Preparation	18
	Protein Concentration	20
	Polyacrylamide Gel Electrophoresis	20
	Cellulose Acetate Electrophoresis	21
	Ultraviolet and Visible Spectral Measurements	21
	Mass Spectroscopy	23
	Amino Acid Analysis	23
	Removal of Heme	23
	Automated Edman Degradation	24
	Sperm Whale Ferrimyoglobin Preparation	24
	Hemoglobin Preparation	24
	Reduction of Ferric Proteins	34
	Separation of Hemoglobin Chains	35
	Recombination of p-Mercuriobenzoate Treated Chains	41
	Preparation of Carbamylated Hemoglobins	41

Methods (continued)

Preparation of Carbamylated Hemoglobins	41
Removal of Carbon Monoxide from Hemoglobin ...	45
Preparation of Ferrihemoglobin	45
2,3-Diphosphoglyceric Acid Preparations	45
Liquid Scintillation Counting	48
Bicarbonate-Carbonate Titration	51
Sample Preparation for ^{13}C NMR	51
^{13}C Fourier Transform NMR Measurements	60
^1H NMR Measurements	63
Resonance Peak Area Integration	63
References	70

Chapter III Interaction of CO_2 with Amino Acids, Peptides and Sperm Whale Myoglobin

Bicarbonate-Carbonate Titration	75
Carbamino Derivative of Glycine	80
pH Dependence of Formation of Glycine Adduct ...	84
Deuterium Isotope Effects	93
Carbamino Formation in Other Amino Acids and Peptides	95
Structural Effects in Valine Derivatives	101
Structural Effects in Proline Derivatives	108
Carbamino Cysteine	111
Spin Lattice Relaxation Times (T_1)	127
Sperm Whale Ferrimyoglobin	135
Discussion and Conclusion	141
References	143

Chapter IV Interaction of CO_2 with Adult Human Hemoglobin

Observation of ^{13}C -Carbamino Resonances in Hemoglobin	151
Chemical Shift Titration Behavior	158
Identification of Resonances	165
Kinetic Effects	178

	Computer Fitting of Observed Spectra	183
	Spin Lattice Relaxation Time and Nuclear Overhauser Enhancement	190
	Quantitation of Carbamate Formation	197
	Discussion	212
	Conclusion	222
	References	224
Chapter V	The Competition of CO ₂ with 2,3-Diphosphoglyceric Acid	
	The Interaction of CO ₂ with Different Hemoglobins	
	Observations of Carbamate Resonances in the Presence of 2,3-DPG	231
	Observation of Carbamino Formation in Human Fetal Hemoglobin (Fo)	253
	Observations of Carbamate Formation in Adult Human Hemoglobin A ₂	261
	Carbamate Formation in Hemoglobin S	261
	Carbamate Formation in Chicken Hemoglobin	265
	Conclusion	269
	References	273
Chapter VI	Carbamino Compounds and Homeostasis	
	Vasopressin	280
	[5-Ile]-Angiotensin II	285
	Discussion	292
	Stability Ranges of Carbamino Derivatives	292
	Conclusion	299
	References	302
Appendix A	Ferrihemoglobin Formation in the Presence of Catalase, Glutathione, or Triethylenetetramine.	305
Appendix B	Interaction of ¹³ CO ₂ and Bicarbonate with Carbonic Anhydrase	309

Appendix C	Computer Programs	315
	CAL3	316
	ISOBAR	345
	ABX Analysis	355
	NMRFIT3	358
	CONVERT	401
Appendix D	Ligand Dependent Aggregation of Chicken Hemoglobin	406
Vita		416

CHAPTER I

Introduction

As for myself, I find it absolutely impossible to produce a work . . . that shall be anything like complete. . . . In completing one discovery we never fail to get an imperfect knowledge of others, of which we could have no idea before; so that we cannot solve one doubt without creating several new ones.

Joseph Priestley (1774)
In "Experiments and Observations on Different Kinds of Air"

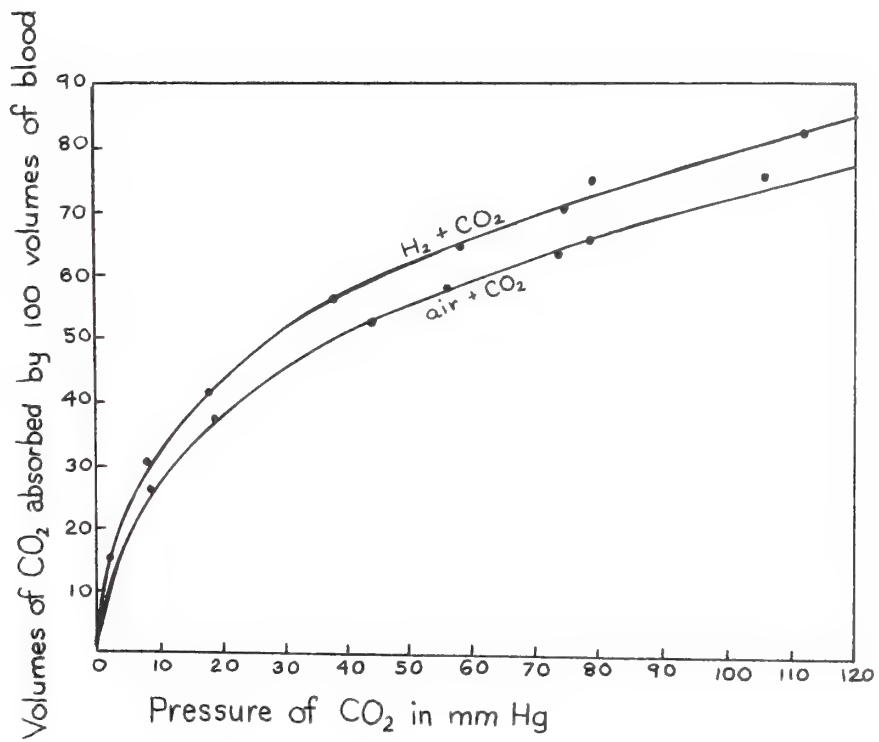
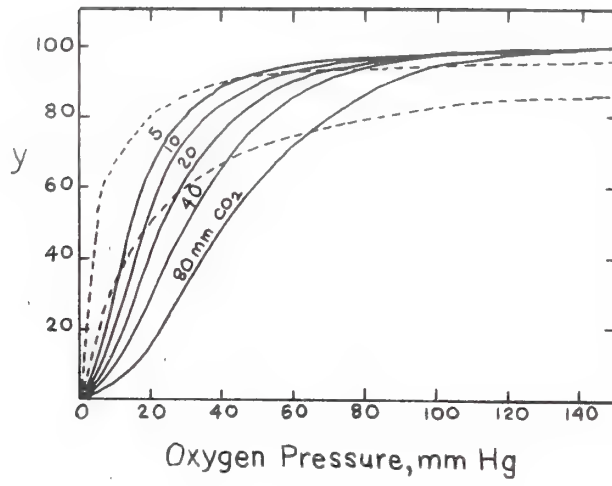
Chapter I

Introduction

The transport of oxygen is the central role of hemoglobin. In performing this task, other molecules and ions also play significant parts, allowing for a modulation of its oxygen affinity without significantly affecting its remarkable cooperativity. Many salts and buffers may exert "non-specific" effects, but the triumvirate of hydrogen ions, carbon dioxide, and 2,3-diphosphoglyceric acid are now known to be the primary allosteric effectors of hemoglobin (1). With the exception of the latter compound, the fundamental picture of hemoglobin as a pigment existing primarily for oxygen transport, modulated by pH and $p\text{CO}_2$, was complete by 1930 (2). In Figure 1A is shown a drawing reproduced from reference (2), and originally taken from the paper of Bohr, Hasselbalch, and Krogh (3). It graphically illustrates two of the most striking properties of hemoglobin: the sigmoid character of its oxygenation curve, and the dramatic effect of CO_2 upon the position of that curve. The reciprocal effect of O_2 upon the CO_2 affinity of hemoglobin, which must exist by thermodynamic necessity, was experimentally verified some years later by Christiansen, Douglas and Haldane (4). The result of their work, reproduced again from reference (2), is shown in Figure 1B.

The concept of hemoglobin function that has emerged since, representing nearly 60 years of effort by countless investigators, is far more subtle, complex, and beautiful than any of the early investigators might

Figure 1. (A) Solid lines represent the binding of oxygen by dog blood, at different $p\text{CO}_2$ levels. Dashed lines represent rectangular hyperbolas, typical of a system without cooperativity. Data of Bohr, Hasselbalch, and Krogh, 1904. (B) Total carbon dioxide content of blood of J. S. Haldane; top curve is deoxy form, bottom curve oxy form. Data from Christiansen, Douglas and Haldane. Figure 1 is redrawn from Reference 2.



ever have imagined. Based largely on crystallographic studies conducted in the laboratory of Perutz (5-7), the conformational change resident upon ligand binding in horse and human hemoglobin is known to exquisite detail. Numerous chemical studies have found satisfactory explanation in the stereochemical models proposed by Perutz (8), although other studies, especially those sensitive to kinetic effects (9-11), have yielded evidence of the dynamic $R \longleftrightarrow T$ (relaxed to taut, oxy to deoxy) equilibrium that most certainly exists (12-15), but remains inaccessible to x-ray analysis. While a complete review of hemoglobin function is far beyond the scope of the present effort, specific aspects of the interaction of hemoglobin with its three "oxygen linked" effectors deserves mention.

Bohr Effect. The term "Bohr effect," while variously assigned to the effect of pH or CO_2 on the O_2 affinity of hemoglobin, is most properly used to designate only the interaction between hydrogen ions and oxygen (1). Phenomenologically, the (alkaline) Bohr effect refers simply to the uptake of protons by hemoglobin upon conversion to the deoxy state. The pH of unbuffered solutions therefore rises, or conversely, diminished pH favors reduced O_2 affinity. The alkaline Bohr effect should be differentiated from the acid, or reverse, Bohr effect which obtains at pH values below 6.0 (1). In this pH range the O_2 affinity is a direct function of the hydrogen ion concentration.

The molecular mechanisms responsible for the alkaline Bohr effect are partially understood. Early work by Hastings et al. (16) indicated that an oxygen linked group changed its pK_Z (the acid dissociation constant) from 8.2 to 6.6 upon oxygenation. The involvement of two oxygen

linked groups was suggested by Wyman (17), who demonstrated that a change in pK_z of these groups from 7.81 to 6.80 would explain his data. Such findings established the physiochemical basis for the Bohr effect, but did little toward its elucidation on the molecular level.

Toward this end, early experiments with CO_2 binding suggested that amino groups might be involved (18), but the most direct evidence has come from chemical modification of the protein. By reacting the NH_2 -terminals of the α - and β -chains of horse hemoglobin with cyanate (19), Kilmartin and Rossi-Bernardi were able to show that the hybrids $(\alpha_2^C\beta_2)^1$ and $(\alpha_2^C\beta_2^C)$ exhibited a Bohr effect diminished by nearly 25%. However, $(\alpha_2\beta_2^C)$ showed a normal Bohr effect. Since the cyanate prevents ionization of the NH_2 -R groups to which it is bound:



the most likely explanation was that the NH_2 -terminal of the alpha chains contributed to the Bohr effect, but that the β -chain NH_2 -termini did not. By differential titration of these hemoglobins, the pK_z of the alpha chain NH_2 -terminus in (horse) oxyhemoglobin was measured to be 7.3, and 7.8 in deoxyhemoglobin. Other workers (20) corroborated the change in pK_z , although differed in their estimates of the actual pK_z values (21). Stereochemically, the change in pK at the α -chain NH_2 -terminus is easily explained, since the C-terminal carboxyl and NH_2 -terminal amino group of adjacent α -chains are salt bridged in deoxy, but not oxyhemoglobin (22).

Similar experiments on des (His 146 β) hemoglobin have shown that ~50% of the Bohr effect can be accounted for by a change in the pK of this imidazole group (23). The source of the remaining 25% of the Bohr effect is not known.

¹ $(\alpha_2^C\beta_2)$ refers to a hemoglobin which has the NH_2 -terminal selectively blocked with HNCO. The other derivatives are likewise designated $(\alpha_2\beta_2^C)$ and $(\alpha_2^C\beta_2^C)$.

2,3-Diphosphoglycerate. As early as 1921, Barcroft speculated that there was "some third substance present...which forms an integral part of the oxygen hemoglobin complex" (24). In 1925, Greenwald discovered high concentrations of 2,3-diphosphoglycerate (DPG) in porcine red blood cells (25). It is thus a remarkable oversight of science that the striking effect of organic phosphates on hemoglobin was not reported until 1966 (26). The pump was primed, however, and in the intervening eight years, a tremendous amount has been learned, culminating in the crystallographic elucidation of the high affinity DPG binding site by Arnone in 1972 (27). The residues involved are about the dyad axis near the β -chain cleft, and include value 1 β , histidines 2 β and 143 β , and lysine 82 β . Reference to Figure 13, Chapter V, will illustrate this point.

Binding at other sites albeit much weaker, has also been postulated, and experimental evidence of such exists (28,29). These secondary sites of binding remain open to investigation as also does the question of competition between 2,3-DPG and the other aforementioned allosteric effectors. The high association constant for deoxyhemoglobin attributed to 2,3-DPG might be expected to dominate any interaction (30), although experimentally this has not always been observed (31).

Carbon Dioxide. In contrast to the case of 2,3-DPG, carbon dioxide was the first allosteric effector of hemoglobin to be discovered (Figure 1), and has enjoyed a long history of investigation. The bibliography to this chapter, a reasonably complete accounting of studies involving hemoglobin and CO₂ (3,4,18,19,32-112,114), reflects this fact. From these studies it is clear that CO₂ expresses itself primarily by carbamino formation with the NH₂-terminal groups of the protein. The reaction involved is shown in Figure 2, along with other reactions

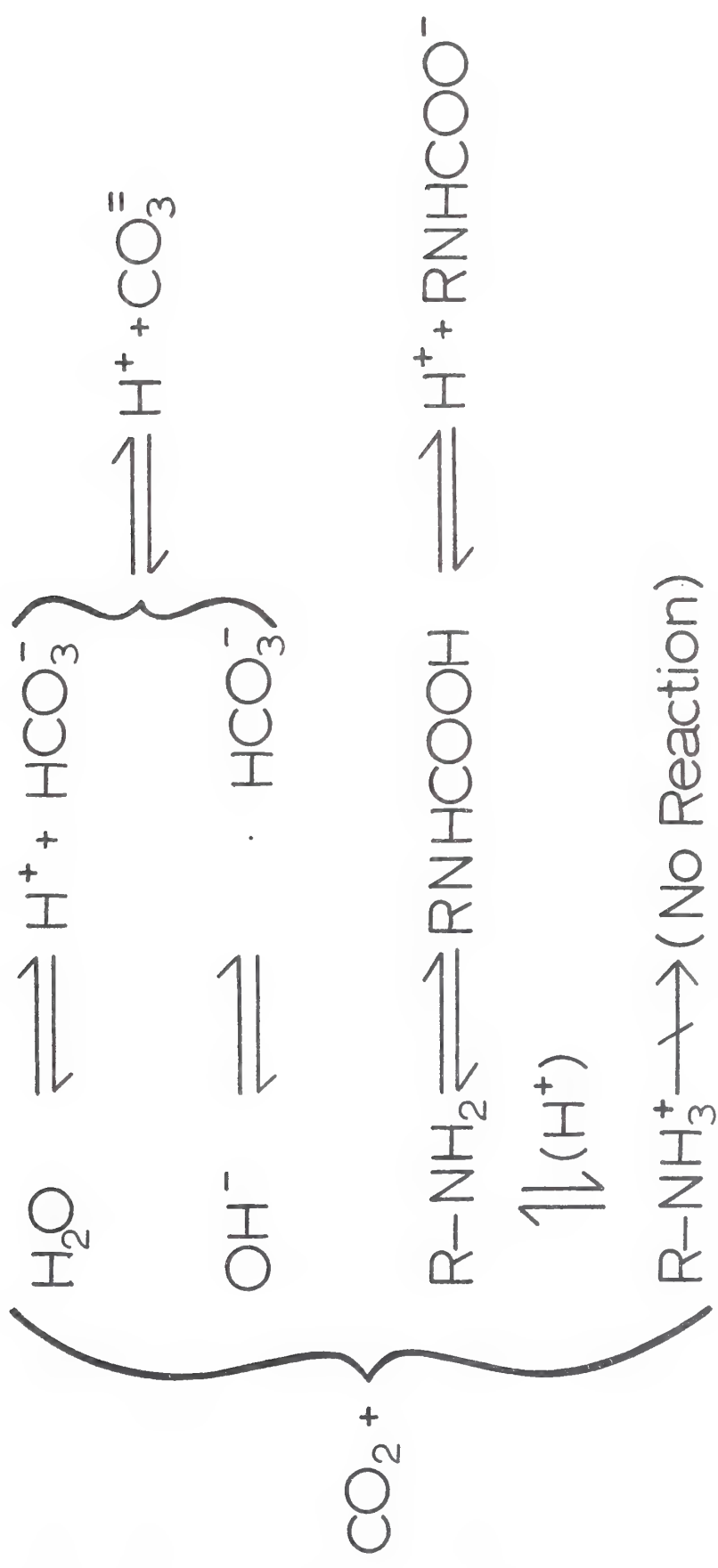


Figure 2. Potential fates of CO₂ in aqueous solutions of amines. The uncatalyzed hydration of CO₂ (top) is relatively slow.

available to CO_2 when dissolved in aqueous solutions of amines. Only the basic form of the amine is reactive, thereby restricting the extent of carbamate formation with ϵ -amino groups under physiological values of pH. This basic reaction scheme was first proposed by Faurholt (113) in 1925, and later extended to hemoglobin by Henriques (44).

However, for all the work that has been done, fundamental questions remain unanswered. The competitive relationship between CO_2 and DPG, while clear in its most general outlines (77,102), is controversial in detail (31,104). Intrinsic to such analysis is a knowledge of the relative affinities of the alpha and beta chains for CO_2 in both the oxy and deoxy states. CO_2 affinity, however, is intricately linked to the amine group pK_z value (Figure 2), and thus to the Bohr effect. To study the CO_2 interaction, one must also study, either directly or indirectly, the remaining partners in the triumvirate.

By traditional methods, the detection and measurement of carbamates has been difficult (113). Most methods employ extremes of pH to "freeze" the system in a given state, and are thus hardly suitable for studies of competitive relationships. The introduction of the CO_2 electrode has provided a partial solution to the problem, although some precision has been sacrificed (104,114).

^{13}C Fourier Transform Nuclear Magnetic Resonance. Within the past five years magnetic resonance techniques have achieved sufficient sensitivity to observe ^{13}C signals at natural abundance in solutions as dilute as 10 mM^2 (115,116). By employing the use of ^{13}C labeled compounds, at enrichment levels (with respect to ^{13}C) exceeding 90%, it is possible

²Assuming the maximal NOE of ~ 3 . See reference 116.

to extend this range of sensitivity over 80 times. Thus, with current technology, the observation of single [^{13}C] enriched loci within a protein is not a difficult problem (117).

By using the atomic nuclei as sensitive probes of their own local magnetic environments, nuclear magnetic resonance potentially offers an attractive alternative to the traditional methods of monitoring carbamate formation.

The work presented here represents primarily a study of the carb-amino reaction in hemoglobin. The lessons learned, however, are general, and the implications transcend the restricted role heretofore attributed to the carbamate reaction (Chapter VI).

With the exception that all chapters depend indirectly on Chapter II (materials and methods), the following chapters have been written so as to be essentially complete in themselves.

References

1. Kilmartin, J. V. and Rossi-Bernardi, L. (1973) *Physiol. Rev.* 53, 836-890
2. Edsall, J. T. (1972) *J. of History of Biol.* 5, 205-257
3. Bohr, C., Hasselbalch, K. A., and Krogh, A.S. (1904) *Skand. Arch. Physiol.* 16, 402-412
4. Christiansen, J., Douglas, E. G. and Haldane, J. S. (1914) *J. Physiol.* 48, 244-247
5. Muirhead, H. and Perutz, M. F. (1963) *Nature* 199, 633-638
6. Muirhead, H., Cox, J. M., Mazzarella, L. and Perutz, M. F. (1967) *J. Mol. Biol.* 28, 117-156
7. Perutz, M. F., Muirhead, H., Cox, J. M. and Goaman, L. C. G. (1968) *Nature* 219, 131-139
8. Perutz, M. F. and Ten Eyck, L. F. (1972) *Cold Spring Harbor Symp. Quant. Biol.* 36, 295-310
9. Cassoly, J. S., Gibson, Q. H. (1972) *J. Biol. Chem.* 247, 7332-7341
10. Olson, J. S., Gibson, Q. H., Nagel, R. L. and Hamilton, H. B. (1972) *J. Biol. Chem.* 247, 7485-7493
11. Moffat, K., Olson, J. S., Gibson, Q. H. and Kilmartin, J. V. (1973) *J. Biol. Chem.* 248, 6387-6393
12. Perutz, M. F., Ladner, J. E., Somon, S. R. and Ho, C. (1974) *Biochem.* 13, 2163-2173
13. Perutz, M. F., Heidner, E. J., Ladner, J. E., Bettlestone, J. G., Ho, C. and Slade, E. F. (1974) *Biochem.* 13, 2187-2200
14. Perutz, M. F., Fersht, A. R., Simon, S. R. and Roberts, G. C. K. (1974) *Biochem.* 13, 2174-2186

15. Adams, M. L. and Schuster, T. M. (1974) Biochem. Biophys. Res. Comm., submitted for publication
16. Hastings, A. B., Seudroy, J., Murray, C. D. and Heidelberger, M. (1924) J. Biol. Chem. 61, 317-335
17. Wyman, J. (1939) J. Biol. Chem. 127, 581-599
18. Ferguson, J. K. W. and Roughton, F. J. W. (1934) J. Physiol. (London) 83, 87-102
19. Kilmartin, J. V. and Rossi-Bernardi, L. (1971) Biochem. J. 124, 31-45
20. Tanford, C. and Nozaki, Y. (1966) 241, 2832-2839
21. Hill, R. J. and Davis, R. W. (1967) J. Biol. Chem. 242, 2005-2012
22. Perutz, M. F., Muirhead, H., Mazzarella, L., Crowther, R. A., Greer, J. and Kilmartin, J. V. (1969) Nature 222, 1240-1243
23. Kilmartin, J. V. and Wootton, J. F. (1970) Nature 228, 766-767
24. Adair, G. S., Barcroft, J. and Bock, A. V. (1921) J. Physiol. (London) 55, 332-338
25. Greenwald, I. (1925) J. Biol. Chem. 63, 339
26. Benesch, R. and Benesch, R. E. (1967) Biochem Biophys. Res. Commun. 26, 162-167
27. Arnone, A. (1972) Nature (London) 237, 146-149
28. Garby, L., Robert, M. and Zaar, B. (1969) Eur. J. Biochem. 10, 110-115
29. Chanutin, A. and Hermann, E. (1969) Arch Biochem. Biophys. 131, 180-184
30. Benesch, R., Benesch, R. E. and Yu, C. I. (1968) Proc. Natl. Acad. Sci. 59, 526-532

31. Caldwell, P. R. B., Nagel, R. L. and Jaffe', E. R. (1971)
Biochem. Biophys. Res. Commun. 44, 1504-1509
32. Bohr, C. (1905) Handbuch der Physiologie des Menschen, Nagel, W.,
ed., Brunswick, 1, 54
33. Campbell, J. M. H. and Poulton, E. P. (1920) J. Physiol. 54,
152-166
34. Joffe, J. and Poulton, E. P. (1920) J. Physiol. 54, 129-151
35. Davies, H. W., Haldane, J. B. S. and Kennaway, E. L. (1920) J.
Physiol. 54, 32-45
36. Buchmaster, G. A. (1921) Proc. Physiol. Soc., J. Physiol. 54, xcii
37. Hill, A. U. (1921) Biochem. J. 15, 577-586
38. Adair, G. S. (1923) J. Physiol. 58, iv
39. Atkins, W. R. G. (1924) J. Marine Biol. Assoc. 13, 437-446
40. Peters, J. P., Bulger, H. A. and Eisenman, A. J. (1924) J. Biol.
Chem. 58, 747-771, 773-791
41. Osborne, W. A. (1926) Aust. J. Exptl. Biol. Med. Sci. 3, 117-118
42. Hayasi, K., Nisimaru, Y. and Okuyama, M. (1927) J. Biophysics
(Japan) 2, 293-303
43. Groak, Bela, (1928) Biochem. Z. 196, 478-487
44. Henriques, O. M. (1928) Biochem. Z. 200, 1-24 (Series of 5 papers)
45. Henriques, O. M. (1929) Ergebnisse Physiol. 28, 625-689
46. Dirken, M. N. J. and Mook, H. W. J. (1930) Biochem. Z. 219, 452-462
47. Dirken, M. N. J. and Mook, H. W. J. (1930) J. Physiol. 70, 373-384
48. Henriques, O. M. (1931) Biochem. Z. 243, 241-255
49. Henriques, O. M. (1931) J. Biol. Chem. 92, 1-11
50. Margaria, R. (1931) J. Physiol. 73, 311-330

51. Goldberger, S., Margaria, R. and Rowinski, P. (1933) Arch. Sci. Biol. (Italy) 18, 378
52. Henriques, O. M. (1933) Biochem. Z. 260, 58-71
53. Janzen, Rudolf and Netter, Hans (1933) Arch. ges. Physiol. (Pflügers) 232, 349
54. Margaria, Rudolf and Green, A. A. (1933) J. Biol. Chem. 102, 611-634
55. Meldrum, N. U. and Roughton, F. J. W. (1933) J. Physiol. 80, 143-170
56. Van Slyke, D. D., Dillon, R. T. and Hiller, A. (1933) PNAS 19, 828-829
57. Ferguson, J. K. W. and Roughton, F. J. W. (1934) J. Physiol. 83, 68-86
58. Ferguson, J. K. W. and Roughton, F. J. W. (1934) Proc. Physiol. Soc., J. Physiol. 81, 21 pp
59. Mirsky, A. E. and Anson, M. L. (1934) Ann. Rev. Biochem. 3, 425-440
60. Groscurth, G. and Havemann, R. (1935) Biochem. Z. 279, 300-313
61. Roughton, F. J. W. (1935) J. Physiol. 85, 17-19 p
62. Roughton, F. J. W. (1935) Physiol. Rev. 15, 241-296
63. Stadie, W. C. (1935) Sci. 81, 207-208
64. Ferguson, J. K. W. (1936) J. Physiol. 88, 40
65. Groscurth, G. and Havemann, R. (1936) Biochem. Z. 285, 153-155
66. Roughton, F. J. W. (1936) Biochem. Z. 285, 150-152
67. Stadie, W. C. and O'Brien, H. (1936) J. Biol. Chem. 112, 723-758
68. Stadie, W. C. and O'Brien, H. (1937) J. Biol. Chem. 117, 439-470

69. Booth, V. H. and Roughton, F. J. W. (1938) *Biochem. J.* 32, 2049-2069
70. Hermann, H., Hudoffsky, B., Netter, H. and Travia, L. (1939) *Arch. ges. Physiol. (Pflüger's)* 242, 311-327
71. Root, R. W. and Irving, Laurence (1941) *Biol. Bull.* 81, 307-323
72. Kallner, Sixten, (1942) *Acta. Med. Scand.* 130, 1-110
73. Margaria, R. (1952) *Schweiz, Med. Wochschr.* 82, 990-993
74. Milla, E., Giustina, G. and Margaria, R. (1952) *Giorn. Biochim.* 1, 357-367
75. Milla, E., Giustina, G. and Margaria, R. (1952) *Ibid.* 1, 475-487
76. Milla, E., Giustina, G. and Margaria, R. (1953) *Bull. Soc. Ital. Biol. Sper.* 29, 805-806
77. Milla, E., Giustina, G. and Margaria, R. (1953) *Giorn. Biochem.* 2, 80-92
78. Milla, E., Giustina, G. and Margaria, R. (1953) *Giorn. Biochem.* 2, 153-165
79. Milla, E., Giustina, G. and Margaria, R. (1953) *Giorn. Biochem.* 2, 357-370
80. Margaria, R. (1957) *Clin. Chem.* 3, 306-318
81. Rossi, L. and Roughton, F. J. W. (1962) *J. Physiol*, 162, 17p
82. Rossi, L. and Roughton, F. J. W. (1962) *Bull. Soc. Ital. Biol. Sper.* 38, 1677-1699
83. Craw, M. R., Constantine, H. P., Morello, J. A. and Forster, R. E. (1963) *J. Appl. Physiol.* 18, 317-324
84. Roughton, F. J. W. (1963) "Oxygen, animal, organism" *Proc. Symp. Lond.* 5

85. Constantine, H. P., Craw, M. R. and Forster, R. E. (1965) *Am. J. Physiol.* 208, 801-811
86. Naeraa, N., Peterson, E. S., Boye, E. and Seoeringhaus, J. W. (1966) *Scand. J. Clin. Lab. Invest.* 18, 96-102
87. Roughton, F. J. W. and Rossi-Bernardi, L. (1967) *J. Physiol.* 189, 1-29
88. Carbon Dioxide: Chemical, Biochemical and Physiological Aspects, Washington: U.S. Government Printing Office (NASA no. SP-188) 1968, (Pub. 1969)
89. Constantine, H. P., Craw, M. R., Forster, R. E., Rotman, H. H., Klock, R. A. and Thyrum, D. (1968) *J. Biol. Chem.* 243, 3317-3326
90. Ishikawa, K., (1968) *Juzen Igakkai Zasshi* 77, 220-230
91. Kernohan, J. C. and Roughton, F. J. W. (1968) *J. Physiol.* 197, 345-361
92. Bauer, C. (1969) *Life Sci.* 8, 1041-1046
93. Kilmartin, J. V. and Rossi-Bernardi, L. (1969) *Nature* 222, 1243-1246
94. Pace, M., Rossi-Bernardi, L. and Roughton, F. J. W. (1970) *Biochem. J.* 119, 67P-68P
95. Roughton, F. J. W. (1970) *Biochem. J.* 117, 801-812
96. Kilmartin, J. V. and Rossi-Bernardi, L. (1971) *Biochem. J.* 124, 31-45
97. Rørth, Mikael (1971) *Acta Anaesthesiologica Scandinavica, Supplementum*, 30-36
98. Tomita, Susumu and Riggs, Austen (1971) *J. Biol. Chem.* 246, 547-554
99. Carreras-Barnes, Jose, Diederich, D. A. and Grisolia, Santiago (1972) *Eur. J. Biochem.* 27, 103-108

100. Salhany, J. M. (1972) J. Biol. Chem. 247, 3799-3801
101. Astrup, P. and Rørth, M., eds. (1972) Oxygen Affinity of Hemoglobin and Red Cell Acid Base Status, Alfred Benzon Symposium IV, Academic Press, New York
102. Arnone, A. (1974) Nature 247, 143-145
103. Bauer, C. and Schröder, E. (1972) J. Physiol. 227, 457-471
104. Brenna, O. M., Luzzana, M., Pace, Perrella, M., Rossi, F., Rossi-Bernardi, L. and Roughton, F. J. W. (1972) Adv. in Exp. Med. and Biol., Brewer, G. J. ed., Plenum Press, New York, 28, 19-37
105. Kernohan, J. C., Kreuzer, F., Rossi-Bernardi, L. and Roughton, F. J. W. (1966) Biochem. J. 100, 49P-50P
106. Kilmartin, J. V., Fogg, J., Luzzana, M. and Rossi-Bernardi, L. (1973) J. Biol. Chem. 248, 7039-7043
107. Rossi-Bernardi, L. and Roughton, F. J. W. (1967) J. Physiol 189, 1-29
108. vonWeiss, H., Meyer, H. and Ruckpaul, K. (1972) Zeit. Klin. Chem. Klin. Biochem. 10, 374-378
109. Morrow, J. S., Keim, P., Visscher, R. B., Marshall, R. C. and Gurd, F. R. N. (1973) Proc. Natl. Acad. Sci 70, 1414-1418
110. Gurd, F. R. N., Morrow, J. S., Keim, P., Visscher, R. B. and Marshall, R. C. (1974) Metal Protein Interaction, Friedman, M., Ed., Plenum Pub. Corp., New York, in press
111. Morrow J. S., Wittebort, R. J. and Gurd, F. R. N. (1974) Nature submitted for publication
112. Matwiyoff, N. A. and Needham, T. E. (1972) Biochem. Biophys. Res. Commun. 49, 1158-1164
113. Faurholt, C. (1925) J. Chem. Phys. 22, 1-44

114. Forster, R. E., Constantine, H. P., Craw, M. R., Rotman, H. H. and Klocke, R. A. (1968) 243, 3317-3326
115. Farrar, T. C. and Becker, E. D. (1971) Pulse and Fourier Transform NMR, Academic Press, New York
116. Allerhand, A., Childers, R. F. and Olfield, E. (1973) Biochem. 12, 1335-1341
117. Nigen, A. M., Keim, P., Marshall, R. C., Morrow, J. S., Vigna, R. A. and Gurd, F. R. N. (1973) J. Biol. Chem. 248, 3724-3732

CHAPTER II

Materials and Methods

Chapter II

Materials

All chemicals were of reagent grade and with the following exceptions were used without further purification.

Dioxane (Fisher) was freed of explosive peroxides by the addition of alumina (Woelm).

Potassium cyanate (Fisher) was twice recrystallized from ethanol, and stored at -20° in vacuo. Examination of this material by infrared spectroscopy established the absence of the strong 833 and 700 cm^{-1} absorptions characteristic of $\text{NH}_4\text{CO}_3(1)$.

Carbon monoxide (Matheson) was scrubbed of trace carbon dioxide by slow passage through 0.2 M NaOH . This precaution was taken only when careful control of carbonate levels was necessary.

2, 3-Diphosphoglyceric acid was obtained as the pentacyclohexylammonium salt from Calbiochem, and was converted to the acid form by passage through a column ($0.9 \times 10\text{ cm}$) of Dowex 50 x 8 (H^+).

Parachloromercuric benzoate (Sigma) was washed by acid precipitation immediately before use, following the method of Boyer (2).

Urea (Fisher) was recrystallized from 95% ethanol, and then stored in vacuo at room temperature. Cyanate was removed from urea solutions by passage through Rexyn[®] I-300 H-OH ion exchange resin shortly before use.

Inositolhexaphosphate (Sigma) was scrubbed of trace metal contamination by batch treatment with Chelex 100 (Bio-Rad) immediately prior to use. The resin was removed by centrifugation.

Acetazolamide (Diamox[®], Lederle) was obtained as the sodium salt, in a preparation suitable for parenteral use.

Hydrochloric acid (constant boiling) was obtained by distillation of concentrated HCl (Mallinckrodt) and water in a 5:4 ratio. The azeotropic mixture boiling at 110° (5.7 N) was collected.

Water was distilled and subsequently passed through two research grade model I ion exchange columns, supplied by the Illinois Water Treatment Co., Rockford, Illinois. Its resultant conductivity was less than 5×10^{-6} mho. The pH of this water was generally not less than 5.0. Totally carbonate free water was prepared by glass distillation and subsequent storage in a flask fitted with an Ascarite (Arthur H. Thomas, Inc.) carbon dioxide trap. The pH of this water was not less than 6.6.

Mercaptoethanol (Pierce) was sequencer grade.

Isotopically enriched compounds were used as obtained. The stable isotope enrichment was verified by mass spectroscopy.

Carbon Dioxide (^{13}C) (Mound Laboratories, Monsanto Chemical Corp.) was found to be enriched to slightly greater than 90% in ^{13}C . The reported contamination by carbon monoxide was less than 0.1%.

$\text{Na}_2^{13}\text{CO}_3$ and $\text{NaH}^{13}\text{CO}_3$ (Bio-Rad) were supplied at a ^{13}C enrichment of 88%.

Glycine (^{15}N) (Prochem) was supplied at a ^{15}N enrichment of 95%.

Potassium cyanate (^{14}C) (New England Nuclear) was supplied at a specific activity of 10.82 mc/mMole. This was reduced to a specific activity of approximately 3.6 mc/mMole before use by the addition of KNCN at natural isotope abundance.

D₂O (Oakridge National Laboratory) was of reported enrichment greater than 99% in deuterium.

Gel filtration media were from Pharmacia, and for most purposes consisted of Sephadex G-25 fine. Sephadex ion exchange resins, DEAE A-50 and CM C-50 were also from Pharmacia. Carboxymethyl cellulose was from Whatman (CM-52), and Bio-Rex 70, 200-400 mesh, was supplied by Bio-Rad. Chelex 100 was also from Bio-Rad. Scintillation fluid was Aquasol (New England Nuclear). For amino-acid analysis, a single column (0.9 x 60 cm) system employing either a Durrum DC1A or DC6A resin was used. The standard reagents (sequencer grade) suggested by Beckman Instrument Co. were used for the automated Edman degradation of the protein and peptide NH₂-terminals (3). Dr. Alan M. Nigen generously provided a sample of hemoglobin alpha-chains specifically carbamylated on the NH₂-terminus. These served as a most valuable reference to the preparations described below.

The di- and tri-peptides used in the model compound studies were from either Sigma or Cyclo Chemical Corp. The pentapeptides, with the exception of pentaglycine (Sigma), had been prepared in this laboratory by the Merrifield solid phase technique for use in other magnetic resonance studies (4, 6). Initial studies on (5-Ile) Angiotensin II were made possible by a generous gift from Dr. F. Merlin Bumpus, while larger quantities of the peptide purchased from Beckman provided the material for later studies. Drs. Miklos Bodansky and Maurice Manning generously provided the initial samples of vasopressin and vasopressin analogues. Additional samples of (Lys) vasopressin and oxytocin were later kindly donated by Dr. Raymond J. Vavrek of Ferring Pharmaceuticals, Malmö, Sweden.

Methods

Measurement of pH. All pH measurements were made with a Radiometer PHM4c pH meter, utilizing a GK2302B combined electrode. Standardization of the meter against two fresh reference buffers (Matheson, Coleman, and Bell at pH 4.01 and 7.00; Radiometer Corp. at pH 9.20) was repeated frequently during any series of measurements. All measurements were made at room temperature, unless otherwise specified.

Measurement of Total Carbonates. A Natelson Microgasometer model #600 with motorized shaker attachment #M-373-20, manufactured by Scientific Industries, Inc., was used to analyze the total carbonates present in small volumes of sample. The principle of operation of this instrument is identical to the classical Van Slyke manometric method (7), wherein the difference in gas pressure over a solution made first acidic and then basic is compared at constant volume and temperature. This difference is representative of the $p\text{CO}_2$, and with appropriate corrections is convertible to the total carbonate concentration. The corrections necessary are adequately described in the literature (7-9), and will not be rederived here. Table I lists the numerical values of the correction factors, which when multiplied by the pressure of liberated CO_2 , yield the millimolar concentrations of carbonates in the original sample. Complete operating instructions are available (Scientific Industries, Inc., Instruction manual #6).

Dialysis Tubing Preparation. Visking cellulose tubing (Union Carbide), 18/32 inch in diameter, was washed four times by boiling twice in a solution containing approximately 4 g NaHCO_3 and 0.5 g Na_2EDTA per liter, followed by two washes with boiling water only. The

Table I
Factors for CO₂ Determination¹

To convert the pressure difference measured between an acid and basic solution of carbonates in the Natelson Microgasometer to either m molar or vol. percent, multiply that difference by the appropriate factor.

Temp.	Factor Vol. Percent	Factor mMol/l
17	0.560	0.253
18	0.558	0.251
19	0.551	0.248
20	0.549	0.247
21	0.548	0.246
22	0.547	0.245
23	0.540	0.244
24	0.539	0.243
25	0.537	0.242
26	0.532	0.241
27	0.530	0.240
28	0.528	0.239
29	0.527	0.238
30	0.524	0.237
31	0.522	0.235
32	0.519	0.234

¹Taken from Scientific Industries Instruction Booklet #6: The Natelson Microgasometer.

tubing was stored at 4° in water containing approximately 0.5 ml per liter of pentachlorophenone, and rinsed immediately before use.

Protein Concentration. Ultrafiltration apparatus supplied by the Amicon Corporation was used exclusively. For most applications, a PM-10 membrane in the Diaflo cells of 15, 50, 200, or 500 ml capacity was employed. After use, the membranes were washed by soaking overnight in an Alconox[®] detergent solution, followed by an EDTA wash and storage at 4° in a 15% Ethanol solution. With such treatment, the membranes retained good flow characteristics for several months.

Polyacrylamide Gel Electrophoresis. Vertical gels for hemoglobin electrophoresis were prepared with a Tris-EDTA-borate buffer, following the recipe of Rosemeyer and Huehns (10). A stock solution containing 69.9 g of trishydroxymethyl aminomethane, 5.8 g disodium EDTA, and 30.9 g boric acid per liter was prepared. Gel solution sufficient to make a single gel slab was then readily obtained by diluting 7.5 ml of the stock solution with 142.5 ml of water, adding 10.5 g Cyanogum 41[®] (95% acrylamide, 5% bis acrylamide; E-C Corporation) and 0.1 ml tetramethylethylenediamine (TMED). Immediately before use the above solution was filtered and mixed with 0.2 g ammonium persulfate. Gel time was less than one hour. A 1:7 dilution of the stock solution was used in the buffer compartment. Electrophoresis was performed for 1 to 2 hours at 250 volts. The gels were stained with 0.2% Amido black 10B for 30 minutes. Destaining by the application of an electrical potential at right angles to the gel slab, in a circulating 1:5:5 solution of acetic acid-methanol-water, required 1 to 2 hours. Further information concerning the acrylamide electrophoresis procedures is described in the E-C Apparatus Technical Bulletin No. 134.

Cellulose Acetate Electrophoresis. Electrophoresis on cellulose acetate membranes (Microzone[®], Beckman Instrument Co.) was carried out in the same buffer as that used for the acrylamide gel electrophoresis. Adequate separation of most hemoglobin components required 45 minutes at 300 volts. The cellulose membranes were stained with a Ponceau-S dye. Complete instructions for the use of the Beckman Microzone[®] system are available in the Beckman Microzone[®] Electrophoresis Manual.

Ultraviolet and Visible Spectral Measurements. All measurements were made on a Cary 14 recording spectrophotometer usually with a pair of 1 cm matched Quartz cuvettes (Hellma). The concentration of sperm whale ferrimyoglobin (Fe^{+++}) was determined as the Soret band (423 nm) absorbance of the cyanide derivative divided by a millimolar extinction coefficient of 109.7 (11). Several different methods of measuring the concentration and heme state of hemoglobin were employed. All hemoglobin concentrations are expressed on a heme basis. For adult human hemoglobin (HbA_0) (12) in the oxy or deoxy state, a close estimation of the state of the solution was possible following the equations of Benesch et al. (13):

$$[\text{HbO}_2] = \frac{1.64 \cdot A_{576} - 0.64 \cdot A_{560} - 0.72 \cdot A_{540}}{1.0 \times 10^4} \quad 1$$

$$[\text{FerriHb}] = \frac{A_{540} - 0.20 \cdot A_{560} - 0.82 \cdot A_{576}}{2.0 \times 10^3} \quad 2$$

$$[\text{Hb}^+] = \frac{1.2 \cdot A_{560} + 0.26 \cdot A_{576} - A_{540}}{7.8 \times 10^3} \quad 3$$

where A_{λ} represents the absorbance at wavelength λ nm.

Since this method was not useful for hemoglobins other than A_0 , a more general method was commonly used, especially if accurate estimations of ferrihemoglobin levels were needed. The most satisfactory procedure was as follows (14):

- 1) An appropriately diluted sample was divided into two aliquots of at least 2 ml each.
- 2) One aliquot was treated with a single crystal of $K_3Fe(CN)_6$, and allowed to stand covered with parafilm[®] at room temperature until oxidation of the heme was complete. This required approximately 10 minutes for HbO_2 , and 30 minutes to one hour for $HbCO$.
- 3) The remaining aliquot was converted to the $HbCO$ derivative by saturation of the solution with moist CO .
- 4) The visible spectrum from 590 to 530 nm of the $HbCO$ solution was recorded. A few grains of $Na_2S_2O_4$ were added, and the spectrum again recorded. This latter measurement represents the spectrum of 100% reduced $HbCO$.
- 5) The spectrum of the 100% oxidized sample was then recorded. Addition of a few grains of KCN yielded the spectrum of cyanoferrihemoglobin.

The millimolar concentration of the hemoglobin solution was then determined as the absorbance of the 576 or 540 bands divided by 13.4, or more reliably as the absorbance at 540 nm of the cyanoferri derivative, divided by 10.04 (15). The percentage of ferrihemoglobin present in the original sample was also readily calculated as:

$$\% \text{ ferriHb} = \left[\frac{A_{576}^{\text{Red}} - A_{576}^{\text{ox}}}{A_{576}^{\text{Red}} - A_{576}^{\text{ox}}} + \frac{A_{540}^{\text{Red}} - A_{540}^{\text{ox}}}{A_{540}^{\text{Red}} - A_{540}^{\text{ox}}} \right] \cdot 50$$

where A_{λ}^{Red} refers to the Hb solution reduced with $\text{Na}_2\text{S}_2\text{O}_4$; A_{λ}^{ox} that of the $\text{K}_3\text{Fe}(\text{CN})_6$ oxidized material; and A_{λ} that of the original sample.

The criterion for complete deoxygenation of the hemoglobin samples was that of Benesch et al. (13), i.e.

$$\frac{A_{670}}{A_{730}} \geq 2.3 \quad 5$$

Mass Spectroscopy. Varian MAT CH7 or Associated Electrical Industries MS-9 magnetic sector mass spectrometers were used to monitor the degree of isotopic enrichment in the ^{13}C samples. Most analysis involved the measurement of the $^{13}\text{C}/^{12}\text{C}$ ratio in the atmosphere within the sealed NMR tubes. The nature of the specially constructed NMR tubes (see below) allowed anaerobic loading of the gas sample directly from the NMR tube. Several mass scans were made of each sample, with the $^{13}\text{CO}_2/^{12}\text{CO}_2$ ratio being calculated from the integral areas of the parent peaks at 45 and 44 m/e units. Integration was done both manually by planimetry (see "Integration Methods") or digitally by means of an on-line Texas Instruments 980 mini-computer. The estimates by either method were generally comparable within 1%.

Amino Acid Analysis. Protein or peptide hydrolyzates were analyzed on one of three Beckman Spinco Automatic Analyzers, models 120C and 121C. While 24 hour hydrolysis of peptides in 6N HCl in vacuo at 110° was adequate, 48 hours was found to be necessary for the complete hydrolysis of hemoglobin samples. Calculation of results was by standard methods (16).

Removal of Heme. Amino-terminal analysis of hemoglobin or myoglobin by the automated Edman procedure (3) requires the prior removal of the heme. This was accomplished either by the method of Teale (17), employing

methyl ethyl ketone extraction, or more conveniently, the method of Rossi-Fanelli et al. (18). This latter method, employing precipitation of the globin from a 0.3% (v/v) 2N HCl-acetone solution at -20° , offers the advantage that it provided dry powdered globin, quite suitable for use in the Beckman Sequencer, in less than two hours' time.

Automated Edman Degradations. Sequential degradation of peptides and proteins from the NH_2 -terminus was performed with the Beckman 890C Sequencer, utilizing standard methods (3). Analysis of the cleaved phenylthiohydantoin (PTH)-amino acids was generally by the amino acid analyzer, following reversion to the free amino acid. The reversion was accomplished by 20 hour hydrolysis in vacuo at 140° in 6N HCl, with one drop of mercaptoethanol added to retard oxidation. An internal standard of 101 nanomoles of PTH-alanine was usually included in these samples, allowing an estimate of the reversion efficiency.

Sperm Whale Ferrimyoglobin Preparation. Sperm Whale ferrimyoglobin (Physeter catodon) was prepared by the method of Hartzell (19) directly from the frozen skeletal muscle. The main fraction (band IV) eluted by 0.1 M ionic strength phosphate buffer on CM-50 Sephadex chromatography at pH 6.5 was collected for study. This protein was homogeneous on polyacrylamide gel electrophoresis, and was deionized immediately before use by passage through a Rexyn I 300 (HOH) ion exchange column.

Hemoglobin preparation. Most adult human hemoglobin was prepared from fresh venous blood collected in citrate-sorbate (Vacutainer[®]) from a single non-smoking donor (the author). The red blood cells were packed by centrifugation at $3000 \times G$ for 10 minutes, and then washed 4 times by resuspension and centrifugation with 0.9% (w/v) NaCl. Following the final wash, the cells were lysed by the addition of 2

volumes of water with gentle agitation. Upon standing at room temperature for 45 minutes, precipitation of the erythrocyte membrane "ghosts" was facilitated by the addition of NaCl to 0.1 M and centrifugation for one hour at 27,000 x G. The hemoglobin solution was decanted, and the packed ghosts rewashed with water and recentrifuged.

If only a hemolyzate was desired, the combined supernatants were adjusted to pH near 7.5 with 0.1 N NaOH, concentrated to a small volume, and then stripped of 2, 3-diphosphoglycerate (2, 3-DPG) by passage through a column (5 x 25 cm) of G-25 Sephadex equilibrated with 0.1 M NaCl. Alteration of the salt environment of the proteins was then achieved either by exhaustive dialysis or gel-filtration. More commonly, additional purification of the protein was carried out by chromatography on A-50 Sephadex. The method was essentially that of Huisman (12,20), with elution by a 0.05 M Tris-HCl pH gradient from 7.9 to 7.0. The initial pH of the column was 8.0, as was that of the hemoglobin solution when loaded.

The buffers needed were most conveniently made from a stock solution of one molar Tris and one normal HCl:

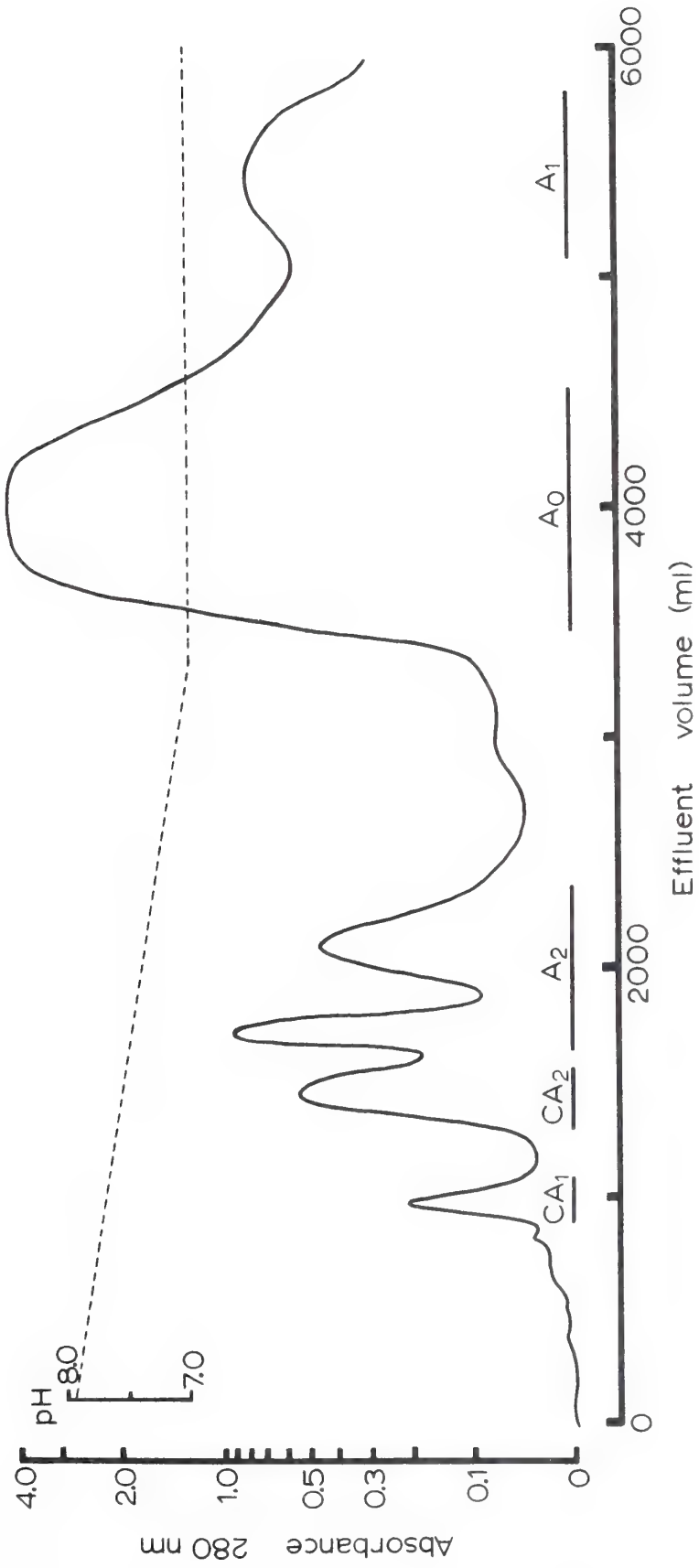
- | | | |
|-------------------|---------------------|------------|
| 1) pH 8.06 buffer | 50.0 ml | 1.0 M Tris |
| | 30.0 ml | 1.0 N HCl |
| | Dilute to 1.0 liter | |
| 2) pH 7.90 buffer | 50.0 ml | 1.0 M Tris |
| | 32.0 ml | 1.0 N HCl |
| | Dilute to 1.0 liter | |
| 3) pH 7.06 buffer | 50.0 ml | 7.0 M Tris |
| | 47.0 ml | 7.0 N HCl |
| | Dilute to 1.0 liter | |

Triethylenetetraamine at 1×10^{-4} molar was included in all buffers (see below).

Most purifications were performed at 4° upon the oxygenated protein. The absorbance at 280 nm of the effluent was monitored with a Beckman model DB spectrophotometer utilizing a one cm flow cell and linked to a Heath model EU-20B chart recorder. A typical elution profile is depicted in Figure 1. The identification of the hemoglobin fractions is based upon published elution profiles (12,20) and was verified by amino acid compositional analysis. The basis of the multiplicity of the fraction labeled A_2 is unknown. Only at 4° and under the most ideal conditions of sample loading, flow rate, and column homogeneity was this multiplicity observed. At room temperature only a single slightly broader peak was found, with a resulting elution profile nearly indistinguishable from published reports (12,20). The two leading non-heme fractions, labeled CA1 and CA2, were found to possess exceedingly high carbonic anhydrase activity on the basis of assays by the method of Wilbur and Anderson (21). Since no other portion of the effluent possessed any similar activity, these fractions were ascribed to the erythrocyte carbonic anhydrases. Electrophoresis by either polyacrylamide gel or cellulose acetate confirmed the purity of the A_0 fraction.

The purification of other hemoglobins was by the same procedure, changes being made only in the nature of the pH gradient. Fetal hemoglobin, HbF, obtained from cord blood at the time of delivery through the courtesy of Dr. Anderson of the Bloomington Hospital, utilized the same pH gradient as that for adult hemoglobin. Sick cell hemoglobin, obtained from a 36 year old black female with documented sickle cell trait, was

Figure 1. Chromatography of adult human hemoglobin hemolyzate on Sephadex DEAE A-50. Column dimensions were 5.0 x 60 cm. Elution was at 4° at 0.05 M Tris-HCl buffer. Flow rate was 70 ml per hour. The components were identified on the basis of their composition, activity assays, and comparison with published reports. The nomenclature of the hemoglobin components is based on Huisman (12,20). See text for details.



purified with a pH gradient of 8.1 to 6.9 (Figure 2). Chicken blood was collected into sodium citrate following decapitation. The immature white leghorn chickens were obtained from a local farm cooperative and kindly provided by Professor Frank Zeller. The two major chicken hemoglobin components, designated A_I and A_{II} , based upon their order of elution on cation exchange chromatography (22), were purified utilizing a similar gradient as that for HbS (Figure 3).

At this point it is worthwhile to digress briefly to comment on the substantial problem of autooxidation in the hemoglobin solutions. While unfractionated hemolyzates were reasonably stable under conditions of the NMR measurements (temperature near 30°), purified solutions, particularly when deoxygenated at low pH, often developed upwards of 50% ferrihemoglobin over a twenty-four hour period. It had been reported that the addition of EDTA (10^{-3} - 10^{-5} M) to the hemoglobin solutions would substantially reduce autooxidation (15). The well known anion binding properties of hemoglobin (15) suggested that such chelating agents as EDTA might perturb the bicarbonate and/or CO_2 interaction, and hence could not be used. A search for an alternative chelating agent suggested that triethylenetetraamine (TETA) might provide a cationic alternative to EDTA. The results of pilot studies (see Appendix A), as well as experience, amply bore this out. If precautions were taken to clean scrupulously all glassware with EDTA, and maintain at least 10^{-5} M TETA in the buffers and hemoglobin solutions, the development of ferrihemoglobin could be reduced to often much less than 15% in the deoxy samples over a 24 hour period at 30° , and less than 2% over a similar period in the carboxyhemoglobin samples. Solutions of oxyhemoglobin were little used, due to their much greater

Figure 2. Chromatography of hemoglobin hemolyzate from donor with sickle cell trait. The column and elution conditions were as in Figure 1. The elution gradient is indicated by the dashed line. The components were identified by comparison with published reports (12,20), and confirmed by the gellation of the fraction indicated S and upon deoxygenation.

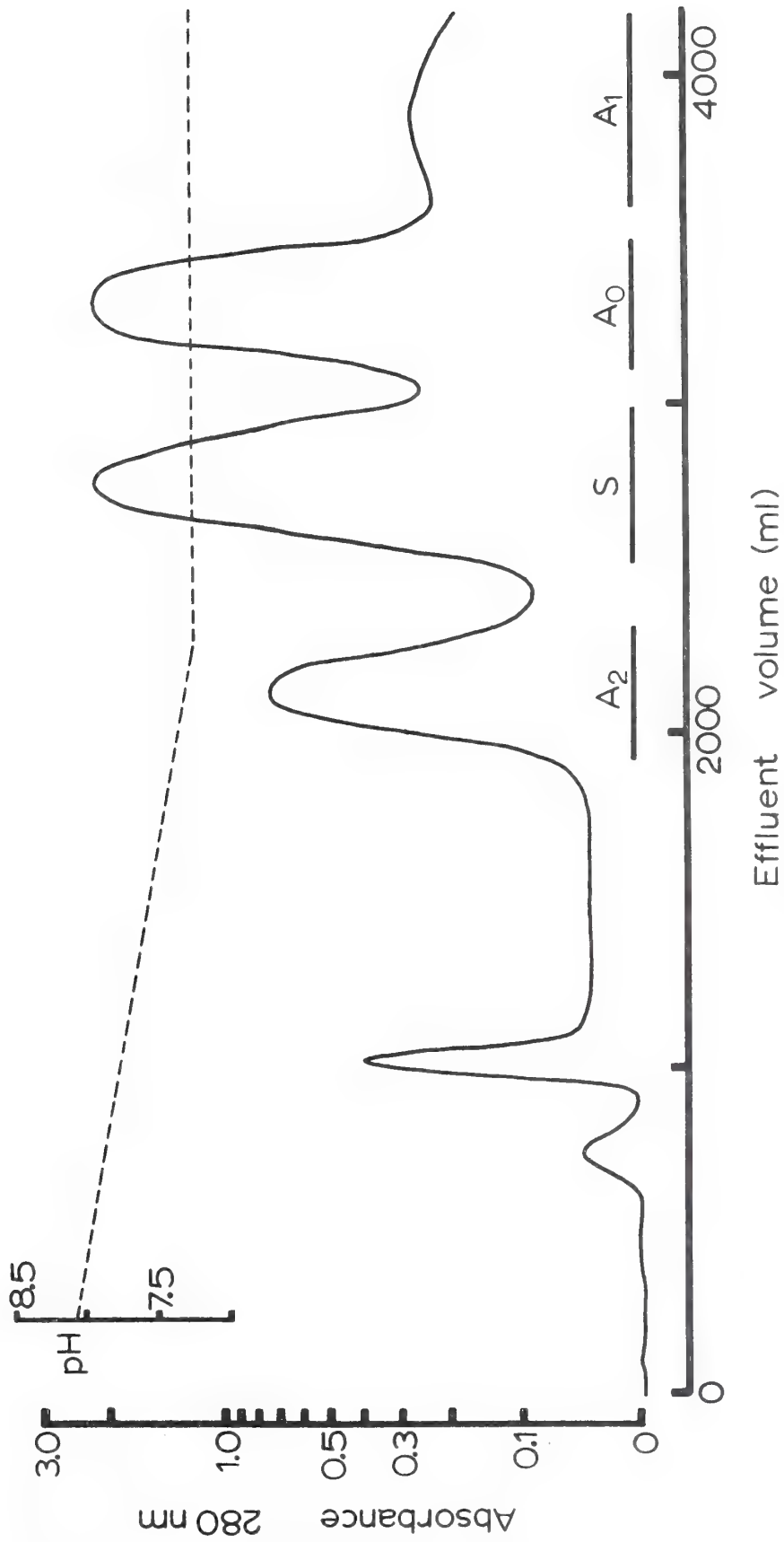
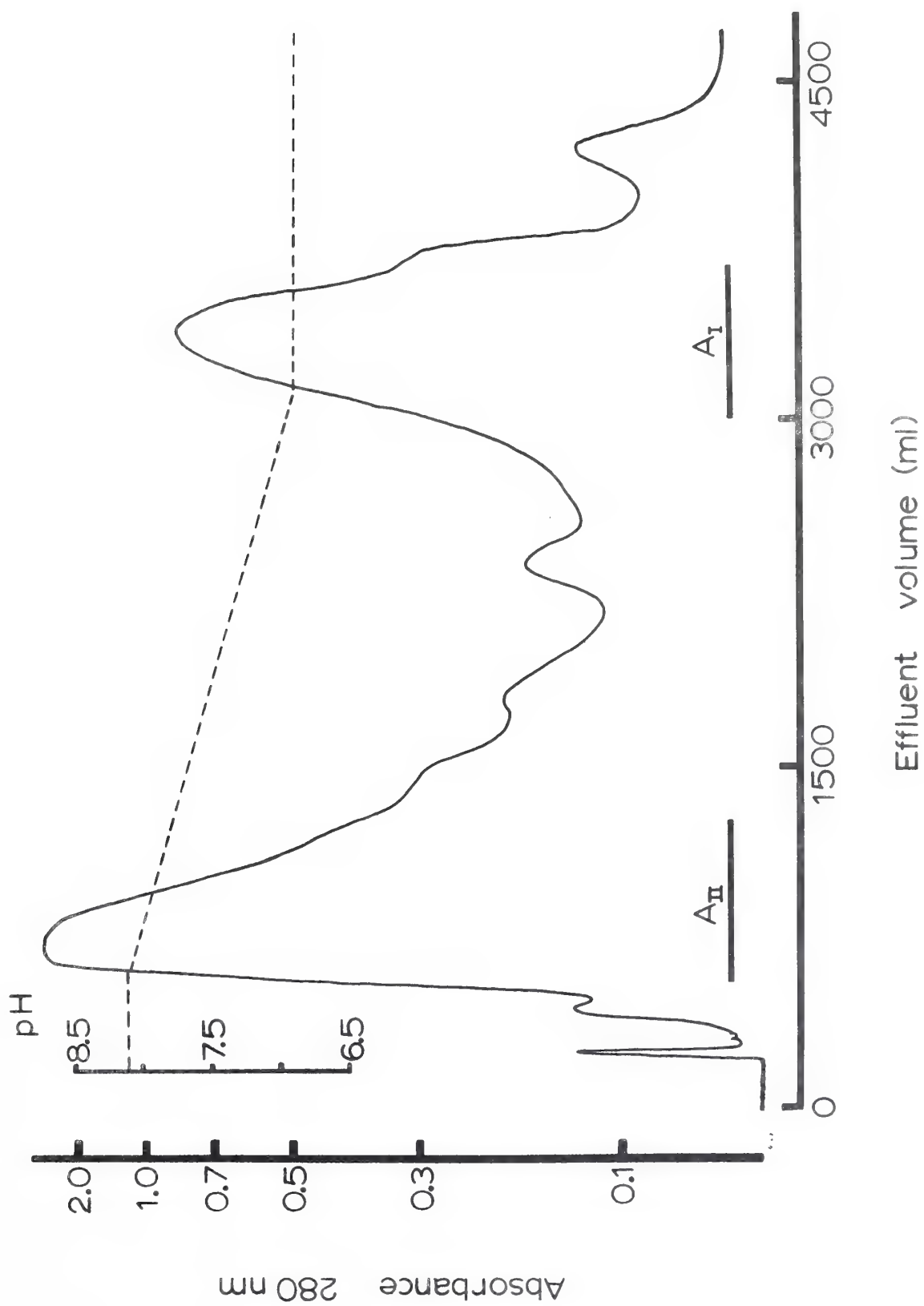


Figure 3. Chromatography of immature white leghorn chicken hemoglobin hemolyzate on Sephadex DEAE A-50. Column dimensions were 5.0 x 60 cm. Elution was at 4° by 0.05 M Tris-HCl buffer, pH 8.1 to 6.9, as indicated by the dashed curve. Hemoglobin component A_{II} eluted from 560 ml to 1300 ml, and A_I from 3000 ml to 3700 ml as shown by the underscoring. The nomenclature of the hemoglobins is based on their order of elution on cation exchange chromatography (22).



tendency to undergo oxidation. Such careful control of metal contamination also had the benefit of limiting the range of variables which might substantially perturb the NMR observations. Very recently, Rifkin (23) has quantitated the effects of trace metals, and in particular copper, upon the oxidation of hemoglobin solutions. His findings provide firm experimental support of the qualitative observations noted here.

Reduction of Ferric Proteins. The chemical reduction of the iron in oxidized hemoproteins is a matter which must be approached with utmost caution. Reports have appeared that the protein is irreversibly damaged by such procedures (24). While such measures are thus to be avoided, circumstances sometimes arise which make it preferable to carefully reduce the protein, rather than start an experiment with elevated ferrihemoglobin levels. Such circumstances almost exclusively are limited to cases where the protein has been modified or it is otherwise difficult to gather fresh material. The procedure for reduction by sodium dithionite was essentially that of Dixon and McIntosh (25). A four to five fold molar excess of $\text{Na}_2\text{S}_2\text{O}_4$ dissolved in 0.05 M NaCl or the elution buffer was layered as a thin band on a column of G-25 Sephadex. This was followed by a very small amount of additional salt solution (buffer), and then protein. As the protein overtakes the dithionite, it is reduced. This technique has the advantage that the protein is only briefly in contact with the reducing solution, thus minimizing chances of damage. Hemoglobins so reduced were indistinguishable from untreated reduced hemoglobin regarding their interactions with the ligands studied here, as well as stability to reoxidation. Reoxidation was accelerated considerably, however, if the gel filtration

column was of insufficient length to insure complete removal of the $\text{Na}_2\text{S}_2\text{O}_4$ from the hemoglobin.

Enzymatic reduction was employed to maintain deoxyhemoglobin solutions essentially free of oxidized protein during the course of some of the NMR measurements. The presence of the reducing system interfered with the CO_2 binding studies, presumably due to the high levels of glucose-6-phosphate. Hence the system was of only limited usefulness. The system chosen was one employing reduced ferridoxin (26). All enzymes and cofactors were obtained from Sigma. To reduce and maintain 10 micromoles of ferrihemoglobin, a solution containing the following was used:

- 1) 45 mg. glucose-6-phosphate dehydrogenase (E.C. No. 1.1.1.49)
(from Bakers yeast)
- 2) 0.12 mg. Ferredoxin (from spinach)
- 3) 0.13 mg. Ferredoxin-TPN reductase (from spinach)
- 4) 0.1 mg. Catalase (1.11.1.6) (from beef liver)
- 5) 0.1 mg. triphosphopyridine nucleotide (TPN)
- 6) 5 mg. glucose-6-phosphate

Complete reduction generally required 10 to 12 hours.

Separation of Hemoglobin Chains. Isolated alpha and beta chains of human hemoglobin A_0 were prepared as the carboxy derivatives, after reaction at pH 6.0 with a 25 molar excess of parachloromercuribenzoate (pCMB) (27,28). The buffer was 0.1 molar ionic strength phosphate, with 0.2 molar NaCl. Temperature was 4° , reaction time 12 hours, and protein concentration 2 millimolar. The pCMB was freshly dissolved in 0.5 M NaOH and then titrated to cloudiness with 6 N HCl immediately before use. The unreacted pCMB was removed by dialysis. Considerable precipitate formed over the course of the reaction, which was removed

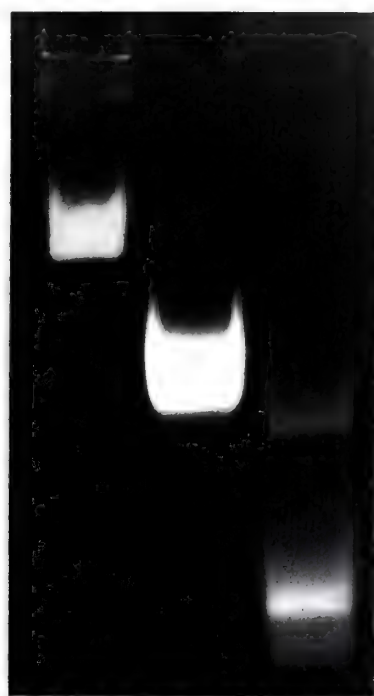
by centrifugation. Electrophoretic examination of the crude reaction mixture (Figure 4) by polyacrylamide gel revealed three distinct bands. On the basis of a comparison with hemolyzate and published reports (28), these may be identified as p-mercuribenzoate reacted alpha-chains, dimer, and β -chains for the slowly to quickly migrating bands, respectively. The apparent heterogeneity of the β -chain fraction is attributed to variable association of the β -chain monomers to form larger aggregates (29).

Preparative separation of the chains was achieved on a CM cellulose column (5 x 15 cm) utilizing a step gradient of CO-saturated phosphate buffers, the first being pH 6.7, 0.01 M phosphate, the second pH 7.1, 0.01 M phosphate, and the third pH 7.6, 0.01 M phosphate. The elution profile obtained at 4° is shown in Figure 5. While a utilization of the step gradient hastened the elution of the trailing α^{pmb} fraction, complete separation of the β^{pmb} chains from the dimer (or tetramer) was not achieved, as evidenced in Figure 4B. The β -chains were subsequently refractionated on a similar column initially at pH 6.47 (Figure 5 inset) which was adequate to provide a clean separation. In subsequent preparations, separation of the β^{pmb} and dimer (tetramer) could be achieved in the first fractionation, if the pH were not above 6.5. Furthermore, a linear gradient, similar to that published by Bucci and Fronticelli (27), proved more convenient than the step gradient used here. When the hemoglobin had been pretreated with KNCN (see below), the pCMB reaction was conducted at lower protein concentrations (0.5 mM). By so doing, the extent of precipitation was reduced and the yield improved. It is significant that when unusual amounts of precipitation occurred, the yield of the alpha chains was disproportionately reduced.

Figure 4. Polyacrylamide gel electrophoresis at pH 8.7 of HbAo following treatment with pCMB. (A-1) crude reaction mixture following treatment for 12 hrs. with p-chloromercuribenzoate at pH 6.0 in 0.2 M NaCl; (A-2) unreacted HbAoCO; (B-1) α^{pmb} -chain fraction following purification of sample shown in (A-1) on CM-cellulose; (B-2) HbAoCO; (B-3) β^{pmb} -chain fraction from purification described in (A-1). The small trace of material near the HbAoCO sample in (B-3) was removed by refractionation (Figure 5, inset). The apparent heterogeneity of the leading band in A or B is attributed to variable states of aggregation in β^{pmb} -chains (29). See text for details.



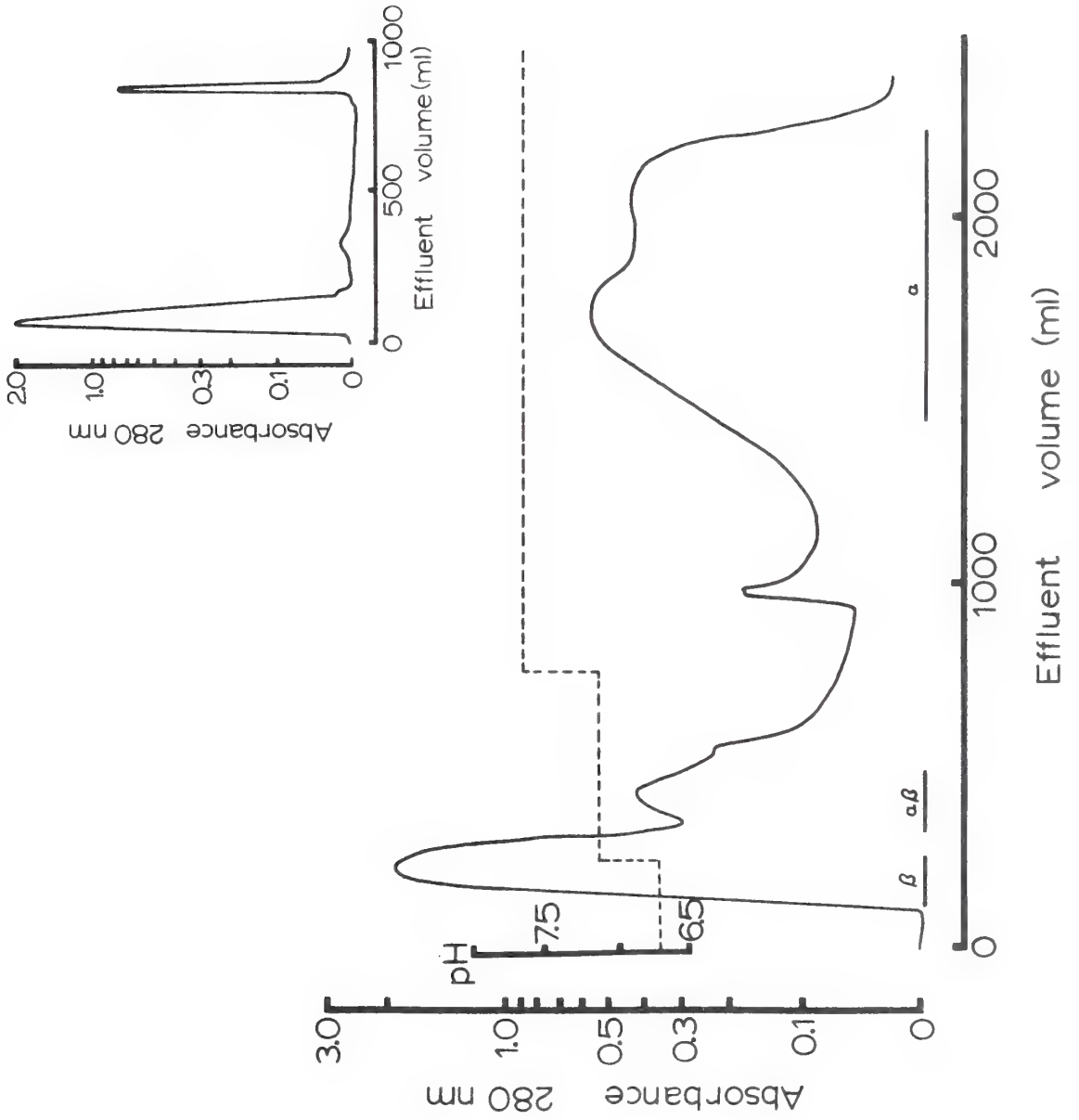
1 2
A



1 2 3
B

Figure 5. Chromatography of pCMB reacted HbAo on CM-52 cellulose at 4°. Column dimensions were 5 x 15 cm. A step gradient was used for elution, as indicated by the dashed line. All buffers were saturated with CO; 10^{-4} M TETA was also included. The first buffer was pH 6.7, 0.01 M phosphate; the second pH 7.1, 0.01 M phosphate, and the third pH 7.6, 0.01 M. phosphate. The components were identified on the basis of their electrophoretic behavior and comparison with published reports (27).

Figure 5 (insert). Chromatography of β fraction derived from the elution shown in Figure 5. Column dimensions and packing material were as above. Elution was by pH 6.47 0.01 M phosphate at 4° until the leading band had eluted, followed by elution with 0.015 M Na_2PO_4 .

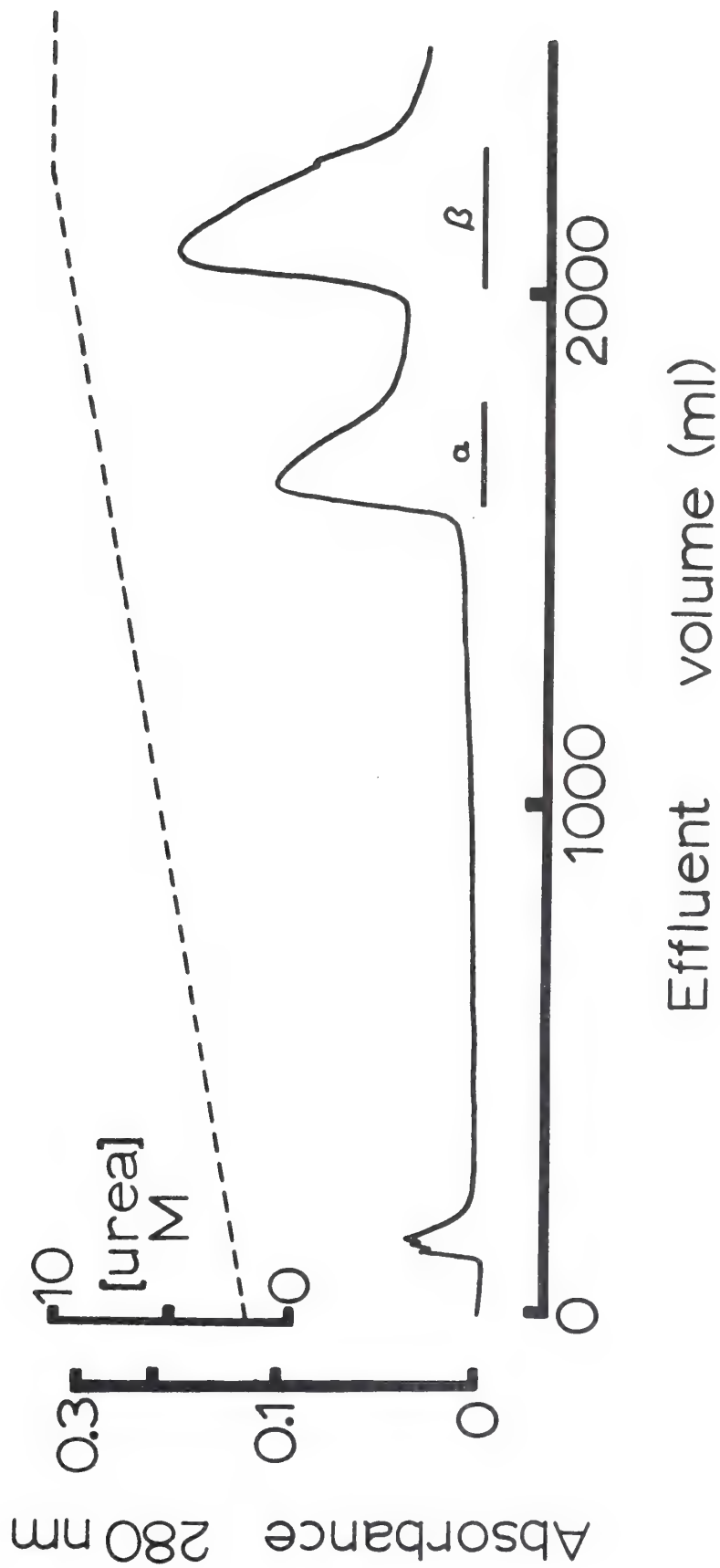


The alpha and beta chains of chicken hemoglobin were prepared for sequence analysis by a modification of the procedure of Matsuda et al. (30). To a column (2 x 40 cm) of Bio-Rex 70, equilibrated with 3N formic acid, was loaded 108 mg of chicken globin which had stood for three days at room temperature in a 10 M urea and 3 N formic acid solution. Elution was by a urea gradient from 2 molar to 10 molar, in 3 N formic acid. The elution profile is depicted in Figure 6. The fractions were identified by their composition and a comparison with published reports (30). Following elution, the excess salts were removed by dialysis against water.

Recombination of p-Mercuriobenzoate Treated Chains. The separated chains were quickly and quantitatively recombined by following the method of Nigen et al. (31). Equimolar amounts of the pmb- α and pmb- β chains (or their carbamylated derivatives) in 0.05 M NaCl were mixed in the presence of a 300-fold molar excess of mercaptoethanol, based on the total sulphydryl content. This solution was allowed to stand for 12 hours at 4°; excess mercaptoethanol was removed either by gel filtration or exhaustive dialysis. Reformation of the tetramer was verified by electrophoresis.

Preparation of Carbamylated Hemoglobins. Several possible approaches to the problem of preparing human hemoglobin selectively carbamylated with cyanate at either the alpha ($\alpha_2^C\beta_2$) or beta ($\alpha_2\beta_2^C$) chain NH_2 -termini exist. These may be divided into three basic categories: (A) reaction of the intact tetramer, then separation of the desired reaction products; (B) reaction of the tetramer, separation and purification of the carbamylated chains, reformation of the desired hybrids; (C) separation of chains, reaction and purification of these, then reformation of the

Figure 6. Chromatography of chicken globin on a 2 x 40 cm column of Bio-Rex 70 equilibrated with 3 N formic acid. Elution was by a urea gradient, from 2 M to 10 M, as indicated by the dashed curve. Components were identified on the basis of their NH₂-terminal sequence (Appendix D).



desired hybrids. Preliminary studies utilizing the first approach suggested that unlike horse hemoglobin (14), the $(\alpha_2^C\beta_2)$ or $(\alpha_2\beta_2^C)$ derivatives of human hemoglobin would not be easily separated as carboxyhemoglobin. A similar result has also been found by Williams and Kuo-Yi Tsay (32). While it has recently been found that the addition of inositol hexaphosphate (IHP) to the carbamylated tetramer facilitates the separation of these analogues (33), no further attempts with this method were tried. Preparation of carbamylated alpha and beta chains by reaction of the tetramer, followed by chain separation, was done essentially exactly as reported by Nigen et al. (31) for HbS. HbA₀ was reacted as the deoxyderivative with a 10-fold molar excess of KNCO at pH 6.15 for 45 minutes at 37°. The reaction was quenched with diglycine. Diglycine carbamate was removed by gel filtration; the hemoglobin solution was reacted overnight with pCMB as previously described. For separation of the carbamylated and uncarbamylated β^{pmb} chains on CM-52 cellulose, an initial column (5 x 20 cm) pH of 5.6 was found to be more satisfactory than the pH 5.85 used for HbS β chains (31,34). However, at this lower pH, a certain amount of the sample bound irreversibly to the top of the column, apparently due to precipitation. A substantially reduced yield (< 10%) of α^{NCO} chains suggested that the precipitation was selective for these chains. While not tried, an initial purification of the fully carbamylated tetramer $(\alpha_2^C\beta_2^C)$, followed by the usual chain separation, would perhaps prove more fruitful for HbA₀. This is the approach that was used successfully by Kilmartin et al. (35).

Alternatively, carbamylated alpha chains were prepared by prior separation of the chains, and subsequent reaction with potassium cyanate at pH 6.2 in 0.01 M phosphate buffer. Alpha chain concentration was 0.6 mM,

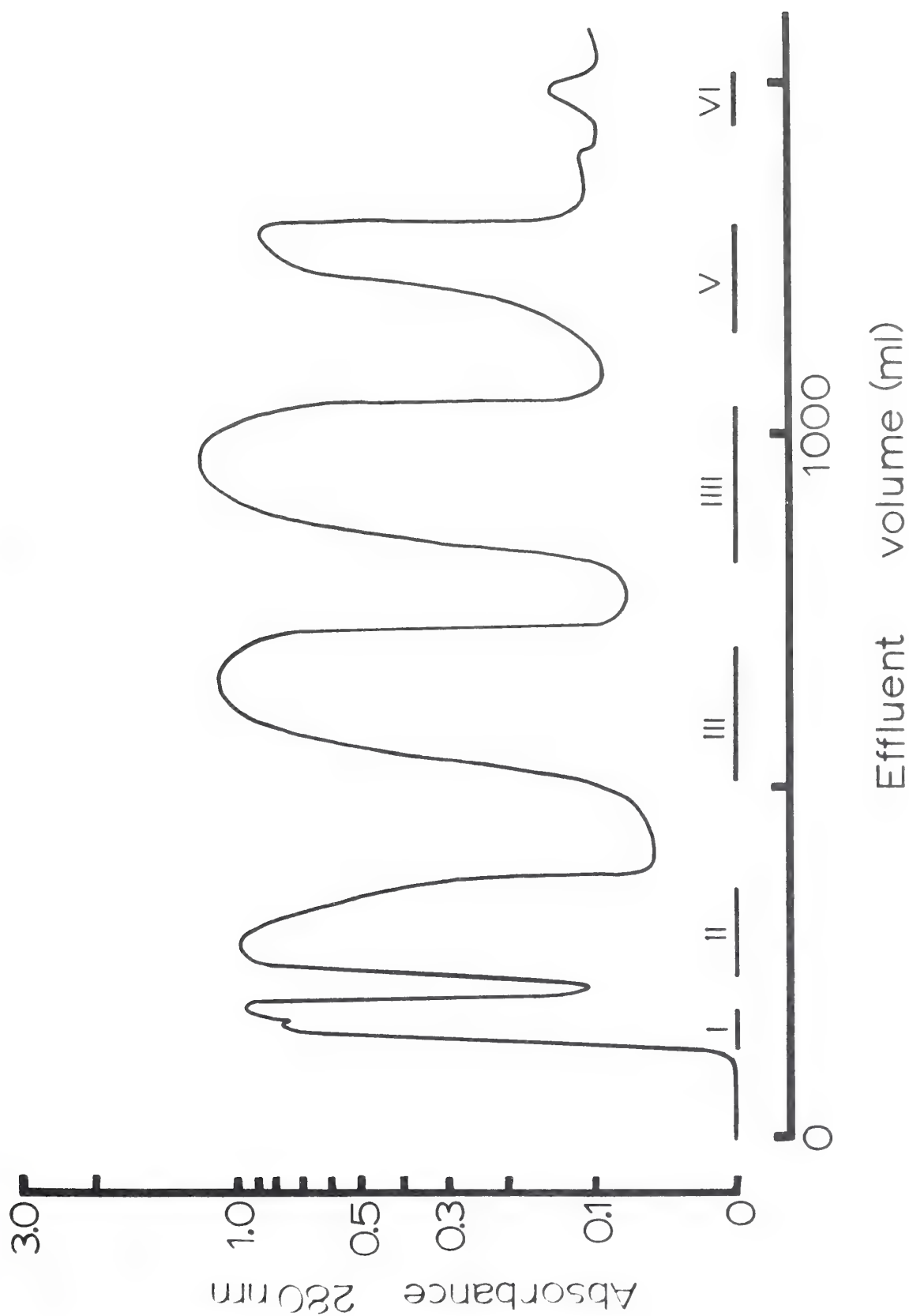
KNCO concentration was 1.0 mM. After 5.5 hours of reaction time at 23°, the reaction was stopped by gel filtration (G-25 Sephadex). The material was purified on a CM-52 cellulose column (5 x 25 cm) as shown in Figure 7. The gradient utilized was pH 6.7, 0.01 M phosphate buffer to 0.015M Na₂HPO₄. Based upon sequencer, electrophoretic, and amino acid analyses, fraction VI represents unreacted material; fraction V alpha chain carbamylated at the NH₂ terminal only; fractions IV to I alpha chains exhibiting multiple sites of carbamylation. Reactions for shorter periods of time with lower KNCO concentrations reduced the extent of multiple reactions.

Removal of Carbon Monoxide from Hemoglobin. Carboxyhemoglobin was readily converted to the oxy derivative by continuously passing scrubbed water-saturated oxygen over the solution. The temperature was kept near 0° with an ice bath; the surface area of the solution was increased and complete mixing assured by rotating it in a rotary-evaporator apparatus (Buchler). A 300 w. flood lamp provided the light necessary for photo-dissociation of carboxyhemoglobin (15). Complete removal, as indicated by a return of the 569 nm absorbance maximum (in CO Hb) to 576 nm, usually required 2 to 3 hours.

Preparation of Ferrihemoglobin. Ferrihemoglobin was prepared from purified oxyhemoglobin by the addition of a 20% molar excess of K₃Fe(CN)₆ at pH 6.3. This solution was allowed to react at room temperature for 3 hours. The excess ferricyanide and its reaction products were removed by exhaustive dialysis against 0.2 M NaCl at 4°.

2, 3- Diphosphoglyceric Acid Determinations. Analysis of the 2, 3-diphosphoglyceric acid (DPG) concentration in prepared stock solutions and protein samples was carried out by monitoring the change in absorbance of NADH due to enzymatic oxidation. This is related to the 2, 3-DPG concentration by the following series of reactions (36-39):

Figure 7. Chromatography of KNC0 treated α -chains on a 15 x 25 cm column of CM-52 cellulose at 4°. The linear gradient, not shown in the figure, was pH 6.7, 0.01 M phosphate to 0.015 M Na₂HPO₄. Equal quantities of each buffer were used, 800 ml. The nature of the components is described in the text.





This reaction is catalyzed by 2,3-DPG phosphatase; phosphoglycolic acid is a necessary cofactor.



The formation of 1,3-DPG is catalyzed by phosphoglycerate kinase.

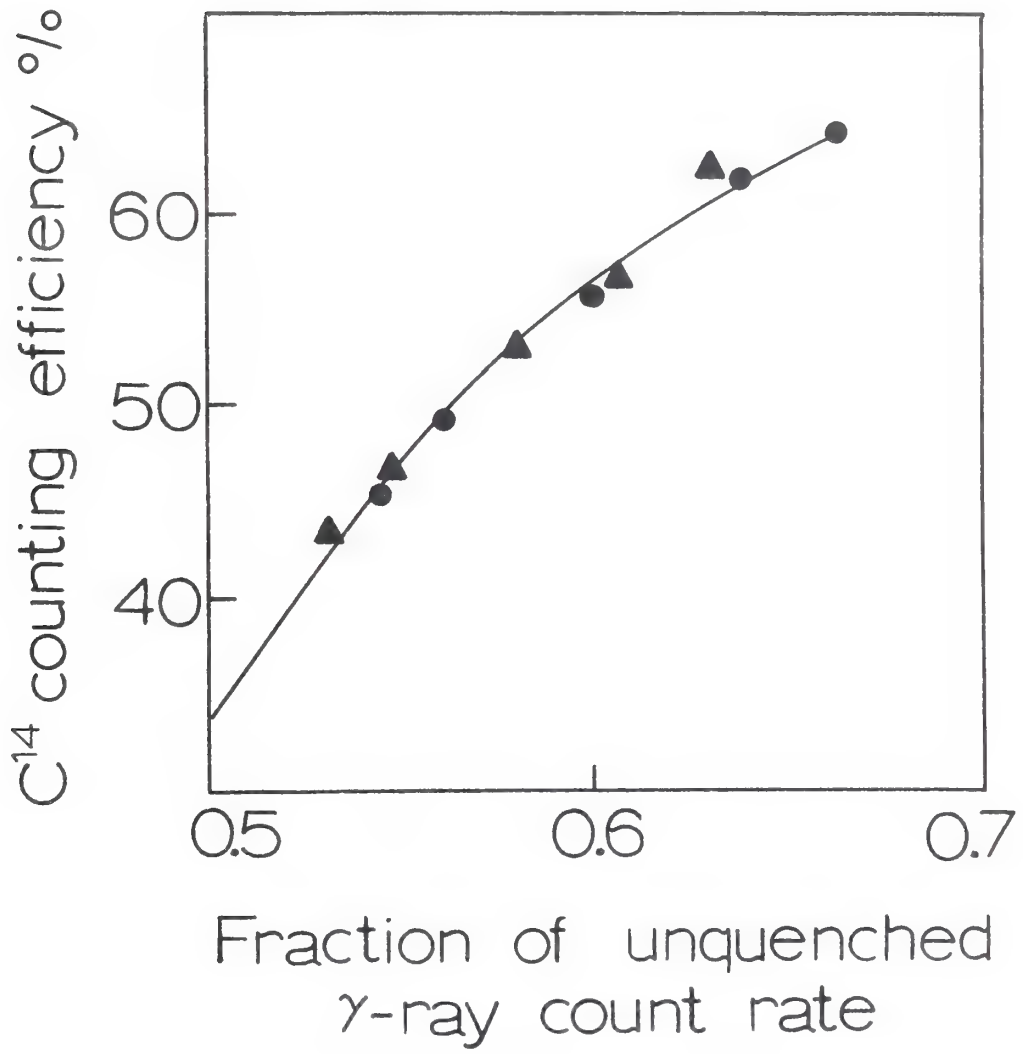


This reaction, catalyzed by glyceraldehyde phosphate dehydrogenase, converts NADH, with a millimolar extinction coefficient of 6.22 at 340 nm (40), to NAD^+ which is transparent at this wavelength.

All enzymes and chemicals were from Sigma. Complete instructions on the use of the assay are given in Sigma Technical Bulletin No. 35-UV.

Liquid Scintillation Counting. In many instances the location and extent of carbamylation was monitored by employing $[\text{}^{14}\text{C}]\text{-KNCO}$. The measurement of proteins so labeled was by means of liquid scintillation detection, utilizing Aquasol[®] as the scintillating agent. Samples were dissolved in 10 ml of fluor, and counted at room temperature in a Beckman LS-230 Liquid Scintillation System. The counting efficiency of the instrument was 95 to 97%, as determined with a Packard standard $[\text{}^{14}\text{C}]\text{-p}$ toluene sample emitting 45.5×10^3 DPM. Quenching errors were corrected by the external standard (^{157}Cs) technique (41,42). A correlation diagram (Figure 8) covering the range over which most protein samples were found to be quenched was determined with $[\text{}^{14}\text{C}]\text{-glycine}$ samples of known activity, obtained from New England Nuclear. Complete details on the use of this technique, as well as liquid scintillation counting in general, are available (42).

Figure 8. Correlation diagram of the relationship between the "External Standard Ratio" determined on the Beckman LS-230 liquid scintillation counter and the relative counting efficiency of the ^{14}C channel of this instrument. The \blacktriangle represents the results of a chemical quencher, citrate buffer, while the \bullet represents the results obtained with water, a dilutional quencher. The ^{14}C standard used for these determinations was a [^{14}C]-glycine sample of known dpm, obtained from New England Nuclear. In each case, 10 ml of fluor solution was used. See reference 42 for further details on the use of the external standard technique.



Bicarbonate-Carbonate Titration. With the exception of samples at pH values greater than 10.3, all solutions were made to contain a constant amount of total carbonates, 0.25 M, and were brought to constant molar ionic strength, 0.46 M, by the addition of NaCl. Above pH 10.3, the total carbonates were 0.20 M and the ionic strength was adjusted to 0.53 with NaCl. This change had little discernible effect on the computed fit of the titration curve (Chapter III). Atmospheric CO_2 was excluded, and water was degassed by boiling. Both pH and NMR measurements were made at 32 to 33° in the bicarbonate titration study. The Radiometer PHM 4c pH meter was standardized with U.S. National Bureau of Standards "Standard Reference Material 187b", sodium tetraborate decahydrate. Approximately 2% (v/v) of dioxane was introduced as an NMR reference.

Sample Preparation for ^{13}C NMR. Amino acid and peptide samples were confirmed by amino acid analysis and the NMR observations themselves. Samples were generally prepared by first dissolving the necessary quantity of the material of interest in water, along with a small amount of dioxane, and then adding the requisite amounts of dry NaHCO_3 and Na_2CO_3 to achieve a desired pH. Adjustment of pH, if necessary, was done by additions of fresh 5N NaOH or constant boiling HCl. The sample solutions were sealed as soon as possible after preparation, and allowed to equilibrate at least two hours at room temperature before the NMR measurements were conducted. Final pH measurements were made immediately after opening the sealed tubes at the end of the NMR runs. In many cases, total carbonates were checked gasometrically. When D_2O was used, pD was defined as the pH meter reading + 0.40 (43). When isotopic enrichment of the

carbamino adduct was desired the sample solutions were equilibrated with $\text{NaH}^{13}\text{CO}_3$ and $\text{Na}_2^{13}\text{CO}_3$, and sealed under the proper pressures of $^{13}\text{CO}_2$, as shown in Table II. To facilitate the handling of the isotopically enriched samples, as well as deoxygenated hemoglobin samples, specially designed NMR tubes were built, as shown in Figure 9. The Wilmad NMR tube was 13 mm OD for use in the DP-60 instrument, or 12 mm OD for the XL-100 instrument (see below). Joined to the top of each tube was a 14/20 ♀ female ground glass joint, modified with a slight bubble extending approximately 6 mm up the joint on one side. Complementing this was a 14/35 male joint, sealed at the bottom, with a small (1mm) hole positioned so that it could just barely reach the bubble of the female joint. By rotating the top joint, the NMR tube could then be sealed. To the open end of the male joint was fused a Fisher-Porter (solvaseal) 14 mm coupling, which facilitated attachment of the tube to a tonometer. This design admirably fulfilled the requirements of a lightweight, symmetrical, compact, and effective seal, which could be spun at velocities up to 20 cps without chatter. The vortex suppressor plugs likewise were modified to allow the transfer of solution through to the bottom of the tube under reduced pressure. As seen in Figure 9, the plugs were constructed of teflon with a 1/4 inch hole down the center. The sharp lip left at the bottom of the plug proved adequate to retard vortexing at normal spin rates. The reservoir from which these tubes were filled consisted of a Keyes, Mizukami and Lumry tonometer (44), modified with a sidearm and valve such that anaerobic transfer could be made to the NMR tubes (Figure 8). The typical procedure for the preparation of a series of deoxyhemoglobin samples at varying pH values was as follows:

Table IIA
FC92 PRESSURES AT VARIOUS TOTAL CARBONATES

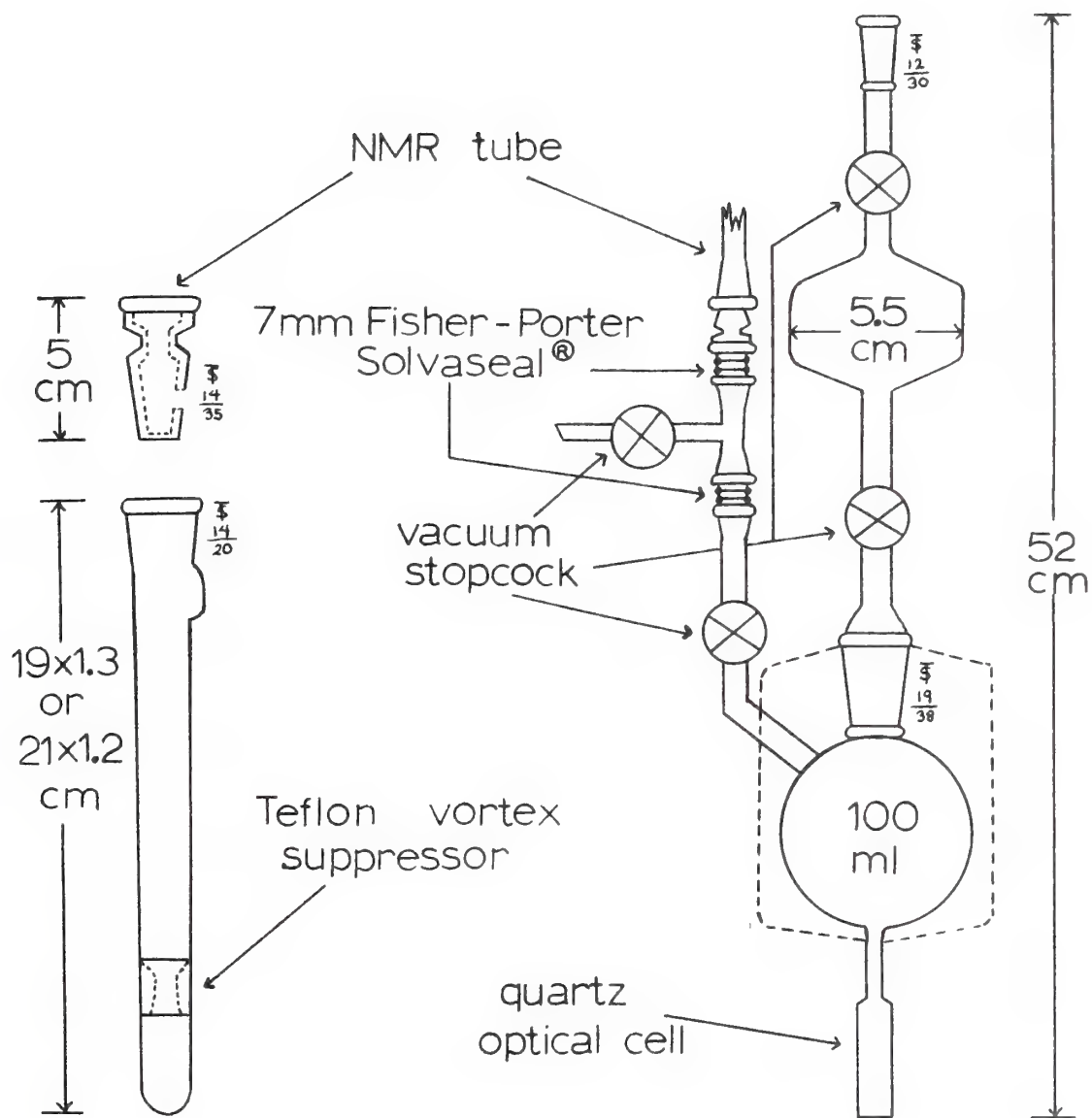
PM	10	20	30	40	50	60	70	80	90	100	110	120	130
6.6000	19.8	29.6	39.4	49.1	58.9	68.7	78.5	88.3	98.1	107.9	127.6	137.4	147.2
6.6000	17.4	27.2	37.0	46.8	56.6	66.4	76.2	86.0	95.8	105.6	125.4	135.2	145.0
6.7000	18.5	28.3	38.1	47.9	57.7	67.5	77.3	87.1	96.9	106.7	126.5	136.3	146.1
6.8000	19.0	28.8	38.6	48.4	58.2	68.0	77.8	87.6	97.4	107.2	127.0	136.8	146.6
6.9000	19.5	29.3	39.1	48.9	58.7	68.5	78.3	88.1	97.9	107.7	127.5	137.3	147.1
7.0000	20.0	29.8	39.6	49.4	59.2	69.0	78.8	88.6	98.4	108.2	128.0	137.8	147.6
7.1000	20.5	30.3	40.1	49.9	59.7	69.5	79.3	89.1	98.9	108.7	128.5	138.3	148.1
7.2000	21.0	30.8	40.6	50.4	60.2	70.0	79.8	89.6	99.4	109.2	129.0	138.8	148.6
7.3000	21.5	31.3	41.1	50.9	60.7	70.5	80.3	90.1	99.9	109.7	129.5	139.3	149.1
7.4000	22.0	31.8	41.6	51.4	61.2	71.0	80.8	90.6	100.4	110.2	130.0	139.8	149.6
7.5000	22.5	32.3	42.1	51.9	61.7	71.5	81.3	91.1	100.9	110.7	130.5	140.3	150.1
7.6000	23.0	32.8	42.6	52.4	62.2	72.0	81.8	91.6	101.4	111.2	131.0	140.8	150.6
7.7000	23.5	33.3	43.1	52.9	62.7	72.5	82.3	92.1	101.9	111.7	131.5	141.3	151.1
7.8000	24.0	33.8	43.6	53.4	63.2	73.0	82.8	92.6	102.4	112.2	132.0	141.8	151.6
7.9000	24.5	34.3	44.1	53.9	63.7	73.5	83.3	93.1	102.9	112.7	132.5	142.3	152.1
8.0000	25.0	34.8	44.6	54.4	64.2	74.0	83.8	93.6	103.4	113.2	133.0	142.8	152.6
8.1000	25.5	35.3	45.1	54.9	64.7	74.5	84.3	94.1	103.9	113.7	133.5	143.3	153.1
8.2000	26.0	35.8	45.6	55.4	65.2	75.0	84.8	94.6	104.4	114.2	134.0	143.8	153.6
8.3000	26.5	36.3	46.1	55.9	65.7	75.5	85.3	95.1	104.9	114.7	134.5	144.3	154.1
8.4000	27.0	36.8	46.6	56.4	66.2	76.0	85.8	95.6	105.4	115.2	135.0	144.8	154.6
8.5000	27.5	37.3	47.1	56.9	66.7	76.5	86.3	96.1	105.9	115.7	135.5	145.3	155.1
8.6000	28.0	37.8	47.6	57.4	67.2	77.0	86.8	96.6	106.4	116.2	136.0	145.8	155.6
8.7000	28.5	38.3	48.1	57.9	67.7	77.5	87.3	97.1	106.9	116.7	136.5	146.3	156.1
8.8000	29.0	38.8	48.6	58.4	68.2	78.0	87.8	97.6	107.4	117.2	137.0	146.8	156.6
8.9000	29.5	39.3	49.1	58.9	68.7	78.5	88.3	98.1	107.9	117.9	137.5	147.3	157.1

Table IIB
PC32 PRESSURES AT VARIOUS TOTAL CARBONATES

PM	140. MM	150. MM	160. MM	170. MM	180. MM	190. MM	200. MM	210. MM	220. MM	230. MM	240. MM	250. MM	260. MM
6.5000	1537.0	1646.8	1756.4	1866.4	1976.1	2085.9	2195.7	2305.5	2415.3	2525.1	2634.9	2744.7	2854.4
6.6000	1222.7	1327.9	1435.1	1482.3	1592.5	1656.7	1743.9	1831.1	1918.3	2005.5	2092.6	2179.8	2267.0
6.7000	969.5	1038.7	1108.0	1177.2	1246.5	1315.7	1385.0	1454.2	1523.4	1592.7	1661.9	1731.2	1800.4
6.8000	763.9	824.9	879.9	934.9	989.9	1044.9	1099.9	1154.9	1209.9	1264.9	1319.9	1374.8	1429.8
6.9000	611.4	655.1	698.7	742.4	786.1	829.8	873.4	917.1	960.8	1004.5	1048.1	1091.8	1135.5
7.0000	485.5	520.2	554.9	589.5	624.2	658.9	693.6	728.3	762.9	797.6	832.3	867.0	901.7
7.1000	385.5	413.0	440.6	468.1	495.7	523.2	550.7	578.3	605.8	633.3	660.9	688.4	715.9
7.2000	306.1	327.9	349.8	371.7	393.5	415.4	437.3	459.1	481.0	502.8	524.7	546.6	568.4
7.3000	243.0	260.3	277.7	295.1	312.4	329.8	347.1	364.5	381.8	399.2	416.5	433.9	451.3
7.4000	192.9	206.6	220.4	234.2	248.0	261.8	275.5	289.3	303.1	316.9	330.6	344.4	358.2
7.5000	153.1	164.0	174.9	185.9	196.8	207.7	218.7	229.6	240.5	251.5	262.4	273.3	284.3
7.6000	121.4	130.1	138.8	147.5	156.1	164.8	173.5	182.2	190.8	199.5	208.2	216.9	225.5
7.7000	96.3	103.2	110.1	117.0	123.9	130.7	137.6	144.5	151.4	158.3	165.1	172.0	178.9
7.8000	76.4	81.8	87.3	92.8	98.2	103.7	109.1	114.6	120.0	125.5	131.0	136.4	141.9
7.9000	60.5	64.9	69.2	73.5	77.8	82.2	86.5	90.8	95.1	99.5	103.8	108.1	112.4
8.0000	48.0	51.4	54.8	58.2	61.7	65.1	68.5	71.9	75.4	78.8	82.2	85.6	89.1
8.1000	38.0	40.7	43.4	46.1	48.8	51.5	54.2	57.0	59.7	62.4	65.1	67.8	70.5
8.2000	30.0	32.2	34.3	36.5	38.6	40.8	42.9	45.0	47.2	49.3	51.5	53.6	55.8
8.3000	23.7	25.4	27.1	28.8	30.5	32.2	33.9	35.6	37.3	39.0	40.7	42.4	44.1
8.4000	18.7	20.1	21.4	22.7	24.1	25.4	26.7	28.1	29.4	30.8	32.1	33.4	34.8
8.5000	14.7	15.8	16.9	17.9	19.0	20.0	21.1	22.1	23.2	24.2	25.3	26.3	27.4
8.6000	11.6	12.4	13.3	14.1	14.9	15.7	16.6	17.4	18.2	19.0	19.9	20.7	21.5
8.7000	9.1	9.7	10.4	11.0	11.7	12.3	13.0	13.6	14.3	14.9	15.6	16.2	16.9
8.8000	7.1	7.6	8.1	8.6	9.1	9.6	10.2	10.7	11.2	11.7	12.2	12.7	13.2
8.9000	5.5	5.9	6.3	6.7	7.1	7.5	7.9	8.3	8.7	9.1	9.5	9.9	10.3

ET-005.40

Figure 9. The pyrex portion of the apparatus used to deoxygenate the protein samples, and subsequently transfer them anaerobically to the sealable NMR tube. The design of the tonometer is basically that of Keyes, Mizukami, and Lumry (44), with the modifications shown. The partially bored stopcock characteristic of the Keyes et al. design, was dispensed with for most experiments, since only totally deoxygenated hemoglobin was desired. The extent of oxygenation could be monitored with the quartz (or pyrex) optical cell. For the NMR measurements, the necessary protein concentration (78 mM) dictated a 1 mm path length cell. The removable "T" on the sidearm is not essential, but facilitates the cleaning of the apparatus between transfers. See text for details on the use of this apparatus.



- 1) After complete deoxygenation, as measured by the A^{670}/A^{730} ratio, 400-600 mm Hg of scrubbed, oxygen free N_2 (prepurified, Matheson) was placed over the solution and into the reservoir bulb.
- 2) A NMR tube with vortex plug in place was attached to the side-arm with the "T" connector, (Figure 8). Already present as a dry powder in the tube was $NaH^{13}CO_3$ and $Na_2^{13}CO_3$, in the proper ratio and amount to achieve the desired carbonate concentration and pH (Table III). These quantities were generally calculated on the basis of a total sample volume of 1.8 to 2.0 ml.
- 3) The tube and connecting pieces were evacuated to a pressure of no more than 50 microns, then filled with the desired $p^{13}CO_2$ (Table II) plus about 20%. The valve of the NMR tube and the connector valve were then closed.
- 4) After removal from the vacuum line, the tonometer with tube attached was tilted so as to fill the sidearm. Approximately 2 ml of hemoglobin solution was bled through to the connector by briefly opening the sidearm valve.
- 5) The transfer was completed by opening the valve atop the NMR tube, thereby allowing the pressure differential to force the solution into the tube.
- 6) After assuring that both the NMR tube valve and the sidearm valve were closed, the NMR tube was removed and vortexed gently to dissolve the carbonates.

Dioxane, 2,3-DPG and IHP, when used, were generally incorporated into the hemoglobin solution within the tonometer.

Table III

Composition of Aqueous Solutions at
Different Total Carbonates and pH Values

The columns beneath " CO_3 " and " HCO_3 " denote the equilibrium millimolar concentration of CO_3^- and HCO_3^- of different pH values for each level of total carbonates. The difference between the sum of the CO_3^- and HCO_3^- values, and the total listed at top of the table, represents the dissolved CO_2 . To determine the pCO_2 over these solutions, consult Table II. The last three columns indicate the approximate charge per heme of hemoglobin at each respective pH. To achieve a given pH with isoelectric hemoglobin, readjust the CO_3^- and HCO_3^- concentrations to account for the number of equivalents of added hemoglobin, then place the pCO_2 indicated in Table II over the solution.

Table III

	CAR3 = 20.0 MM	CAR3 = 30.0 MM	CAR3 = 40.0 MM	CAR3 = 50.0 MM	CAR3 = 60.0 MM	
W	CW	CW	CW	CW	CW	HB HB02 HB+
6.500	.012 13.557	.013 20.012	.004 28.259	.004 35.857	.005 43.680	.08 .5 .6
6.600	.013 14.546	.014 20.285	.005 30.177	.006 38.203	.007 46.338	.05 .2 .3
6.700	.013 15.442	.015 20.585	.006 31.858	.008 40.246	.009 48.728	.02 .01 .01
6.800	.015 16.243	.007 24.708	.008 33.302	.010 41.994	.012 50.765	.00 .04 .05
6.900	.016 16.812	.018 25.655	.011 34.525	.013 43.468	.015 52.476	.03 .07 .08
7.000	.008 17.477	.011 26.467	.014 35.547	.017 44.695	.020 53.897	.05 -1.0 -1.2
7.100	.010 17.948	.014 27.133	.018 36.392	.022 45.707	.025 55.066	.08 -1.3 -1.5
7.200	.013 18.336	.018 27.680	.023 37.084	.028 46.534	.032 56.020	.11 -1.6 -1.9
7.300	.016 18.654	.023 28.126	.029 37.647	.035 47.205	.041 56.792	.14 -1.9 -2.2
7.400	.021 18.911	.028 28.486	.037 38.100	.045 47.744	.052 57.412	.17 -2.2 -2.6
7.500	.024 19.118	.031 28.774	.047 38.463	.057 48.176	.066 57.908	.20 -2.5 -2.9
7.600	.033 19.282	.047 29.003	.060 38.750	.072 48.517	.084 58.300	.23 -2.7 -3.2
7.700	.042 19.412	.060 29.183	.074 38.975	.091 48.784	.106 58.606	.25 -3.0 -3.6
7.800	.053 19.511	.075 29.321	.096 39.148	.115 48.989	.133 58.841	.28 -3.2 -3.8
7.900	.067 19.586	.094 29.424	.121 39.278	.145 49.142	.168 59.016	.30 -3.4 -4.1
8.000	.085 19.639	.120 29.498	.152 39.369	.183 49.250	.212 59.139	.33 -3.6 -4.3
8.100	.107 19.674	.151 29.545	.192 39.428	.230 49.320	.267 59.218	.35 -3.8 -4.5
8.200	.134 19.691	.180 29.569	.241 39.457	.290 49.353	.336 59.255	.37 -3.9 -4.6
8.300	.169 19.693	.230 29.570	.304 39.457	.365 49.352	.422 59.253	.39 -4.1 -4.9
8.400	.212 19.678	.305 29.548	.382 39.429	.458 49.317	.531 59.212	.41 -4.2 -5.1
8.500	.267 19.647	.377 29.503	.479 39.371	.575 49.247	.666 59.130	.42 -4.4 -5.3
8.600	.334 19.597	.473 29.433	.601 39.281	.721 49.138	.835 59.004	.43 -4.4 -5.4
8.700	.419 19.527	.592 29.333	.752 39.154	.903 48.986	1.046 58.827	.43 -4.5 -5.5
8.800	.524 19.434	.740 29.201	.941 38.986	1.129 48.783	1.309 58.591	.46 -4.7 -5.6
8.900	.653 19.313	.923 29.030	1.174 38.768	1.410 48.521	1.634 58.287	.49 -5.6 -5.9

.002.27

After the NMR measurement, each protein sample was analyzed for pH, total carbonate concentration, heme concentration, the extent of its oxidation, and in many instances the degree of ^{13}C enrichment.

These latter measurements were not made in all cases, since withdrawal of a portion of the gas phase for the mass spectrometer perturbed the pH, and the results of over 30 such samples so measured indicated that the expected maximal [^{13}C] abundance was $88 \pm 1\%$, where the error represents two standard deviations.

^{13}C Fourier Transform NMR Measurements. Measurements at 15.075 MHz were made on a Varian high resolution DP-60 NMR spectrometer modified for Fourier transform (FT) operation (45,46). Signal averaging was accomplished with a Fabri-Tek 1074 instrument computer while data processing required an on-line PDP-8/I computer supplied by Digital Equipment Corporation. Also included in the apparatus was an external ^{19}F lock and noise-modulated proton decoupling equipment sufficiently powerful to decouple all protons. A pulse width of 90° was routinely used, requiring 21 μsec . In some instances, it was advantageous to use lesser pulse widths at increased recycle rates (46). For relaxation time measurements, a $180-\tau-90$ degree pulse sequence was employed (47). Acquisition time was 0.542 sec. for a spectral width of 250 ppm (3768.8 Hz). After Fourier transformation of the 4095 word free induction decay (FID) signal, the real portion of the frequency domain utilized 2048 channels, yielding a digital resolution of 0.12 ppm for a 250 ppm window. The digital resolution was appropriately improved at lesser spectral widths.

Programs for the Fourier transform were supplied by Fabri-Tek and Digital; these consisted of the DEC-08-LBAA-PM binary loader and

the FTII 70/8-7002-B Fourier transform. In addition overlays were appended to provide an apodization correction, baseline correction, and digital filtering. These latter two options are available as an "Exponential Filter Patch" package from Robert E. Addleman, Indiana University. Peak positions were determined from their respective channel locations, as determined by manual interrogation of the memory with the 1074. A more complete description of this instrument is in the literature (45,48,49).

Spectral measurements at 25.196 MHz were made on a standard Varian XL-100 spectrophotometer equipped with the external ^{19}F lock accessory. Initial measurements with this instrument utilized the Varian 620/I computer for data aquisition and processing. Later measurements and data processing were performed with the aid of a TTI-100 Fourier transform accessory employing a Nicolet 1089 20 bit, 36 K (32K for data accumulation) instrument computer interfaced with an on-line random access disk unit (Diablo). This allowed the storage of the free induction decay signals for later or repeated processing, as well as providing a large library of specialized programs which could be loaded at will.

The program found most useful, and by which almost all of the data processing was done, was "FTMOD3". This is an extensively modified version of the Nicolet FTNMR/1972 program NIC-80/S-7202D, modified by Dr. Robert A. Craig, and kindly provided for this study by Dr. Adam Allerhand. FTMOD3 is the original FTNMR program, updated with patch "MOD2" (NUS-80/U-7328), and to which the additional "in house" options of "BA" (Baseline Adjust) and "SS" (Spectrum Shift) have been incorporated. These latter two options operate as a patch which is swapped in from the

disk prior to execution, and is returned afterwards. Their application is detailed more completely below.

After the processing of the data in the 1089, many of the spectra were punched on binary paper tape using a high speed punch (Remex) so that further evaluation and line-shape analysis could be done using a Control Data Corporation 6600 series computer.

The general procedure for recording spectra on either machine was to adjust the magnet homogeneity prior to each run by maximizing the amplitude while minimizing the decay of the free induction signal of ethylene glycol. The carrier frequency of the pulse was generally set to 2260 Hz or 3268.7 Hz above the Larmor frequency of ethylene glycol, for the 15.1 and 25.2 MHz instruments respectively. This corresponds to a -20.16 ppm offset relative to external CS_2 for the DP-60 instrument, and 0.0 ppm from external CS_2 for the XL-100. All peptide, amino acid, and some protein samples included 0.1 to 2% (v/v) dioxane as an internal reference marking 126.20 ppm relative to external CS_2 . Positive and negative chemical shift differences refer to the upfield and downfield directions, respectively. These values may be converted to the internal TMS scale by subtracting them from 193.6 ppm. Recycle times, especially in situations where the integral areas were important, were usually not less than three times the longest T_1 value for the peaks of interest. Most measurements were made in the range of 29.5 to 35.5° for both instruments, with individual cases specified in the text or legends.

Measurements of nuclear Overhauser enhancement (NOE)¹ factors (Chapters III and IV) were made by comparing the integrated areas of each resonance peak under conditions of complete proton decoupling with analogous areas obtained in the absence of proton decoupling. The

latter spectra were recorded by offsetting the proton-decoupling frequency 50 KHz at 15.1 MHz and 75 KHz at 25.2 MHz off-resonance without noise modulation (50,51). Most protein spectra for which the carboxyl resonance integrals were to be measured were also run in the uncoupled mode (see below).

¹H NMR Measurements. Measurements were made in D₂O at 220 MHz on the Varian HR 200 instrument, operating in the field sweep mode. In some cases, measurements were made in collaboration with Dr. Philip Keim at the University of Chicago. These measurements were made by him on a Bruker HX-270 instrument, operating at 270 MHz. Spectral width was usually 1000 Hz. Temperature was maintained at 30 or 37° with the Varian temperature controller, and 5 mm OD sample tubes were employed. Chemical shifts (δ) are referenced to internal sodium 2, 2-dimethyl-2-silapentane-t-sulfonate (DSS)¹.

Resonance Peak Area Integration. The reproducible integration of ¹³C resonance peak areas has proven to be an exceedingly difficult and not completely solved problem. Quite aside from the question of spectrometer stability, the potential sources of error are manifold. If a resonance line becomes too narrow, it may be insufficiently represented digitally. In the limit, sampling theory will predict the minimum number of spectral points necessary to define a frequency (52); no such theory applies to the integral. Accurate integration demands a precise knowledge of the baseline position. Most protein spectra, however, contain a sizeable component of noise making exact baseline estimation impossible. Resonance peaks of greater than minimum width, while sufficiently represented digitally, often suffer from artificial

baseline irregularities and severe overlap with neighboring resonances, both of which contribute substantially to the integral uncertainty. Furthermore, the resonance integral itself, no matter what its accuracy, need not be linearly related to the population of the species from which it originated. Under conditions of proton decoupling, as routinely employed in ^{13}C NMR, a given resonance area may exhibit up to a three fold enhancement (53) due to the Nuclear Overhauser effect. If the pulse repetition rate is too high, a given resonance may lose area to saturation. If [^{13}C] isotopically enriched compounds are used, uncertainties in the enrichment level further cloud the extrapolation from resonance area to species abundance. Thus, the integration of the carbamino resonances demanded that several precautions be observed. The available computer memory, coupled with a minimum width of the carbamino resonance of at least 5 Hz assured that each resonance peak encompassed at least 30 data channels, and usually many more. This 30 channel minimum for each peak was considered adequate for integration purposes. Moreover, usually only information concerning the mole fraction of carbamino formed was desired. Thus, the problem of instrumental instability between spectra was minimized, the integral of the carbamino being compared with the integral of all of the protein carboxyls in the same spectrum. By recording the spectra undecoupled, and at recycle times satisfying the $3T_1$ criterion, uncertainties in the relationship of the integral to the abundance of the contributing species were minimized. Unfortunately, fulfilling the $3T_1$ criterion required recycle times of 3.0 sec. at 15.1 MHz, and 3.5 sec. at 25.2 MHz. Thus, the accumulation of 16K transients on the XL-100 required nearly 16 hours for each spectrum. The baseline and spectral overlap problems were not so readily solved. Integration

by the programs available for the Nicolet 1080 is performed by simply summing the intensities of each data channel over the region of interest. Tangential baselines cannot be adequately handled. If the mean baseline noise is not zero, the integral for a given region will be incorrect by a constant, but unknown, amount. A partial solution to this problem was available in FTMOD3. The baseline correction option "BA" (as previously described), allows the operator to select up to 9 points throughout the spectrum which are to be moved to zero intensity. The distance from baseline of a straight line connecting each of the 9 points determines the correction that is applied to the spectrum itself at each channel. With judicious use, "BA" can flatten tangential baselines and minimize the ambiguity of the positioning of the apparent baseline with respect to true "computer zero". Problems with peak overlap also arose, particularly with the tail or spinning-sideband of the large bicarbonate peak present in most spectra. To minimize the spinning-sideband problem, optimum magnetic field homogeneity was required, and the samples were seldom spun at rates greater than 12 cps. The general procedure followed for the integration of a typical carbamino-hemoglobin spectra on the XL-100 with FTMOD3 was:

- 1) Transform free induction decay, following digital filtering with a time constant of -5 sec. for a 16K accumulation and 5050 Hz spectral width. Acquisition time (AT) under these conditions was 1.62 sec.; thus a -5 sec. exponential filter produces $5/\pi \cdot AT$ or 0.98 Hz line broadening (46).
- 2) Phase correct transformed spectrum accurately.
- 3) Use "BA" to flatten and bring overall baseline to center. The "AC" option available in FTMOD3, whereby the operator may manually adjust the spectrum up or down should never be used.

Proper placement of the baseline about true (computer) zero using "AC", demands that the center of the CRT correspond exactly to (computer) zero. In practice, this condition was seldom found to hold.

- 4) "BA" may then be repeated, if necessary, to remove traces of the tail of the bicarbonate resonance in the carbamino region. This limited form of curve resolving was avoided in most cases, since the exact shape of the bicarbonate tail in this region was seldom apparent, and its contribution to the area probably minimal.
- 5) The entire carboxyl resonance region of the protein was integrated by defining the limits of the region with computer options "F1" and "F2", and then using "IR-I" to return a digital sum of the area of this region. This region typically included the area from 10 to 26 ppm.
- 6) The region from 24 to 34 ppm was integrated using the "IR-L" command, with a peak intensity threshold value of 200. The result was a listing of the positions of the peaks recognized as such by the computer, their areas, and the limits of the integration. A typical output appears below.

```

IP
THRESHOLD = 200
1164 - 717.6254 - 28.4811 PPM 1057 > 1182 1.7767215 4943
1193 - 735.5044 - 29.1907 PPM 1183 > 1204 1.2748605 11800
1221 - 752.7668 - 29.8758 PPM 1205 > 1255 2.1667715 15031
1230 - 819.9672 - 32.5429 PPM 1250 > 1375 2.1045836 176700
1383 - 852.6425 - 33.8397 PPM 1370 > 1406 2.7920014 1390

```


- 7) The computer's choice of integration limits was checked by visual examination. If other choices seemed more reasonable, these were integrated with the "F1", "F2", and "IR-I" options. Any peaks not recognized as such by the computer would also be integrated in this manner and their position noted.

Other integration methods were also tried. The regions of interest were evaluated from the recorded spectra by manual tracing (planimetry) using a Technicon[®] model AAG Integrator/calculator. In each case, the mean of three or more tracings was used as the best estimate. Alternatively, the resonance peak areas were compared by cutting out and weighing the peaks of interest from a Xerox copy. A comparison of these methods, as applied to NMR spectra typical of those obtained in this study, is shown in Table IV.

While the foregoing methods served adequately when the resonances of interest were well resolved as at high pH, at lower pH values chemical exchange effects resulted in severe broadening and overlap (Chapter IV). A general solution to the integration and derivation of site populations for such situations was developed as program NMRFIT3 (Appendix C). Basically, this consists of a series of Fortran routines which will fit by the criterion of least squares, selected regions of the actual experimental spectrum to expected theoretical lineshapes and positions. The parameters returned are the relative site populations and exchange rates. Integration of the experimentally determined protein carboxyl region is also performed, and when compared with the integral area of the fitted spectrum and the relative site populations, yields estimates of the mole fraction (Z) of each binding site which is reacted with CO_2 . Details on the use of this program, as well as program CONVERT,

Table IV

Precision of NMR Spectral Integration
Comparison of Methods for Determination of Z

Spectra number XL196 and XL198 were integrated repeatedly by different methods. In the "cut and weigh" and "planimetry" methods, a single spectrum was repeatedly integrated. For the digital integration, performed as described in the text with the Nicolet 1089 computer, the same free induction decay was repeatedly processed and then integrated. The larger apparent standard deviation (σ) of the latter measurements reflects contributions from a larger number of variables, and is more representative of the true integral uncertainty. The σ of the other methods reflects primarily the precision of the integration method itself, apart from errors introduced in the transformation process. Z is the mole fraction carbamate per $\alpha\beta$ dimer, defined as:

$$Z \propto \frac{\text{Area carbamate resonance}}{\text{Area Protein carbonyl resonances}} \cdot \text{constant.}$$

Spectrum No. and Carbamate Resonance Position	INTEGRATION METHOD								
	Cut and Weigh			Planimetry			Digital		
	Avg. Z.	σ	No. of Meas.	Avg. Z	σ	No. of Meas.	Avg. Z	σ	No. of Meas.
XL196 29.8 ppm	0.641	0.029	4	0.648	0.009	4	0.738	0.061	3
29.2 ppm	0.492	0.013	5	0.505	0.007	4	0.582	0.048	3
28.4 ppm	0.259	0.006	5	0.267	0.007	4	0.288	0.025	3
XL198 29.8 ppm	0.652	0.019	5	0.709	0.014	4	0.729	0.062	3
29.2 ppm	0.501	0.013	5	0.522	0.006	4	0.504	0.023	3
28.4 ppm	0.262	0.016	5	0.264	0.004	4	0.264	0.045	3

are in Appendix C. CONVERT, kindly supplied by Mr. Chris Hasenkampf, converts the paper tape output from the Nicolet 1080 to decimal integers on cards.

Integration of resonance peak areas on the DP-60 instrument was carried out by utilizing the hard-wired integration feature of the 1074. The intensity of the line integral so obtained was interrogated digitally, having visually chosen the channel limits of each peak. Strictly tangential baselines could be corrected by adding a complementary line using the "additive transfer" feature; correction of the more complex problems of baseline roll or variable slope were hampered by the vastly more limited computing options on this instrument when compared to the TTI-100 system. Thus, the manual methods of integration described above assumed greater importance when analyzing data obtained with this instrument.

REFERENCES

1. Sadtler Index Standard Spectra (1967) Sadtler Research Laboratories, Philadelphia, nos. 5718 and 8106
2. Boyer, P. D. (1954) J. Amer. Chem. Soc. 76, 4331-4337
3. Edman, P. (1970) in Protein Sequence Determination, S. B. Needleman, ed., Springer-Verlag, Berlin, Chap. 8
4. Keim, P., Vigna, R. A., Marshall, R.C. and Gurd, F. R. N. (1973) J. Biol. Chem. 248, 6104-6113
5. Keim, P., Vigna, R. A., Morrow, J. S., Marshall, R. C. and Gurd, F. R. N. (1973) J. Biol. Chem. 248, 7811-7818
6. Keim, P., Vigna, R. A., Nigen, A. M., Morrow, J. S. and Gurd, F. R. N. (1974) J. Biol. Chem., in press
7. Van Slyke, D. D. and Neill, J. M. (1924) J. Biol. Chem. 61, 523-573
8. Van Slyke, D. D. and Sendroy, J. (1927) J. Biol. Chem. 73, 127-144
9. Holaday, D. A. and Veresky, M. (1956) J. Lab. Clin. Med. 47, 634-644
10. Rosemeyer, M. A. and Huehns, E. R. (1967) J. Mol. Biol. 25, 253-273
11. Nakhleh, E. T. (1971) Ph.D. Thesis, American University of Beirut, Beirut, Lebanon
12. Huisman, J. H. J. and Dozy, A. M. (1965) J. Chromotog. 19, 160-169
13. Benesch, R., MacDuff, G. and Benesch, R. E. (1965) Anal. Biochem. 11, 81-87
14. Kilmartin, J. V. and Rossi-Bernardi, L. (1971) Biochem J. 124, 31-45
15. Antonini, E. and Brunori, M. (1971) Hemoglobin and Myoglobin in Their Reactions with Ligands, North Holland Publishing Co., Amsterdam
16. Spackman, D. H., Stein, W. H. and Moore, S. (1958) Anal. Chem. 30, 1190-1206

17. Teale, F. W. J. (1959) *Biochem. Biophys. Acta* 35, 543
18. Rossi-Fanelli, A., Antonini, E. and Caputo, A. (1958) *Biochem. Biophys. Acta* 30, 608-615
19. Hartzell, C. R., Bradshaw, R. A., Hapner, K. D. and Gurd, F. R. N. (1968) *J. Biol. Chem.* 243, 690-696
20. Dozy, A. M., Kleihauer, E. F. and Huisman, T. H. J. (1968) *J. Chromatog.* 32, 723-727
21. Wilbur, K. M. and Anderson, N. G. (1948) *J. Biol. Chem.* 176, 147-154
22. Matsuda, G. and Takei, H. (1963) *J. Biochem. (Tokyo)* 54, 156-160
23. Rifkin, J. M. (1974) *Biochem.* 13, 2475-2481
24. King, N. K. and Winfield, M. E. (1963) *J. Biol. Chem.* 238, 1520-1528
25. Dixon, H. B. F. and McIntosh, R. (1967) *Nature* 213, 399-400
26. Asakura, T., Tamura, M. and Shin, M. (1972) *J. Biol. Chem.* 247, 3693-3701
27. Bucci, E. and Fronticelli, C. (1965) *J. Biol. Chem.* 240, PC551-552
28. Rosemeyer, M. A. and Huehns, E. R. (1967) *J. Mol Biol.* 25, 253-273
29. Bucci, E., Fronticelli, C., Cliaucone, E., Wyman, J., Antonnini, E. and Rossi-Fonelli, A. (1965) *J. Mol Biol.* 12, 183-192
30. Matsuda, G., Maekawa, T. and Otsubo, Y. (1965) *J. Biol. Chem., Tokyo*, 57, 228-229
31. Nigen, A. M., Njikam, N., Lee, C.K. and Manning, J.M. (1974) *J. Biol. Chem.*, submitted for publication
32. Williams, R. C. and Kuo-Yi Tsay, personal communication
33. Schuster, T. M., personal communication
34. Njifutié Njikam, Jones, W. M., Nigen, A. M. Gillette, P. N., Williams, R. C., Jr. and Manning, J. M. (1973) *J. Biol. Chem.* 248, 8052-8056

35. Kilmartin, J. V., Fogg, J., Luffana, M. and Rossi-Bernardi, L. (1973) J. Biol. Chem. 248, 7039-7043
36. Joyce, B. K. and Grisolia, S. (1959) J. Biol. Chem. 234, 1335-1337
37. Lowry, O. H., Passonneau, J. V., Hasselberger, F. X. and Schulz, D. W. (1964) J. Biol. Chem. 239, 18-30
38. Rose, F. B. and Liebowitz, J. (1970) J. Biol. Chem. 245, 3232-3241
39. Rose, R. B. and Liebowitz, J. (1970) Anal. Biochem. 35, 177-180
40. Keitt, A. S. (1971) J. Lab Clin. Med. 77, 470-475
41. Higashimura, T., Yamada, O., Nohara, N. and Shidei, T. (1967) Intern. J. Appl. Radiation Isotopes 13, 308-309
42. Wang, C. H. and Willis, D. L. (1965) Radiotracer Methodology in Biological Science, Prentice-Hall, Englewood Cliffs, N. J., 104-137
43. Glasoe, P. K. and Long, F. A. (1960) J. Phys. Chem. 64, 188-190
44. Keyes, M., Mizukami, H. and Lumry, R. (1967) Anal. Biochem. 18, 126-142
45. Allerhand, A., Cochran, D. W. and Doddrell, D. (1970) Proc. Nat. Acad. Sci. USA, 67, 1093-1096
46. Ernst, R. R. and Anderson, W. A. (1966) Rev. Sci. Instru. 37, 93-102
47. Farrar, T. C. and Becker, E. D. (1971) Pulse and Fourier Transform NMR, Academic Press, New York, Chap 2
48. Allerhand, A., Doddrell, D., Glushko, V., Cochran, D. W., Wenkert, E. W., Lawson, P. J. and Gurd, F. R. N. (1971) J. Amer. Chem. Soc. 93, 544-546
49. Glushko, V., Lawson, P. J. and Gurd, F. R. N. (1972) J. Biol. Chem. 247, 3176-3185
50. Allerhand, A. and Oldfield, E. (1973) Biochemistry 12, 3428-3433
51. Schaefer, J. and Natusch, D. F. S. (1972) Macromolecules 5, 416-427
52. Ferrar, T. C. and Becker, E. D. (1971) Pulse and Fourier Transform NMR, Academic Press, New York, Chap. 5

53. Doddrell, D., Glushko, V. G. and Allerhand, A. (1972) J. Chem. Phys. 56, 3683-3689

Chapter III

Interaction of CO₂ with Amino Acids,
Peptides and Sperm Whale Myoglobin

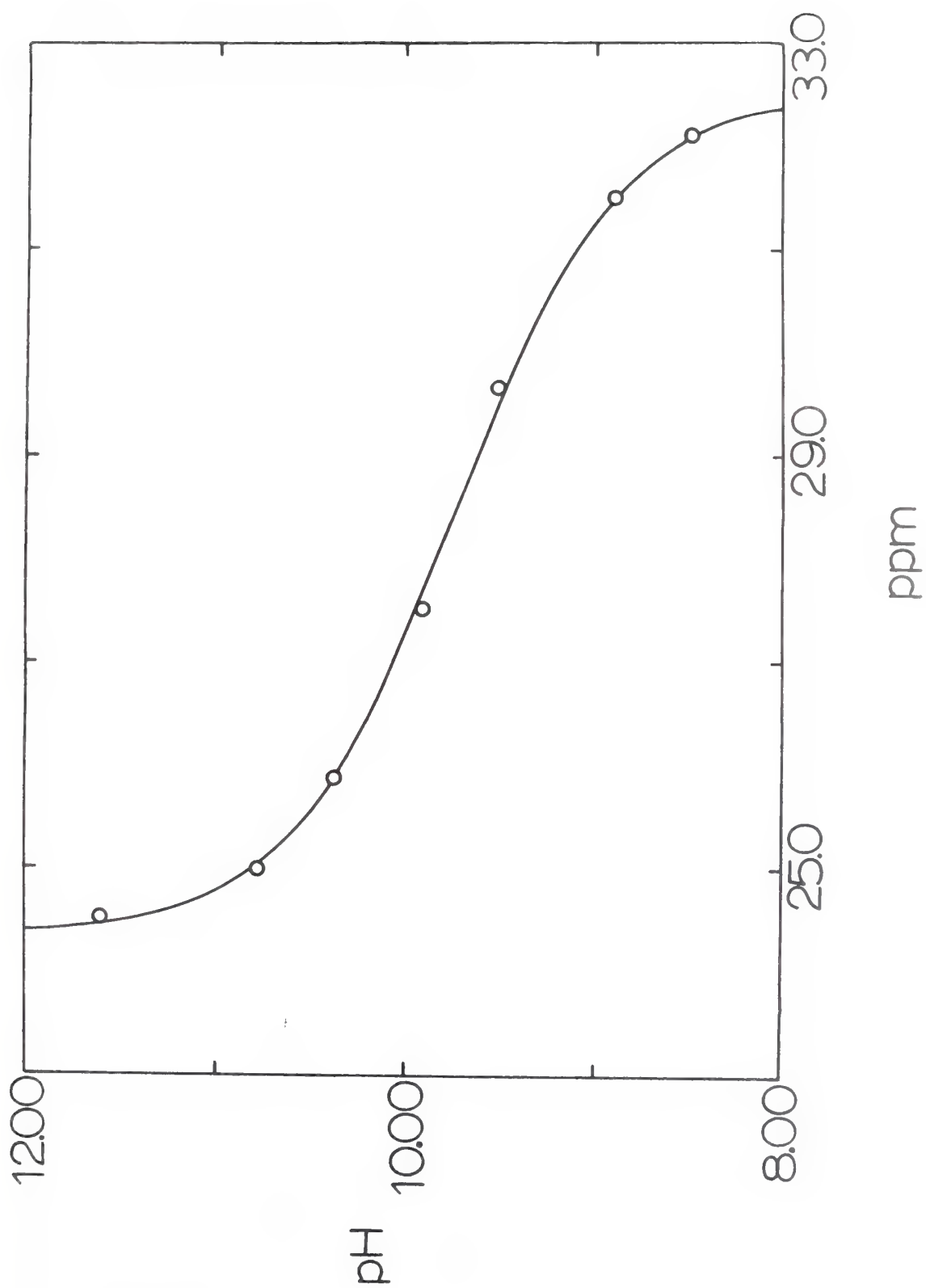
Chapter III

Interaction of CO₂ with Amino Acids, Peptides and Sperm Whale Myoglobin

A firm experimental basis for the ¹³C NMR study of the interaction of CO₂ and bicarbonate with hemoglobin (Chapters IV and V) or biologically active peptides (Chapter VI) was needed. Toward this goal, Chapter III describes the study of carbamino formation in a wide variety of model compounds. The bicarbonate-carbonate chemical shifts are described as a function of pH. The carbamino adduct of glycine is studied in some detail. The structural consequences of carbamino formation in several small valine containing peptides, in proline and in cysteine are discussed. Spin lattice relaxation time measurements (T₁) in a variety of peptide carbamates are described, including an unexplained effect of certain peptides upon the relaxation rate of bicarbonate.

Bicarbonate-Carbonate Titration. The ¹³C NMR behavior of bicarbonate-carbonate was found to follow the case of the limit of fast exchange, wherein the position of a single narrow resonance of constant integrated intensity varied with increasing pH between the limits of 24.38 ± 0.13 and 32.63 ± 0.12 ppm upfield of external CS₂. The position of the resonance of dissolved CO₂, detectable in the less alkaline samples, varied only minimally as a function of pH. Figure 1 shows the titration of the bicarbonate-carbonate resonance, while Figure 2 that of the CO₂ resonance. The curve in Figure 1 represents a least squares fit of the Henderson-Hasselbalch equation to the experimental points. The apparent pK₂¹ at ionic strength $\mu = 0.46$ M

Figure 1. Relation between pH and chemical shift of the ^{13}C resonance of bicarbonate-carbonate mixtures. Ionic strength was 0.46 M, at 32° , as described in the text. Data were obtained at 15.1 MHz. The fit was by least squares to the Henderson-Hasselbalch function with $\text{pK}'_2 = 9.75 \pm 0.03$.



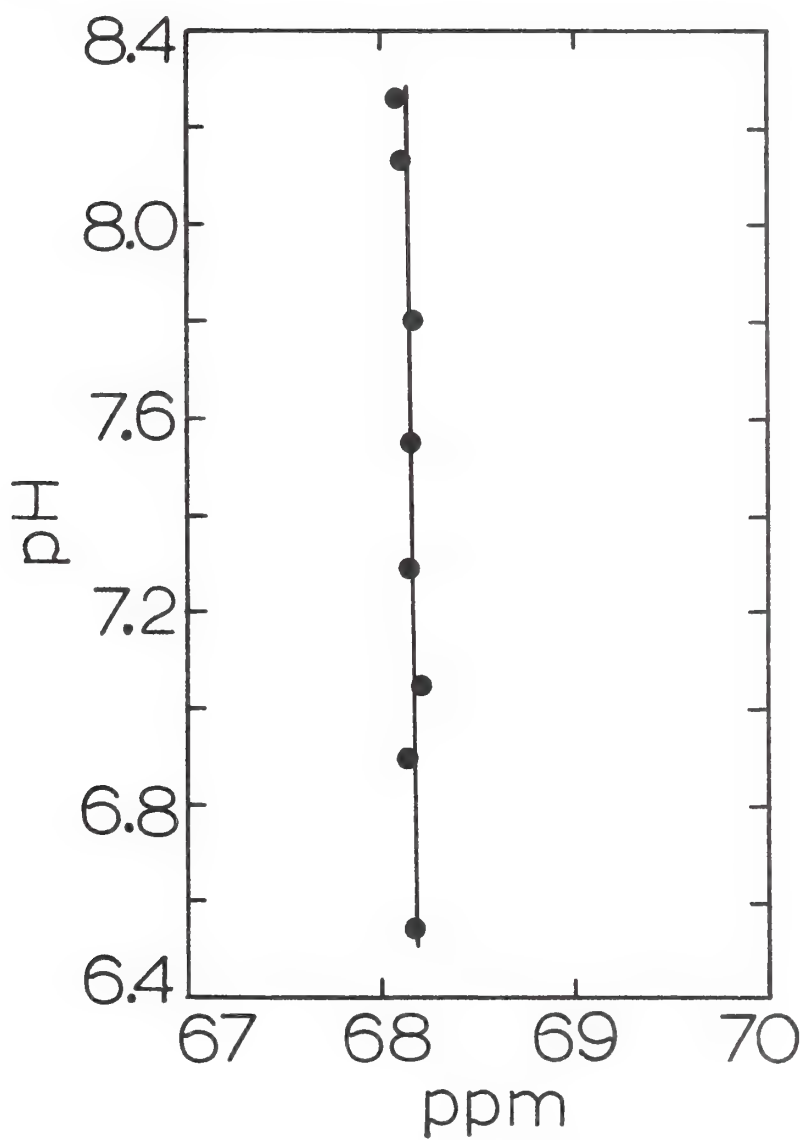


Figure 2. ^{13}C chemical shift of dissolved CO_2 vs. pH. Measurements were made at 15.1 MHz; dioxane was used as an internal standard.

and 32° is 9.75 ± 0.03 for the reaction



The apparent second ionization constant of carbonic acid, pK_2' is defined in terms of the measured pH and the molar concentration of bicarbonate and carbonate ions. This constant is related to the thermodynamic ionization constant pK_2° by the expression

$$\text{pK}_2' = \text{pK}_2^\circ - \log(\gamma_{\text{HCO}_3^-} / \gamma_{\text{CO}_3^{=}}) \quad 2$$

where γ_i represents the activity coefficient of species i .

The results obtained above by the NMR method are in good agreement with the corresponding values for this constant obtained by other workers (1,2) when such values are appropriately reexpressed in the terminology used here, Equation 2. The studies of MacInnes and Belcher (1,2) may be taken as a reference, in which potentiometric measurements were made on solutions of KHCO_3 , K_2CO_3 and KCl at different ionic strength values. The apparent second ionization constants so obtained differ from ours by the form of the activity coefficient term, $-\log(\gamma_{\text{HCO}_3^-} \gamma_{\text{Cl}^-} / \gamma_{\text{CO}_3^{=}})$. Solutions identical with those used for the potentiometric measurements (2) were prepared and the pH determined. After making the necessary corrections for temperature, hydrolysis of carbonate, and the ion product of water (2), the results were used to recalculate the pK_2' values of these solutions based on Equation 2. Extrapolation of pK_2' values against μ to obtain a value for $\mu = 0.46$ M was performed either linearly, as suggested by MacInnes and Belcher (1,2) or by estimating the activity coefficients according to the Davies equation (3). The former extrapolated value for pK_2' was 9.78 and

the latter value was 9.76.

Carbamino Derivative of Glycine. Figure 3 shows various glycine spectra taken at pH 8.90 and 9.25 with or without the presence of 1M total carbonates. Figure 3A shows glycine without CO₂, in which the upfield resonance at 150.5 ppm represents C^α and the downfield resonance at 18.5 ppm represents the carboxyl carbon, C^o. In this and the other spectra of Figure 3, the dioxane resonance is visible at 126.2 ppm upfield of external CS₂. In Figure 3B the conditions are comparable except that now the glycine has been equilibrated with CO₂ in the form of 1 M total carbonates. This addition results in the partial conversion of the glycine to the adduct form ⁻OOCNHCH₂COO⁻. The resonances of the free glycine are easily recognized. Just downfield of each of these is a new resonance reflecting the C^α and C^o. The resonance at 31.6 ppm represents the bicarbonate-carbonate component. The resonance of the ¹³C-enriched carbamino group, 0.09 mole fraction ¹³C, is at 28.4 ppm. Because of the high pH of the measurements the resonance of CO₂ is not apparent.

Small differences in pH between the experiments recorded in Figures 3A and 3B are responsible for the differences in chemical shift position of the resonances of both carbons of free glycine. The carbamino moiety itself is represented by a resonance that is not sensitive to pH under these conditions.

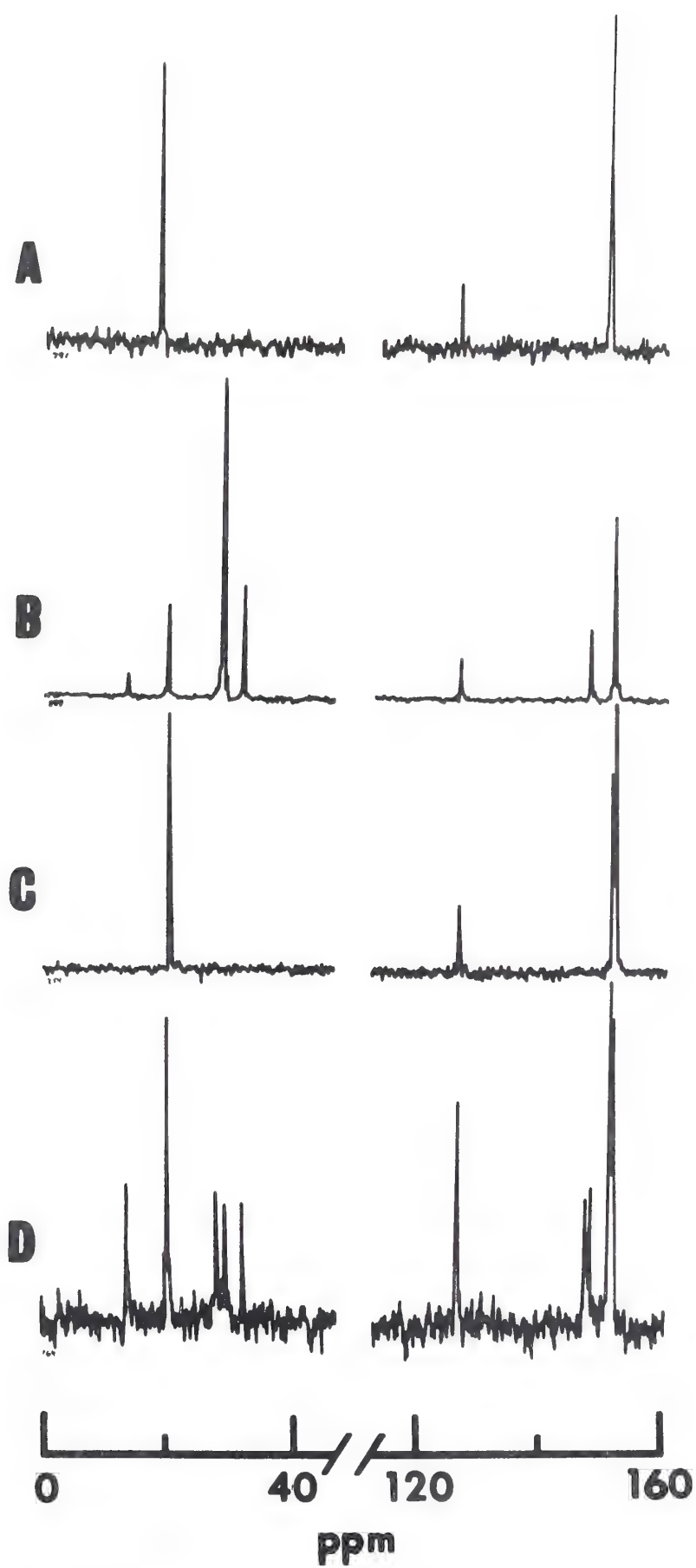
The assignment of the resonance at 28.4 ppm to the carbamino adduct is verified by the spectra in Figure 3C and 3D in which glycine enriched 95% with ¹⁵N was substituted to take advantage of the splitting patterns arising from scalar coupling between ¹³C and ¹⁵N. In Figure 3C this splitting is seen in the simple C^α doublet,

characterized by $J_{C^{\alpha}-N}$ of approximately 6 Hz. Figure 3D corresponds to the conditions of Figure 3B, in which enriched $^{13}CO_2$ and carbonates were allowed to equilibrate with ^{15}N -glycine. The $J_{C^{\alpha}-N}$ for the C^{α} of the glycine with the carbamino adduct is now enhanced to 11 Hz, as a result (4) of changes in the charge density at C^{α} (see below). The carboxyl (C^O) resonances for the free and carbamylated glycine forms are at 19.8 and 13.3 ppm respectively, and the bicarbonate-carbonate resonance is at 31.8 ppm. The remaining 2 resonances are centered about 28.4 ppm, with a separation of 20 Hz, and reflect the ^{15}N - ^{13}C spin-spin coupling between the ^{13}C nucleus of the carbamino adduct and the directly bonded ^{15}N atom.

The increase of $J_{C^{\alpha}-N}$ with carbamino formation, approximately from 6 Hz to 11 Hz, and the value of $J_{cam-^{15}N}$ of 20 Hz can be taken as evidence for considerable sp^2 character of the hybrid orbitals of nitrogen (5) in the carbamino form. The value of 20 Hz compares favorably with those for several amides (6). This interpretation supports the proposal (7) that the increased pK of the carbamic acids derived from amino acids and peptides (8) is the result of the contribution of the canonical form $R(H^+)N=C(O^-)OH$.

The deprotonated amine form of glycine exhibits chemical shifts for C^O and C^{α} of 12.2 and 147.8 ppm, respectively. Thus the effect of $-COO^-$ substitution for $-H$ in glycine is approximately 1.1 and -0.7 ppm for C^O and C^{α} , respectively. The average values for this effect are 1.2 and -1.0, respectively, for all amino acids and peptides listed in Table II, with the exception of L-lysine, L-proline, L-serine, L-threonine and L-cysteine (at pH 8.8). The effects of carbamino formation on the resonances of C^{α} and C^O are qualitatively

Figure 3. ^{13}C NMR spectra of glycine solutions with or without $^{13}\text{CO}_2$ addition to form the carbamino derivative. A, ^{13}C natural abundance glycine, 2 M, pH 9.25, 128 accumulations, recycle time 10 sec; B, ^{13}C natural abundance glycine, 3 M, pH 8.90, equilibrated with 1 M total carbonates, 9 atom % ^{13}C , 232 accumulations, recycle time 10 sec; C, glycine enriched to 95% ^{15}N , 2 M, pH 9.00, 159 accumulations, recycle time 10 sec; D, ^{15}N enriched glycine, 1 M, pH 8.90, equilibrated with 1 M total carbonates at ^{13}C natural abundance, 132 accumulations, recycle time 10 sec. The measurements were made at 15.1 MHz. The temperature was 30 to 32°.

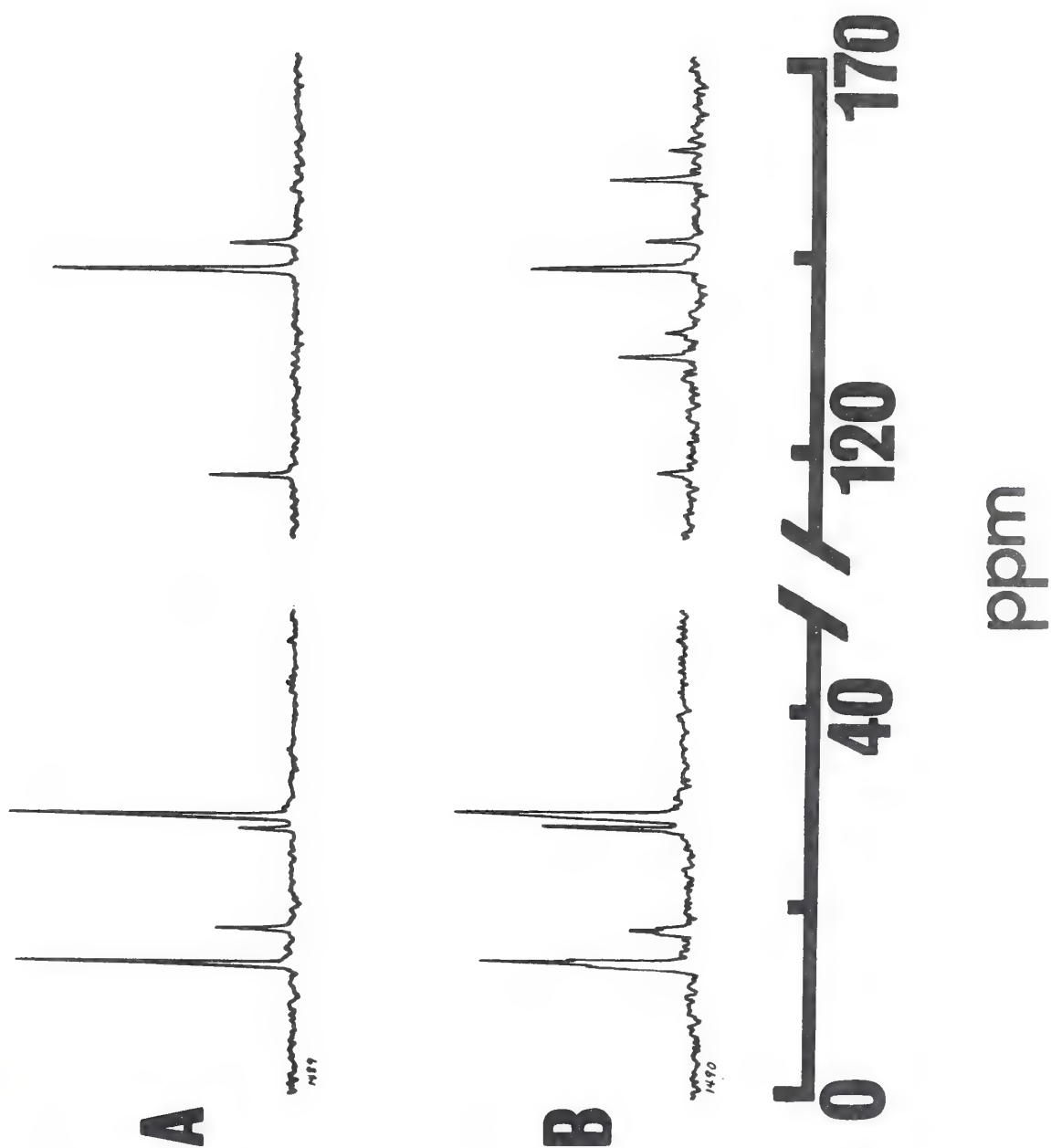


in accord with estimates based on mono- and dicarboxylic acids (9,10) derived from aliphatic compounds.

pH Dependence of Formation of Glycine Adduct. The formation of the glycine carbamino adduct as a function of pH has been defined by the classical methods by Stadie and O'Brien (11). A comparable study was undertaken here to test for the quantitation of the extent of the carbamino reaction by the ^{13}C NMR technique. Apart from the instrumental limitations in determining integrated intensities with sufficient accuracy, there are further limitations as discussed in Chapter II related to the T_1 value and the nuclear Overhauser enhancement factor for each carbon nucleus (12,13). To provide full spectral intensity, the instrumental recycle time must be at least 3 to 5 times longer than the T_1 of the measured nucleus. A recycle time of 20 sec. amply satisfied this criterion for the α -carbon resonance of either the free or carbamino forms. The carboxyl resonances of both forms were partially, but equally, saturated at these recycle times. In the following study the NOE factors were carefully estimated under certain representative conditions for all resonances in glycine and in the carbamino adduct form. It should be borne in mind that glycine is a sufficiently small molecule that the ^{13}C - ^1H dipole-dipole relaxation mechanism, even for protonated carbon nuclei, may not be dominant (13-15). Significant contributions from other relaxation mechanisms, notably paramagnetic or spin-rotation, will result in NOE values less than 2.99, the characteristic upper limit with dipolar relaxation (12,14).

Figure 4 shows a comparison of spectra of 2.0 M glycine with 2.0 M total carbonates at pH 9.89 recorded in the usual proton decoupled mode, shown above, and in the fully coupled form, shown below.

Figure 4. ^{13}C NMR spectra of 2 M ^{13}C natural abundance glycine at pH 9.89 in 2 M total carbonates at ^{13}C natural abundance. A, fully proton-decoupled, 128 accumulations, recycle time 21.7 sec; B, proton-coupled spectrum made with ^1H radio frequency offset 50 KHz relative to ethyleneglycol without noise modulation, 1024 accumulations, recycle time 21.7 sec. The measurements were made at 15.1 MHz, 30° .



The upper spectrum, A, is fully analogous to that in Figure 2B, except that the adduct formation is more pronounced and the bicarbonate-carbonate resonance is now downfield of the carbamino adduct resonance as a result of the higher pH used here (cf. Figure 1).

The lower spectrum in Figure 4B shows the expected splitting patterns due to ^1H - ^{13}C coupling. The coupling constant $J_{\text{C}^\alpha-\text{H}}$ is 141 Hz for the α -carbon of free glycine, and 136 Hz for the carbamino derivative form. Splitting of C^O resonances of glycine is also discernible, amounting to about 5 Hz in both the free and carbamino derivative forms. Neither the carbamino adduct nor the bicarbonate-carbonate resonance shows any evidence of spin-spin splitting.

Table I lists NOE factors determined at two pH values. Within experimental error, these factors appear to be the same for each class of carbon nucleus in both the free and carbamino derivative forms. Other experiments indicated that these similarities extended to relaxation times. The NOE values near 3.0 for the protonated C^α -nuclei in free glycine and in the carbamino form confirm the dominance of the ^{13}C - ^1H dipolar relaxation mechanism. The pH dependence of the NOE factors suggests that other mechanisms, in addition to the ^{13}C - ^1H dipolar one, contribute to the relaxation of C^O nuclei at pH 8.18. In this pH range the only species experiencing a substantial change in its ionic state is free glycine. Since at the lower pH values the spin-lattice relaxation time may be longer than the mean time of CO_2 exchange (16-18) between the solution and the carbamino forms, the observed NOE values may represent average values, weighted relative to the abundance of the three forms, dipolar glycine, anionic glycine, and carbamino glycine. Although free CO_2 could not be

Table I

¹³C Nuclear Overhauser Enhancement Factors at
15.1 MHz for Glycine and Its Carbamino Derivative

Measurements were made at 31° as described in the text. Total glycine was 2.0 M, total carbonates 2.0 M. The error of the estimates of resonance intensities puts practical confidence limits of ± 0.3 in the listed values. The NOE factors are expressed as $(1 + \eta)$ (12).

Resonance Assignment		Nuclear Overhauser Enhancement Factor	
<u>Free Glycine</u>	<u>Carbamino Derivative</u>	<u>pH 9.89</u>	<u>pH 8.18</u>
C ^α		3.1	3.2
	C ^α	2.9	2.8
C ^O		2.5	1.5
	C ^O	2.6	1.8
	C ^O , adduct	2.3	1.5
	HCO ₃ ⁻ - CO ₃ ⁼	1.1	1.2
	Dioxane	2.7	2.6

observed at the high pH of the study, it is interesting to speculate whether dissolved CO_2 would thus experience an intermolecular NOE as observed in other exchangeable systems (19).

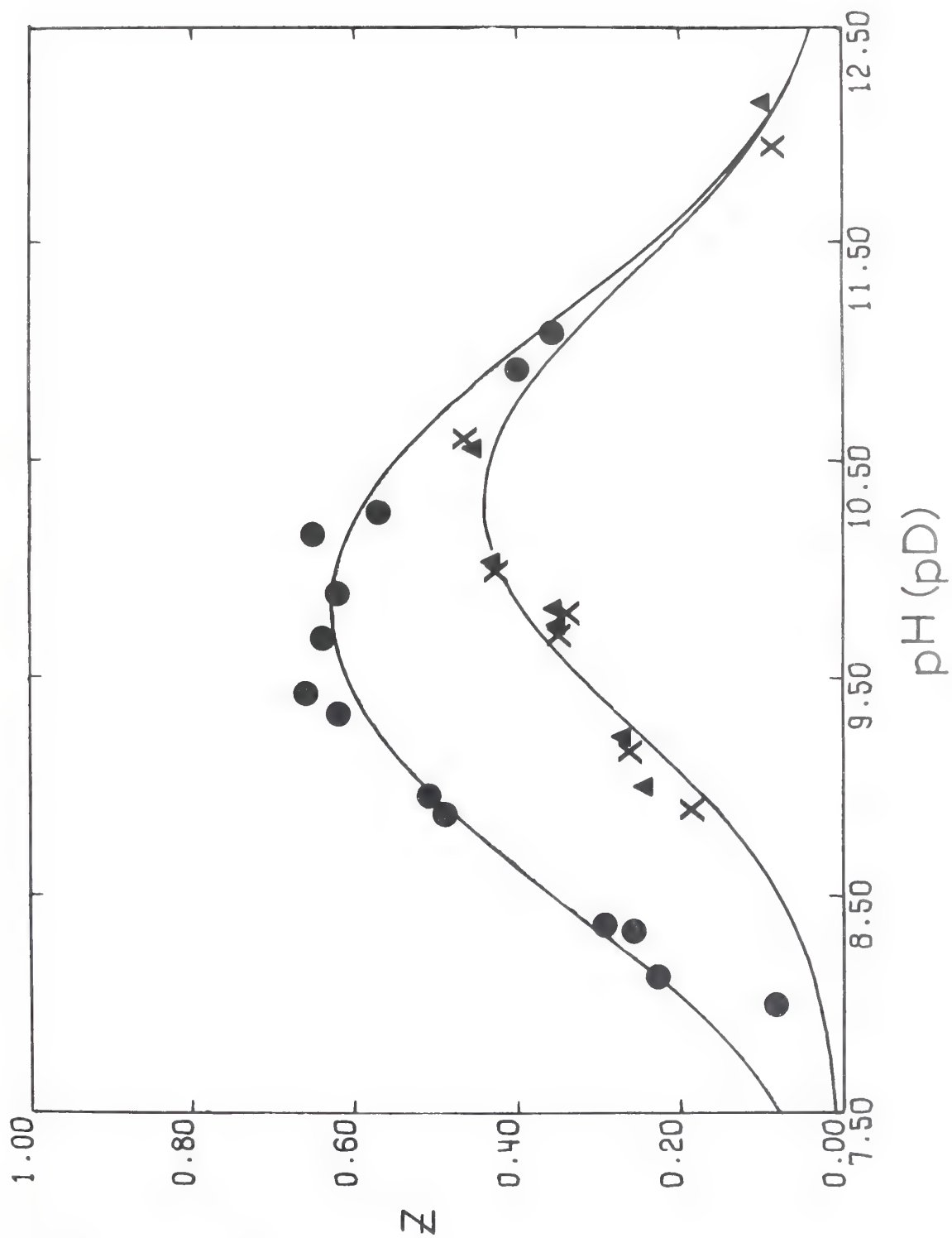
Integrated intensities for the C^α and C° resonances (Chapter II), where separate resonances were clearly discernible, were used to estimate the amount of carbamino product formed in a series of solutions containing 0.5 M total glycine and 0.5 M total carbonates. The mole fraction of the carbamino form was calculated to be

$$Z = \frac{[\text{Gly}-\text{CO}_2]}{[\text{Total Gly}]} = \frac{1}{2} \left[\frac{I_{\text{cam}}^\alpha \cdot \text{NOE}_{\text{free}}^\alpha}{I_{\text{cam}}^\alpha \cdot \text{NOE}_{\text{free}}^\alpha + I_{\text{free}}^\alpha \cdot \text{NOE}_{\text{cam}}^\alpha} + \frac{I_{\text{cam}}^\circ \cdot \text{NOE}_{\text{free}}^\circ}{I_{\text{cam}}^\circ \cdot \text{NOE}_{\text{free}}^\circ + I_{\text{free}}^\circ \cdot \text{NOE}_{\text{cam}}^\circ} \right] \quad 3$$

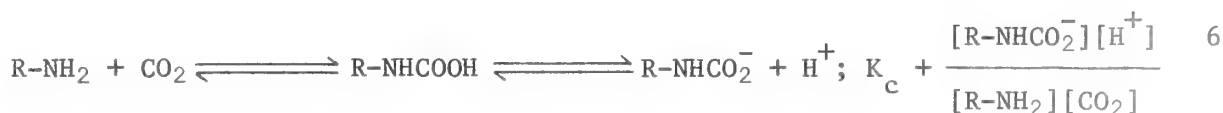
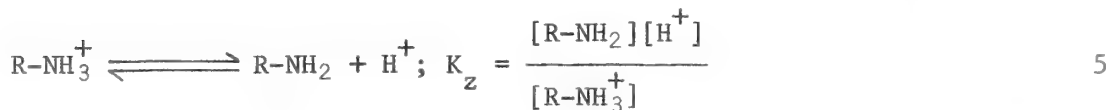
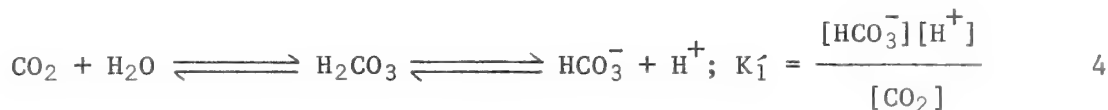
where I represents an integrated intensity, NOE the Overhauser enhancement factor, the superscripts refer to the α - and carboxyl-carbons of the glycine, and the subscripts refer to the carbamino derivative or the free glycine form. In practice, the NOE values were assumed to be identical for each class of carbon in both the free and carbamate forms (cf. Table I); in cases where the signal to noise ratio for the C° carbon was not comparable to that for C^α , Z was estimated from the C^α resonance areas alone.

The calculated results for these experiments are shown as circles in Figure 5, plotted as Z , the mole fraction of glycine present as carbamate, against pH. The maximum mole fraction of carbamino form, about 0.60, is reached near pH 9.9. At lower pH values the formation of the anionic glycine is limiting, and at high pH values the availability of dissolved CO_2 is limiting. In addition

Figure 5. Relation between pH or pD and Z, the mole fraction of glycine in carbamino form. Total glycine was 0.5 M and total carbonates 0.5 M. Temperature was 30-31°. The curves are fit by least-squares based on Equation 10, and yield values of $pK_Z = 9.78 \pm .09$, and $pK_C = 4.71 \pm .06$, for the top curve done in H₂O, and $pK_Z = 10.17 \pm .08$ and $pK_C = 5.3 \pm 0.1$ for the bottom curve done in D₂O. The filled circles (●) and triangles (▲) represent ¹³C NMR results, while the crosses (x) were from ¹H NMR methods. See the text for details.



to the equilibrium described in Equation 1 defining K'_2 , the following equilibria are important.



The total mass balances for this system are described by:

$$\text{Total carbonates, } [\text{TC}] = [\text{CO}_2]_{\text{free}} + [\text{CO}_2]_{\text{bound}} + [\text{HCO}_3^-] + [\text{CO}_3^{=}] \quad 7$$

$$\text{Total amine, } [\text{TA}] = [\text{R-NH}_2] + [\text{R-NH}_3^+] + [\text{R-NH-CO}_2^-] + [\text{R-NH-COOH}] \quad 8$$

The last term in Equation 8 may be assumed to be negligible (8). It follows that the mole fraction of amine present as carbamate, is given by (20)

$$Z = \frac{K_c K_z [\text{CO}_2]_{\text{free}}}{K_c K_z [\text{CO}_2]_{\text{free}} + K_z [\text{H}^+] + [\text{H}^+]^2} \quad 9$$

Since it is more economical with the isotope to work at constant total carbonates rather than at constant $[\text{CO}_2]$, Equation 9 was recast as

$$Z = \frac{1}{2} (b \pm (b^2 - 4\text{TC}/\text{TA})^{1/2}) \quad 10$$

$$\text{where } b = \frac{K'_1 K'_2 K_z + [\text{H}^+] (K_c K_z (\text{TC} + \text{TA}) + K_z K'_1 + K'_1 K'_2) + [\text{H}^+]^2 (K'_1 + K_z) + [\text{H}^+]^3}{K_c K_z [\text{H}^+] \text{TA}}$$

The root that satisfies the requirement that $0 \leq Z \leq 1$ is the one obtained by subtraction of the square root term in Equation 10.

The correct values for the apparent K'_1 and K'_2 were estimated by the Davies equation (3) at each experimental ionic strength. Alternatively,

the pK'_2 may be directly measured from the chemical shift behavior of the bicarbonate-carbonate resonance (cf. Figure 1) and then pK'_1 estimated after MacInnes and Belcher (1,2). Estimates by either method were generally comparable within ± 0.01 pH unit.

The upper curve in Figure 5 represents a least-squares fit to the data based on Equation 10 (Fortran program CAL3, Appendix C), and yielded values of $pK'_Z = 9.78 \pm .09$, and $pK'_C = 4.71 \pm 0.06$ at 30° , where the error limits represent two standard deviations. The ordinate variance (Z) was 0.002. The apparent pK'_1 and pK'_2 values determined for these experiments were 6.18 and 9.76, respectively. Roughton and Rossi-Bernardi (8) cite 4.7 for pK'_C at 5° . Stadie and O'Brien (11) found approximately 4.8 for pK'_C at 25° . The present results necessarily cover a considerable range of ionic strength, most heavily weighted between 0.5 and 1.3 M. This is a range in which sensitivity to ionic strength variations is relatively small (3). The computed variation in pK'_1 and pK'_2 , 0.02 in this range, agrees with the direct observations on the bicarbonate-carbonate chemical shift. Direct observation of the chemical shift of C^α of the free form of glycine in the same series of solutions yielded, furthermore, a value for pK'_Z of 9.82 ± 0.06 . This value is in keeping with previous results (21).

Deuterium Isotope Effects. The lower curve in Figure 5 represents the identical experiment done in solutions of D_2O , with carbamino formation being monitored by either the relative proton resonance areas on the HR220 instrument, as represented by the points designated X, or by utilization of the above method with ^{13}C NMR, represented by the triangles (\blacktriangle). Either NMR method gives indistinguishable results, data variance 0.001, suggesting that no systematic errors arising from

saturation or NOE effects as discussed in Chapter II exist in the ^{13}C measurements. The pK_z of glycine in D_2O determined from these measurements was 10.17 ± 0.08 , which when compared with the corresponding value in H_2O , yields an apparent $\text{K}^{\text{H}}/\text{K}^{\text{D}}$ ratio of 2.5 ± 1.0 , in reasonable agreement with previous estimates (22).

Of greater interest is the large effect that deuterium replacement has on the carbamino reaction itself, the determined pK_c value being 5.3 ± 0.1 . Taken with the value determined in H_2O this corresponds to an apparent $\text{K}^{\text{H}}/\text{K}^{\text{D}}$ ratio of 4.3 ± 1.5 . The isotopic effect actually may be thought of as reflecting a two-step process, Equation 6. If one assumes a $\text{K}^{\text{H}}/\text{K}^{\text{D}}$ ratio of 3.4 for the ionization of the carbamate based upon its estimated pK (8) and the relationship between pK and $\text{K}^{\text{H}}/\text{K}^{\text{D}}$ first reported by Rule and LaMer (23), the $\text{K}^{\text{H}}/\text{K}^{\text{D}}$ ratio for the carbamate formation alone would then be, very approximately, 1.3. Apart from the question of experimental errors, the exact magnitude of the ratio is a function of the values chosen for pK_1^0 and pK_2^0 in D_2O (cf. Equation 10). The $\text{K}^{\text{H}}/\text{K}^{\text{D}}$ ratio for Reaction 1 has been reported (24), hence a pK_2^0 value in D_2O of 10.87 could be chosen with some confidence. An accurate value for the $\text{K}^{\text{H}}/\text{K}^{\text{D}}$ ratio for hydration of CO_2 is not available, only incomplete reports having appeared (25). Based on analogy with the hydration of aldehydes (26, 27), a value of ≈ 4 might be expected. However, at higher pH values base catalysis intervenes (17,28), and the $\text{K}^{\text{H}}/\text{K}^{\text{D}}$ ratio reportedly falls to ≈ 0.8 (25). Hence, a $\text{K}^{\text{H}}/\text{K}^{\text{D}}$ ratio of 1.0 was assumed for the hydration constant of CO_2 in the above calculations. The error inherent in this assumption reflects itself particularly in the derived value of pK_c , and hence of $\text{K}_c^{\text{H}}/\text{K}_c^{\text{D}}$.

Carbamino Formation in Other Amino Acids and Peptides. Table II presents the chemical shift characterization of carbamino compounds of a number of amines. The range of total amine concentration was 0.2 M to 3.0 M. Sufficient $^{13}\text{CO}_2$ was introduced to provide a signal to noise ratio (29), of at least 12. The pH of the measurement is listed in the second column. Many more measurements were made to establish that the carbamino chemical shift was independent of pH except as noted below. These observations reinforce the interpretation that the bound CO_2 at these pH values is in the slow exchange limit with either bicarbonate-carbonate or dissolved CO_2 . The table shows the observed chemical shift of the carbamino adduct, δ_{cam} , followed by that of the α -carbon of the residue bearing the adduct, $\delta_{\text{cam}}^{\alpha}$. The next column lists the difference between the latter value and that obtained for the α -carbon of the residue under basic conditions with the amino group free and uncharged. The last two columns deal with the chemical shift of the carbonyl carbon of the residue bearing the adduct and compare that value again with the free base form of the unprotonated, free amine. The low solubility of L-tyrosine limited the information obtained for that sample.

The results in Table II show first that, with some exceptions, the chemical shift of the carbamino carbonyl is not very sensitive to the nature of the substitution on C^{α} nor to peptide bond formation. The carbamino resonance in a glycine residue has a chemical shift of 28.4 ppm in the free amino acid and of 28.8 ppm in glycyl-glycine and pentaglycine. In the pentapeptides of the form Gly-Gly-X-Gly-Gly the value was 28.6 ppm. It is not known whether the optically active central residue, as compared with optically inactive glycine, plays a role in this behavior (30-33).

Table II

^{13}C Chemical Shift of Carbamino Adduct and C^α and C^O of Carbamino Amino Acids and Peptides

Measurements were made at 50-34° as described in text. The accuracy of many of the chemical shift measurements was limited by the digital resolution of the instrument, 0.12 ppm, although in some cases the XL-100 instrument was used, at a digital resolution of 0.05 ppm. Such measurements contain an additional significant digit. The columns $\delta\text{C}^\text{cam}$ - $\delta\text{C}^\text{base}$ give the chemical shift difference between the base and carbamino forms for either the α -carbon (C^α) or the carbonyl carbon (C^O).

Sample	pH	$\delta\text{C}^\text{cam}$	$\delta\text{C}^\alpha\text{cam}$	$\delta\text{C}^\alpha\text{cam} - \delta\text{C}^\alpha\text{base}$	$\delta\text{C}^\text{Ocam}$	$\delta\text{C}^\text{Ocam} - \delta\text{C}^\text{Obase}$
Glycine	8.90	28.36	147.14	-0.7	13.33	1.1
glycylglycine	10.34	28.81	147.66	-1.0	18.65	1.4
Pentaglycine	9.45	28.79	147.54	-1.2	17.44	1.1
L-Valine	8.56	28.8	130.3	-0.4	11.6	1.4
L-Valylglycine	8.93	28.8	131.3	-0.8	17.0	1.2
L-Valylglycylglycine	9.61	28.8	131.0	-1.3	15.8	1.2
L-Leucine ^a	9.22	28.9	136.8	-1.0	10.0	1.5
L-Lysine α -amino adduct	8.80	29.09	135.95	-0.7	11.50	2.3
ϵ -Amino adduct	10.10	28.24	151.71 ^b	-0.6 ^b	11.19	--
ϵ -Amino caproate	9.40	28.16	151.40 ^b	-0.7 ^b	9.20	0.0
L-Histidine ^c	9.98	29.28	135.72	-0.7	12.23	1.4
Histamine	10.60	28.6	NO ^d	--	NO ^d	--
L-Glutamine	9.67	29.0	134.1	-0.5	NO	--

Table II (Continued)

Sample	pH	δ_{cam}	$\delta C^{\alpha}_{\text{cam}}$	$\delta C^{\alpha}_{\text{cam}} - \delta C^{\alpha}_{\text{base}}$	$\delta C^{\alpha}_{\text{cam}}$	$\delta C^{\alpha}_{\text{cam}} - \delta C^{\alpha}_{\text{base}}$
L-Aspartate	8.66	28.8	137.7	-1.0	11.6	1.4
L-Arginine	8.90	28.8	136.2	-0.7	11.6	1.6
L-Tyrosine	9.60	29.2	NO	--	NO	--
L-Proline	8.64	30.0	131.1	0.0	10.0	-0.4
Phenylhydrazine	7.35	28.4	--	--	--	--
L-Cysteine ^e	8.80	29.2	134.4	2.0	14.0	3.5
L-Cysteine ^e	11.04	28.4	131.7	-0.7	11.3	0.9
L-Serine	8.72	28.8	133.9	-0.4	13.9	2.2
L-Threonine	9.63	28.7	130.5	0.1	13.3	1.6
L-Methionine	9.43	29.0	136.4	-1.0	11.9	1.6
Glycylglycyl-L-Histidylglycylglycine ^f	8.33	28.6	147.4	-1.2	17.6	1.1
Glycylglycyl-L-glutamylglycylglycine ^f	8.83	28.7	147.6	-1.2	17.6	1.1
Glycylglycyl-L-tyrosylglycylglycine ^f	9.10	28.6	147.6	-1.2	17.7	1.1
Glycylglycyl-L-leucylglycylglycine ^f	8.62	28.6	147.4	-1.4	17.6	0.9
Glycylglycyl-L-serylglycylglycine ^f	8.87	28.6	147.4	-1.4	17.6	1.1

a (δ) base form from Gurd, et al. (42).b refers to C ^{ϵ} of lysine or ϵ -amino caproate.

c N-acetyl-L-histidine at pH 9.60 or Imidazole at pH 8.66 formed no detectable carbamino resonance.

d NO - not observed

e Mercaptoethanol at pH 9.45 formed no detectable adduct with ¹³CO₂.f (δ) base form from Keim et al. (31-33).

The formation of the ϵ -carbamino adduct may be clearly observed at 28.2 ppm in solutions of ϵ -aminocaproic acid of lysine above pH 9. As seen in Table II this chemical shift represents a displacement downfield of less than 1 ppm relative to the α -carbamino adduct.

Free imidazole or N-acetyl-L-histidine formed no detectable adduct with CO_2 , in keeping with previous reports crediting the imidazole moiety with an effect in catalyzing the hydration of CO_2 but not with the formation of stable adducts (17,34).

The sulfhydryl group did not yield detectable adducts with CO_2 as judged from experiments on mercaptoethanol or L-cysteine (Table II, and below). However, the chemical shift behavior of carbamino cysteine is of considerable interest, as discussed in greater detail below. In nearly all cases studied, the concentration of dissolved CO_2 is so much less than the concentration of the bound CO_2 , that even infinitely fast exchange with dissolved CO_2 could not shift the observed carbamino resonance by more than 0.1 ppm (18,19).

The carbamino chemical shift can be approximated with additive substituent effects (35), as the methyl substituent parameters for carbonyl chemical shifts in aldehydes, ketones and carboxylic acids (9,10,36,37) are qualitatively applicable. In the case of amino acids and peptides, the only important consideration is substitution at the glycine α -carbon, substitution γ with respect to the carbamino carbon. The predicted effect is a shielding equivalent to less than one part per million. The values for δ_{cam} in Table II bear out the relative positions of the glycine and other adducts based on the above predictions. In addition the insensitivity of the carbamino carbon to substitution at C^α is consistent with the

small shift effects observed for the C^O of residue 2 due to substitution at C^α of residue 3 in the pentapeptides Gly₁-Gly₁-X₃-Gly₄-Gly₅ (31-33). Finally, a lack of sensitivity of the carbamino resonance chemical shift would be expected by analogy with ethyl carbamate (38) and ethyl methyl carbamate (39) where the carbonyl resonances are nearly identical at 35.9 ppm.

The pattern of chemical shifts for the carbamino forms of Val, Val-Gly, Val-Gly-Gly, and ϵ -amino caproic acid is illustrated in Table III. The directly bonded nitrogen nucleus must be counted as alpha to the carbamino adduct in valine. Therefore, the alpha carbon becomes a beta substituent, and the beta carbon a gamma substituent. A similar analysis applies to ϵ -amino caproic acid. The tabulated chemical shift differences are in the direction of, and of approximately the same magnitudes as, the effects of $-COO^-$ substitution for $-H$ in aliphatic chains (9,10). They are reminiscent of the patterns seen in alkyl chains of carboxylic esters (40). In these model systems (40) the shielding at the γ -position has been compared with the shielding effect of methyl substitution in aliphatic chains (41) which has been explained as the result of steric perturbation (charge polarization) of C-H bonds (41).

The chemical shift pattern for the carbamino adduct of L-proline is distinctive in most respects. The δ_{cam} value of 30.0 ppm, Table II, is the farthest upfield found here. This is an especially interesting observation since it corresponds closely to a prominent carbamino resonance observed in hemoglobin solutions and indeed in packed, deoxygenated erythrocytes equilibrated with $^{13}CO_2$ (Chapters IV and V). The details of the spectrum of the carbamino derivative

Table III

Effect of the Carbamino Adduct on ^{13}C
Chemical Shifts of the Parent Compound

Measurements were made as described in the text. Results are expressed for each locus as the difference in chemical shift (δ) between the carbamino derivative and the free base (anionic) form. The γ -methyls of the valine derivatives are discussed separately, see text and Tables IV, and V.

Sample	$(\delta_{\text{cam}} - \delta_{\text{base}})$					
	C^{O}	C^{α}	C^{β}	C^{γ}	C^{δ}	C^{ϵ}
L-Valine	1.4	-0.4	0.8	--	--	--
L-Valylglycine	1.2	-0.8	1.6	--	--	--
L-Valylglycylglycine	1.2	-1.3	1.8	--	--	--
ϵ -Amino caproate	0.0 ₁	-0.0 ₂	0.0 ₃	-0.0 ₄	2.2	-0.7

of L-proline are dealt with below.

Structural Effects in Valine Derivatives. An analysis of the proton coupling constants and of both the ^1H and ^{13}C NMR chemical shifts allows a semi-quantitative examination of the structural consequences inherent upon carbamino formation in small peptides. A series of valine containing peptides, including the free amino acid, was chosen as a suitable model set for this purpose and was studied in collaboration with Dr. Philip Keim at the University of Chicago. The valine series was chosen because human hemoglobin and sperm whale myoglobin have valine as their NH_2 -terminal amino acid, and because the well known isopropyl methyl nonequivalence in ^{13}C and ^1H NMR of valine (31,35,42-44) provides a fertile ground for conformational analysis. This nonequivalence arises from differences in the populations, probably of the three staggered rotamers (45,46) designated $\gamma(\text{III}, \text{II})$, $\gamma(\text{II}, \text{I})$, and $\gamma(\text{I}, \text{III})$ as illustrated in Figure 6 (a), (b), and (c) respectively. By utilizing Karplus-type relationships, the fractional population of $\gamma(\text{III}, \text{II})$ may be estimated from the magnitude of the vicinal $\text{C}_\text{H}^\alpha - \text{C}_\text{H}^\beta$ proton-proton coupling constant (44,47-51). The mechanisms by which the above structural non-equivalence may be reflected in the methyl group chemical shifts can take many forms, including the σ -inductive effect (52), magnetic anisotropy (53), steric crowding (48,54-57), and alterations in the average excitational energy (57). However, in the present study, the effects of electric fields are likely to play the most prominent role (58,59), a point illustrated by a comparison of the methyl nonequivalence as expressed for both ^1H and ^{13}C NMR in the peptides listed in Table IV.

As the $-\text{COO}^-$ grouping is displaced by lengthening the peptide,

Figure 6. Newman projections representing the three staggered conformations of the valine side chain. The pairs of dihedral angles defining the positions of the γ -methyl groups are (a): $\gamma(\text{III}, \text{II})$, (b): $\gamma(\text{II}, \text{I})$, (c): $\gamma(\text{I}, \text{III})$.

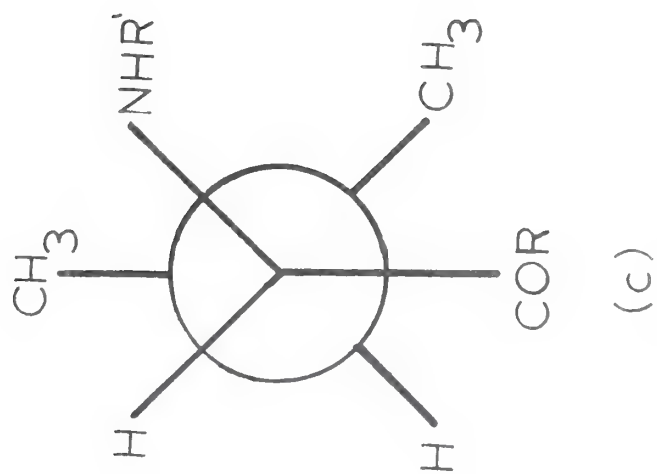
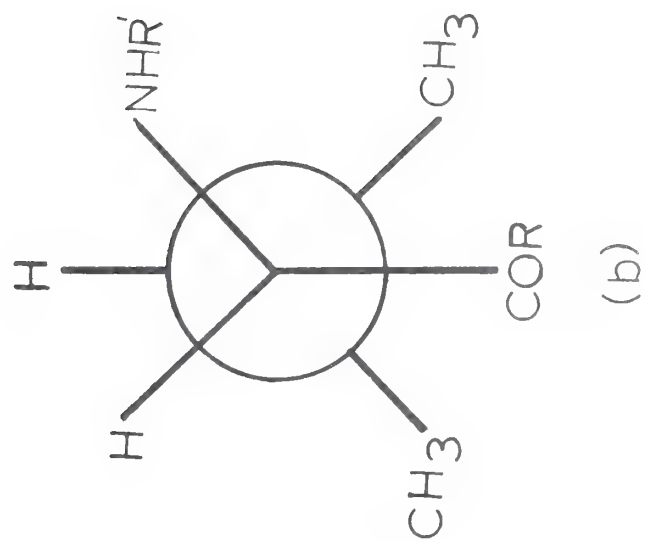
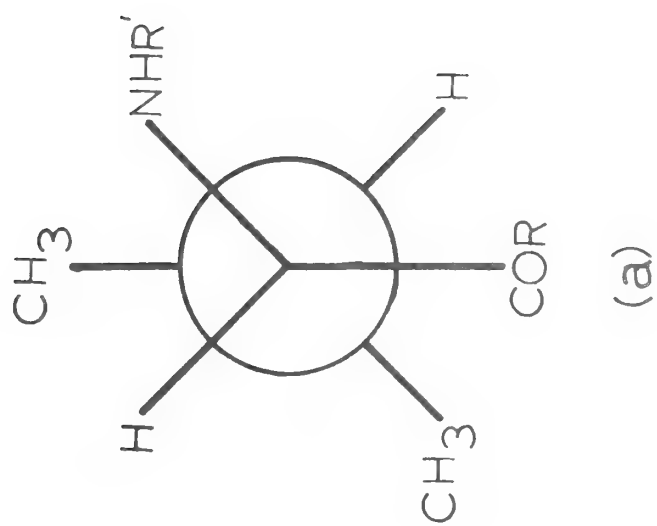


Table IV

Proton and ^{13}C Chemical Shifts of the γ -Methyl Resonances in L-Valine and L-Valine Containing Peptides in Various States of Ionization

Proton shifts as ppm are referenced downfield of internal DSS. The charge states of the free amino and carboxyl groups are represented schematically in parentheses following the name of the compound. Temperature was 37° for the proton studies, and $32\text{--}34^\circ$ for the ^{13}C work. The last two columns report the α - β proton coupling constants in Hz ($J_{\alpha\beta}$), and a corresponding estimate of the mole fraction (χ_t) of the γ (III, II) configuration. See text for details.

Sample	^1H			^{13}C			$J_{\alpha\beta}$	χ_t
	δ_1	δ_2	$\Delta\delta_1$	δ_1	δ_2	$\Delta\delta_1$		
Valine (+ -)	1.04	0.98		174.7	176.0		4.6	0.18
Valine (0 -)	0.93	0.85	0.11	173.6	175.9	-1.1	5.1	0.23
Valylglycine (+ -)	1.02	1.01		175.0	175.6		6.8	0.38
Valylglycine (0 -)	0.91	0.88	0.11	174.0	175.7	-1.0	6.2	0.33
Valylglycylglycine (+ -)	1.01	1.01		175.2	175.8		6.4	0.35
Valylglycylglycine (0 -)	0.91	0.88	0.10	174.2	175.9	-1.0	6.2	0.33

the methyl non-equivalence virtually disappears for ^1H , but approaches a limiting value of 0.6 ppm for ^{13}C . Deprotonation of the α -amino group is reflected to a slightly unequal extent in ^1H NMR, but results almost exclusively in a downfield shift of the more downfield of the two resonances in ^{13}C NMR. An analysis of the population of the $\gamma(\text{III}, \text{II})$ configuration from the $\text{C}_\text{H}^\alpha - \text{C}_\text{H}^\beta$ ^1H coupling constants (Table V) indicates that the effects of ionization upon the rotamer population are modest in relation to those due to increased chain length. The effects on ^1H chemical shifts of intramolecular magnetic and electric fields arising from centers with considerable anisotropy are of similar size, but for ^{13}C resonances the effects of electric fields dominate by at least an order of magnitude (53,58,59). Therefore, it appears that the reported nonequivalence relates to changes in local electric fields incompletely averaged over the three rotamer states.

Thus, based upon the foregoing considerations and also on the expected shielding and deshielding effects of $-\text{COO}^-$ and $-\text{NH}_3^+$ respectively (58,59) due to linear electric field components, it appears (60) that for free valine the population of $\gamma(\text{II}, \text{I})$ is greater than either $\gamma(\text{III}, \text{ID})$ or $\gamma(\text{I}, \text{III})$. Specific solvation effects may be involved (44,54). In contrast, the uncarbamyated peptides listed in Table IV seem to exist predominantly in the $\gamma(\text{III}, \text{II})$ and $\gamma(\text{I}, \text{III})$ configurations. Theoretical calculations accounting for simple electrostatic and nonbonded interaction predict a predominance of the $\gamma(\text{III}, \text{II})$ form (45,46). Although this is what is found for the α -helical regions in many proteins (46), the predictions fail in other cases (44,49,61,62), perhaps due to

Table V

Non-Equivalence of Valine (γ)-Methyls in
Various L-Valine Containing Compounds

Conditions were as described in text and preceding tables. The $\alpha\beta$ and $\beta\gamma$ proton coupling constants are listed in the first two columns; the separation of the methyl proton resonances (in ppm) is designated $\Delta\delta(^1\text{H})$, while the corresponding separation of the methyl ^{13}C resonances is designated $\Delta\delta(^{13}\text{C})$. The ^{13}C chemical shifts of the methyl carbons is also listed, with the estimated mole fraction of $\gamma(\text{III}, \text{II})$ configuration (χ_t) based on the proton coupling constants.

Sample	$J_{\alpha\beta}$	$J_{\beta\gamma}$	$\Delta\delta(^1\text{H})$	$\delta_1(^{13}\text{C})$	$\delta_2(^{13}\text{C})$	$\Delta\delta(^{13}\text{C})$	χ_t
Valine (+ -)	4.6	7.0	0.06	174.7	176.0	1.3	0.18
Valine (0 -)	5.1	6.9	0.08	173.6	175.9	2.3	0.23
Carbaminovaline (- -)	5.5	7.0	0.07	173.7	175.5	1.8	0.26
Acetylvaline (0 -) ^a	5.5	7.0	0.03	--	--	--	0.26
Valylglycine (+ -)	6.8	6.8	0.1	175.0	175.6	0.6	0.38
Valylglycine (0 -)	6.2	6.5	0.03	174.0	175.7	1.7	0.33
Carbaminovalylglycine (- -)	5.6	6.6	--	173.8	175.8	2.0	0.27
Valylglycylglycine (+ -)	6.4	6.8	ca.0.0	175.2	175.8	0.6	0.35
Valylglycylglycine (0 -)	6.2	6.8	0.03	174.2	175.9	1.7	0.33
Carbaminovalylglycylglycine (- -)	5.4	6.9	--	174.0	175.8	1.8	0.26
Glycylvaline (+ -) ^a	5.5	7.0	0.03	--	--	--	0.26
Glycylvaline (0 -) ^a	5.5	7.0	0.02 ₅	--	--	--	0.26

^a From reference 61.

aforementioned solvation effects or more likely due to a stabilizing interaction between the C-H bonds in the isopropyl side chain, and a carbonyl grouping, in a manner similar to that for substituted amides (63). The case for interaction of this sort is further strengthened by the reduced rate of hydrolysis of esters of the form $R\text{-COOR'}$, when R is $i\text{-C}_4\text{H}_9$ (64). Such interactions may account for the considerable stability of the $\gamma(\text{II}, \text{I})$ configuration in the absence of CO_2 , and may be the basis for the additional destabilization of the $\gamma(\text{III}, \text{II})$ configuration upon formation of the carbamino adduct in valine peptides (cf. Table V). It is noteworthy that the effect of amino group deprotonation is significantly less than that due to carbamino formation.

Thus, it is likely that the interaction of CO_2 with NH_2 -terminal valine residues produces significant structural consequences, destabilizing the $\gamma(\text{III}, \text{II})$ conformation, the one in which the side chain methyl groups are least sterically crowded with respect to the polypeptide backbone. This conformation is characteristically found in valine residues in α -helical regions of several proteins (46).

Such destabilization makes the -CO_2^- adduct α -helix breaking. For a protein such as sperm whale myoglobin where the terminal valine region is quite flexible (65) the structural constraint of the -CO_2^- adduct may be easily accommodated. However, the addition of CO_2 to a more highly organized NH_2 -terminal valine might have substantial structural ramifications not only in the local environment of the amino terminus, but also in the long range three-dimensional organization of the protein. Such effects may contribute to the allosteric control of oxygen affinity by CO_2 in hemoglobin (Chapter I).

Structural Effects in Proline Derivatives. The pattern of chemical shifts for proline in the dipolar, anionic and carbamino forms is listed in Table VI. A comparison of chemical shift changes for C^α and C^O of proline upon carbamino formation with those for other carbamylated amines (Table II) points to some unique features resident in the structural requirements for the carbamino form of the imino acid. These features are more clearly illustrated for C^β , C^γ , and C^δ in Table VI. With reference to the proline anion, carbamino formation is most prominently reflected by chemical shift variations at C^γ and C^δ with some alteration for C^β . Such alterations can be qualitatively understood by consideration of the pyrrolidine ring structure.

The dipolar imino acid proline may exhibit considerable ring flexibility in which the most stable conformations allow any one of the five ring atoms to be out of the average plane of the other four (67,68). On the other hand, prolyl residues in peptides should exhibit less flexibility, restricted largely to structures in which the C^γ is displaced on the same side (conformation B) or on the opposite side (conformation A) of the ring plane relative to the carboxyl carbon of the α -carboxyl group (67). The greater ring flexibility for the free imino acid compared with the peptide form appears to relate to the presence of the tetrahedral nitrogen in the former and the trigonal nitrogen in the latter forms (67). Based on analogy with neutral N-substituted derivatives of proline, the nitrogen atom of the carbamino form of the proline should have greater sp^2 character than sp^3 and the carbamino carboxylate group

Table VI

¹³C Chemical Shifts of Proline under Various Conditions

Chemical shifts are expressed in ppm upfield of external CS₂. See text for details.

Sample	Form	Chemical Shift (ppm)				
		C ^O	C ^α	C ^β	C ^γ	C ^δ
Proline	(+ -)	18.3	131.6	163.9	169.0	146.7
Proline	(0 -)	10.4	131.1	162.0	167.5	146.6
Carbamino- proline	(- -)	10.0	131.1	161.7	168.9	145.7

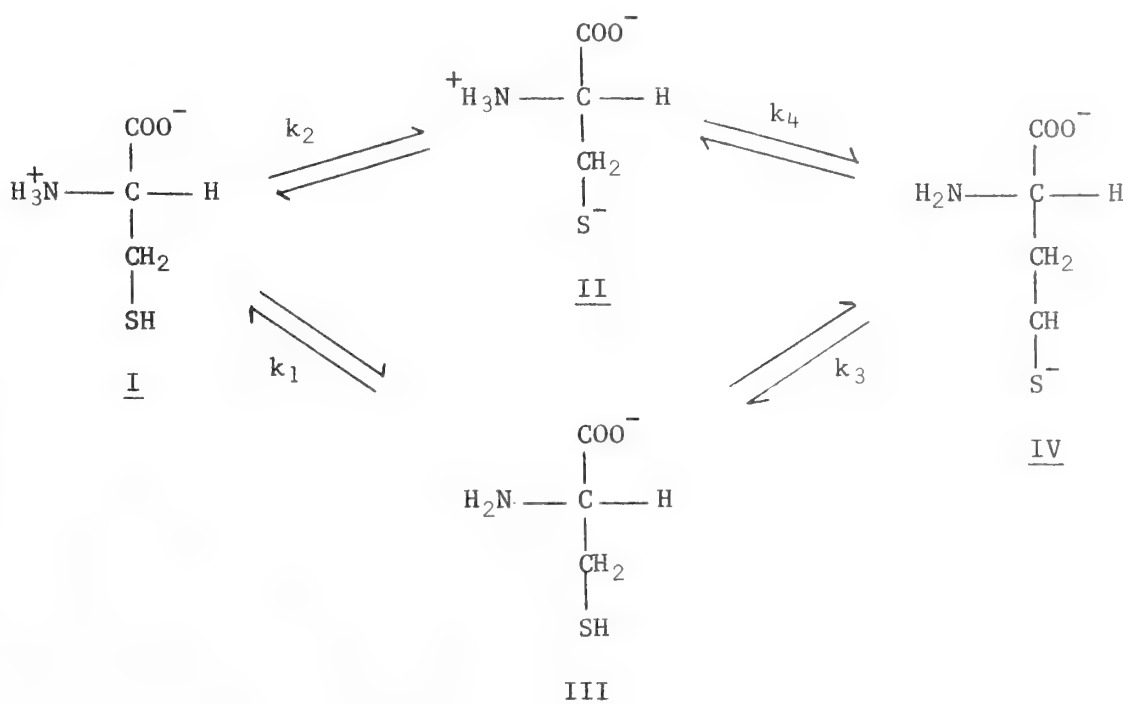
should be roughly coplanar with the imino nitrogen (68,69). In this case, ring flexibility will probably be restricted to forms in which C^δ and C^α may not be strictly coplanar with the carbamino function and C^γ is displaced above or below the average plane encompassing N, C^α , C^β , and C^δ . The change in nitrogen hybridization and the restrictions in ring flexibility appear to be reflected to different extents in all the ring carbon nuclei. An atom by atom interpretation, however, is beyond the scope of the present investigation.

Significantly, the chemical shift of the carbamino adduct (30.0 ppm) falls about 1 ppm upfield of corresponding adducts in acyclic systems (Table II). By virtue of the expected proline ring geometry the factor most probably responsible for this shift anomaly is the interaction between the carbamino carboxylate, coplanar with the imino nitrogen, and the α -carboxylate group of proline. In contrast with other carbamylated amino acids and peptides, the distance of separation between these interacting carboxyl groups is probably much reduced in proline. Potential energy calculations for the carbamino form of L-proline, kindly done by Dr. Sarathy and Dr. Keim at the University of Chicago, in which the nonbonded interactions are estimated for the A and B ring conformations (67) with the carbamino adduct and nitrogen atom coplanar support this interpretation. For the α -carboxyl group, two relatively sharp minima of approximately -2.8 to -3.4 kcal/mole are found at the dihedral angles $\Psi(260-360^\circ)$ and $\Psi(90-170^\circ)$. Within these limits, the effects of noncoplanarity of the carbamino adduct by $\pm 20^\circ$ contribute only a few tenths of a kcal to the energy minima and hardly alter the predicted dihedral angles. Although the predicted distance

between the carbamino adduct and the alpha carboxylate carbons, 3.00 and 3.12 Å for A and B conformations respectively, falls within the estimated van der Waals contact distance of 3.4 Å, the predicted stable conformations are allowed (70). Despite the absence of the electrostatic terms, this type of calculation often works well (45,46,67,70). Introduction of these factors, requiring a precise knowledge of the carbamino geometry, would allow the selection of the most favored Ψ_i , but would not be expected to alter significantly the basic picture (68).

Based upon the above considerations, it is likely that electric field gradients or steric compression, or both may prove to be important mechanisms responsible for the shielding of carbamino carbons in proteins and peptides.

Carbamino Cysteine. The ionization of cysteine is a multi-step process involving the thiol as well as the amino and carboxyl groups (71). At pH values favorable to carbamino formation the carboxyl group may be treated as completely ionized, leaving the following ionizations to be considered:



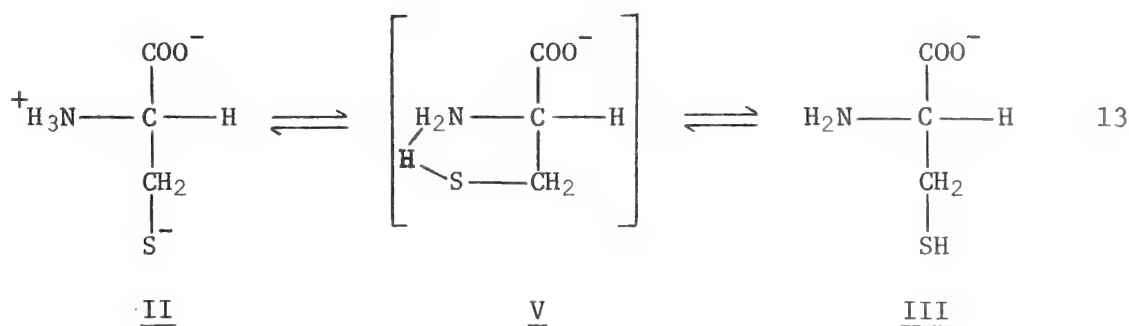
Where k_1 to k_4 represent the microscopic dissociation constants and are related to the macroscopic titration values pK_2' and pK_3' by the equations (71):

$$K_2' = k_1 + k_2$$

$$\frac{1}{K_3'} = \frac{1}{k_3} + \frac{1}{k_4}$$

12

Moreover, the existence of inter or intramolecular exchange of a proton between tautomers has also been postulated (72-75), although the formation of a longlasting hydrogen bond with the thiol group seems unlikely (74,76, 77). Measurements of the rate of intramolecular proton exchange in cysteamine (78,79) and penicillamine (80) have demonstrated rates on the order of 10^6 to 10^7 sec^{-1} . If such an exchange holds for cysteine, a fifth (intermediate) state may then be depicted (74):



Cysteine is thus an attractive model in which to study the consequences of electrostatic interactions with the carbamino adduct. The importance of similar interactions in proton equilibria in proteins is well documented (79-81).

A series of solutions of L-cysteine (Pierce) containing approximately 0.5 M cysteine and 0.5 M carbonates were freshly prepared, and

the ^{13}C chemical shifts of both the free and carbamylated forms measured as a function of pH. The titration behavior of the free component was in complete accord with a published NMR study (75), yielding biphasic curves for all carbon nuclei and fitting the sum of two ionizations (Equation 12) with approximate values of $\text{pK}_2' = 8.1$ and $\text{pK}_3' = 10.5$. Grafius and Neilands (82) have reported values of 8.30 and 10.40 for these constants respectively, based on potentiometric measurements at ionic strength 0.150 M. The proton exchange between species (equations 11 and 13) presumably denies a direct examination of the microconstants (k_1 to k_4) by ^{13}C NMR.

The behavior of the cysteine carbamate in this same series of solutions is shown in Fig. 7. All of the cysteine resonances titrated in a sigmoidal fashion, presumably due solely to the ionization of the thiol group. The acid and base limits of chemical shift, and the corresponding fitted pK values (Figure 7) for the carbon nuclei of cysteine carbamate are shown in Table VII. The observed pK values correspond closely to those reported for the sulfhydryl ionization in analogues with the NH_2 -group blocked (76) and also approximate the estimated value of the microscopic pK_3 (equation 11) of 10.03 (71). The marked lack of sensitivity of the C^β nucleus to the $-\text{SH}$ ionization is similar to that observed in homocysteine (75) and in control studies on N-acetylcysteine (Table VII).

The pH dependence of the carbamino adduct chemical shift (Figure 7) is especially interesting since it is the only compound yet examined to show this behavior. At high pH values, the observed shift may be fit to the Henderson-Hasselbalch function, with an estimated pK value of 9.8 (Table VII). However, under increasingly more acidic conditions

Figure 7. ^{13}C titration behavior of Cysteine carbamate and bicarbonate. Moving upfield at pH 8.5, the resonances represent respectively: C^{O} , C^{adduct} , HCO_3^- , C^{α} and at highest field, C^{β} .

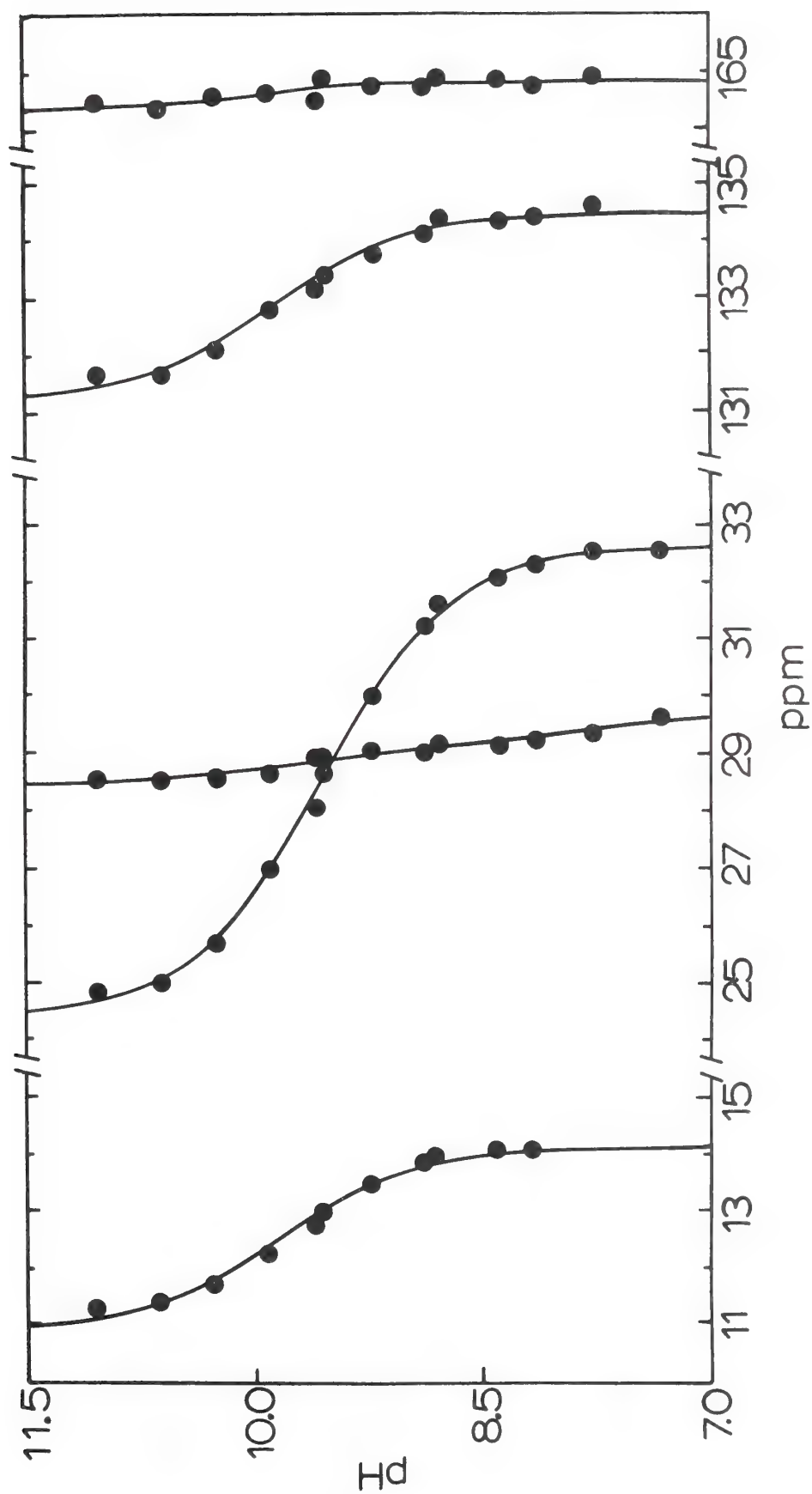


Table VII

¹³C Chemical Shifts and Titration Results
of Carbamino Cysteine and N-acetylcysteine

Chemical shifts (δ) are expressed relative to external CS₂. The δ_{acid} indicates the chemical shift of the dipolar forms. The error limits represent (\pm) two standard deviations, based on the fit of the entire titration curve. See text for details.

Nucleus	δ_{base}	δ_{acid}	$\delta_{\text{base}} - \delta_{\text{acid}}$	pK
Carbamino Cysteine				
C ^O	11.0 \pm 0.2	14.2 \pm 0.1	-3.2	9.8 \pm 0.1
C ^{α}	131.3 \pm 0.2	134.5 \pm 0.1	-3.2	9.9 \pm 0.1
C ^{β}	164.4 \pm 0.2	164.9 \pm 0.1	-0.5	9.9 \pm 0.7
C ^O , adduct	\sim 28.5	\sim 29.1	-0.6	9.8 and 7.9 ¹
HCO ₃ ⁻	24.4 \pm 0.2	32.6 \pm 0.1	-8.2	9.6 \pm 0.1 ²
N-Acetylcysteine ³				
C ^O	13.8	16.5	-2.7	--
C ^{α}	132.4	135.9	-3.5	--
C ^{β}	165.3	166.2	-0.9	--
C ^O , acetyl	19.1	19.2	-0.1	--
CH ₃ , acetyl	170.5	170.6	-0.1	--

¹ See text.

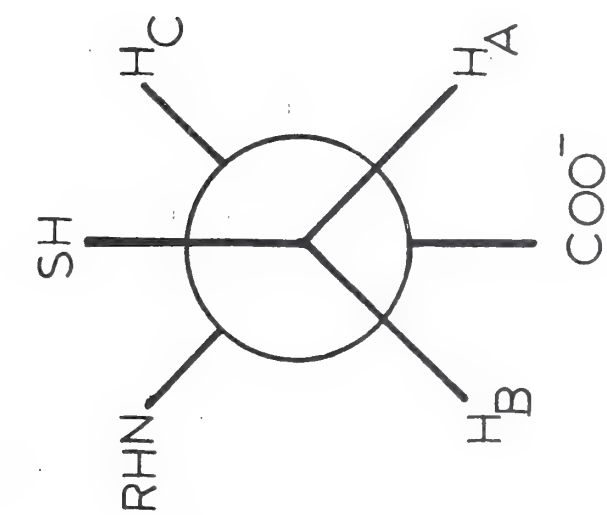
² Compare with Figure 1.

³ δ_{acid} was measured at pH = 6.60; δ_{base} at pH = 12.28.

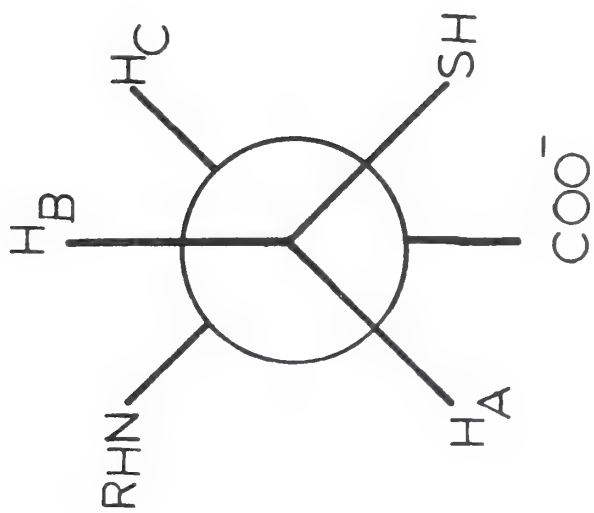
the position of this resonance shifts gradually upfield, a definite limit never being reached within the adduct's range of pH stability. The fitted curve in Figure 7 is based on the sum of two ionizations with pK values of 9.8 and 7.9. This latter value is probably not physically meaningful. The sulfhydryl ionization presumedly is responsible for the shift at the higher pH values. The lack of a definite limit at more acidic pH values may be related to the increasing degeneracy of the rotamer populations.

As with the case of the valine peptides previously described, analysis of the coupling constants observed in ^1H NMR allows, in favorable cases, an estimation of the preferred conformations. Numerous such studies of cysteine and related analogues have been reported (44,47,48,83-36). If, as in the case of valine, the assumption is made that the classical staggered configurations predominate without significant angle distortions, and that the gauche and trans coupling constants remain unchanged in these rotamers, semi-quantitative estimates of the relative residence times in each configuration may be made. These rotamers, designated t, g, and h (86) are depicted as Newman projections in Figure 8. Proton magnetic resonance spectra of cysteine or its carbamate at high pH exhibit 12 observable lines, typical of a three-spin ABX spectra (87). At lower pH values, the spectra collapse into a deceptively simple 5 line ABX system, reminiscent of the classical A_2X spectrum. The pD of this transition is near 9.0 for L-cysteine, and near 10.0 for L-cysteine carbamate. Analysis of the coupling constants and line positions by standard techniques (87) in spectra obtained at 220 MHz yielded the values shown in Table VIII. The signs of the coupling

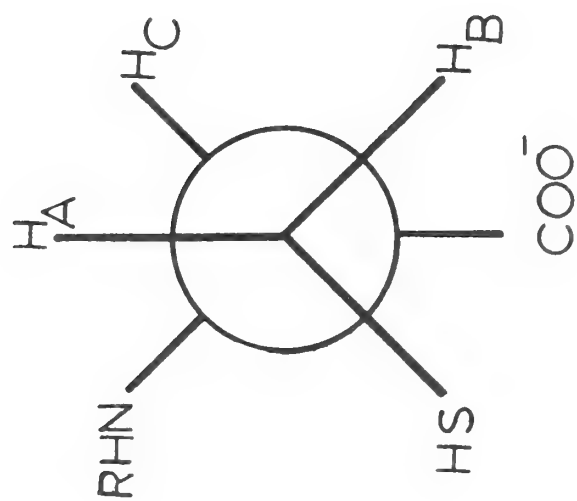
Figure 8. Newman projections representing the three staggered conformations of L-cysteine; (a) trans (t); (b) gauche (g); (c) hindered (h).



(a)



(b)



(c)

Table VIII

Cysteine and Cysteine Carbamate Proton Magnetic Resonance Parameters
at 220 MHz

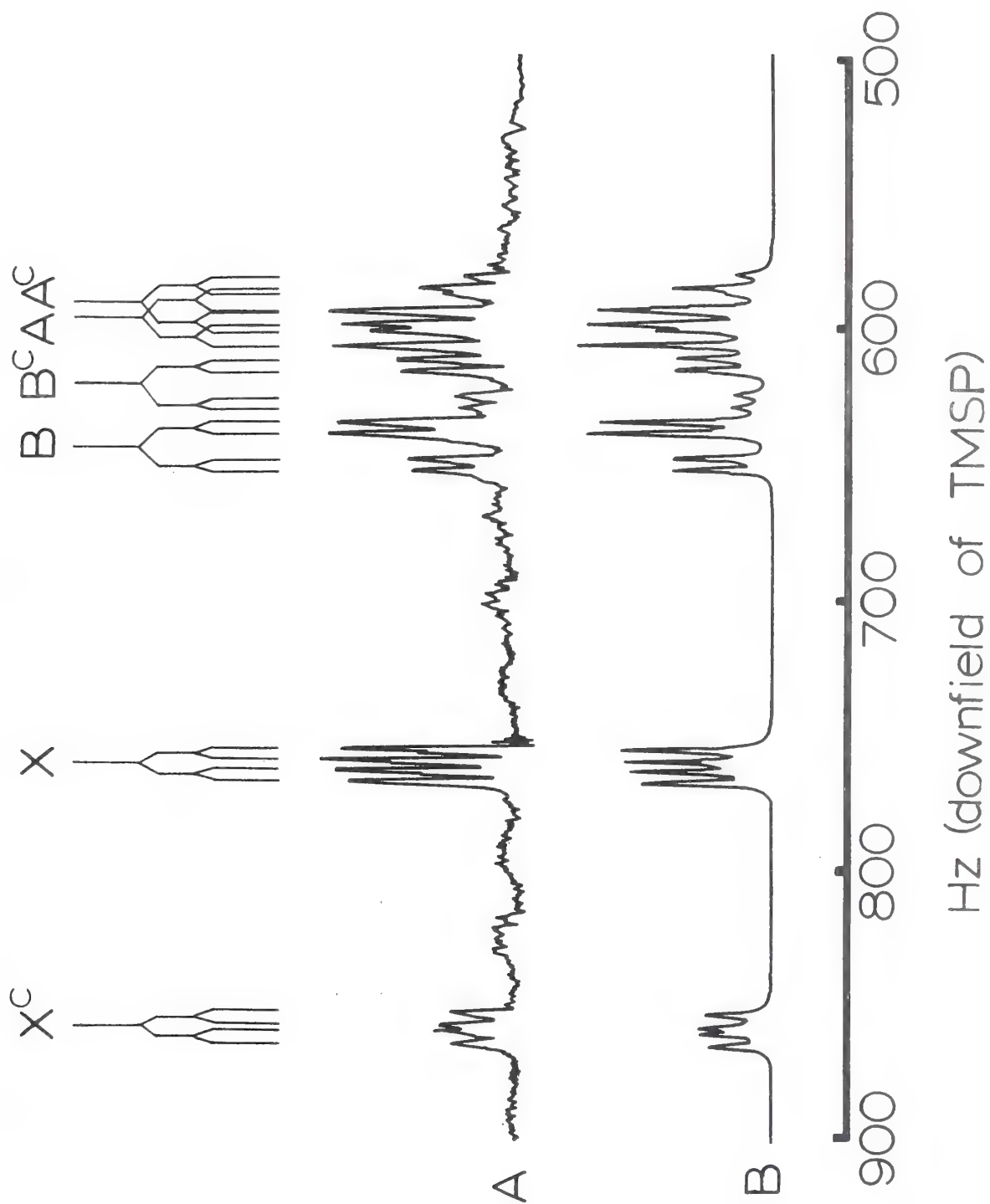
Chemical shifts (ν_i) are expressed as Hz downfield of internal DSS. The chemical shifts and coupling constants were calculated on the basis of an ABX type spectrum, except at lower pD values, where an A₂X analysis was more appropriate. χ_i indicates the calculated mole fraction of rotamer i (Figure 8), based on a trans vicinal coupling constant of 12.0 Hz, and a gauche vicinal coupling constant of 2.0 Hz. Temperature was 35°. Estimated precision is $\pm .2$ Hz in the frequency measurements. See text for details.

Sample	pD	ν_X	ν_A	ν_B	$-J_{AB}$	J_{AX}	J_{BX}	χ_T	χ_G	χ_H
L-Cysteine	11.24	710.8	632.1	562.6	13.0	3.9	8.8	.68	.19	.13
	10.89	732.5	637.1	577.1	13.1	3.6	8.4	.64	.16	.20
	10.72	744.6	638.9	585.6	13.3	4.3	8.2	.62	.23	.15
	10.40	762.0	643.4	598.0	13.4	4.2	7.9	.59	.22	.19
	10.00	774.0	645.0	605.8	13.3	4.1	7.9	.59	.21	.20
	9.92	780.0	647.1	611.5	13.5	4.3	8.3	.63	.23	.14
	9.56	793.5	649.0	619.7	13.5	4.2	8.0	.60	.22	.18
	9.24	807.9	651.0	629.3	14.0	4.0	7.5	.55	.20	.25
	9.19	806.4	651.5	628.6	13.9	4.2	7.2	.52	.22	.26
	8.69	831.8	651.2		5.8					
	8.09	837.5	663.5		5.3					
L-Cysteine Carbamate	10.89	841.4	617.5	582.4	13.1	3.8	8.3	.63	.18	.19
	10.72	846.2	617.1	586.2	13.3	4.2	8.2	.62	.22	.16
	10.40	858.7	619.6	593.2	13.5	4.3	7.2	.52	.23	.25
	10.00	870.6	620.2	601.4	13.3	4.8	6.6	.46	.28	.26
	9.92	879.7	618.0		5.6					
	9.56	892.4	620.6		~5.2					
	9.19	899.0	622.6		~5.3					
	8.69	902.0	624.2		~5.3					
	8.09	921.5	630.5		~5.2					

constants have been chosen by comparison with published reports (44, 47, 48, 83-86). A comparison of a calculated and experimental spectrum is shown in Figure 9, validating the spectral assignment and choice of coupling constants. Also shown in Table VIII are the relative populations of each rotamer, based on a trans coupling constant (J_t) of 12.0 Hz and a gauche coupling constant (J_g) of 2.0 Hz. These values of J_t and J_g were found to be more applicable to the study of cysteine conformers (85) than the values of 13.56 and 2.60 Hz, typical of many other amino acids (44, 47).

Most surprisingly, the results in Table VIII show that the addition of the CO_2 adduct affected the rotamer population very little at high pD values (Table VIII). However, at pD values below about 10, the rotamer populations of cysteine carbamate rapidly approached equality, with subsequent collapse to a simple 5 line spectrum. A comparison with the similar behavior of L-cysteine, which also shows a 5 line spectrum at lower pD values, reinforces an earlier suggestion that the energy difference responsible for the predominance of the trans rotamer arises from strong electrostatic repulsion between the carboxylate and the thiolate anions (44). Why the carbamate anion does not significantly perturb the stability of this conformation is not clear. Stabilizing solution effects (85) may play a role, perhaps due to the high ionic strength of these studies. Inadequacies in the aforementioned assumptions upon which the analysis was based likewise cannot be excluded. However, the variable ^{13}C chemical shift of the carbamate following protonation of the thiol group is consonant with a redistribution of rotamer populations (54).

Figure 9. 220 MHz spectrum (A) of L-cysteine and L-cysteine carbamate at pD 10.40 and 35°; (B) simulated spectrum based on the coupling constants and chemical shifts reported in Table VIII, which were calculated on the basis of an ABX type spectrum. A^C, B^C, or X^C refers to the protons of carbamino cysteine.



The extent of carbamino formation in 0.5 M cysteine solutions containing 0.5 M total carbonates also was measured in D₂O by NMR methods as previously described. The integral area of the C^α proton, H_x in the above analysis, was used for quantitation purposes. The observed mole fraction of carbamate vs. pD is shown in Figure 10. The curve passing through the points represents a least square fit based on equation 10, with fitting values of $pK_z = 8.70 \pm .14$ and $pK_c = 6.02 \pm .04$. These values must be interpreted cautiously since in the present case the equilibrium upon which they are based does not rigorously apply (cf. equations 5-10).

The alternative ionizations available to cysteine (equation 11) produce two forms (III and IV) presumably reactive toward CO₂. It is likely that each form has an associated (and unequal) K_c. A third constant (k₅) will describe the thiol equilibrium of the carbamylated amino acid. Schematically, these additional ionizations may be represented as (cf. equation 11):

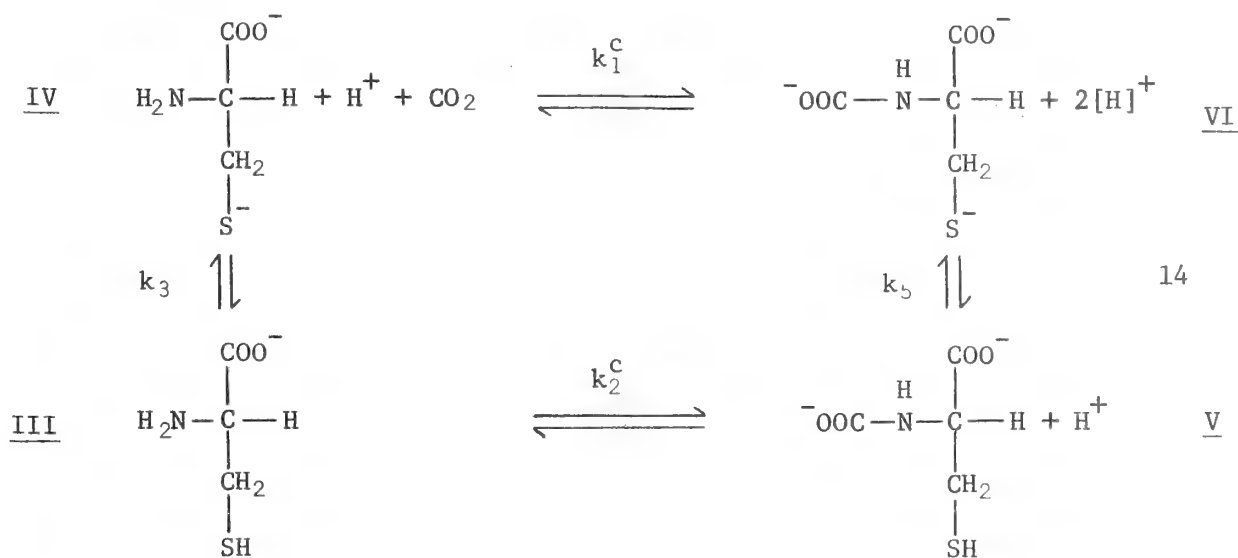
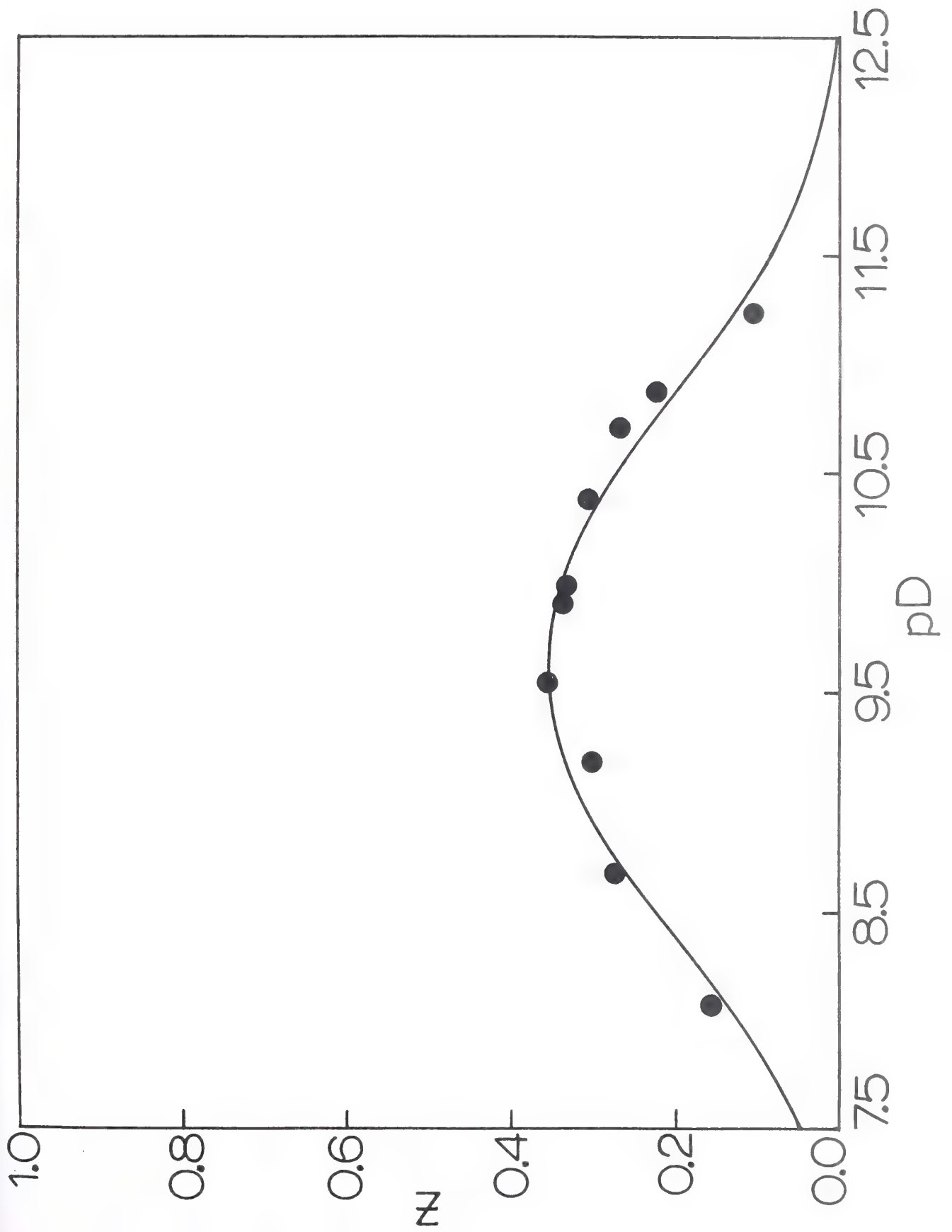


Figure 10. Mole fraction of carbamino cysteine (Z) as a function of pD at 35°. Z was determined by a comparison of the integral areas of the "X" proton in both cysteine and cysteine carbamate (see Figure 9).



Interestingly, if one considers the apparent equilibrium constant (K_z^{app}) of the amine to be defined by

$$[\text{NH}_3^+ - \text{X}] \rightleftharpoons [\text{NH}_2 - \text{X}] + [\text{H}^+]; K_z^{\text{app}} = \frac{[\text{NH}_2 - \text{X}][\text{H}]}{[\text{NH}_3^+ - \text{X}]} \quad 15$$

where X represents the rest of the molecule with either a charged or uncharged thiol group, then it can be shown that K_z^{app} is pH dependent and is related to the microscopic constants (Equation 11) by:

$$K_z^{\text{app}} = \frac{k_1[\text{H}] + k_4k_2}{[\text{H}^+] + k_2} \quad 16$$

Thus at low values of pH, K_z^{app} approaches k_1 , while at higher values of pH, k_4 is approached. Although such studies on cysteine were not pursued, it is obvious that by monitoring the extent of carbamate formation under conditions of constant pH and different pCO_2 pressure, and by knowing pK_2' and pK_3' (cf. Equation 12), all of the microscopic ionization constants are in theory accessible.

Spin Lattice Relaxation Times (T_1). T_1 values were measured for several sets of pentapeptide carbamates of the form glycylglycyl-X-glycylglycine, as well as for the bicarbonate-carbonate resonance under different conditions. The relaxation of protonated carbon nuclei is dominated by the ^{13}C -H dipolar mechanism, as defined by equation 17 relating T_1 to an effective correlation time, τ_{eff} , for rotational reorientation (12).

The gyromagnetic ratios of ^{13}C and ^1H are represented by γ_{C} and γ_{H} respectively; N is the number of directly bonded hydrogen atoms, r_{CH} the C-H distance, and ω_{C} and ω_{H} the ^{13}C and ^1H Larmor frequencies

$$\frac{1}{T_1} = \frac{N_H^2 \gamma_c^2 \gamma_H^2}{10 r_{CH}^6} \left[\frac{\tau_{eff}}{1 + (\omega_c - \omega_H)^2 \tau_{eff}^2} + \frac{3\tau_{eff}}{1 + \omega_c^2 \tau_{eff}^2} + \frac{6\tau_{eff}}{1 + (\omega_c + \omega_H)^2 \tau_{eff}^2} \right] \quad 17$$

in radians per sec. Incomplete dominance of a single relaxation mechanism hinders a similar interpretation for the non-protonated carbon nuclei. The observed T_1 values in milliseconds of the protonated carbon nuclei are expressed as NT_1 values to allow for the effect of the number of directly bonded hydrogen atoms (N).

Figure 11 sets out in schematized form the T_1 or NT_1 values observed for a number of different peptides and their carbamino derivatives. In all instances, control measurements were made after those on the carbamates, the CO_2 having been removed by acidification and evacuation. Such controls yielded values indistinguishable from measurements under similar conditions made before the addition of the carbonates (32). No attempt was made to control ionic strength; peptide concentrations ranged from 0.3 to 0.5 M. Table IX lists the experimental conditions of pH and temperature for the T_1 values shown in Figure 11. The error associated with each value, representative of two standard deviations and based on the estimated data variance, is generally not greater than 10%.

As is evident from Figure 11, the NT_1 values of the protonated carbons systematically increase as one moves away from the central residue, either along the peptide backbone or the side chain. This behavior, indicative of a graded increase in the freedom of motion, is well known (31-33). Also evident is the similarity between the

Table IX
Spin-Lattice Relaxation Experiments

Experimental conditions corresponding to the relaxation results illustrated in Figure 11 are listed for each pentapeptide or pentapeptide carbamate. The pentapeptide carbamates are designated X *CAM.

Central Amino Acid	Figure 11 Designation	pH	Temperature
Tyrosine	A	9.11	34°
Tyrosine *CAM	B	9.10	34°
Serine	C	9.48	36°
Serine *CAM	D	8.87	35°
Histidine	E	9.52	34°
Histidine *CAM	F	7.48	34°
Histidine *CAM	G	8.33	35°
Glutamic Acid	H	9.50	34°
Glutamic Acid *CAM	I	8.55	34°
Leucine	J	9.88	35°
Leucine *CAM	K	8.62	35°

Figure 11. T_1 or NT_1 values expressed schematically for various pentapeptides of the form glyglycyl-X-glycylglycine, in both free and carbamate forms. See text and Table IX for the conditions of each measurement.

A.

	Gly	Gly	Tyr	Gly	Gly	0
H ₂ N-	850-4173-	392-3179-	291-2788-	392-3250-	850-4173	0
			370			
			2401			
		373		373		
		389		389		
			2078			
			OH			

B.

0 ⁻		Gly	Gly	Tyr	Gly	Gly	0
	1916-N-	456-1679-	263-2516-	160-2213-	263-2570-	501-6982	
0				193			0 ⁻
				867			
	HCO ₃ ⁻		188		188		
	165		175		175		
				379			
				OH			

C.

	Gly	Gly	Ser	Gly	Gly	0
H ₂ N-	1277-3419-	479-2777-	356-4036-	479-3527-	864-3228	
			464			0 ⁻
			OH			

D.

0		Gly	Gly	Ser	Gly	Gly	0
	3391-N-	355-3546-	282-2596-	223-3023-	282-2846-	606-4980	
-0				302			0 ⁻
		HCO ₃		OH			
		104					

E.

	Gly	Gly	His	Gly	Gly	0
H ₂ N-	523-1670-	276-2242-	171-2151-	276-2362-	427-3189	
			194			0 ⁻
			1657			
		260		N		
		N		245		

F.

0	Gly	Gly	His	Gly	Gly	0
1273-N-	255-1356-	166-1613-	193-1543-	166-1703-	278-2679	
-0			122			0 ⁻
			855			
HCO ₃ ⁻		177		N		
2054		N		149		

G.

0	Gly	Gly	His	Gly	Gly	0
1761-N-	347-1893-	170-1818-	185-1813-	170-1704-	411-3103	
-0			162			0 ⁻
			1094			
HCO ₃ ⁻		192		N		
1365		N		186		

H.

	Gly	Gly	Glu	Gly	Gly	0
H ₂ N-	1253-2563-	514-5156-	312-3240-	514-7396-	817-8340	
			527			0 ⁻
			742			
			3731			
		0		0 ⁻		

I.

0	Gly	Gly	Glu	Gly	Gly	0
	3433-N-539-3688-416-3632-274-3453-466-4260-888-7710					
-0			369			0 ⁻
	HCO ₃ ⁻		566			
	801		5506			
		0		0 ⁻		

J.

	Gly	Gly	Leu	Gly	Gly	0
	H ₂ N-1118-3948-420-4441-246-4638-420-4040-728-5783					
			439			0 ⁻
			445			
		1291	1497			

K.

0	Gly	Gly	Leu	Gly	Gly	0
	4823-N-420-3065-287-2670-204-3065-287-2766-598-5632					
-0			289			0 ⁻
	HCO ₃ ⁻		278			
	2256	1599	1710			

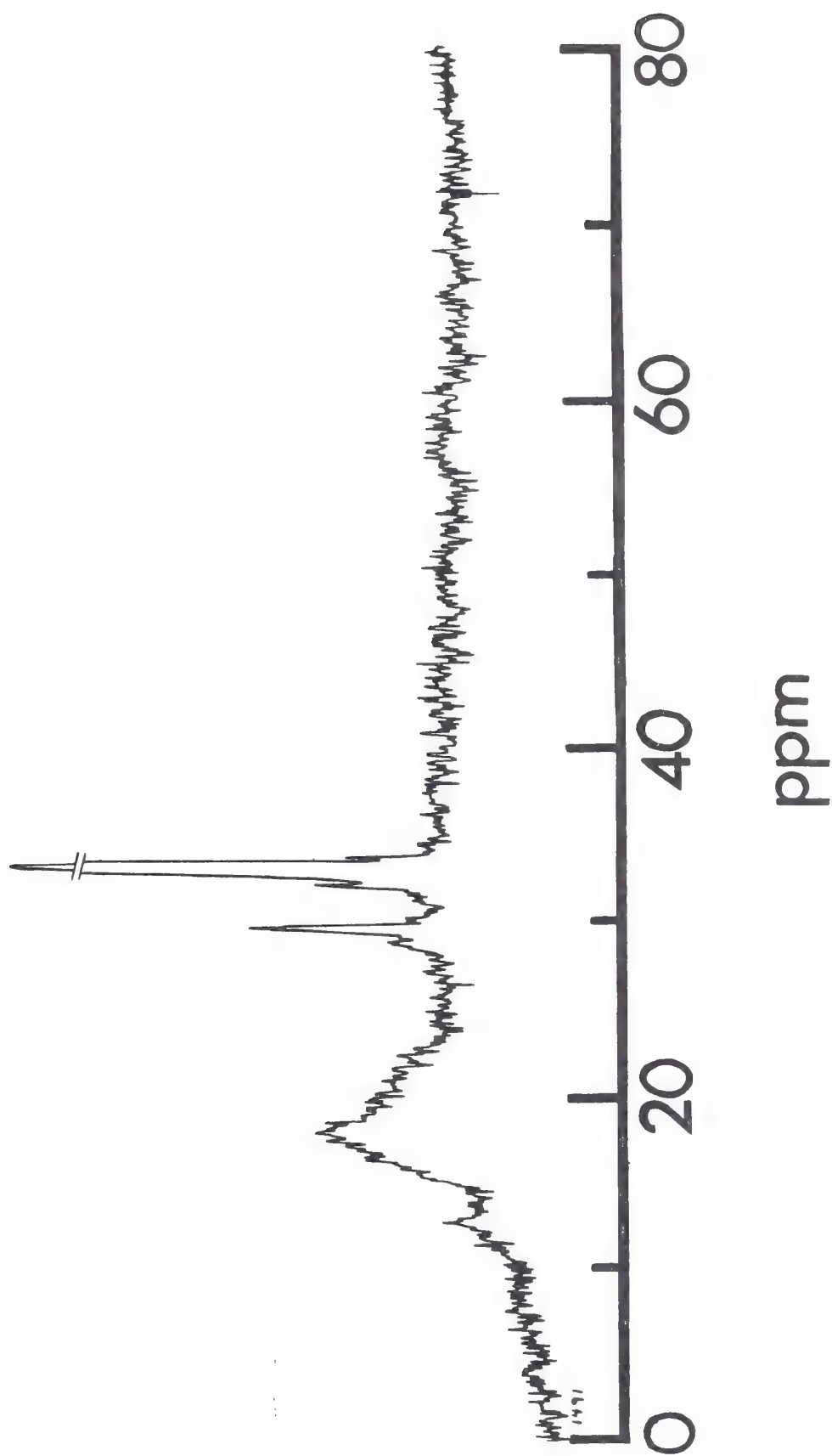
T_1 value of the carbamino adduct and a backbone amide, especially when contrasted with the much longer T_1 values characteristic of C-terminal carboxyls. A comparison of the glycine 1 alpha carbon NT_1 value between the free and carbamylated forms suggests that the carbamate markedly limits the mobility of this group. The effect is greater than a similar one due to protonation of the NH_2 -terminus (31-33), in analogy with the structural studies of valine peptides or cysteine reported above. Another very striking effect in some peptides was a dramatic reduction in the T_1 values of carbon nuclei distant from the NH_2 terminus. Most notable in this respect was glycylglycyl-L-tyrosylglycylglycine carbamate, Figure 11B, in which the T_1 values of the non-protonated ring carbons, C and C^δ , were reduced by a factor of nearly 3, while the NT_1 values of the other ring carbons underwent a two-fold reduction. Accompanying these changes, the relaxation time of the bicarbonate-carbonate resonance (Figure 1) was found to be reduced to 165 ms, when compared with a measured value of ~ 10 sec. alone, or of about 2 sec. in a 15% (w/v) solution of dextran. As shown in Figure 11, the T_1 of the bicarbonate-carbonate resonance varied widely in the other solutions, glycylglycyl-L-serylglycylglycine carbamate yielding a $HCO_3^- \cdot CO_3^{=}$ T_1 value of 104 ms, and glycylglycyl-L-leucylglycylglycine carbamate a $HCO_3^- \cdot CO_3^{=}$ T_1 value of 2256 ms. As is reported in Appendix B, this variability also extended to the protein solutions.

The precise mechanism of these effects is unclear. Contamination by trace paramagnetic impurities cannot be ruled out. This explanation, however, seems inadequate since the control studies were made after the removal of only volatile components. Careful exclusion of dissolved

O₂ had no measurable effect. Additional studies on glycylglycyl-L-tyrosylglycylglycine carbamate, in which the bicarbonate-carbonate component was removed by dialysis at high pH, suggested that it was this component and not the carbamate which was responsible for the reduced T₁ values of the ring nuclei; similar studies with phenol, however, could show no effect on the $\text{HCO}_3^- \cdot \text{CO}_3^{=}$ relaxation time. The possible role of other factors, including pH, temperature, and the ionic milieu needs to be explored before any conclusions may be reached. However, the results reported here raise the question of whether bicarbonate or carbonate may themselves interact directly with the biological analogues studied here.

Sperm Whale Ferrimyoglobin. To test the application of the ¹³C NMR method to a protein, a study of the pH dependence of carbamino formation was made with sperm whale ferrimyoglobin. A representative spectrum is shown in Figure 12. The proton irradiation frequency was offset 50 KHz without noise modulation so as to produce a fully coupled spectrum in which the nuclear Overhauser effect is absent (Chapter II). The protein concentration was 9.1 mM, total carbonates were 46 mM with 0.87 mole fraction ¹³C, and the pH was 8.27. The measurement was made at 15.1 MHz at 30°. The main features of the spectrum reproduced here are the protein carbonyl band between 11 and 24 ppm upfield of external CS₂, the bicarbonate-carbonate resonance at 32.5 ppm, and the carbamino resonances at 28.8 ppm and 29.3 ppm. The upfield carbamino resonance was identified as the α-amino adduct on the basis of its preferential deletion when the protein was pretreated with cyanate (88). The carbamylated sperm whale myoglobin was a gift from Dr. M. H. Garner. The shift of this

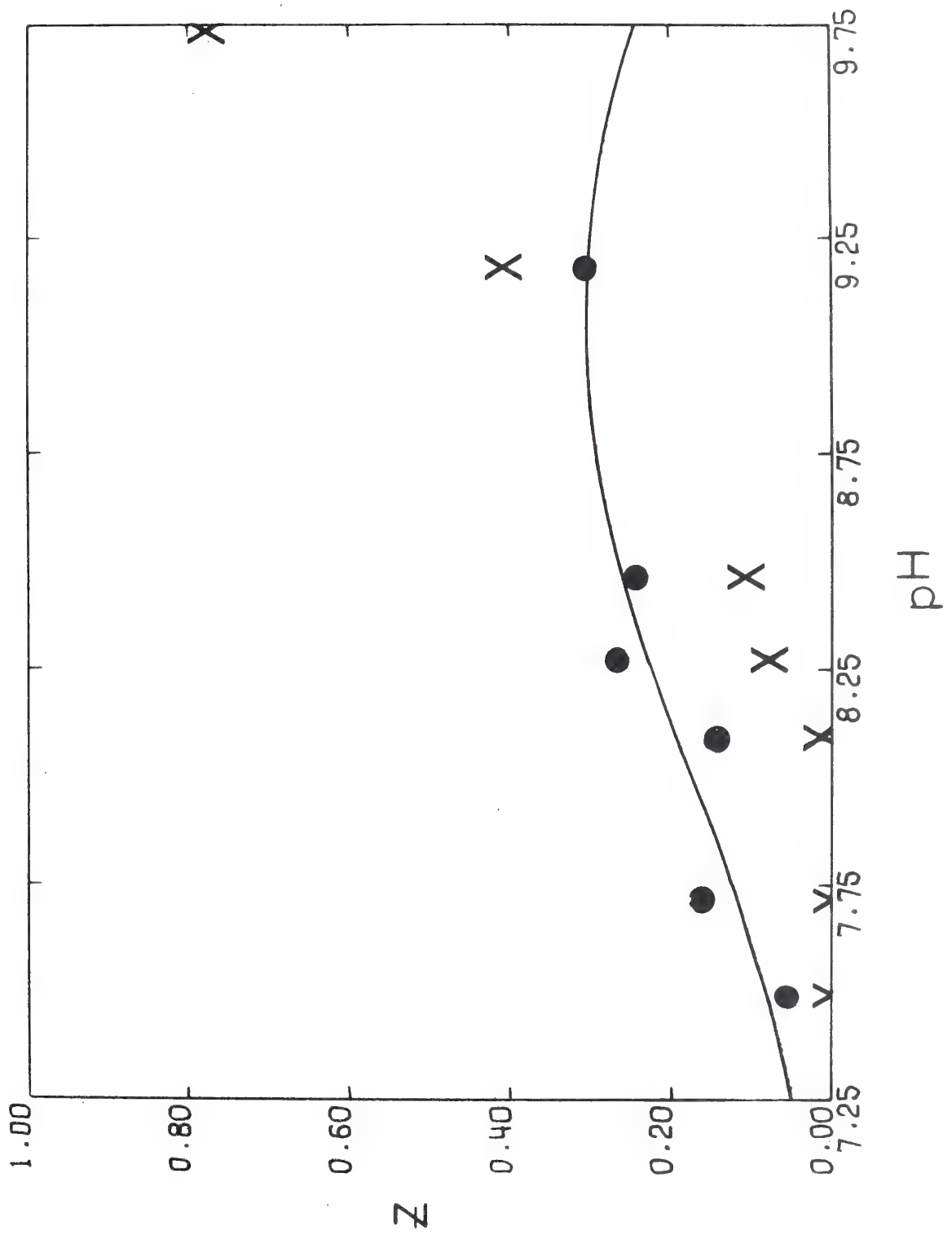
Figure 12. Undecoupled 15.1 MHz ^{13}C NMR spectrum of sperm whale ferrimyoglobin equilibrated with 46 mM ^{13}C enriched (mole-fraction $^{13}\text{C} = 0.87$) carbonates. Protein concentration was 9.1 mM, pH was 8.27. The resonance at 32.5 ppm represents free bicarbonate-carbonate, and is too large to be fully represented at the scale shown. The small resonances immediately on either side are spinning sidebands. The next large resonance, downfield at 29.3 ppm, is the CO_2 adduct bound to the terminal α -amino group of the protein, whereas the small resonance slightly further downfield at 28.8 ppm, and barely perceptible at this pH probably represents ϵ -amino CO_2 adducts. Recycle time was 3.05 sec, with 9536 accumulations, and the temperature was 30° . See text for details.



adduct relative to that observed in the model compounds reflects the effects imposed by its unique environment within the protein. As the pH of the equilibration was increased from 7.7 to 9.7 the resonance at 28.8 ppm first increased in intensity and then broadened with the appearance of shoulders and finally moved downfield to 28.2 ppm. It appears to represent one or more ϵ -amino adducts.

Figure 13 shows the dependence on pH of the mole fraction of myoglobin in the carbamino form following equilibration with 46 mM total carbonates. The stoichiometry of adduct formation was estimated by relating the areas under the carbamino resonances to the total protein carbonyl resonance area in the given sample, making use of the fully coupled spectra for the purpose (Chapter II). The filled circles refer to the α -amino adduct and the ϵ -amino values are shown by X. The latter are of limited significances since this resonance appears to be multiple; hence, no curve has been drawn through the data points. The values obtained for the α -amino adduct are $pK_z = 8.2 \pm 0.2$, and $pK_c = 5.1 \pm 0.1$, with an estimated data variance of 0.002. The value corresponding to pK_z obtained by Garner *et al.* (88) with the cyanate method was 7.96 at ionic strength 0.2 M and 25°. A significant perturbation of the pK value obtained here by mechanisms similar to that found in cysteine (Equation 16) is unlikely, since few groups in the protein (besides the NH_2 -terminus) ionize in the pH range studied (7.5 - 9.5), and independent studies with cyanate (88) have demonstrated only a single pH independent rate constant for the reaction at the NH_2 -terminal of myoglobin.

Figure 13. Relation between pH and the mole fraction (Z) of a given amino group existing as the carbamate in sperm whale myoglobin (\bullet), the NH_2 -terminal valine is represented by the filled circles. (X), probably multiple lysine carbamino adducts; no curve has been drawn since the model described by Equation 9 or 10 does not rigorously apply. Total carbonate was 45 mM, temperature was 30 to 31°.



Discussion and Conclusion

In Chapter III, it has been demonstrated that the carbamino derivative in a wide array of compounds can be directly observed with ^{13}C NMR. Under the conditions of slow exchange (16) which have been encountered up to now (cf. Chapter IV) the recognition of a given component can be based on the observed chemical shift. For quantitation, especially in proteins, the proton decoupling mode carries no advantages, since the NOE observed for the adduct carbon is small. Measurements of spin-lattice relaxation times, T_1 , indicate that the adduct carbon attached to the α -amino group in a peptide undergoes relaxation at a rate generally comparable to that of the amide carbon nuclei of the peptide proper.

The unusual relaxation behavior of bicarbonate in certain peptide solutions may be indicative of a direct and previously unrecognized interaction, but other substantive evidence for this is lacking. The equilibria of CO_2 with amino groups has a complex pH dependence as described by Equations 5 and 6, or their transformations, Equations 9 or 10. The precise distribution of products as a function of pH is dependent on pK_z , pK_c and pCO_2 . Although the dependence on pCO_2 and pK_c is obvious, the pK_z is a strongly determining variable (Chapter VI) that can range from below 7 to above 8.

The present work has been concerned with kinetic effects in showing that the rates of the formation and decomposition reactions at equilibrium did not influence the NMR observations, although the slow exchange limit (16) can be breeched in solutions of hemoglobin (Chapter IV). The factors involved in the reactions have been explored ably by Caplow (33). In biological systems transient effects may

be important. For example, in the absence of carbonic anhydrase, metabolic CO_2 can be present at concentrations that differ from the equilibrium concentration in the immediate environment.

The formation of the carbamate changes the chemical function borne by the NH_2 -terminus of the peptide chain, alters the charge, introduces bulk, and has an effect on the conformation of the terminal region of the chain. The pK of a nearby charged group is altered. The possibility is raised by the results given here for the terminal valine peptides that the carbamate form will enter a helical peptide geometry with greater difficulty than the free peptide. Since the end of the peptide chain is usually looked upon as a point of unraveling, it may be that the carbamate form will stabilize the unraveled form for an appreciable length of time on the scale of molecular motions.

REFERENCES

1. MacInnes, D. A. and Belcher, D. (1933) J. Amer. Chem. Soc. 55, 2630-2646
2. MacInnes, D. A. and Belcher, D. (1935) J. Amer. Chem. Soc. 57, 1683-1685
3. Butler, J. N. (1964) Ionic Equilibrium, A Mathematical Approach, Addison Wesley Publishing Co. Inc., Reading, Massachusetts, 436-439
4. Grant, D. M. and Litchman, W. M. (1965) J. Amer. Chem. Soc. 87, 3994-3995
5. Stothers, J. B. (1972) Carbon-13 NMR Spectroscopy, Academic Press, New York, 375
6. Lichter, R. L., Fehder, C. G., Patton, P. H. and Combes, J. (1974) Chem. Commun., 114-115
7. Edsall, J. T. and Wyman, J. (1958) Biophysical Chemistry, Academic Press, Inc., New York, 1, 571-578
8. Roughton, F. J. W. and Rossi-Bernardi, L. (1969) in Carbon Dioxide: Chemical, Biochemical and Physiological Aspects, Forster, R. E., Edsall, J. T., Otis, A. B. and Roughton, R. J. W., eds., NASA SP-188, Washington, D. C., 41-45
9. Lippmaa, E. and Pehk, T. (1967) Kem. Teollisuus 24, 1001-1011
10. Hagen, R. and Roberts, J. D. (1969) J. Amer. Chem. Soc. 91, 4504-4506
11. Stadie, W. C. and O'Brien, H. (1936) J. Biol. Chem. 112, 723-758
12. Doddrell, D., Glushko, V. and Allerhand, A. (1972) J. Chem. Phys. 56, 3683-3689
13. Gurd, F. R. N. and Keim, P. (1973) Methods Enzymol., Hirs, C. H. W. and Timasheff, S. N. eds., Academic Press, New York, 27D, 836-911

14. Kuhlmann, K. F., Grant, D. M. and Harris, R. K. (1970) J. Chem. Phys. 52, 3439-3448
15. Farrar, T. C., Druck, W. J., Shoup, R. R. and Becker, E. D. (1972) J. Amer. Chem. Soc. 94, 699-703
16. Johnson, C. S., Jr. (1965) in Advan. Mag. Res., J. S. Waugh ed., Academic Press, New York, 7, 33-102
17. Caplow, M. (1968) J. Amer. Chem. Soc. 90, 6795-6803
18. McConnell, H. M. (1958) J. Chem. Phys. 28, 430-431
19. Bothner-By, A. A. and Gassend, R. (1973) Ann. N. Y. Acad. Sci. 222, 668-675
20. Kilmartin, J. V. and Rossi-Bernardi, L. (1973) Physiol. Rev. 53, 836-890
21. Cohn, E. J. and Edsall, J. T. (1943) Proteins, Amino Acids and Peptides as Ions and Dipolar Ions, Reinhold Publishing Corp., New York, New York, 78-88
22. Schwarzenbach, G. (1938) Z. Electrochem. 44, 46-55
23. Rule, C. K. and LaMer, V. K. (1938) J. Amer. Chem. Soc. 60, 1974-1981
24. Glasoe, P. K. and Long, F. A. (1960) J. Phys. Chem. 64, 188-190
25. Pocker, Y. (1969) in Carbon Dioxide: Chemical, Biochemical and Physiological Aspects, Forster, R. E., Edsall, J. T., Otis, A. B. and Roughton, R. J. W., eds., NASA SP-188, Washington, D. C., 31
26. Pocker, Y. and Meany, J. E. (1967) J. Phys. Chem. 71, 3113-3120
27. Pocker, Y. and Meany, J. E. (1968) J. Phys. Chem. 72, 655-659
28. Edsall, J. T. (1969) in Carbon Dioxide: Chemical, Biochemical and Physiological Aspects, Forster, R. E., Edsall, J. T., Otis, A. B. and Roughton, F. J. W., eds., NASA SP-188, Washington, D. C., 15-27

29. Levy, G. C. and Nelson, G. L. (1972) in Carbon-13 Nuclear Magnetic Resonance for Organic Chemists, Wiley-Interscience, New York, 19
30. Gurd, F. R. N., Keim, P., Glushko, V., Lawson, P. J., Marshall, R. C., Nigen, A. M. and Vigna, R. A. (1972) in Chemistry and Biology of Peptides, Meienhofer, J., ed., Ann Arbor Science Publishers, Inc., Ann Arbor, Michigan, 45-49
31. Keim, P., Vigna, R. A., Morrow, J. S., Marshall, R. C. and Gurd, F. R. N. (1973) J. Biol. Chem. 248, 6104-6113
32. Keim, P., Vigna, R. A., Morrow, J. S., Marshall, R. C. and Gurd, F. R. N. (1973) J. Biol. Chem. 248, 7811-7818
33. Keim, P., Vigna, R. A., Nigen, A. M., Morrow, J. S. and Gurd, F. R. N. (1974) J. Biol. Chem., in press
34. Roughton, F. J. W. and Booth, V. H. (1938) Biochem. J. 32, 2049-2069
35. Horsley, W. J., Sternlicht, J. and Cohen, J. S. (1970) J. Amer. Chem. Soc. 92, 680-686
36. Stothers, J. B. and Lauterbur, P. C. (1964) Canad. J. Chem. 42, 1563-1576
37. Stothers, J. B., (1972) Carbon-13 NMR Spectroscopy, Academic Press, New York, 282-283
38. Johnson, L. F. and Jankowski, W. C. (1972) Carbon-13 Spectra, Wiley-Interscience, New York, 37
39. Johnson, L. F. and Jankowski, W. C. (1973) Carbon-13 Spectra, Wiley Interscience, New York, 86
40. Stothers, J. B. (1972) Carbon-13 NMR Spectroscopy, Academic Press, New York, 150
41. Grant, D. M. and Chener, B. V. (1967) J. Amer. Chem. Soc. 89, 5315-5318

42. Gurd, F. R. N., Lawson, P. J., Cochran, D. W. and Wenkert, E. (1971) J. Biol. Chem. 246, 3725-3730
43. Christl, M. and Roberts, J. D. (1972) J. Amer. Chem. Soc. 94, 4565-4573
44. Taddei, F. and Pratt, L. (1964) J. Chem. Soc. 1553-1559
45. Ponnuswamy, P. K. and Sasisekharan, V. (1971) Int. J. Protein Research 3, 1-8
46. Ponnuswamy, P. K. and Sasisekharan, V. (1971) Biopolymers 10, 565-582
47. Pachler, K. G. R. (1963) Spectrochim. Acta 19, 2085-2092
48. Pachler, K. G. R. (1964) Spectrochim. Acta 20, 581-587
49. Bovey, F. A. (1972) High Resolution NMR of Macromolecules, Academic Press, New York, Chap. 3
50. Kopple, K. D., Wiley, G. R. and Taube, R. (1973) Biopolymers 12, 627-636
51. Weinkam, R. J. and Jorgensen, E. C. (1973) J. Amer. Chem. Soc. 95, 6084-6090
52. Morishima, I., Yoshikawa, K., Okada, K., Yonezawa, T. and Goto, K. (1973) J. Amer. Chem. Soc. 95, 165-171
53. McFarlane, W. (1970) Chem. Commun. 418-419
54. Kroschwitz, J. I., Winkur, M., Reich, H. J. and Roberts, J. D. (1969) J. Amer. Chem. Soc. 91, 5927-5928
55. Grover, S. H., Guthrie, J. P., Stothers, J. B. and Tan, C. T. (1973) J. Magn. Resonance 10, 227-230
56. Stothers, J. B., Tan, C. T. and Theo, K. C. (1973) Can. J. Chem. 51, 2893-2901

57. Quirt, A. R., Lyerla, J. R., Jr., Peat, J. R., Cohen, J. S., Reynolds, W. F. and Freedman, M. H. (1974) *J. Amer. Chem. Soc.* 96, 570-574
58. Horsley, W. J. and Sternlicht, H. (1968) *J. Amer. Chem. Soc.* 90, 3738-3748
59. Batchelor, J. G., Prestegard, J. H., Cushley, R. J. and Lipsky, S. R. (1973) *J. Amer. Chem. Soc.* 95, 6358-6364
60. Tran-Dinh, S., Fermandjian, S., Sala, E., Mermet-Bouvier, R., Cohen, M. and Fromageot, P. (1974) *J. Amer. Chem. Soc.* 96, 1484-1493
61. Beecham, A. F. and Ham, N. S. (1968) *Tetrahedron* 24, 2773-2781
62. Ramachandran, G. N., Chandrasekaran, R. and Kopple, K. D. (1971) *Biopolymers* 10, 2113-2131
63. Fillaux, F. and deLozé, C. (1972) *Biopolymers* 11, 2063-2077
64. Taft, R. W., Jr., (1956) in *Steric Effects in Organic Chemistry*. M. S. Newman ed., John Wiley, and Sons, London, 578
65. Watson, H. C. (1969) *Progr. Stereochem.* 4, 299-333
66. Kilmartin, J. V. and Rossi-Bernardi, L. (1971) *Biochem. J.* 124, 31-45
67. Ramachandran, G. N., Lakshminarayanan, A. V., Balasubramaniam, R. and Tegoni, G. (1970) *Biochem. Biophys. Acta* 221, 165-181
68. Balasubramaniam, R., Lakshminarayanan, A. V., Sabesan, M. N., Tegoni, G., Venkateson, K. and Ramachandran, G. N. (1971) *Int. J. Protein Research* 3, 25-33
69. Dorman, D. E. and Bovey, F. A. (1973) *J. Org. Chem.* 38, 2379-2383
70. Ramachandran, G. N. and Sasisekharan, V. (1968) *Advan. Prot. Chem.* 23, 283-437

71. Edsall, J. T. and Wyman, J. (1958) Biophysical Chemistry, Academic Press, New York, 1, 496-504
72. Deken, R. H., de Broekhuysen, J., Biechlet, J. and Mortier, A. (1956) Biochim. Biophys. Acta 19, 45-52
73. Wallenfels, K. and Streffer, C. H. (1966) Biochem. Z. 346, 119-132
74. Edsall, J. T. (1965) Biochem. 4, 28-31
75. Flohé, L., Breitmaier, E., Günzler, W. A., Voelter, W. and Jung, G. (1972) Hoppe-Seyler's Z. Physiol. Chem. 353, 1159-1170
76. Benesch, R. E. and Benesch, R. (1955) J. Amer. Chem. Soc. 77, 5877-5881
77. Mori, N., Takahashi, Y. and Tsuzuki, Y. (1967) Bull. Chem. Soc. Jap. 40, 2720-2721
78. Eigen, M. and DeMaeyer, L. (1963) in Technique of Organic Chemistry, 2nd ed., Freiss, S. L., Lewis, E. S. and Weissberger, A., eds., New York, Academic Press, 8, Part II, 1040
79. Tanford, C. (1962) Adv. Prot. Chem. 17, 69-165
80. Shire, S. J., Hanania, G. H. and Gurd, F. R. N. (1974) Biochem. 13, in press
81. Shire, S. J., Hanania, G. H. and Gurd, F. R. N. (1974) Biochem. 13, in press
82. Grafius, M. A. and Neilands, J. B. (1955) J. Amer. Chem. Soc. 77, 3389-3390
83. Fujiwara, S. and Arata, Y. (1963) Bull. Chem. Soc. Japan 36, 578-579
84. Fujiwara, S. and Arata, Y. (1964) Bull. Chem. Soc. Japan 37, 344-349
85. Martin, R. B. and Mathur, R. (1965) J. Amer. Chem. Soc. 87, 1065-1070

86. Casey, J. P. and Martin, R. B. (1972) J. Amer. Chem. Soc. 94, 6141-6151
87. Bovey, F. A. (1969) Nuclear Magnetic Resonance Spectroscopy, Academic Press, New York, Chapter IV
88. Garner, M. H., Garner, W. H. and Gurd, F. R. N. (1973) J. Biol. Chem. 248, 5451-5455



CHAPTER IV

Interaction of CO₂ with Adult Human Hemoglobin

Chapter IV

Interaction of CO₂ with Adult Human Hemoglobin

Great importance is attributed to the interaction of carbon dioxide with hemoglobin (1,2). Particular attention has been directed to the "oxygen linked" (3) nature of the interaction, reportedly by carbamino formation with the four NH₂-terminal groups of the α - and β -chains (4-6). Binding of CO₂ at other sites is considered negligible under physiological conditions (4-7), although non-carbamate binding has been reported (3,8-15). In Chapter IV, the analytical discrimination of ¹³C Fourier transform NMR is used to explore the hemoglobin interaction with CO₂. The results are in accord with the expected allosteric linkage to the ligand state of the heme, and find ready stereochemical explanation based on the x-ray studies of Arnone and Perutz et al. (11,16-19). However, some findings if accepted would reverse previous interpretations (6,20) attributing to the α -chain NH₂-terminus the most significant role in CO₂ binding. An alternative interpretation of the data would suggest the existence of at least two slowly interconverting ($k \leq 1 \text{ sec}^{-1}$) deoxyhemoglobin conformations in the solutions studied.

Observation of [¹³C]-Carbamino Resonances in Hemoglobin. The equilibration of 5 to 15 millimolar solutions of hemoglobin with ¹³CO₂ and [¹³C] bicarbonate and carbonate (Chapter II) allowed carbamino resonances (Chapter III) to be clearly observed. At the lowest levels of carbonates and at pH values near 7, the enhanced

CO_2 affinity characteristic of deoxyhemoglobin (21) was plainly apparent. Examples of the observations obtained in such experiments on adult human hemoglobin are shown in Figure 1. The solution in Figure 1A was a hemolyzate containing 0.9 mM acetazolamide necessary to inhibit the carbonic anhydrase present in such preparations. As discussed in Appendix B, active carbonic anhydrase broadens the bicarbonate and CO_2 resonances markedly. In Figure 1A, 9.9 mM hemoglobin was equilibrated with 7.2 mM total carbonates at pH 7.20; the corresponding pCO_2 pressure was near 15 mm Hg. In Figure 1B 14.5 mM HbCO was equilibrated with 17.0 mM total carbonates at pH 6.98. In Figure 1C, 13.0 mM ferrihemoglobin was equilibrated with 17.6 mM total carbonates at pH 6.78. The ^{13}C mole fraction in CO_2 was not less than 0.80 in any spectrum. As is apparent from the figure, only the deoxyhemoglobin solution clearly exhibited a ^{13}C resonance attributable to the carbamino adduct. The large bicarbonate-carbonate resonance, present in all solutions, was at 32.6 ± 0.1 ppm as previously described (Chapter III). Dissolved $^{13}\text{CO}_2$ is only weakly represented in Figure 1A, but is apparent in 1B and 1C near 68.3 ppm. The broad resonances between 10 and 24, and 40 and 70 ppm arise from the natural abundance ^{13}C in the protein, comparable to the NMR spectrum of myoglobin in Chapter III.

Raising the pH and/or carbonate levels does not erase the contrast between deoxyhemoglobin and the oxidized or liganded forms. In Figure 2 examples of observations at increased carbonate and pH levels are shown. All samples are purified hemoglobin component A_0 . In

Figure 1. 15.1 MHz ^{13}C NMR spectra of human hemoglobin equilibrated with $^{13}\text{CO}_2$ under various conditions. (A) Hb; (B) HbCO; (C) ferri Hb. All solutions contained 0.9 mM acetazolamide to inhibit the carbonic anhydrase present in these hemolyzate preparations. Temp. was 33-34°. See text for details.

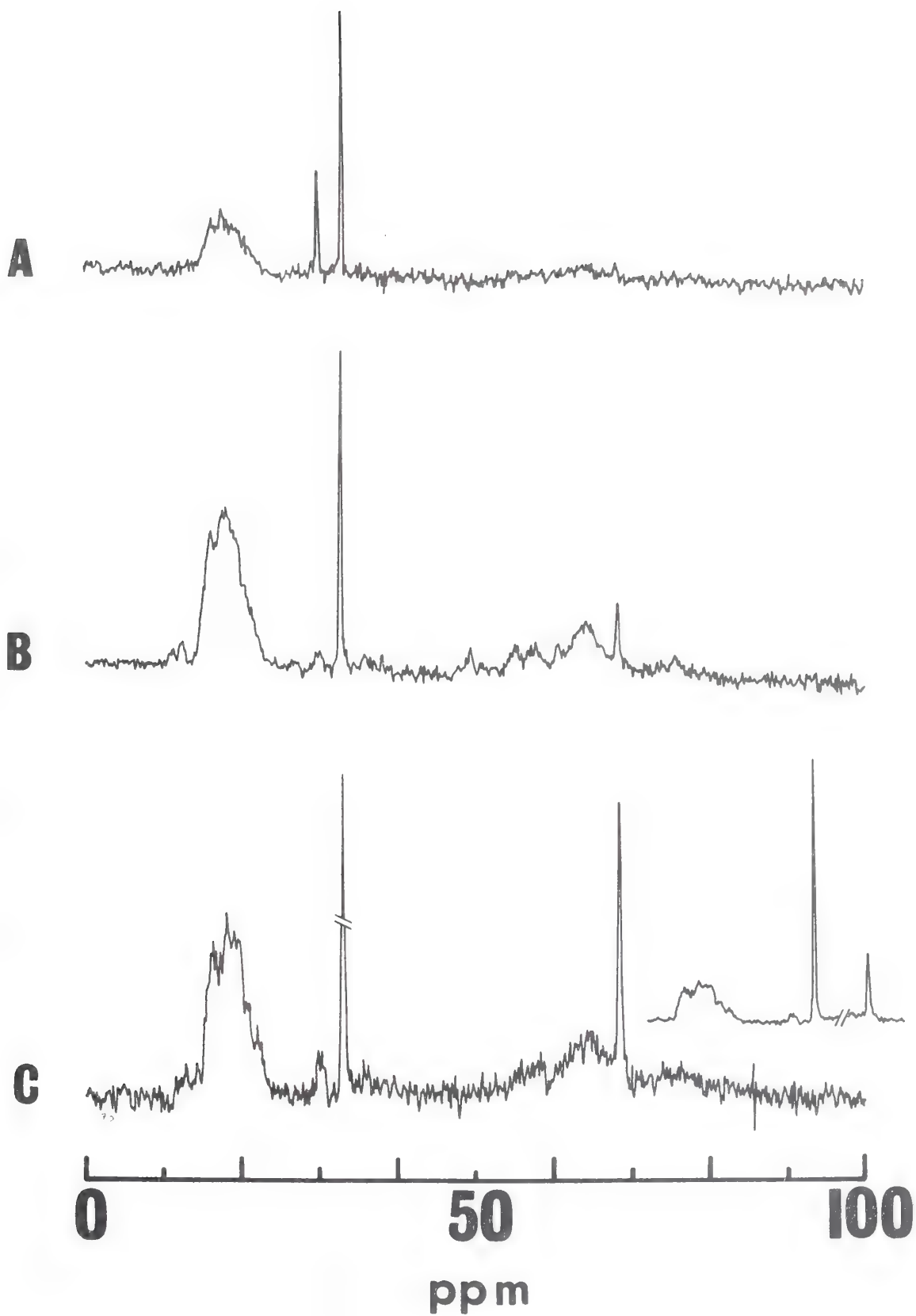
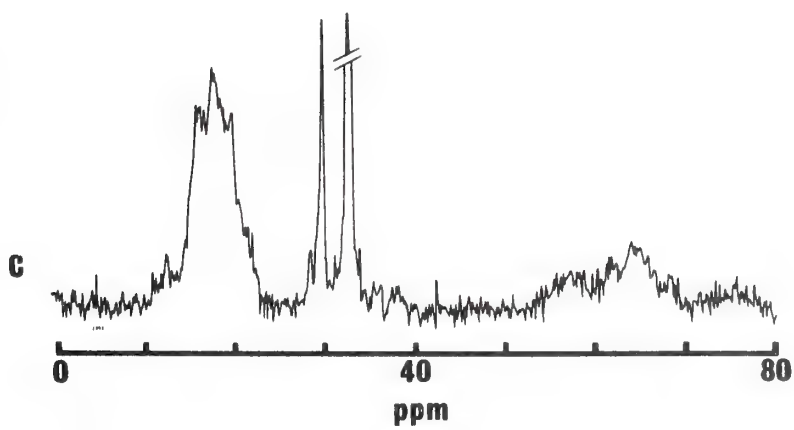
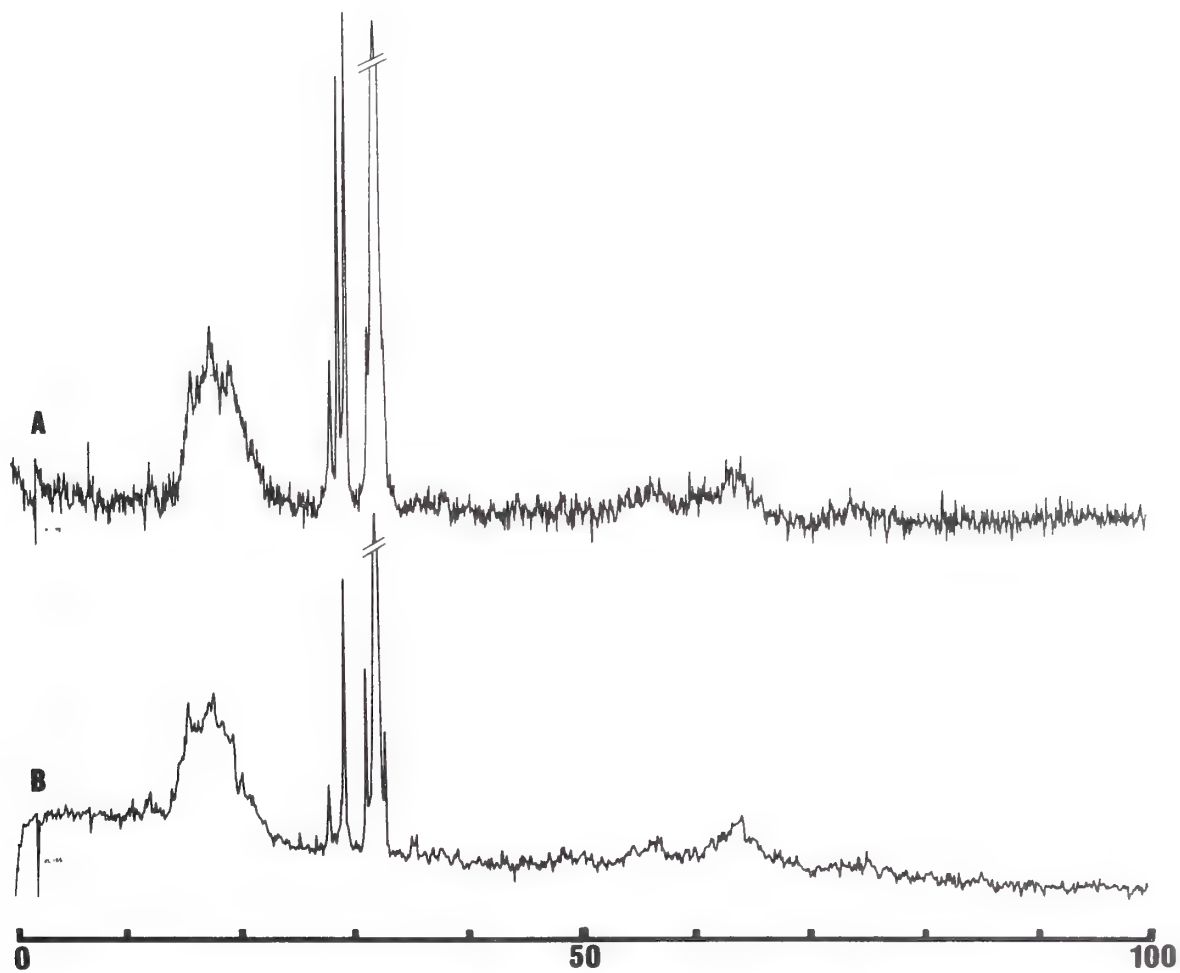


Figure 2A, 13.07 mM deoxyhemoglobin is equilibrated with 68 mM total carbonates at pH 8.47. Most strikingly, three resonances are now clearly discernible in the carbamino region. The largest and most upfield resonance (excluding bicarbonate-carbonate) is as before at 29.8 ppm. Immediately downfield is another resonance near 29.2 ppm, and a third much smaller resonance falls at 28.4 ppm. Conversely, carboxyhemoglobin, Figure 2B, shows only two resonances in this region under similar conditions, an upfield peak at 29.8 ppm, and a small peak at 28.4 ppm. The ferrihemoglobin spectrum, Figure 2C, was recorded at a lower magnetic field strength than the spectra shown in 2A and 2B. Nevertheless, the nearly identical resonance pattern as that of carboxyhemoglobin under these conditions is evident. In Figure 2B, the hemoglobin concentration was 16.80 mM, the pH was 8.47, and total carbonates were 46 mM. In Figure 2C, 10.44 mM ferrihemoglobin was in equilibrium with 49 mM total carbonates at a pH of 8.23. The ^{13}C enrichment levels are similar to those in Figure 1. The relative chemical shift of the large bicarbonate-carbonate resonance reflects the higher pH of this study (Chapter III).

Apart from the resonances which fall in the "carbamino region" from 28 to 30 ppm as shown in Figures 1 and 2, an additional resonance was apparent in some solutions, particularly under the conditions of low pH and high carbonate levels. In most instances, this resonance, near 33 to 34 ppm, was detectable only as a shoulder on the large bicarbonate-carbonate resonance, indistinguishable in

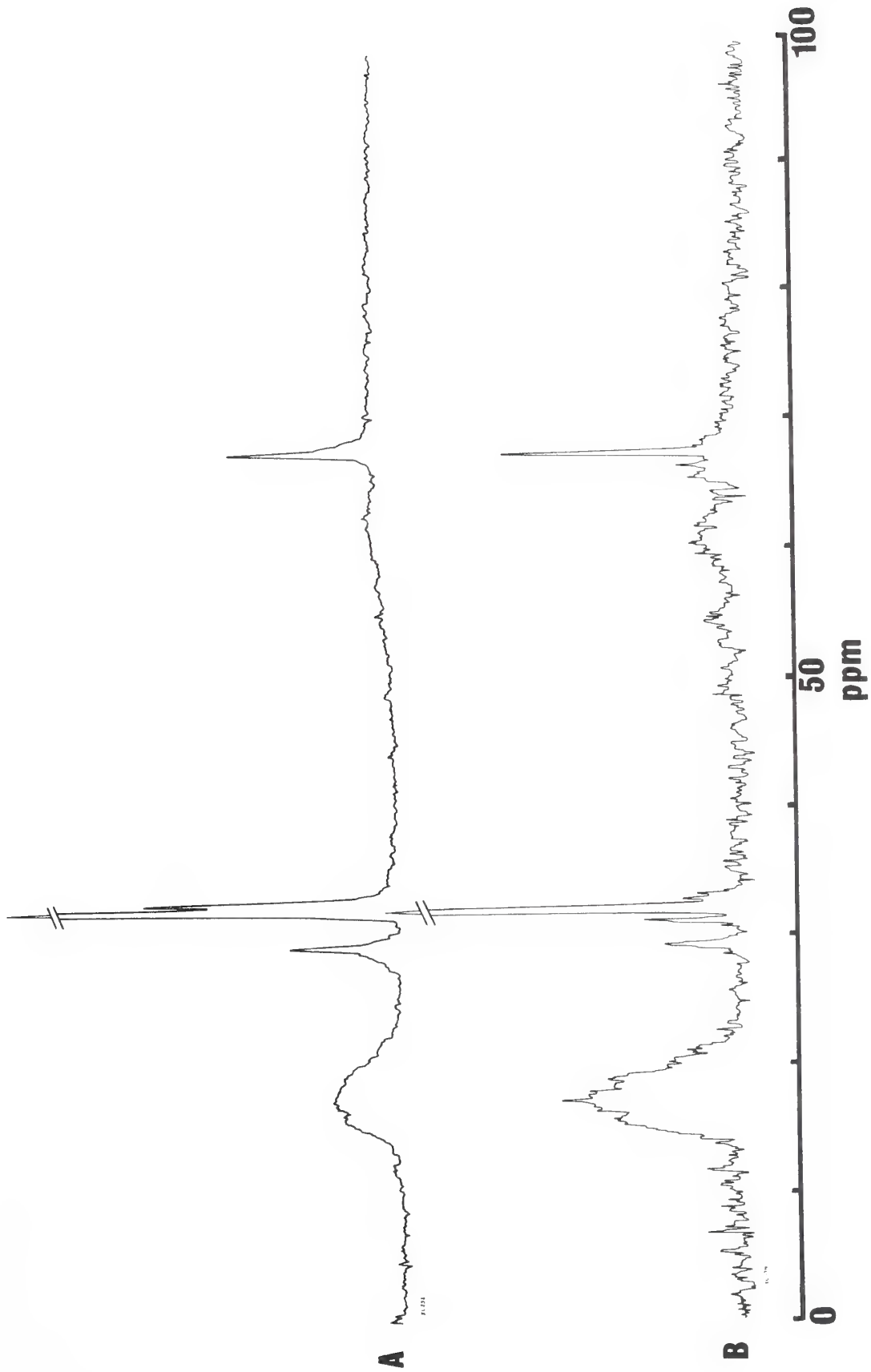
Figure 2. ^{13}C NMR spectra of purified HbAo equilibrated with $^{13}\text{CO}_2$ at higher values of pH than in Figure 1. (A) HbAo, pH 8.47, 68 mM total carbonates; (B) HbAoCO, pH 8.47, 46 mM total carbonates; (C) ferri HbAo, pH 8.23, 49 mM total carbonates. The latter spectrum was recorded at 15.1 MHz , while the rest were recorded at 25.2 MHz .



most instances from a spinning side band. Its intensity was highly variable, but its position when observed was insensitive to the rate of sample spinning. Under optimum conditions it could be resolved, as shown in Figure 3, for both deoxyhemoglobin (A) and carboxyhemoglobin (B). The hemoglobin concentrations were 16.25 and 10.64 mM, total carbonate concentrations were 69 and 64 mM, and the pH of the experiments 7.14 and 6.92 for A and B, respectively. The chemical shift of this resonance, if observable, was variable, but tended to shift to lower fields with increasing pH (Figures 4 and 5). It has been noted in solutions of both deoxy and carboxyhemoglobin, in deoxyhemoglobin with the alpha NH₂-terminal blocked, and in the presence of IHP (see below). It is not present under the combined conditions of low pH and low carbonate levels (Figure 1), nor is it regularly observed at high pH values when the bicarbonate-carbonate resonance titrates downfield. Its precise chemical nature remains a mystery, although on the basis of the pH dependence and chemical shift it is unlikely to be a carbamate. A possible identity as the CO₂ or bicarbonate observed near the heme pocket on x-ray analysis (11), or as a contributor to increased CO₂ binding under acid conditions (8,9) is evident. It does not appear to be appreciably "oxygen linked".

Chemical Shift Titration Behavior. Observations of the carbamate resonance chemical shifts over their pH ranges of stability showed only small changes (Figures 4-6). At pH values below 7.3, in solutions with sufficient total carbonates to form measurable

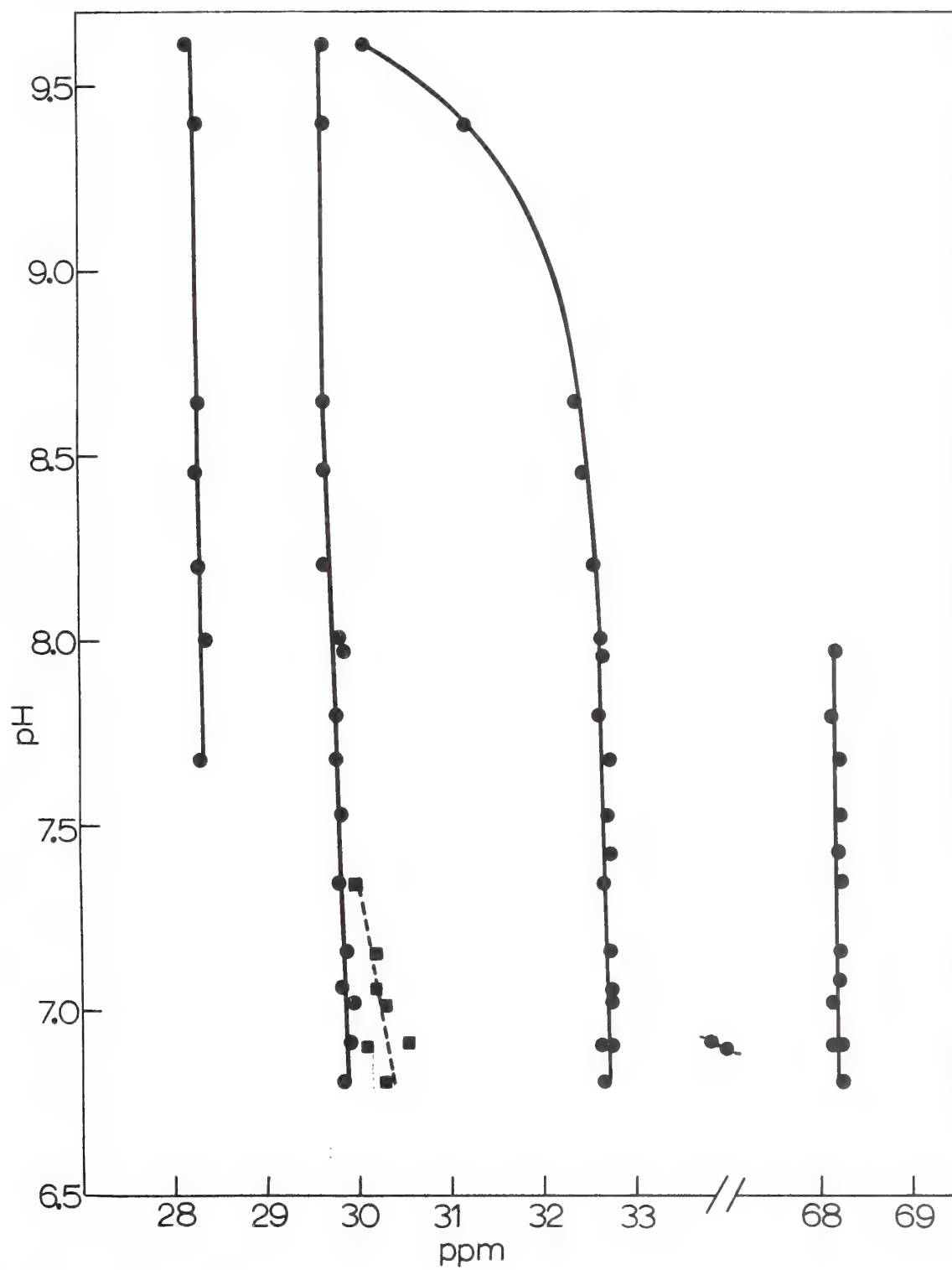
Figure 3. 25.2 MHz ^{13}C NMR spectra of (A) HbAo; (B) HbAoCO. Of interest is the resonance near 33.4 ppm, just upfield of the large bicarbonate - carbonate resonance. It is most clearly seen in the deoxy sample, but still apparent upfield of the large bicarbonate resonance in HbAoCO. Interference from a spinning sideband in this region introduces some ambiguity into the exact assignment in the HbAoCO sample. Conditions of the measurements were pH 7.14 and 6.92, at total carbonate levels of 69 and 64 mM respectively.



levels of carbamates (Equation 10, Chapter III), two resonances of approximately equal intensity were apparent near 29.9 and 30.5 ppm in carboxyhemoglobin (Figure 4). At slightly higher pH values, these resonances merge, yielding the single previously described resonance near 29.8 ppm. The titration results are thus suggestive that the resonance observed at 29.8 ppm in carboxyhemoglobin above pH 7.3 enjoys contributions from at least two different sites, which become magnetically distinct at low pH values. The shift behavior is reminiscent of that seen in the case of cysteine carbamate (Chapter III). As such, the increasing magnetic nonequivalence of the two sites at low pH may arise from a changing electrostatic environment (22,23) presumably due to protonation of a nearby group. The pKa of this group would fall between 6 and 7.5. Protonation of the carbamate itself (22-24), or what is more likely the existence of multiple long lived protein conformations (25-27) also must be considered. The chemical shift of the small resonance appearing only at high pH values was near 28.4 ppm. Its position and requirement for high pH point to ϵ -amino adducts (Chapter III).

In solutions of deoxyhemoglobin (Figure 5), the carbamate resonance positions were generally little affected by changes in pH. However, at pH values below 7.2, the carbamate resonance ordinarily near 29.2 ppm broadens and shifts to higher magnetic fields. Below neutrality this diminutive resonance contributes only a broad base to the much larger (and narrower) unshifted resonance at 29.8 ppm. As discussed in greater detail below, the observed resonance broadening

Figure 4. Titration behavior of ^{13}C resonances observed upon introduction of $^{13}\text{CO}_2$ into solutions of HbAOCO; temperature was 29-31°. Chemical shifts are expressed relative to external CS_2 .



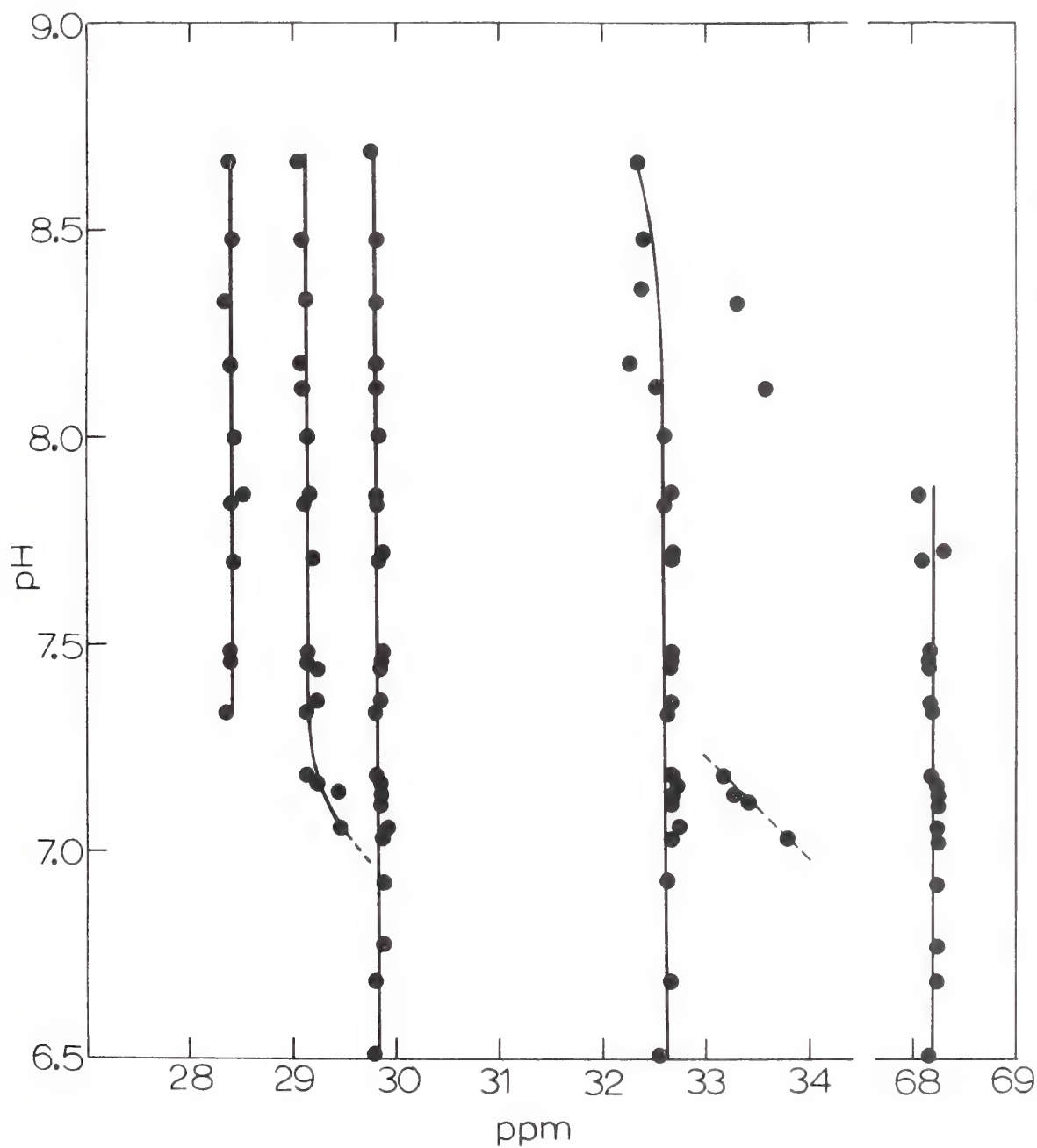


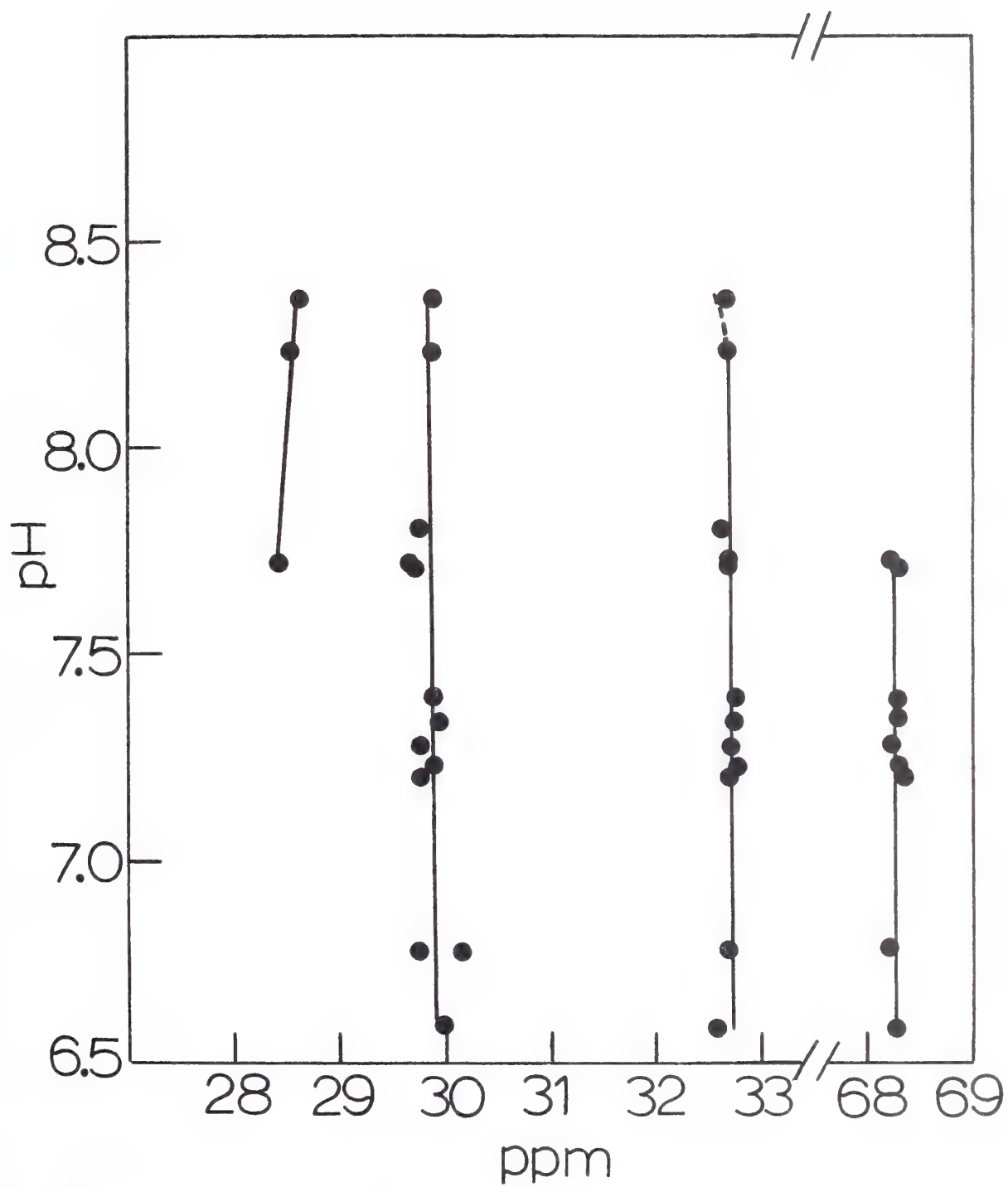
Figure 5. Titration behavior of ^{13}C resonances observed upon introduction of $^{13}\text{CO}_2$ into solutions of deoxy HbAo. Conditions were as in Figure 4.

and shift are indicative of exchange effects either with dissolved CO_2 (28,29) or between different deoxyhemoglobin conformations (25-28). Similar effects were observed for the carbonic anhydrase modulated exchange of the bicarbonate-carbonate and CO_2 resonances (see Appendix B).

Except for the absence of the small resonance near 30.5 ppm, the titration of the carbamates in ferrihemoglobin (Figure 6) is essentially indistinguishable from that of carboxyhemoglobin. This is consonant with reports of their nearly identical crystallographic structure (16,17). The aforementioned peak upfield of the bicarbonate resonance was never observed in ferrihemoglobin; the lower magnetic field strength at which most of the ferrihemoglobin titrations were measured may be responsible (14.1 versus 24.5 kG). An interpretation implicating the paramagnetic ($S = 5/2$) iron (30) is weakened but not excluded by the clear observation of this resonance in deoxyhemoglobin ($S = 4/2$).

Identification of Resonances. If the carbamate resonances observed in neutral solutions of hemoglobin represent adducts of the NH_2 -terminal valine residues of the α - and β -chains (4-7,20), their chemical shifts are unusual when compared with the valine peptides described in Chapter III. Magnetic non-equivalence arising from conformational and electrostatic constraints, as characteristic of proteins, is well known (31,32). Examples of similar constraints with perturbations of the carbamate chemical shift were evident in Chapter III for L-proline and L-cysteine. Thus, the chemical shift

Figure 6. Titration behavior of ^{13}C resonances observed upon introduction of $^{13}\text{CO}_2$ into solutions of ferri HbAo. These measurements were made at 15.1 MHz , whereas those reported in Figures 4 and 5 were made at 25.2 MHz . Conditions otherwise were the same. See text for details.



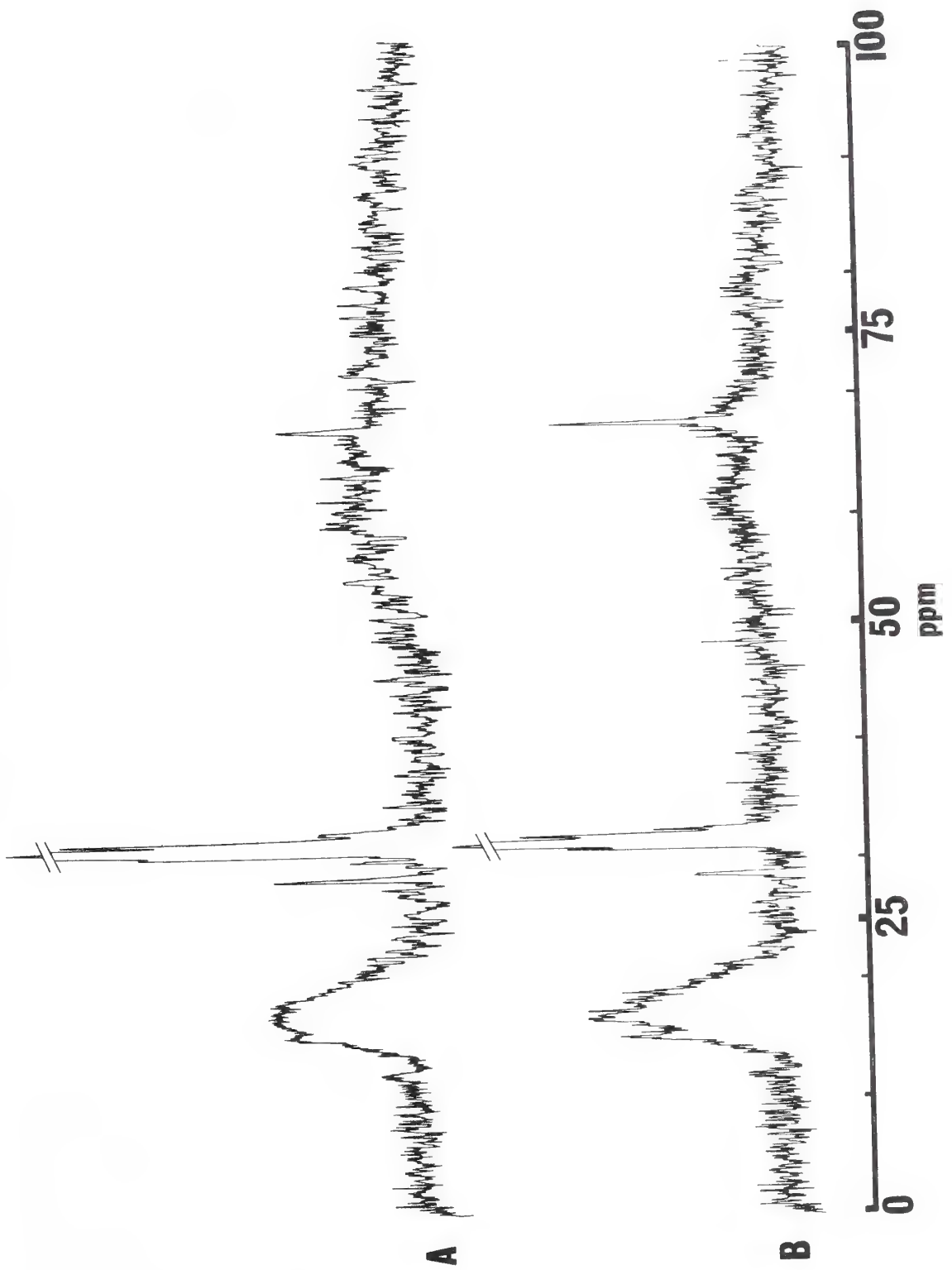
of the carbamate resonances suggests only that there exist two conformationally constrained sites in deoxyhemoglobin, one of which changes dramatically upon conversion to the "oxy" or "R" form of the protein. Such criteria can describe either NH₂-terminus (16-19).

The question of assignments was approached by chemical modification of the NH₂-terminals, by observation of the competition between IHP and CO₂ for a common binding site (33,34), and by the observation of carbamino formation in hemoglobin H, the β -chain tetramer, a protein reportedly exhibiting the "deoxy" or "T" conformation independent of ligand state (35).

In Figure 7 are shown the results following equilibration with CO₂ of hemoglobin A₀ ($\alpha_2^C\beta_2$), a protein which had been prepared from alpha-chains blocked at the NH₂-terminus with cyanate. Sequential Edman degradation confirmed a reduction in reactive alpha chain of 90%. The conditions of Figure 7 were (A) 7.07 mM deoxyhemoglobin ($\alpha_2^C\beta_2$), 62 mM total carbonates, pH 7.42; (B) 7.07 mM carboxyhemoglobin ($\alpha_2^C\beta_2$), 52 mM total carbonates, pH 7.68. In Figure 7A, the single adduct resonance is at 29.8 ppm. Under comparable conditions, unmodified HbA₀ would be expected to show at least two resonances of nearly equal intensity (Figure 2A).

While an assignment of the missing peak at 29.2 ppm to the alpha chain is thus reasonable, the matter is clouded by the diminished intensity of the remaining carbamino resonance relative to the protein carboxyl resonances. The precise reason for this is not apparent, although it may be related to the formation of ferrihemoglobin over the duration of the measurement. The problem of auto-

Figure 7. 25.2 MHz ^{13}C NMR spectra of hemoglobin Ao, which had been modified by selective blockage of the alpha chain NH_2 -terminus with cyanate. In (A) deoxy Hb ($\alpha_2^c\beta_2$), pH 7.42, 62 mM total carbonates; (B) carboxyhemoglobin ($\alpha_2^c\beta_2$), pH 7.68, 52 mM total carbonates. See text for details.



oxidation of deoxy Hb ($\alpha_2\beta_2^C$) proved to be quite severe even with precautions against trace metal contamination (36). After the spectral measurement shown in Figure 7A was complete (requiring 18.4 hrs. at 30°), the measured ferrihemoglobin level was 25%.

In carboxyhemoglobin ($\alpha_2\beta_2^C$) (Figure 7B) autooxidation was not a problem. The single carbamate resonance falls at 29.8 ppm, identical to that found in unmodified carboxyhemoglobin. A comparison of its integral area with unmodified samples under similar conditions (see below) indicates that the adduct resonance is nearly 50% smaller than expected. Thus, in carboxyhemoglobin the carbamino adducts bound to either the alpha chain or beta chain NH_2 -terminals appear to be magnetically equivalent and of nearly equal populations. The magnetic equivalence of the carbamino groups is reminiscent of the lone α -amino adduct resonance observed in solutions of [^{13}C] cyanate treated carboxyhemoglobin (37).

Observations on hemoglobin solutions under conditions in which the β -chain NH_2 -terminus would be unreactive to CO_2 are shown in Figure 8. In Figure 8A, 2.39 mM deoxyhemoglobin specifically reacted with cyanate at the β -chain NH_2 -terminus ($\alpha_2\beta_2^C$) is shown after equilibration with 47 mM total carbonates at pH 7.91. While the reduced signal to noise ratio of this spectrum limits detailed interpretation, it is apparent that the resonance at 29.2 ppm is now of increased intensity relative to that near 29.8 ppm. In stripped unmodified hemoglobin A_0 , this is never observed; under the conditions of the figure the resonance at 29.8 ppm would be expected at least

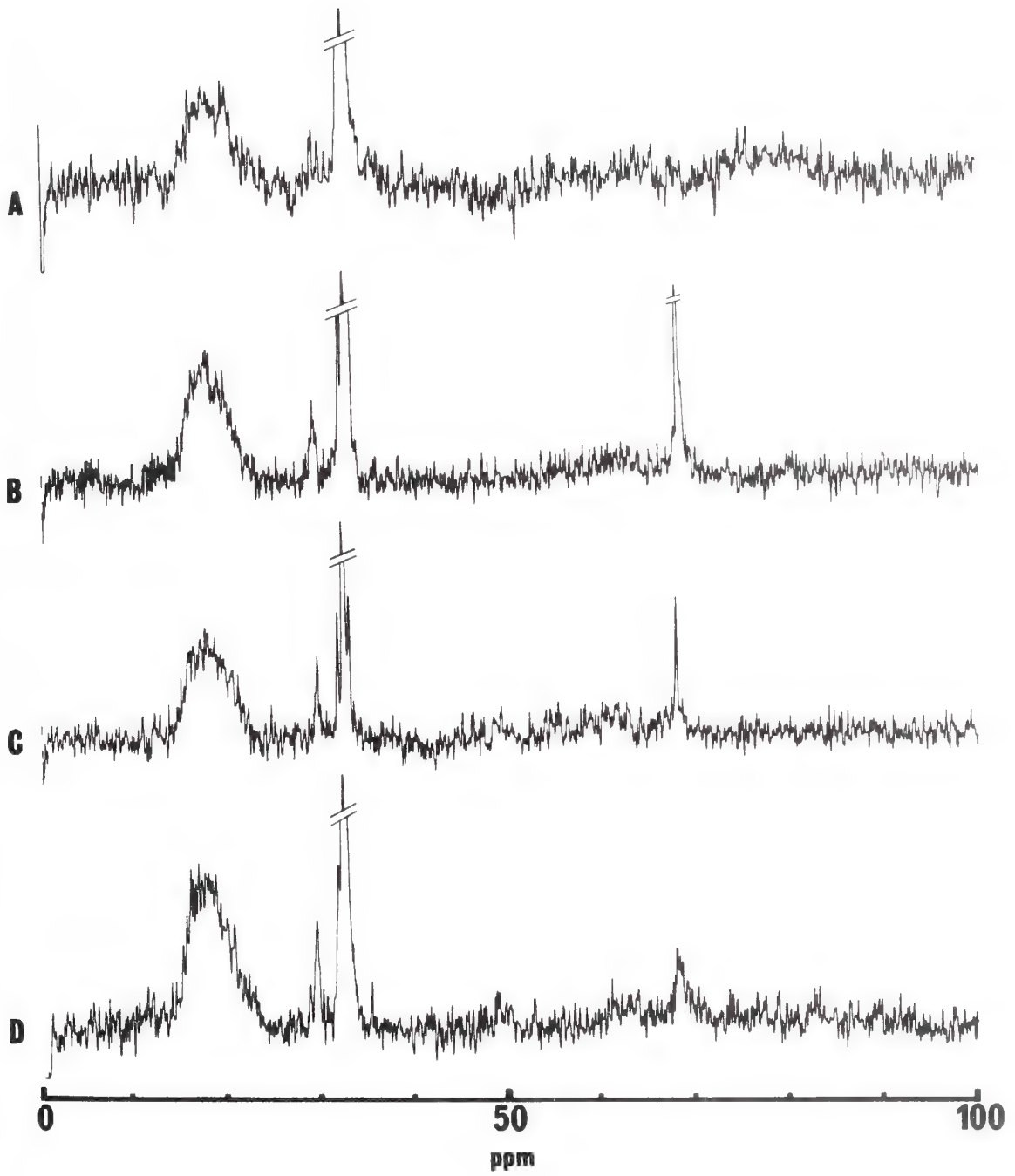
to match the intensity of the protein carboxyl resonances (cf. Figure 2). The sample used for the measurement in Figure 8A showed less than 5% of its β -chain to be reactive to the Edman reagent. The assignment suggested in Figure 8A of the missing resonance at 29.8 ppm to the β -chain NH_2 -terminal CO_2 adduct is strengthened by the observations shown in Figure 8B on a 9.16 mM deoxyhemoglobin solution equilibrated with 64 mM total carbonates at pH 7.20, in the presence of 3 to 4 mM inositol hexaphosphate (IHP). IHP is known to bind very strongly to the anion binding site of hemoglobin (34). The residues involved are valine 1 β , histidine 2 β and histidine 143 β , and lysine 82 β . No such interaction near the alpha-chain NH_2 -terminus has been found (34). The complete elimination of the resonance expected at 29.8 ppm in solutions containing IHP (Figure 8B) is thus consistent with the above assignment. The sole carbamate resonance in Figure 8B is at 29.2 ppm. While broader than the comparable resonance in solutions without IHP, its integral area is unchanged within the limits of experimental error ($\pm 10\%$). In Figure 8C is shown the spectrum of a 10.06 mM carboxyhemoglobin A_0 sample with 37 mM total carbonates, pH 7.65, and an IHP concentration of 3 to 4 mM. The single carbamate resonance is at 29.8 ppm; its integral area relative to the protein is only marginally reduced ($\sim 10\text{-}30\%$) when compared with samples under the same conditions without IHP.

Observations on a single sample of carboxy β -chain tetramer are shown in Figure 8D. The reduced level of isotopic enrichment of the

Figure 8. 25.2 MHz ^{13}C NMR spectra of hemoglobin equilibrated with $^{13}\text{CO}_2$, under conditions in which the β -chain NH_2 -terminus would not be expected to form a carbamate.

- (A) 2.39 mM solution of deoxy HbAo ($\alpha_2\beta_2^c$), a preparation with the β -chain NH_2 -terminus blocked with cyanate. pH was 7.91, 47 mM total carbonates.
- (B) 9.16 mM deoxyhemoglobin solution equilibrated with 64 mM total carbonates at pH 7.2, in the presence of 3-4 mM IHP.
- (C) 10.06 mM carboxyhemoglobin with 3-4 mM IHP. pH was 7.65; total carbonates 37 mM.
- (D) 9.74 mM solution of beta chain tetramers (β_4), equilibrated with $^{13}\text{CO}_2$. pH was 7.58 with 31 mM total carbonates.

See text for further details.



carbonates in this measurement ($\chi^{13\text{C}} = 0.31$ versus 0.88) must be considered in any comparison with the other spectra of Figure 6. However, measurement of the integral area of the large carbamate resonance at 29.6 ppm suggests a mole fraction (Z) of CO_2 bound per β -chain near 0.4. The conditions of the measurement were 9.74 mM hemoglobin and 31 mM total carbonates at pH 7.58. The high affinity for CO_2 suggested by the above resonance as well as its chemical shift are reminiscent of the most upfield carbamate resonance (Figure 2) observed in solutions of deoxyhemoglobin. The origin of the very small resonance at 29.0 ppm in Figure 8D is unknown, but may be related to slight heterogeneity in this β -chain preparation, as evidenced by electrophoretic tailing following recombination of the chains. Multiple conformational states of the protein are also possible.

The simplest interpretation consonant with the above results would thus assign in deoxyhemoglobin the resonance near 29.2 ppm to the α -chain adduct, and the resonance near 29.8 ppm to the β -chain adduct. The resonance observed near 28.4 ppm under conditions of high pH most likely represents one or perhaps multiple ϵ -amino adducts. In carboxy (or oxy) hemoglobin, and probably ferrihemoglobin as well, the carbamate resonance near 29.8 ppm may be assigned to approximately equal contributions ($\pm 20\%$) from the NH_2 -terminal adducts of both chains.

The identity of the adduct shifted to slightly higher fields under more acidic conditions is unproven, although only the β -chain

NH₂-terminus is near groups ionizing in this pH range (22,23,33). The observation of the resonance near 33 ppm (Figure 3) in HbA₀ ($\alpha_2\beta_2$) and HbA₀ solutions with IHP makes its assignment to a carbamate implausible. The pCO₂ pressures under the conditions of these experiments exceed 200 mm Hg at low pH values (Table II, Chapter II). The protein also becomes increasingly more protonated as the pH falls. Either factor could contribute to enhanced non-carbamate binding.

The chemical shift behavior of the adducts is consistent with the foregoing interpretations. In carboxyhemoglobin, the pK's of both NH₂-terminals are abnormally low, but approximately equal (38-40). In deoxyhemoglobin the pK of the alpha-chain returns to a near normal value, while that of the beta-chain remains unchanged (38,40). Based on the proposed assignments, the chemical shift behavior of the CO₂ adducts exactly mimics the variations in the pK of these groups.

Other interpretations of the resonance assignments are also plausible, and must be considered. Ligand binding studies on several mutant hemoglobins, hybrid hemoglobins in which one pair of like chains is selectively oxidized, and hemoglobins modified by removal of the carboxyl terminal histidine (146 β) (25-27) have shown the existence of two spectrophotometrically and kinetically distinct forms. The time course for the interconversion of these forms is considered to be slow, probably not faster than 0.1 sec⁻¹ (25-27). While the interconversion is probably between R- and T-like states (25), the presence of new conformations has also been postulated (27).

Such slowly interconverting forms have not been reported for normal hemoglobin, although a dynamic R to T equilibrium most certainly exists (41-44). Thus, as discussed below, if the R-T equilibrium in the carbamylated hemoglobins is as slow as in the mutant hemoglobins, it is possible that the carbamate resonances observed at 29.2 and 29.8 ppm represent contributions from carbamate formation at both NH_2 -terminals, with their relative areas representing not the amount of carbamate on each NH_2 -terminal, but rather the relative total carbamate bound by each conformation.

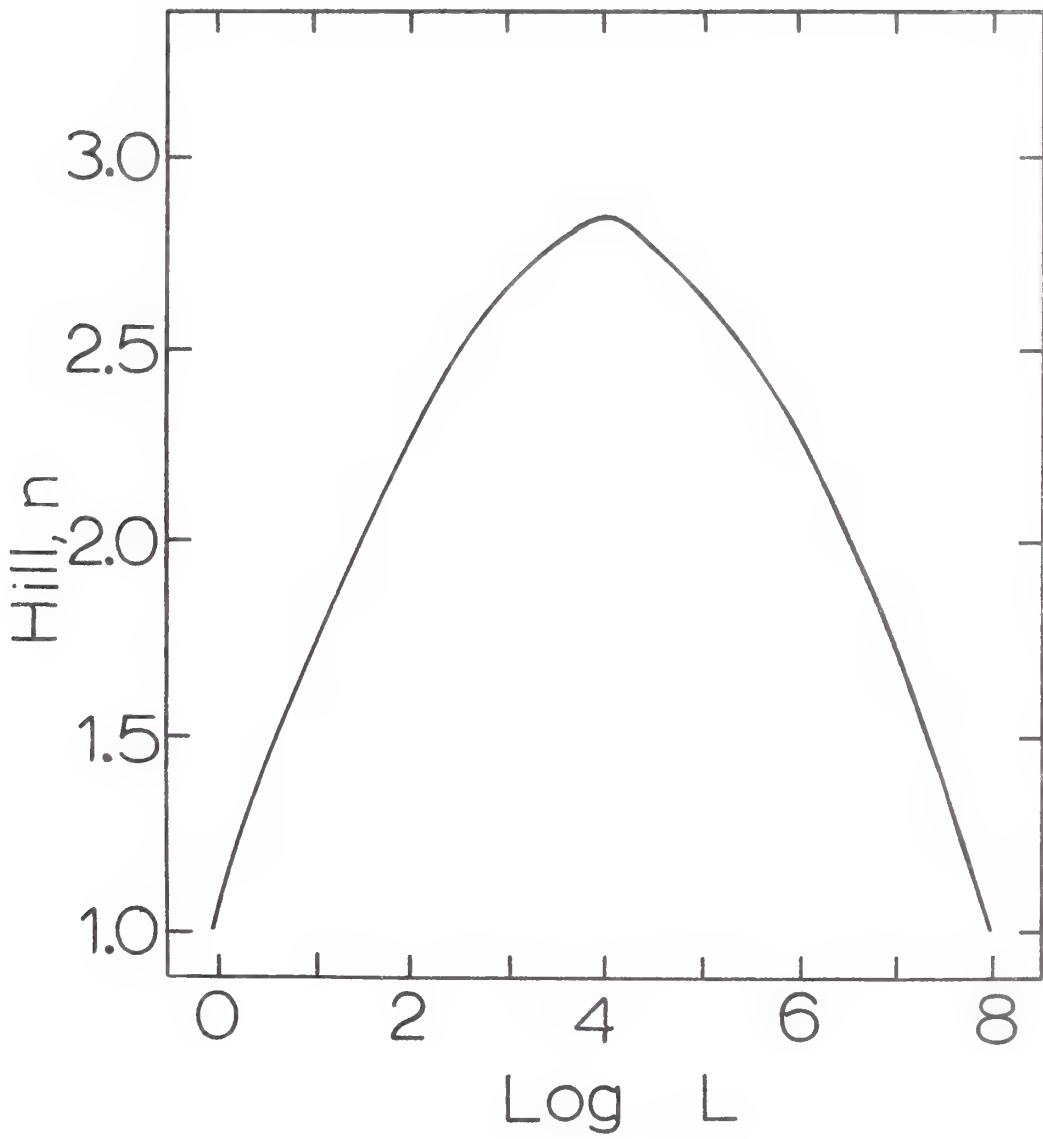
Under this scheme, the results of the $\alpha_2^c\beta_2$ experiments would imply a redistribution of the conformer population to the "R" state, based on the known enhancement of oxygen affinity in such preparations (45). Likewise, the addition of IHP or blockage of the β -chain would lead to an increased relative population of the "T" state (41-45). Concomitant with these changes would be a reduction in the total carbamate levels. Such an explanation is attractive, in that it accounts for the reduced area of the 29.8 ppm resonance in Hb ($\alpha_2^c\beta_2$), as well as avoiding conflict with a report that the deoxyhemoglobin α -chain NH_2 -terminus carries the major portion of the bound CO_2 (20). Significant inconsistencies arise in the foregoing interpretation however. If the resonances are indeed representative of the abundance of "R" and "T" configurations in deoxyhemoglobin, and these conformations are assumed to have differing oxygen affinities (16-19), then the value of (L) in the Monod, Wyman, and Changeux two-state model of cooperative interactions (46) would

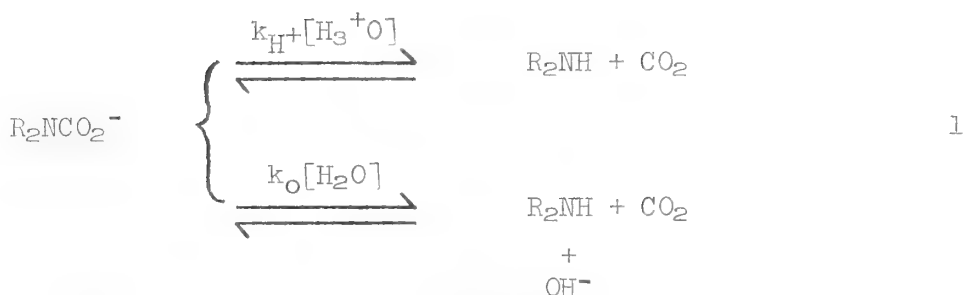
be near unity. In this treatment $L = [T]/[R]$, the ratio of the "T" to "R" oligomers, and represents an isomerization equilibrium or allosteric constant.

The relationship between L and the Hill constant \underline{n} is shown in Figure 9, as redrawn from the literature (47). The value of \underline{n} for adult hemoglobin is widely known to be 2.8 to 3.0 (48), independent of CO_2 concentration. This value is clearly inconsistent with the foregoing interpretation of the carbamino data. In fact, the expected value of L near 10^4 (Figure 9) would render any carbamate resonances characteristic of the "R" state unobservable in deoxy-hemoglobin. Arguments both for and against this conformational interpretation can be generated. Other explanations are also possible, such as slow amine inversion (49). These questions will be returned to, but for the present, reliance will be placed on Ockham's razor. All of the present results are compatible with the alpha and beta chain assignments described above.

Kinetic Effects. In Chapter III chemical exchange of the carbamate with dissolved CO_2 did not affect the observed NMR spectrum. This was primarily due to the high pH of those studies which limited both the population of the dissolved CO_2 (cf. Equation 4, Chapter III) and the rate of carbamate decarboxylation. The acid catalyzed decarboxylation of carbamates is well known, although an uncatalyzed pathway also exists (29). The reaction scheme presented by Caplow (29) for the decarboxylation of carbamates is:

Figure 9. Dependence of cooperativity (the Hill constant n) on $\text{Log } L$, the allosteric constant. ($L = [T]/[R]$ for deoxyhemoglobin). The value of L near unity, suggested by the interpretation that the observed resonances at 29.2 and 29.8 ppm represent the T and R conformational states of the protein, is clearly inconsistent with the known values of n in unmodified HbAo. Graph is redrawn from reference (47).





where the observed first order rate constant k_{obs} is given by

$$k_{obs} \text{ (sec}^{-1}\text{)} = k_{H^+} [H_3^+O] + k_O [H_2O] \quad 2$$

Under all but the most basic conditions, the $k_{obs} \cong k_{H^+} [H_3^+O]$. Typical values of k_{H^+} for basic amines ($pK_z > 6$) are on the order of $10^{+8} \text{ sec}^{-1} \text{ mole}^{-1}$, and vary little with amine basicity (29). The expected decarboxylation rate at neutrality would thus be on the order of 10 sec^{-1} . The mean lifetime of the carbamate, τ_{cam} , is related to the dissociation rate as $\tau_{cam} = 1/k_{obs}$. The nearly 1000 Hz separation of the carbamate and CO_2 resonances at 25.2 MHz (Chapter III) insures that at all pH values for which the adduct is stable, the observed carbamate resonances will fulfill the criteria of "slow exchange" (28):

$$|\omega_i - \omega_j| \gg \left(\frac{1}{T_2^i} + \frac{1}{\tau_i P_j} \right) ; \tau_i P_j = \tau_j P_i \quad 3$$

where P_j represents the fractional population of site j . In the limiting case each resonance (i) is Lorentzian in shape with a width (in Hz) at half-height give by (50):

$$(\Delta\nu)_{\frac{1}{2}} = \frac{1}{\pi T_2^i} + \frac{1}{\pi \tau_i} \quad 4$$

From equations (3) and (4) it is evident that if the resonances are of unequal intensity, the weaker one will be the more broadened.

The residual linewidth of site i in the absence of exchange ($\tau_i = \infty$) is $\frac{1}{\pi T_2}$, and was estimated by measurement at high pH to be approximately 5 Hz for the carbamate resonances in deoxyhemoglobin at 25.2 MHz. A consideration of Equations 2 and 4 and Equation 9 of Chapter III thus predicts that as the pH falls, the carbamate resonances will broaden. If the population of carbamate vanishes before $\frac{1}{\tau_i} \approx \frac{1}{T_2}$, however, observable broadening will be unlikely. Such was the case for the model compounds studied in Chapter III.

An example of the effect of increasing the dissociation rate of the carbamino groups in a system of constant population is shown in Figure 10A. For systems involving more than one carbamino site, as in hemoglobin, the common assumption implicit in Equation 4, that the probability of transfer to a site is independent of the initial site, is invalid. A constraint on transfer probabilities arises due to the improbability of direct carbamate-carbamate interchange, all exchanges proceeding through the intermediate free CO_2 . The computations necessary for the general case are arduous, and will not be reiterated here. Instead, the spectra illustrated in Figure 10 were simulated by DNMR, a general NMR line shape program by G. Binsch and D. A. Kleier. This program, available from the Indiana University Quantum Chemistry Program Exchange, was also used in a modified form as the basic line-shape generating routine in NMRFIT3, described below and in Appendix C.

The relative populations chosen in Figure 10A were 0.35, 0.40, and 0.25 for the two major carbamino resonances and CO_2 , respectively. These populations correspond to those expected near pH 7.6 and 60 mM total carbonates for a 10 mM deoxyhemoglobin solution (see below). The large bicarbonate-carbonate resonance has been omitted. Estimates of the carbamate dissociation rate in deoxyhemoglobin by potentiometric methods (51) have approximated its value as 500 sec^{-1} at pH values slightly above neutrality. A comparison of the spectra in Figure 10A with experiment (Figures 1, 2) clearly indicates that the dissociation rate in the solutions reported here is much slower, certainly no greater than 10 to 50 sec^{-1} . The temperature difference between experiments (51) may be responsible for some of this discrepancy. However, a calculation of the dissociation rate (51) using the data of Roughton and Rupp (52) for ferrihemoglobin yielded estimates near 125 sec^{-1} at 37° , a value more likely to be within error of the NMR observations when corrected for the 7° to 8° temperature difference.

Computer Fitting of Observed Spectra. The highly correlated parameters of site populations and exchange rate (Equations 3 and 4) as well as the added complication of bicarbonate- CO_2 exchange, hinder a direct analysis of these constants in any given spectrum. A partial solution to this problem was found by least squares analysis of the carbamate and CO_2 line-shapes and resonance positions. To accomplish this task, Fortran program NMRFIT3 was written (Appendix C). Selected regions of an entire 4096 data points digitized spectrum could then

Figure 10. Computer simulated spectra illustrating the effects of exchange.

- (A) Three site exchange between two carbamino resonances at 735 and 755 H_z , and dissolved CO_2 at 1720 H_z . The exchange rate between the two downfield resonances (representative of two carbamate species) was set to zero in all cases. The relative populations of the three sites were held constant at 0.35; 0.40; and 0.25, respectively. The carbamino dissociation rate constant used for each calculation is listed in the center.
- (B) Simulated effect of two site exchange between the resonances at 735 and 755 H_z , as might occur if the two resonances represented different slowly exchanging conformations of the protein.

See text for further details.



be fitted to the case of three-site exchange, yielding estimated site populations and exchange rates. Examples of experimental and fitted spectra are shown in Figure 11 for deoxyhemoglobin at different pH values. Details of the program are in Appendix C.

The conditions of these measurements are described in the legend and the derived carbamate dissociation constants are shown in Table I. While in theory such an approach should completely solve the spectrum, in practice uncertainties in the exact resonance positions and less than optimal signal-to-noise, as well as a neglect of the slowly exchanging bicarbonate- CO_2 resonances (53) (in the absence of active carbonic anhydrase, Appendix B) denies an unambiguous determination of the parameters. Such uncertainties are particularly severe in the fitting of protein spectra since, for example, the contribution of exchange to the observed chemical shifts (Figures 4, 5, 6) of the carbamates cannot be differentiated from other mechanisms, and the extent of the linewidth changes when observed were at best small. Even spectra with accurate fits contain potential errors in the fitted parameters in excess of those anticipated on the basis of simple criteria (54). Consequently, the derived parameters must be assumed to be only semi-quantitative. Nevertheless, the pH dependence of the dissociation rates (Table I) is apparent, as expected for simple carbamates (29) but not previously determined for hemoglobin. Also of interest is the difference in dissociation rates between the two resonances (Table I). As shown below, both resonances yield identical estimates of pK_C (but not pK_Z).

Figure 11. Least squares analysis of experimental ^{13}C NMR spectra.

^{13}C NMR spectra were recorded on deoxyhemoglobin solutions in the presence of approximately 40 mM total [^{13}C] carbonates. Also present in these solutions, with the exception of the measurement at pH 8.47, was the enzymatic reducing system described in Chapter II; thus the ionic strength of these solutions was higher than those of the spectra reported in Figures 1 or 2. Control experiments established that in the presence of this enzyme system, the net amount of carbamate formed under the conditions of the control was suppressed by about 10 to 20 %.

The peaks of interest were fit using NMRFIT 3, Appendix C. The parameters yielding the best fits are shown in Table I. For the spectra at pH 6.51, the computer's choice of parameters yielded a poor fit by visual criterion. A constrained fit, holding the dissociation rate of the downfield resonance constant at 50 sec^{-1} , yielded the simulated spectrum shown as an insert. Visually, this seems to be a better fit; a peculiarity in the baseline or peak symmetry of the actual experimental spectrum may be responsible for the failure of NMRFIT 3 to accurately reproduce the experimental spectrum.

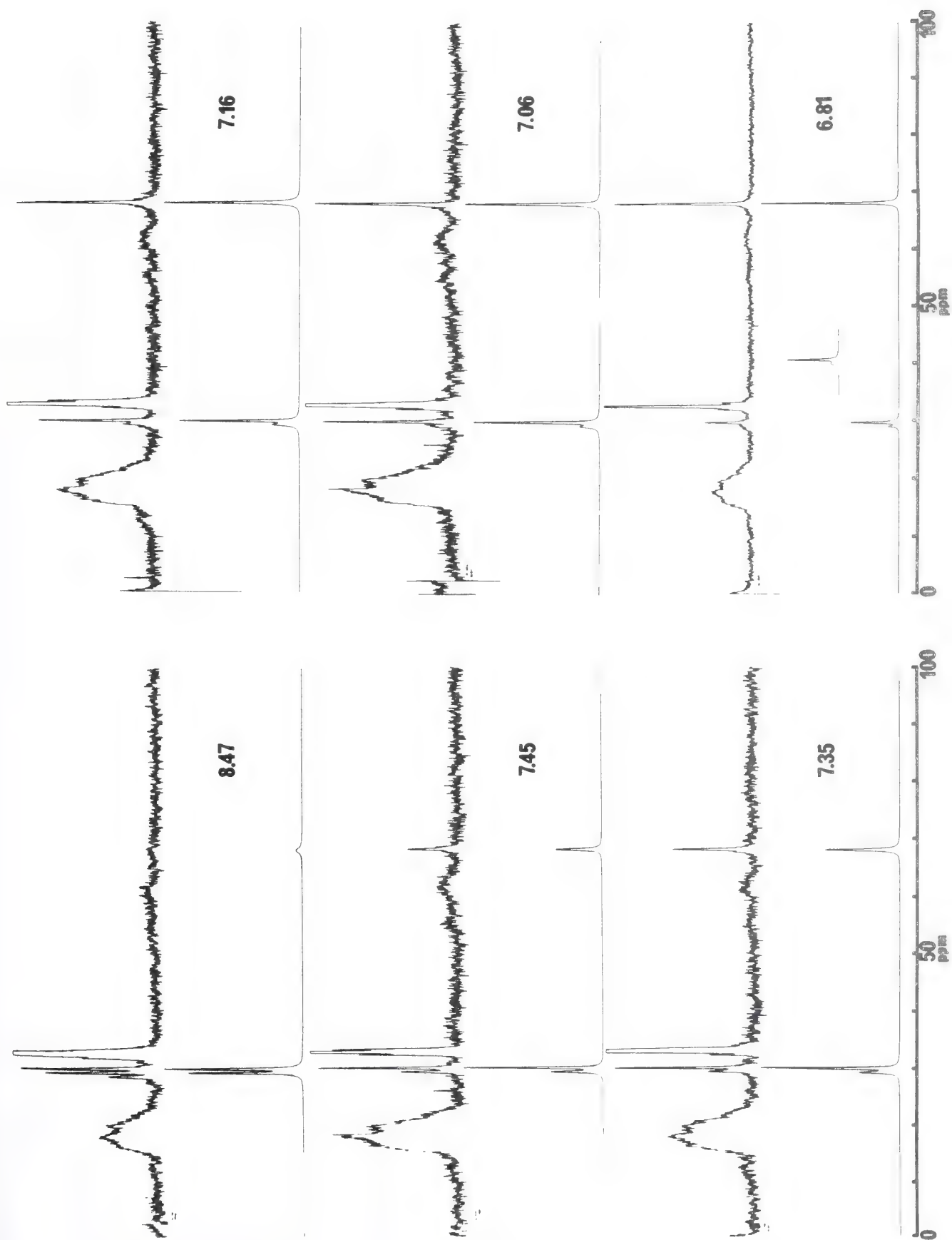


Table I

Carbamino Dissociation Rate Constants in Deoxyhemoglobin

The dissociation constants for the carbamino adducts of deoxyhemoglobin were calculated on the basis of a least squares fit to the observed spectrum (NMRFIT3), based on three site exchange with CO_2 and the two NH_2 -terminal carbamino adducts. Each resonance was assumed to represent the adduct at one site (see text). The apparent T_2 used for the fitting procedure was 0.064 sec. At pH 6.81, the reported values correspond to a fit which visually is poor, but is reproducibly approached by NMRFIT3. The values in parentheses are those derived from a (better) visual fit to the data (See Figure 11). The values reported below must be regarded as only semi-quantitative, due to the uncertainties involved in the fitting procedures. The column designated pop. gives the relative populations of the resonances at 29.2, 29.8, and 68.3 ppm (CO_2) as estimated by the fitting procedure. See Figure 11 for details of this particular hemoglobin preparation, which was maintained nearly free of ferrihemoglobin by the addition of an enzymatic reducing system. Separate measurements indicated that the calculated exchange rates were apparently unaffected by the presence of this enzyme system, although the goodness of fit was usually improved in their presence.

pH	Estimate Variance of fit	k sec ⁻¹		Pop.
		at 29.2 ppm	at 29.8 ppm	
8.47	0.027	5	6	.39/.51/.10
7.47	0.021	11	1	.27/.46/.27
7.35	0.033	18	1	.23/.40/.37
7.16	0.018	27	1	.16/.31/.53
7.06	0.093	21	3	.10/.39/.51
6.81	0.021 (0.044)	8 (50)	4 (2)	.07/.26/.67 (.11/.20/.69)

Therefore, the association rate constant at the site with the largest dissociation rate must also be greater. If, as suggested above, the resonance at 29.2 ppm represents the alpha chain NH_2 -terminal, then its enhanced reactivity (Table I) corresponds well with the 3-4 fold greater pH independent rate constant determined for this site in its reaction with HNCO (38).

If the alternative interpretation of the resonances favoring slow exchange between two protein configurations is adhered to, then the expected lineshape dependence on the rate of conformer interconversion is shown in Figure 10B for equally populated sites. A comparison with experiment (Figures 2, 11) clearly places an upper limit near 1.0 sec^{-1} for the rate in deoxyhemoglobin, similar to the rate postulated in des-(146 His) hemoglobin (27) but three orders of magnitude slower than the proposed rates of conformational change in normal hemoglobin (55).

Spin Lattice Relaxation Time and Nuclear Overhauser Enhancement.

As discussed in Chapter III, accurate quantitation of ^{13}C resonance areas demands a consideration of saturation and NOE effects. As expected, the spin lattice relaxation time (T_1) for the carbamino resonances was found to be magnetic field strength dependent (32), preserving the parallel between their relaxation behavior and that of the carbonyl amides of the backbone (Chapter III). At 15.1 MHz, the T_1 values found for the resonance at 29.8 ppm (Figure 1) in deoxyhemoglobin hemolyzate was $700 \pm 80 \text{ msec}$, indistinguishable from the value of $690 \pm 30 \text{ msec}$ for the protein carboxyl resonance envelope. The conditions of this measurement were nearly identical to those shown in Figure 1A, except that the pH was 7.12. At 25.2

MHz, the T_1 of this same resonance in deoxyhemoglobin solutions at pH 8.17 was now 860 ± 160 msec. Also observable at this pH were the other carbamate resonances (Figure 12), the one at 28.4 ppm yielding a T_1 value of 760 ± 200 msec and that at 29.2 ppm a value of 980 ± 214 msec. The protein carboxyl envelope itself yielded a T_1 value of 830 ± 180 msec. The error limits represent an estimated two standard deviations. The poorer fit of these measurements compared with those done on the hemolyzate at 15.1 MHz may be attributed to the formation of considerable levels of ferrihemoglobin in the purified preparation over the nearly 3 day period in which the sample remained in the instrument.

In Figure 13 are shown typical observations in the presence (A) and absence (B) of proton decoupling. The conditions of these measurements were 13.07 mM deoxyhemoglobin, 68 mM total carbonates at pH 8.47. Temperature was 33° . While the two spectra are quite similar, close inspection reveals that the carbamate resonances are of slightly reduced intensity and slightly greater linewidth in Figure 13B compared with the spectrum in Figure 13A. Integration of the resonances could detect no loss of area (Table II). Contributions from the NOE to the carbamate resonances are thus negligible under these conditions. The protein carboxyl envelope also shows no measurable NOE (Table II). The increased linewidth of the carbamates in Figure 13B is probably attributable to long-range ^{13}C - ^1H spin-spin coupling (32). Since the decoupling mode offered only minimal advantages for the observation of carbamate or protein carbonyl

Figure 12. Spin lattice relaxation time (T_1) measurements on a 13.85 mM deoxy HbA₀ solution equilibrated with 58 mM total carbonates at pH 8.17. The values listed along the right edge represent τ , in millisec., where τ is the delay time between 180 and 90° pulses, in an 180 - τ - 90° pulse sequence.

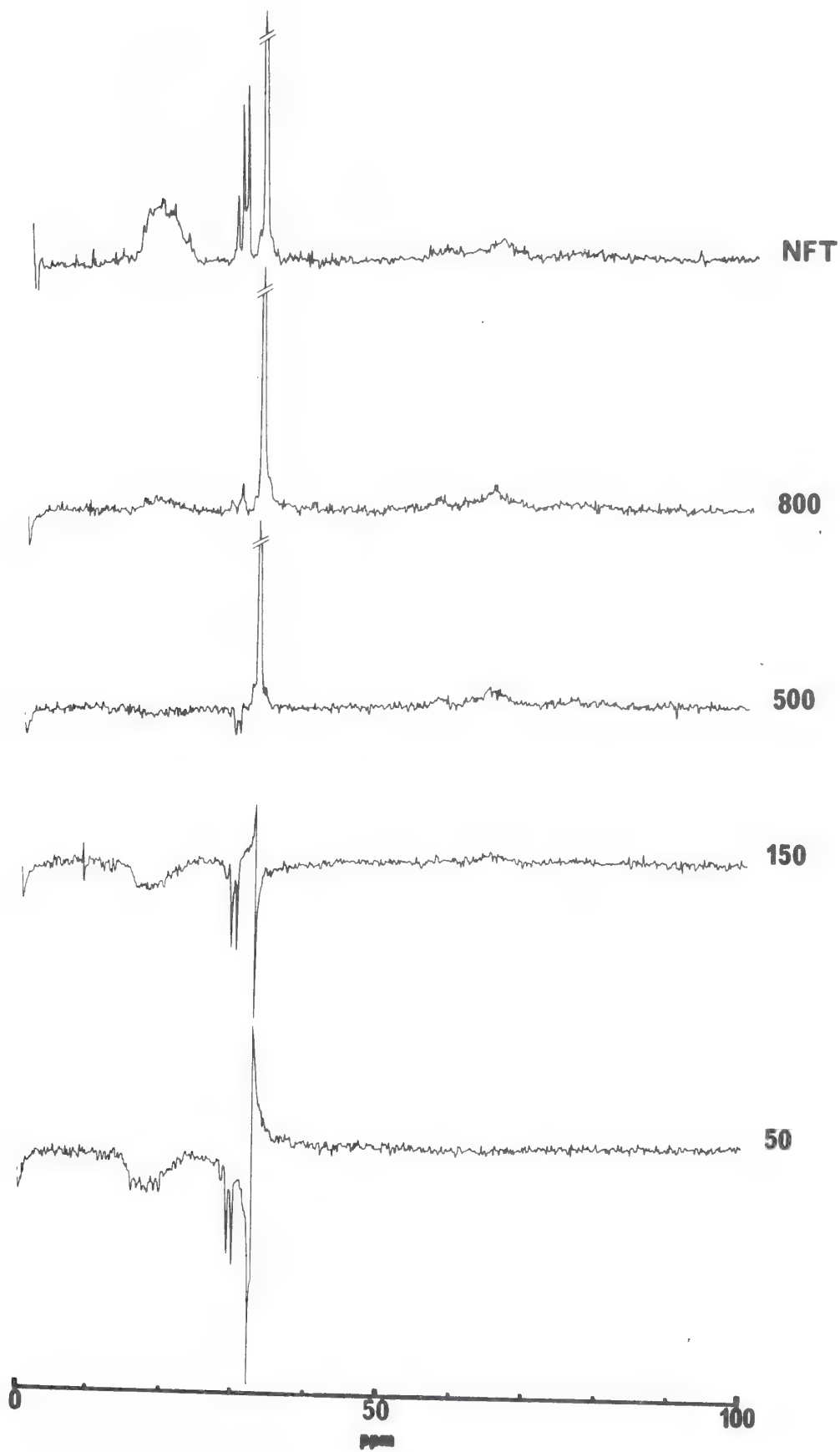


Figure 13. ^{13}C NMR spectrum at 25.2 MHz of deoxy Hb, equilibrated with 68 mM total carbonates at pH 8.97. (A) With complete proton decoupling. (B) In the absence of proton decoupling.

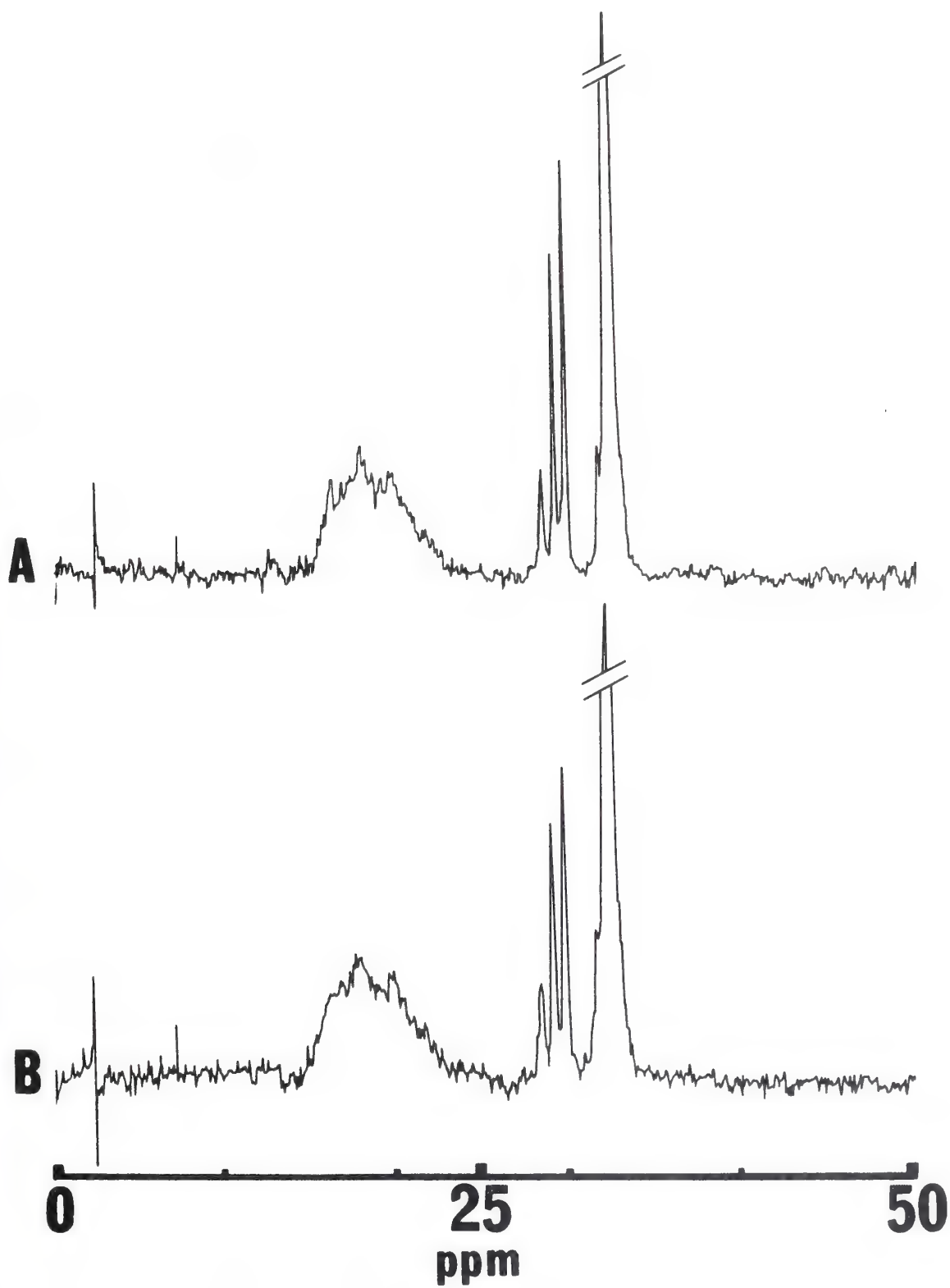


Table II

NOE Measurements on Deoxyhemoglobin Carbamate

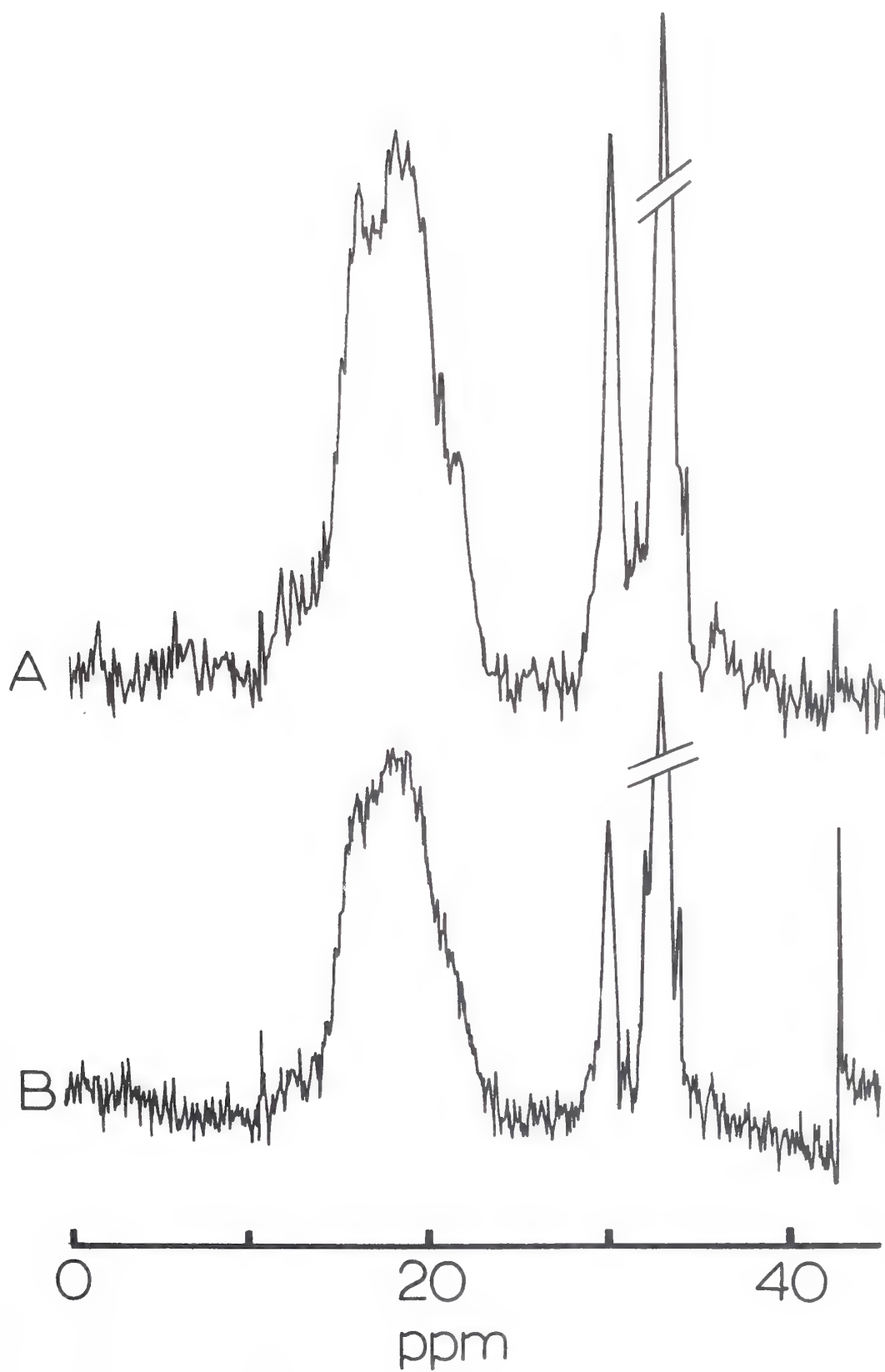
Measurements were made at 30° as described in the text. Data listed without units were obtained by digital integration on the Nicolet 1089 computer. Data listed with units of grams were obtained by "cut and weigh." The error in the estimates of resonance areas and the increasing levels of ferrihemoglobin over the course of the experiment puts practical confidence limits of ± 0.3 in the listed values of NOE. NOE is expressed as $(1 + \eta)$ (58).

Resonance (ppm)		Decoupled Area	Undecoupled Area	Avg. NOE
Protein Carbonyl 10 → 25 ppm		(8.90963×10^5) 0.1234 g	(8.75137×10^5) 0.1345 g	1.0
Carbamino Peaks	29.8	(1.40469×10^5) 0.0181 g	(1.45452×10^5) 0.0186 g	1.0
	29.2	(1.05038×10^5) 0.0144 g	(1.17070×10^5) 0.0151 g	0.9
	28.4	(5.20480×10^4) 0.0069 g	(5.68580×10^4) 0.0081 g	0.9

resonances but serious disadvantages with regards to reliable quantitation of site populations, most spectra used for integration purposes were obtained without it.

Quantitation of Carbamate Formation. Within the limitations discussed in Chapter II, the analytical discrimination of the NMR method is potentially capable of quantitating the population of carbamate represented by each resonance. Toward this goal, a large number of measurements were made on hemoglobin solutions with various ligand states and pH values under conditions of approximately constant total carbonates. The selection of constant total carbonates rather than the more easily analyzed (Equation 9, Chapter III) case of constant $p\text{CO}_2$ represented an economic and practical compromise. It also allowed the ionic strengths of the protein solutions to be more readily held constant. This was particularly important at low pH values. Below $\text{pH} \sim 7.1$, several factors conspired to render reproducible integration of the carbamate resonances exceedingly difficult. Some of these factors have already been alluded to (Figure 11); a particularly important variable was ionic strength. As shown in Figure 14A, spectra recorded at low pH in deionized water contained a very large and broad component underlying the carbamino resonances. At slightly higher salt concentrations, Figure 14B, most of this broad base vanished. The integral area of such broad envelopes suggested a significant amount of carbonates or carbamino was being bound, usually greater than 1 mole/mole $\alpha\beta$ -dimer. The conditions of the measurements in Figure 13 were, (A), 12.84 mM

Figure 14. Effects of ionic strength on nature of resonances in carbamino region. (A) Ferrihemoglobin at pH 7.20, 52 mM total carbonates, ionic strength 47 mM. (B) Ferrihemoglobin at pH 7.22, 50 mM total carbonates, NaCl 50 mM, ionic strength 96 mM.



ferrihemoglobin, pH 7.20, total carbonates 52 mM, and ionic strength 47 mM; (B), 11.20 mM ferrihemoglobin, pH 7.22, total carbonates 50 mM, NaCl 0.05 mM, and ionic strength 96 mM. Increased scatter of the data under conditions of reduced ionic strength severely hampered accurate determination of the apparent pK_Z .

Figure 15 shows a representative series of observations at various pH values on deoxyhemoglobin solutions containing 0.05 M NaCl and a mean carbonate level of 58 mM. The ionic strength of these solutions over the pH range from 6.51 to 8.47 was thus 0.11 to 0.12 M.

Quantitation of the carbamate resonance areas and comparison with the protein carbonyl envelope, representing 328 carbons at natural abundance in $[^{13}\text{C}]$ per $\alpha\beta$ -dimer, yielded the plots shown in Figure 16. The abscissa and ordinate representations are as in Chapter III, with Z representing the moles carbamate per $\alpha\beta$ -dimer. The experimentally determined Z values representative of the resonances at 29.2 ppm (●) and 28.4 ppm (■) could be readily fit by the equation described in Chapter III, yielding the estimates of pK_Z and pK_C in Table III. The resonance at 29.8 ppm (▲) was perturbed at low pH values by remnants of the underlying broad absorption discussed above. If simple integration over the peak was performed, the resultant area yielded markedly increased values of Z. At the lowest pH value plotted in Figure 16 for the 29.8 ppm resonance a straight line was drawn across the apparent base of the narrow resonance, and the integral area of the peak above this was used in Figure 16. Correspondingly, the value of pK_Z obtained for this curve

Figure 15. pH dependence of carbamino resonances in deoxy HbA₀. All spectra were recorded in the absence of proton decoupling. See text for details.

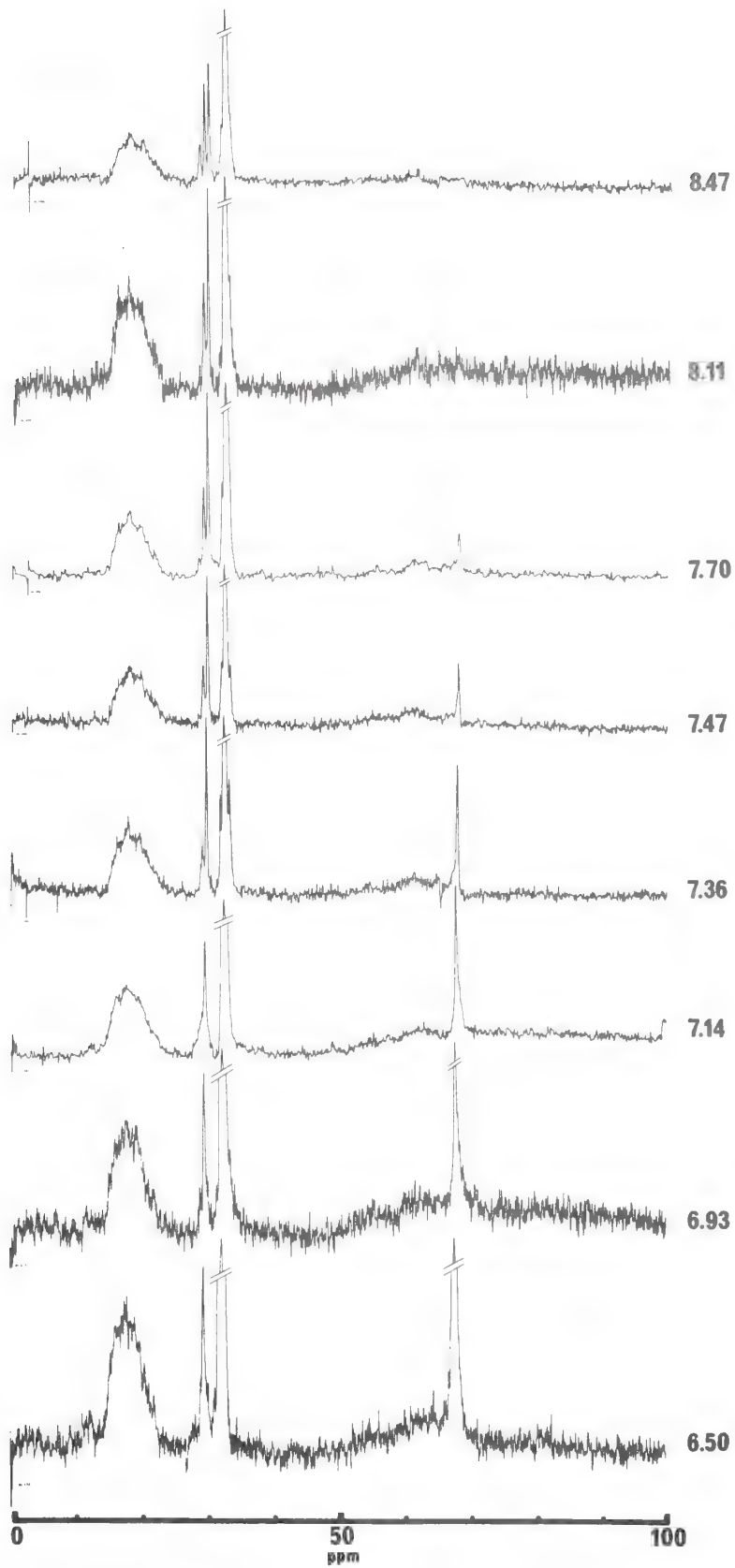


Figure 16. Comparison of Z vs. pH as calculated from spectra similar to those shown in Figure 15.

(●) represents the resonance at 29.2 ppm.

(▲) represents the resonance at 29.8 ppm.

(■) represents the resonance at 28.4 ppm.

Closed symbols represent measurements made in 0.05 M NaCl; the open symbols (○, △) represent measurements made with no added NaCl. See text for details.

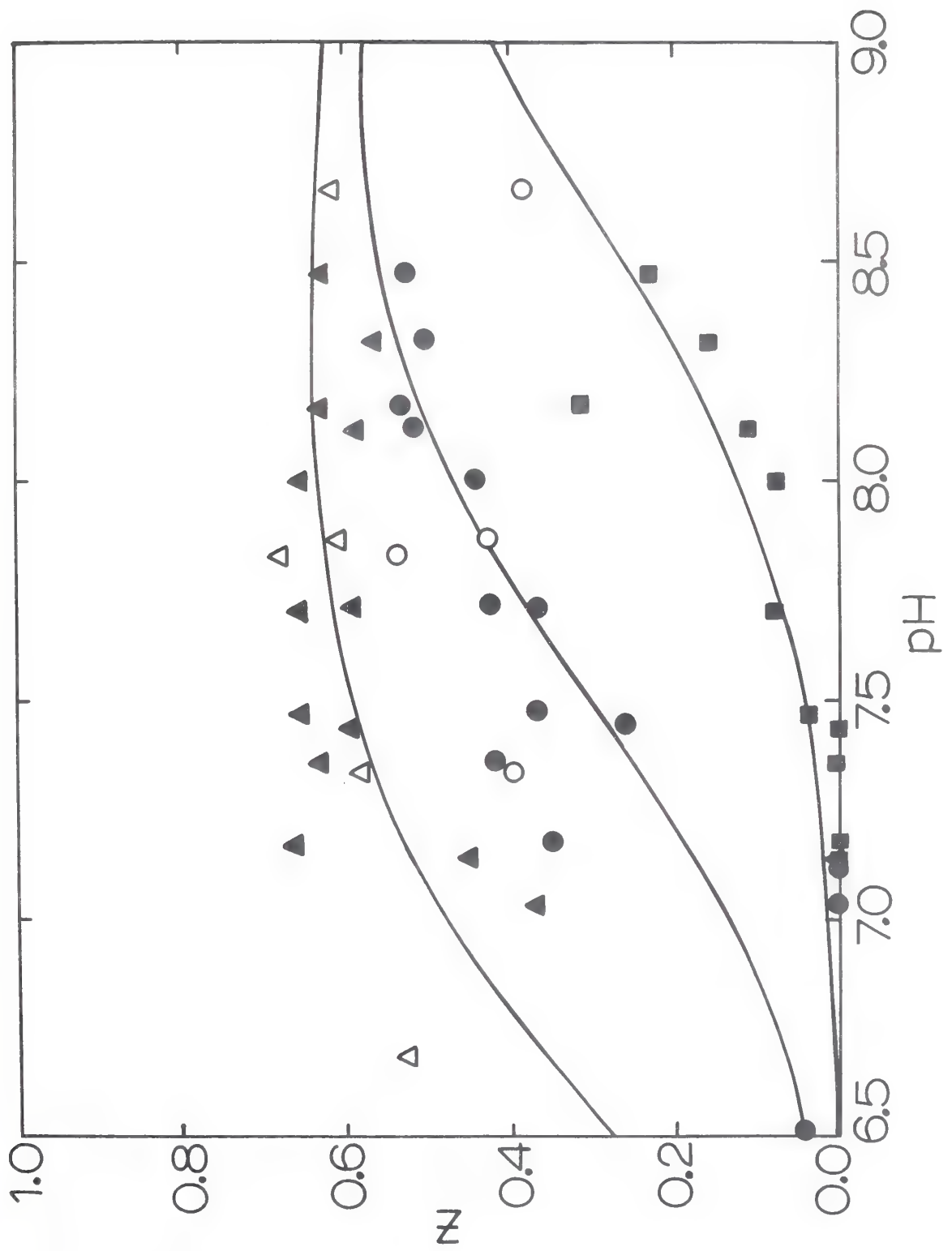


Table III

Carbamino Formation Data for Human Hemoglobin A₀

The assumed number of equivalent sites contributing to the observed resonance is listed in Column 3. The ionic strength variation reflects the changes due to the progressive ionization of hydrated CO₂. The error limits assigned to pK_C and pK_Z represent two estimated standard deviations, based on the goodness of the data fit. The values at 29.2 ppm in deoxy Hb were corrected for the presence of ferri Hb. The 2,3-DPG concentration was zero in all samples. Temperature of the measurements was 29-32°.

Carbamate Resonance ppm	No. Equiv. Sites per αβ dimer	[NaCl] mM	Ionic Strength mM	[Hb] mM	\overline{TC} mM	pK _C	pK _Z	No. of Meas.
Deoxy	1	50	85-123	14.70	58	4.64 ± .08	6.91 ± .32	13
	1	50	85-123	14.95	59	4.69 ± .12	7.96 ± .20	15
	1	50	85-123	14.91	58	4.83 ± .16	8.91 ± .20	11
Hb	1	0	40-59	10.19	53	4.71 ± .06	6.05 ± .66	5
	1	0	40-59	10.19	53	4.95 ± .22	7.32 ± .64	5
	1	0	40-59	10.19	53	4.66 ± .10	9.16 ± .12	5
Carboxy	2	50	102-153	13.85	60	5.57 ± .10	6.57 ± .22	11
	1	50	102-153	13.68	59	4.20	~9.87	7
	2	0	46-56	11.52	55	5.30 ± .24	5.67 ± 2.78	4
Hb	1	0	46-66	13.33	55	4.35	~9.72	9
	2	50	85-96	11.21	42	5.39 ± .08	6.50 ± .72	4
	2	0	39-63	13.97	53	5.30 ± .06	6.47 ± .50	7
Ferri	1	0	39-53	14.62		5.07 ± .08	9.00 ± .10	5
Hb								

is of reduced significance. Symptomatic of the increased scatter in the data at reduced ionic strength are the curves marked by open symbols in Figure 16 (o, Δ , \square) representative of the 28.4 to the 29.2 ppm resonances, respectively.

The pK_Z and pK_C values yielding a best fit to these points are also shown in Table III. The curve, however, is not shown. All points plotted in Figure 16 have been adjusted to a carbonate level of 55 mM, a task accomplished by expanding Equation 9, Chapter III, in a Taylor series about $[CO_2]_i$:

$$Z([\overline{CO_2}]) = \left\{ \sum_j \frac{1}{j!} \frac{\partial^j Z_i}{\partial [CO_2]^j} \right|_{[CO_2]_i} ([\overline{CO_2}] - [CO_2]_i)^j \right\} \quad 5$$

where $[\overline{CO_2}]$ is the mean or desired CO_2 concentration, and $[CO_2]_i$ the CO_2 concentration for Z_i . The partial derivatives of Z_i with respect to $[CO_2]_i$ were found by inspection to follow the recursion formula:

$$\frac{\partial^j Z_i}{\partial [CO_2]^j} \bigg|_{[CO_2]_i} = \frac{(-1)^j j! Z_i^j (Z_i - 1)}{[CO_2]_i^j} ; \quad j > 0 \quad 6$$

Thus the expected Z value at any (mean) carbonate level $[\overline{TC}]$ may be obtained from a known Z_i value at a known carbonate $[TC]_i$ level as:

$$Z([\overline{TC}]) = Z_i + \sum_{n=1} (-1)^n Z_i^n (Z_i - 1) \left(\frac{[\overline{TC}] - [TC]_i}{[TC]_i} \right)^n ; \quad 7$$

$$[\overline{TC}] < 2 \cdot [TC]_i$$

This is because at any given pH $\text{CO}_2 = \alpha \cdot \text{TC}$, where α is a constant that drops from Equation 7. A value of $n = 4$ was usually sufficient to ensure a negligible error in $Z([\overline{\text{TC}}])$.

Rough corrections to account for the amount of ferrihemoglobin present in the solutions were also applied to the resonance integrals at 29.2 ppm. Since ferrihemoglobin exhibits no resonances at this position, the correction consisted only of

$$Z_{\text{corrected}} = \frac{Z_{\text{observed}}}{(100 - \% \text{ferriHb})} \times 100 \quad 8$$

In Figure 17 are presented spectra of carboxyhemoglobin at different pH values and a mean carbonate concentration of 60 mM in 0.05 M NaCl. The multiple component character of the resonance at 29.8 ppm alluded to earlier is clearly apparent below pH 7.2. Integration of the observed resonances, with correction to 55 mM total carbonates (Equation 7) yields the points plotted in Figure 18. The filled triangles (\blacktriangle) represent the resonance near 29.8 ppm or alternatively the sum of the two observed carbamate resonances at pH values less than 7.2. The curve drawn through these points is based on the assumption that the observed resonance results from two individual sites with equal values of K_C and K_Z . The $\text{p}K_C$ and $\text{p}K_Z$ values yielding the fitted curve are shown in Table III. The open triangles in Figure 18 represent measurements of the 29.8 ppm resonance made in deionized water. Increased scatter and a generally greater level of apparent carbamate binding is evident. The lower curve (\blacksquare) in Figure 18 represents the resonance at 28.4 ppm. The

Figure 17. Dependence of ^{13}C NMR spectra of carboxy Hb equilibrated with 60 mM mean carbonates as a function of pH. See text for details.

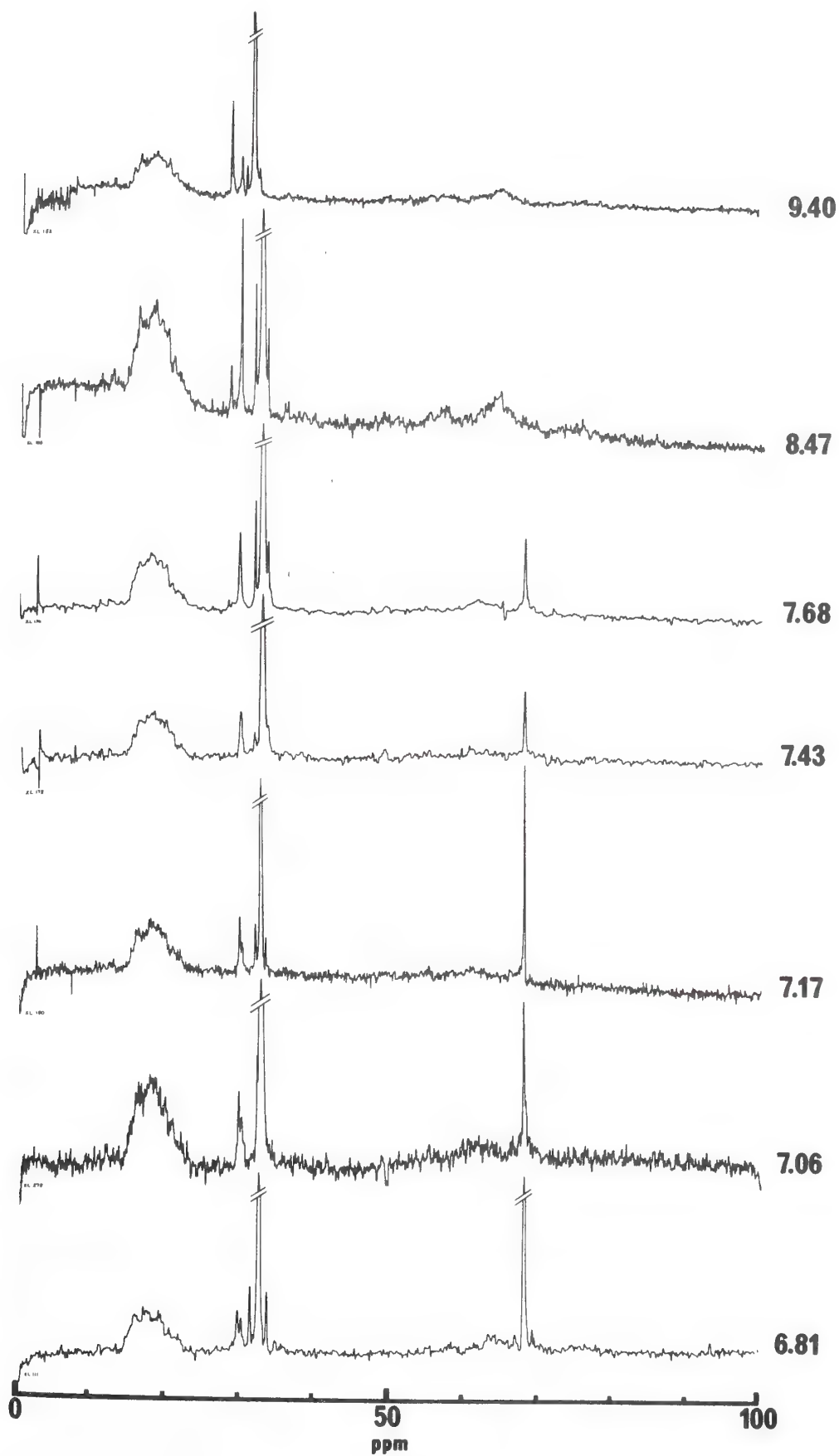
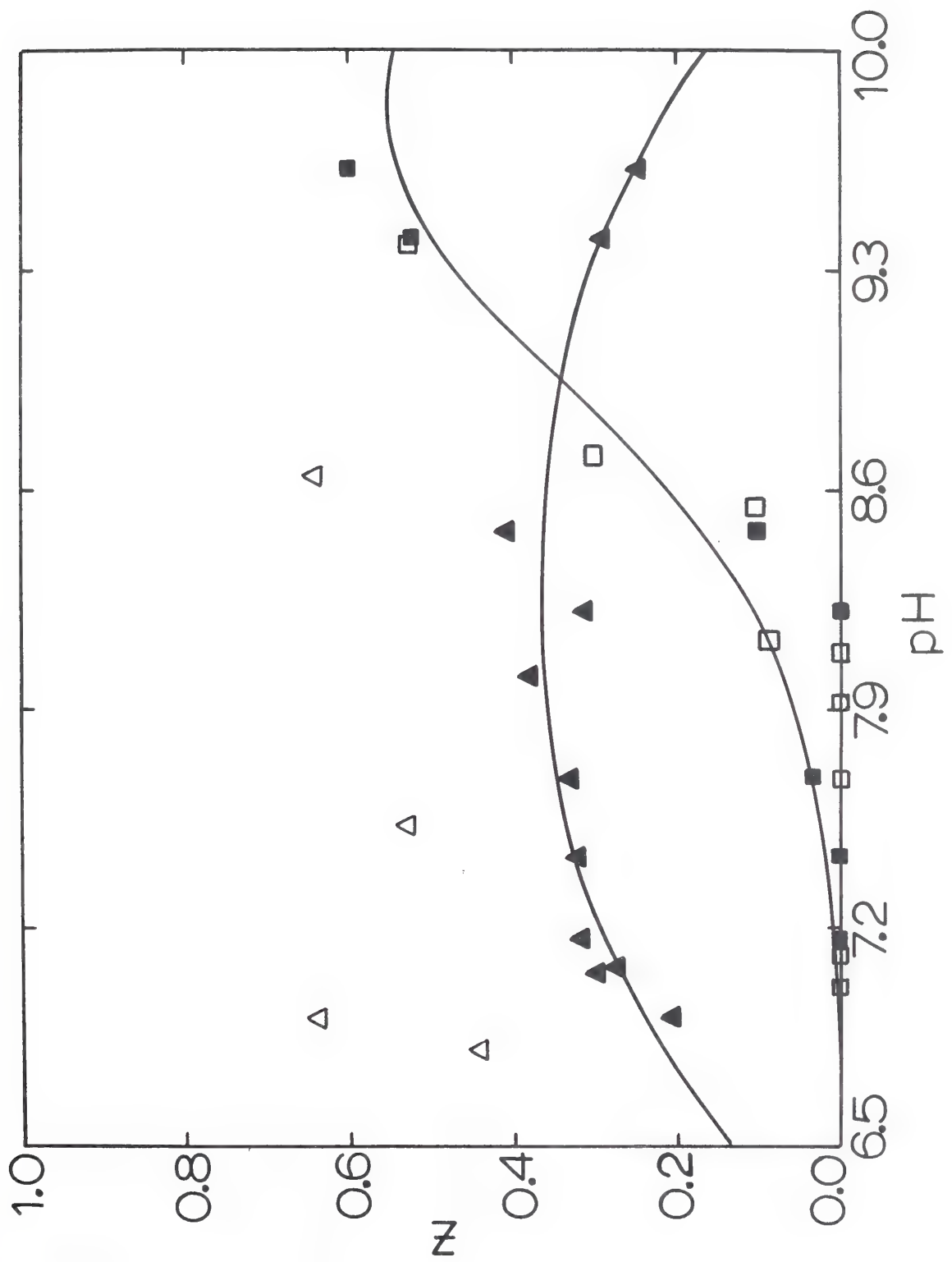


Figure 18. Mole fraction carbamate per α,β dimer as a function of pH, derived from spectra similar to those shown in Figure 17.

(▲) 29.8 ppm resonance in 0.05 M NaCl.

(■) 28.4 ppm resonance in 0.05 M NaCl.

The open symbols represent comparative measurements made in the absence of any added NaCl.



leveling at high pH values indicated by the fitted curve is artificial, since the fitting procedure in this case assumes a single reactive site when in reality numerous lysine residues are probably reactive. It is noteworthy that conversion to the liganded form retards the formation, not only of the 29.2 ppm resonance, but also the onset of the 28.4 ppm resonance.

In Figure 19 is shown a series of measurements on ferrihemoglobin in the presence of 53 mM carbonates. These measurements were made at 15.1 MHz, while those shown in Figures 15 and 17 were made at 25.2 MHz. The pattern of carbamate formation depicted in Figure 20 is reminiscent of that seen in carboxyhemoglobin, although the CO_2 affinity in ferrihemoglobin is somewhat improved ($\text{pK}_c^{\text{ferriHb}} < \text{pK}_c^{\text{COHb}}$, Table III). As in carboxyhemoglobin, the fit to the data was based on the assumption of two equally reactive sites. The upper curve (Δ) was measured in deionized water, the lower two curves (\blacktriangle , \blacksquare) in 0.05 M NaCl. Further measurements need to be made to determine if the differences in CO_2 affinity indicated here between ferrihemoglobin and carboxyhemoglobin are real. Such a difference would not be unexpected, however, since appreciable amounts of ferrihemoglobin exist in the "T" state, or "deoxy" configuration (41-43), a configuration with substantially improved CO_2 binding affinity (Table III).

Discussion. It is quite possible that some carbamino species have been overlooked in the foregoing analysis, either because of spectral overlap or very rapid exchange. A comparison of the results reported here with those of other workers (20) suggests that such

Figure 19. The pH dependence of the 15.1 MHz ^{13}C NMR spectrum of ferri Hb, in the presence of approximately 53 mM total carbonates. The numbers along the right border represent the pH values at which the measurements were made.

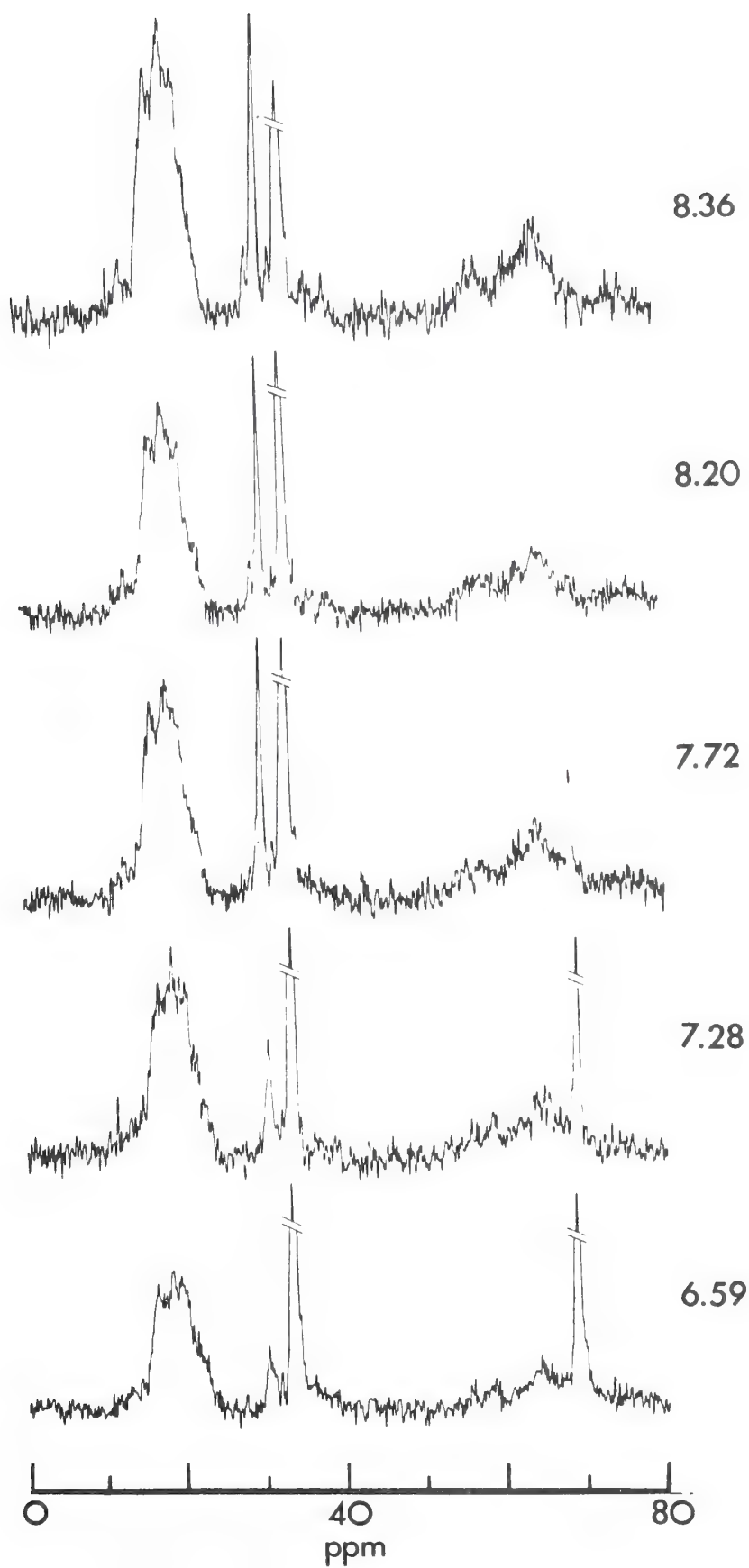
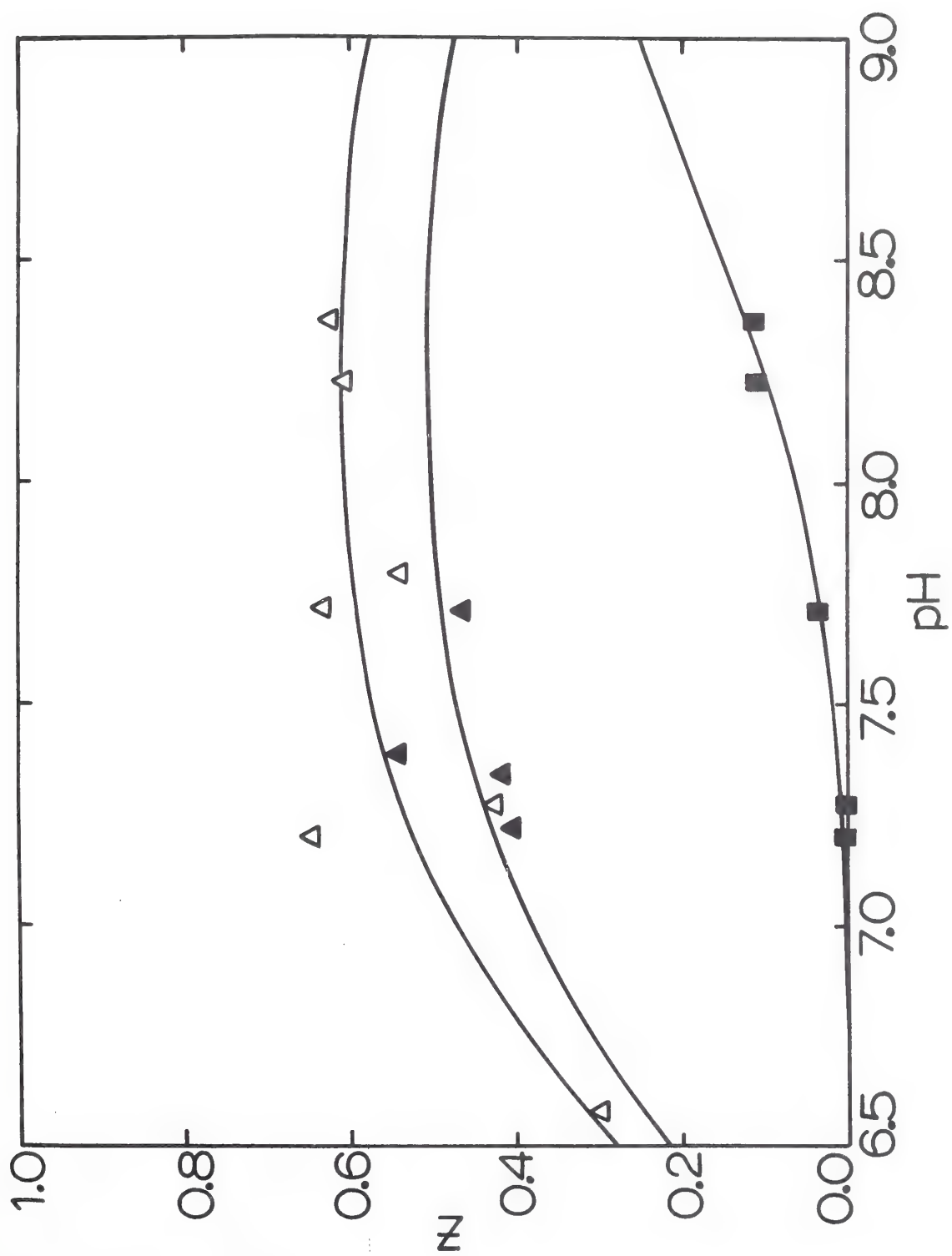


Figure 20. Mole fraction carbamate per α,β dimer, as determined from NMR measurements similiar to those shown in Figure 19.

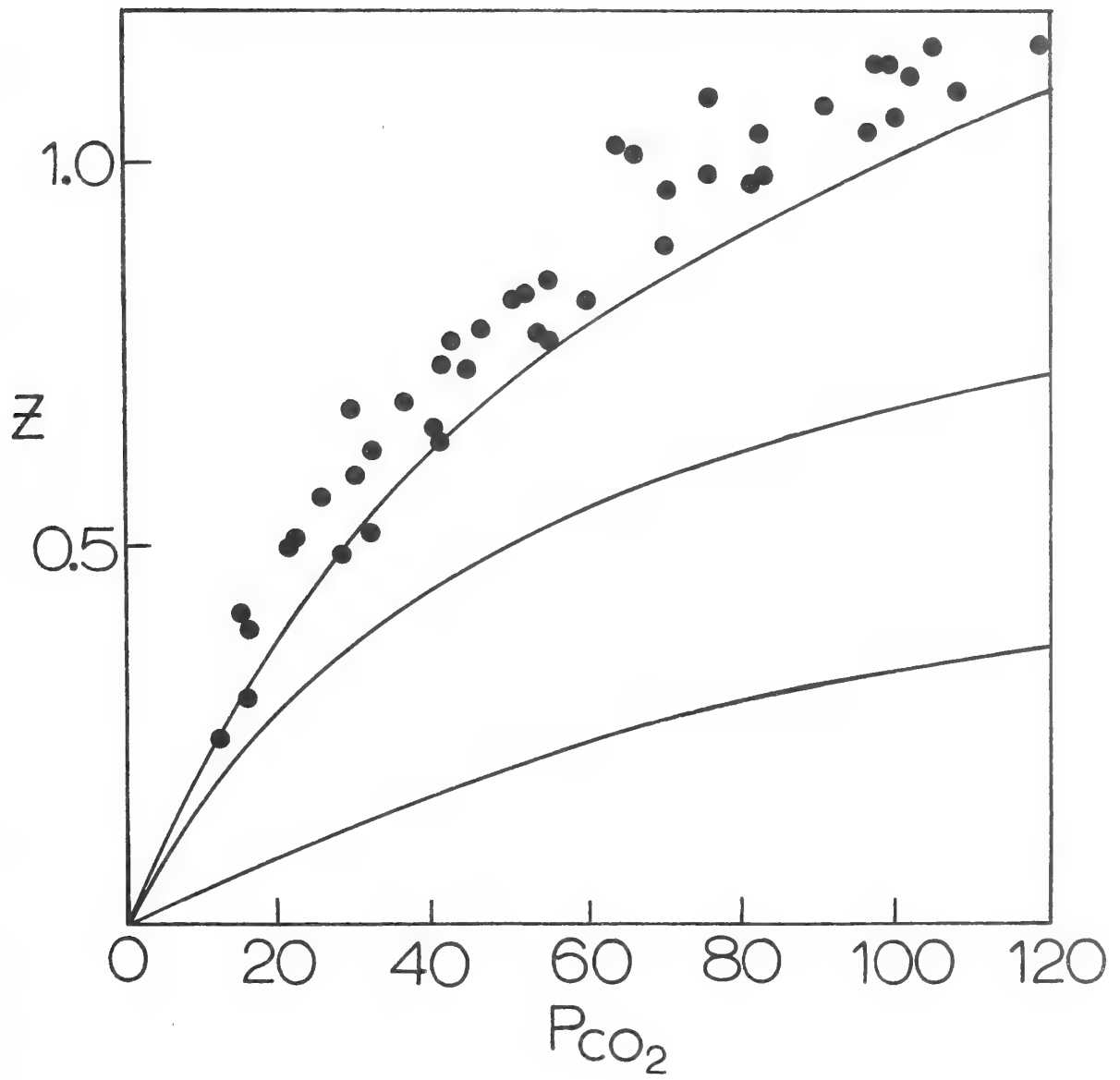
- (▲) 29.8 ppm resonance in 0.05 M NaCl
- (■) 28.4 ppm resonance in 0.05 M NaCl
- (△) 29.8 ppm resonance in absence of salt.



potential omissions cannot be very significant. The pK_C and pK_Z values (Table III) estimated by the NMR method for each resonance in 0.05 M NaCl in deoxyhemoglobin were used to predict the total fraction of carbamate bound under the conditions of constant pH and varying pCO_2 . This comparison is shown in Figure 21. The points have been replotted from the data of Brenna, et al. (20). The bottom and middle curves represent the expected binding at pH 7.4 under various pCO_2 pressures for the resonances at 29.2 and 29.8 ppm respectively. The top curve represents the total of these plots. The correspondence between the results obtained from the NMR method and those by conventional methods (20) is quite satisfying. If the small amount of carbamate represented by the resonance at 28.4 ppm is included in the total in Figure 21, the fit is further improved. Thus it seems inescapable that the total carbamates represented by the resonances at 29.8, 29.2, and 28.4 ppm completely account for the classically observed CO_2 binding in deoxyhemoglobin. As previously discussed, the assignment of these resonances to specific sites in the protein is not without ambiguity. The most likely assignment remains, however, the β -chain NH_2 -terminal, the α -chain NH_2 -terminal, and an ϵ -amino group(s) as the sites of origin for the resonances at 29.8, 29.2, and 28.4 (to 28.2 ppm) respectively.

The estimated values of pK_C and pK_Z derived for each resonance (Table III) is in accord with the above assignments. The best available estimate of pK_C in the literature is that calculated by

Figure 21. Comparison of results of NMR method with published reports. The data points are values replotted from the work of Brenna et al. (20). The bottom curve represents the expected carbamate formation at the site represented by the resonance at 29.2 ppm, based on the estimated values of pK_C and pK_Z (Table III). The intermediate curve is plotted in the same manner, but based on the pK_C and pK_Z values derived for the site represented by the 29.8 ppm resonance. The top curve represents the sum of the two bottom curves. Not shown is the curve for carbamate formation at the site represented by the 28.4 ppm resonance. This resonance would be expected to contribute approximately 0.05 to 0.1 units of Z at a pCO_2 of 120 mM Hg.



Rossi-Bernardi and Roughton (56). They found a value of 4.62 at 37° for deoxyhemoglobin, in excellent agreement with the values reported here. Current theories regarding the nature of the Bohr effect attribute a substantial role (~25%) to a change in the pK_Z of the α -chain NH_2 -terminal (4,5,57). Estimates of this pK in both oxy and deoxyhemoglobin have been made. Differential titration studies suggest that $pK_{oxy}^{\alpha} = 7.3$, and $pK_{deoxy}^{\alpha} = 7.8$ (7). Measurements by Hill and Davis (39) using the rate of reaction with fluorodinitrobenzene yielded a value for $pK_{oxy}^{\alpha} = 6.7$. Very recently in this laboratory the NH_2 -terminal pK values of both chains in deoxy, carboxy, and ferrihemoglobin have been determined by studying the rate of reaction of each NH_2 -terminal with $HNCO$ (38). The values obtained by Garner were $pK_{CO}^{\alpha} = 6.95$, $pK_{deoxy}^{\alpha} = 7.79$, $pK_{ferri}^{\alpha} = 6.74$; $pK_{CO}^{\beta} = 7.05$, $pK_{deoxy}^{\beta} = 6.84$, and $pK_{ferri}^{\beta} = 6.93$. The pK_Z values determined by the NMR method and based upon the proposed assignments concur remarkably well with the cyanate study.

The NMR results also give clear evidence of bicarbonate-carbonate or CO_2 binding over and above that measurable by the classical methods. As early as 1938 Sidwell et al. (15) suggested that bicarbonate anion may itself be bound by hemoglobin. Later studies by Milla et al. (8) and Giustina et al. (9) demonstrated by a thermodynamic method that substantial CO_2 binding must be occurring at low pH values. These papers have received remarkably little attention. More recently, Arnone (11) demonstrated by x-ray analysis a presumably non-carbamic CO_2 or bicarbonate trapped near the heme pocket. Also, significantly, Arnone could not demonstrate any carbamino formation with the NH_2 -terminal of

the α -chains under the high salt conditions of crystallization.

It seems likely that the large broad envelope observed in the carbamino region under conditions of low ionic strength and pH, as well as the narrow elusive resonance found near 33 ppm, corresponds to the non-carbamic bound CO_2 reported by the workers cited above. The broad envelope possibly represents electrostatically bound bicarbonate anions, exhibiting variable rates of exchange between the bound and free forms and multiple chemical environments. The sensitivity of this envelope to inhibition by increased ionic strength supports such an interpretation. Conversely, the narrow resonance near 33 ppm showed little ionic strength variation, consonant with a highly tentative assignment to a free CO_2 molecule trapped within the hydrophobic pocket behind the heme (11).

Three additional measurements made on solutions of deoxyhemoglobin containing 0.4 M NaCl and approximately 50 mM total carbonates suggested that the resonance near 29.2 ppm was more sensitive to ionic strength than the one at 29.8 ppm. A rough estimate of the pK_c of this resonance in 0.4 M NaCl suggested values of 4.9 to 5.0. If this estimate is true, then the lack of an α -chain carbamate in Arnone's study (11) might be expected.

The potential physiologic role of the non-carbamate binding is unknown. While the extent of CO_2 bound in such fashion under normal physiologic conditions may be negligible, the potentiality for such binding at pathologic pCO_2 pressures (as in severe respiratory acidosis) may constitute an important mechanism for facilitating

the transport of CO_2 back to the lungs. Alternatively, it may function normally as a local "buffer" against rapid fluctuations in the pCO_2 pressure.

The enhanced dissociation rate with dissolved CO_2 of the resonance at 29.2 ppm, relative to that at 29.8 ppm, is noteworthy. As previously discussed, the near identity of pK_c for these two resonances implies that the association rate must also be greater. Such a finding is consonant with the rapid rate of reaction with amino-phylic reagents characteristic of the α -chain NH_2 -terminal (38,39).

Conclusion

Based on the evidence presented in Chapter IV, it can be strongly argued that the carbamino adducts of deoxyhemoglobin yield unique resonances, which are degenerate in carboxy or ferrihemoglobin. The beta chain NH_2 -terminus binds the major fraction of CO_2 in the deoxy state, while both chains contribute approximately equally in carboxyhemoglobin. Ferrihemoglobin gives some evidence of existing in an intermediate structure, binding more CO_2 than carboxyhemoglobin, but less than deoxy. The derived pK_c and pK_z values correspond well with estimates in the literature; the kinetics of carbamino exchange at the alpha chain NH_2 -terminus is at least twice as fast as is exchange at the beta chain NH_2 -terminus. Under conditions of reduced pH, ionic strength, and/or high pCO_2 levels, non-specific bicarbonate and/or CO_2 binding probably becomes significant.

The foregoing interpretation must be tempered with the possibility that a slow equilibrium of multiple conformers, perhaps between "R" and "T" configurations, could explain many of the results equally as well.

REFERENCES

1. Lambertsen, C. J. (1968) in Medical Physiology, Mountcastle, V. A., ed., C. V. Mosley Co., St. Louis, Mo., Chap. 37
2. Roughton, F. J. W. (1964) in Handbook of Physiology, Section 3: Respiration, Feun, W. O. and Rahn, N., eds., American Physiological Society, Washington, D. C., 1, 767
3. Roughton, F. J. W. (1970) Biochem. J. 117, 801-812
4. Kilmartin, J. V. and Rossi-Bernardi, L. (1969) Nature 222, 1243-1246
5. Kilmartin, J. V. and Rossi-Bernardi, L. (1971) Biochem. J. 124, 31-45
6. Kilmartin, J. V., Fogg, J., Luzzana, M. and Rossi-Bernardi, L. (1973) J. Biol. Chem. 248, 7039-7043
7. Kilmartin, J. V. and Rossi-Bernardi, L. (1973) Physiol. Rev. 53, 836-890
8. Milla, E., Giustina, G. and Margaria, R. (1953) Gior. Bio. 2, 153-165
9. Giustina, G., Milla, E. and Margaria, R. (1953) Gior. Bio. 2, 357-370
10. Kernohan, J. C., Kreuzer, F., Rossi-Bernardi, L. and Roughton, F. J. W. (1966) Biochem. J. 100, 49P-50P

11. Arnone, A. (1974) *Nature* 247, 143-145
12. Keuzer, F. (1968) in *Biochemie des Sauerstoffs* 19 Colloquium Ges. Biol. Chem., Hess, B. and Staudinger, H., eds., Springer-Verlag, Berlin
13. Kreuzer, F. (1967) in *Exercise at Altitude*, Margaria, R. ed., Excerpta Medica Foundation, Amsterdam, 148-158
14. Kreuzer, F., Roughton, F. J. W., Rossi-Bernardi, L. and Kernohan, J. C. (1972) in *Oxygen Affinity of Hemoglobin and Red Cell Acid Base Status*, Rørth, M. and Astrup, P., eds., Academic Press, New York, 208-215
15. Sidwell, A. E. Jr., Munch, R. H., Guzman Barron, E. S. and Hogness, T. R. (1938) *J. Biol. Chem.* 123, 335-350
16. Perutz, M. F., Muirhead, H., Cox, J. M. and Goaman, L. C. S. (1968) *Nature* 219, 131-139
17. Perutz, M. F. (1970) *Nature* 228, 726-739
18. Perutz, M. F. and Ten Eyck, L. F. (1972) *Cold Spring Harbor Symp. Quant. Biol.* 36, 295-310
19. Perutz, M. F., Muirhead, H., Mazzarella, L., Crowther, R. A., Greer, J. and Kilmartin, J. V. (1969) *Nature* 222, 1240-1246
20. Brenna, O., Luzzana, M., Pace, M., Perrella, M., Rossi, F., Rossi-Bernardi, L. and Roughton, F. J. W. (1972) in *Advances in Experimental Medicine and Biology*, Brewer, G. J. ed., Plenum, New York, 28, 19-37
21. Meldrum, N. V. and Roughton, F. J. W. (1932) *J. Physiol.* (London) 75, 4P

22. Shire, S. J., Hanania, G. H. and Gurd, F. R. N. (1974)
Biochem. 13, 2967-2974
23. Shire, S. J., Hanania, G. H. and Gurd, F. R. N. (1974)
Biochem. 13, 2974-2979
24. Roughton, F. J. W. and Rossi-Bernardi, L. (1969) in Carbon
Dioxide: Chemical, Biochemical and Physiological Aspects,
Forster, R. E., Edsall, J. T., Otis, A. B., and Roughton,
F. J. W., eds., NASA SP-188, Washington, D. C., 41-45
25. Cassoly, R. and Gibson, Q. H. (1972) J. Biol. Chem. 247,
7332-7341
26. Olson, J. S., Gibson, Q. H., Nagel, R. L. and Hamilton, H. B.
(1972) J. Biol. Chem. 247, 7485-7493
27. Moffat, K., Olson, J. S., Gibson, Q. H. and Kilmartin, J. V.
(1973) J. Biol. Chem. 248, 6387-6393
28. Johnson, C. S. Jr. (1965) in Adv. Mag. Res., Waugh, J. S. ed.,
Academic Press, New York, 1, 33-102
29. Caplow, M. (1968) J. Amer. Chem. Soc. 90, 6795-6803
30. Abragam, A. (1961) The Principles of Nuclear Magnetism, Oxford
Press, London, 303-304
31. Allerhand, A. and Trull, E. A. (1970) Ann. Rev. Phys. Chem.
21, 317-348
32. Gurd, F. R. N. and Keim, P. (1973) in Methods in Enzymology,
Hirs, C. H. W. and Timasheff, S. N., eds., 27, Chap. 34
33. Arnone, A. (1974) Nature 247, 143-145
34. Arnone, A. and Perutz, M. F. (1974) Nature 249, 34-36

35. Perutz, M. F. and Mazzarella, L. (1963) *Nature* 199, 639
36. Rifkin, J. M. (1974) *Biochem.* 13, 2475-2481
37. Moon, R. B., Nelson, M. J., Richards, J. H. and Powars, D. F. (1974) *Physiol. Chem. and Phys.* 6, 31-40
38. Garner, M. H. (1974) Ph.D. Thesis, Indiana University
39. Hill, R. J. and Davis, R. W. (1967) *J. Biol. Chem.* 242, 2005-2012
40. Tanford, C. and Nozaki, Y. (1966) *J. Biol. Chem.* 241, 2832-2839
41. Perutz, M. F., Ladner, J. E., Simon, S. R. and Ho, C. (1974) *Biochem.* 13, 2163-2173
42. Perutz, M. F., Fersht, A. R., Simon, S. R. and Roberts, G. C. K. (1974) *Biochem.* 13, 2174-2186
43. Perutz, M. F., Heidner, E. J., Ladner, J. E., Beeston, J. G., Ho, C. and Slade, E. F. (1974) *Biochem.* 13, 2187-2200
44. Adams, M. L. and Schuster, T. M. (1974) *Biochem. Biophys. Res. Comm.*, submitted for publication
45. Nigen, A. M., Njifutié, N., Lee, C. K. and Manning, J. M. (1974) *J. Biol. Chem.*, submitted for publication
46. Monod, J., Wyman, J. and Changeux, J. P. (1965) *J. Mol. Biol.* 12, 88-118
47. Edelstein, S. J. (1971) *Nature* 230, 224-227
48. Antonini, E. and Brunori, M. (1971) *Hemoglobin and Myoglobin in Their Reactions with Ligands*, North-Holland, London
49. Saunders, M. (1967) in *Magnetic Resonance in Biol. Systems*, Wenner-Gren Center Internatl. Symp. Series, 9, 85-99
50. Piette, L. H. and Anderson, W. A. (1959) *J. Chem. Phys.* 30, 899-908

51. Forster, R. E., Constantine, H. P., Craw, M. R., Rotman, H. H. and Klocke, R. A. (1968) J. Biol. Chem. 243, 3317-3326
52. Roughton, F. J. W. and Rupp, J. C. (1958) Ann. N. Y. Acad. Sci. 75, 156-166
53. Edsall, J. T. (1969) in Carbon Dioxide: Chemical, Biochemical and Physiological Aspects, Forster, R. E., Edsall, J. T., Otis, A. G. and Roughton, F. J. W., eds., NASA SP-188, Washington, D. C., 15-27
54. Bevington, P. R. (1969) Data Reduction and Error Analysis for the Physical Sciences, McGraw-Hill, New York, Chap. 7
55. Antonini, E. and Brunori, M. (1969) J. Biol. Chem. 244, 3909-3912
56. Rossi-Bernardi, L. and Roughton, F. J. W. (1967) J. Physiol. (London) 189, 1-29
57. Kilmartin, J. V. and Rossi-Bernardi, L. (1969) in CO₂: Chemical Biochemical and Physiological Aspects, Forster, R. E., Edsall, J. T., Otis, A. B. and Roughton, F. J. W., eds., NASA SP-188, Washington, D. C., 73-81
58. Doddrell, D., Glushko, V. G. and Allerhand, A. (1972) J. Chem. Phys. 56, 3683-3689

CHAPTER V

The Competition of CO_2 with 2,3-Diphosphoglyceric Acid

The Interaction of CO_2 with Different Hemoglobins

Chapter V

The Competition of CO₂ with 2,3-Diphosphoglyceric AcidThe Interaction of CO₂ with Different Hemoglobins

With the discovery in 1967 that organic phosphates profoundly affect the oxygen affinity of many hemoglobins (1-3), a new dimension was added to the complexity of hemoglobin function. In the seven years which have since lapsed, a voluminous literature has accumulated. Several reviews of the subject exist (4-11). Current belief holds that at least for 2,3-diphosphoglyceric acid (DPG), adenosine triphosphate (ATP), and inositol hexaphosphate (IHP) there is a single high affinity binding site per tetramer. This site is along the dyad axis in deoxyhemoglobin (12,13) and involves the conjugate acids of valine 1 β , histidines 2 β and 143 β , and lysine 82 β . The exact association constant (K_{ass}) for this binding,

$$K_{ass} = \frac{[Hb_4 \text{ DPG}]}{[Hb_4] [DPG]} \quad (1)$$

has been the subject of some dispute, although it is obviously high, with estimates ranging from 10^2 to 10^5 mole⁻¹ (14-16).

Much of the discrepancy in results is no doubt attributable to the variety of experimental conditions employed, K_{ass} having been reported to be a function of protein concentration (17), ionic strength (18), pH (14-19), and temperature (18). Moreover, various reports have appeared indicating binding in excess of one DPG per tetramer for both deoxy and oxyhemoglobin (14, 15), particularly at low ionic strengths. Binding at such additional sites probably is not "oxygen-linked"(11).

Since the binding of 2,3-DPG thus involves the NH_2 -terminals of the β -chains, a competition with the CO_2 binding at these sites would be expected. Such a competition was first reported by Bauer in 1969 (21) and later widely confirmed (17, 19, 22-25).

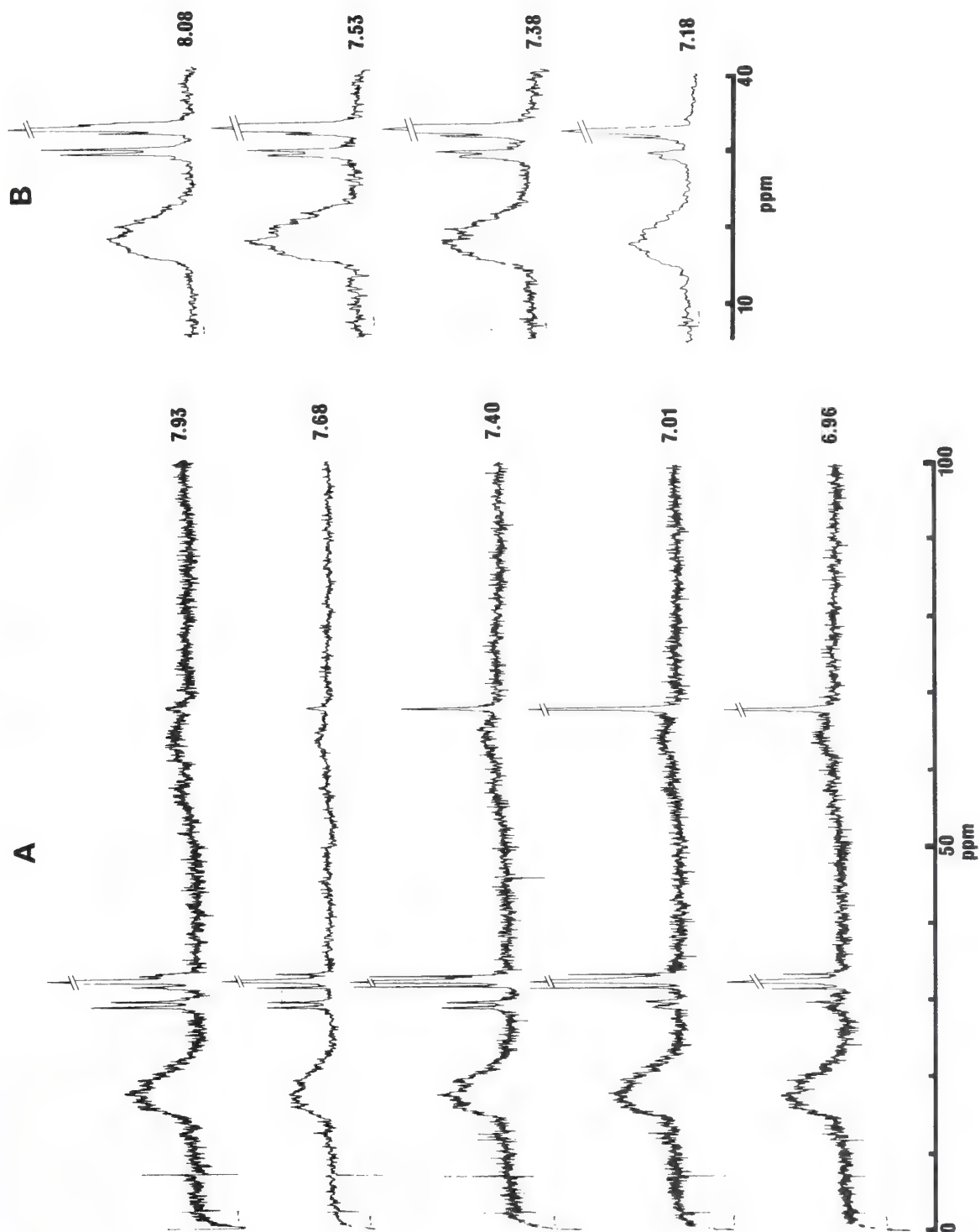
In the present chapter, this competition is examined by ^{13}C NMR. The effect of IHP has already been noted in Chapter IV, where it was found that 3 to 4 mM IHP was sufficient for the complete elimination of the carbamate resonance at 29.8 ppm in deoxyhemoglobin. The results with 2,3-DPG reported here are less dramatic, probably due to the 1000-fold weaker binding of DPG compared to IHP (26). As with IHP, however, only the resonance at 29.8 ppm is substantially perturbed. In Chapter IV, the alternative hypothesis of slow configurational exchange as an explanation for the multiple resonances was suggested. The evidence presented in Chapter V strengthens the argument against such a contingency, but fails to exclude it rigorously.

Observation of Carbamate Resonances in the Presence of 2,3-DPG.

In Figure 1 are shown observations typical of those obtained in deoxyhemoglobin solutions in the presence of (A) 8 ± 2 mM and (B) 5 ± 2 mM 2,3-DPG. The mean hemoglobin concentration for the measurements in Figure 1A was 10.06 mM at a mean carbonate concentration of 53 mM. In Figure 1B, the mean protein concentration was 11.97 mM, at a mean carbonate level of 53 mM. The chemical shifts of the carbamino adducts apparent in either Figures 1A or B were unaffected by the addition of DPG. The high ionic strength of the solutions studied here (Table I) minimized spurious contributions to the well resolved carbamate resonances, even at low pH values.

Figure 1. Dependence of the observed NMR spectrum on pH for solutions of deoxy Hb equilibrated with [^{13}C] carbonates, and in the presence of 2,3-DPG.

- (A) 10.06 mM Hb equilibrated with approximately 53 mM total carbonates. 2,3-DPG concentration was near 8 mM, temperature was 29 - 31°.
- (B) 11.97 mM Hb, identical carbonate levels as in (A), 2,3-DPG concentration near 5 mM.



The inherent differences in exchange rate of the two resonances with dissolved CO_2 , noted in Chapter IV, persisted in the presence of DPG (Figure 1A). The formation of the small resonance near 28.4 ppm was almost totally suppressed under the conditions of these experiments, while the relative intensities of the resonances at 29.2 and 29.8 ppm were often reversed.

A comparison of the Z values obtained from these experiments is shown in Figure 2. The squares (■) and circles (●) represent the measurements in 8 mM DPG for the resonances at 29.8 and 29.2 ppm respectively. The triangles (▲) and X's (x) represent the same respective peaks in solutions of 5 mM DPG. Significantly, in neither case was any resonance entirely eliminated. When compared with the expected pattern in the absence of DPG (Chapter IV), only the resonance at 29.8 ppm was found to be significantly suppressed, most dramatically at low pH values. The basis of the slight reduction in carbamate levels at high pH is not well understood, since K_{ass} falls markedly above pH 7.5 (14). The increased ionic strength (Table I) of the DPG solutions may be a factor (cf. Chapter IV).

The curves passing through the points in Figure 2 represent a least squares fit to the data, and are based on the same equations as used in Chapters III and IV. When describing carbamate formation at the β -chain NH_2 -terminus in the presence of 2,3 DPG, however, these equations are clearly not valid. The values of $\text{p}K_{\text{c}}$ and $\text{p}K_{\text{z}}$ determined in such instances do not represent true equilibrium constants, but nevertheless remain empirically useful to describe the extent of carbamate formation. The similarity of the values of $\text{p}K_{\text{c}}$ and $\text{p}K_{\text{z}}$ estimated for the resonance at 29.2 ppm, attributed to the α -chain adduct, in the 5 mM DPG solution

Figure 2. Mole fraction (Z) of carbamate per α, β dimer in solutions of deoxy Hb + DPG.

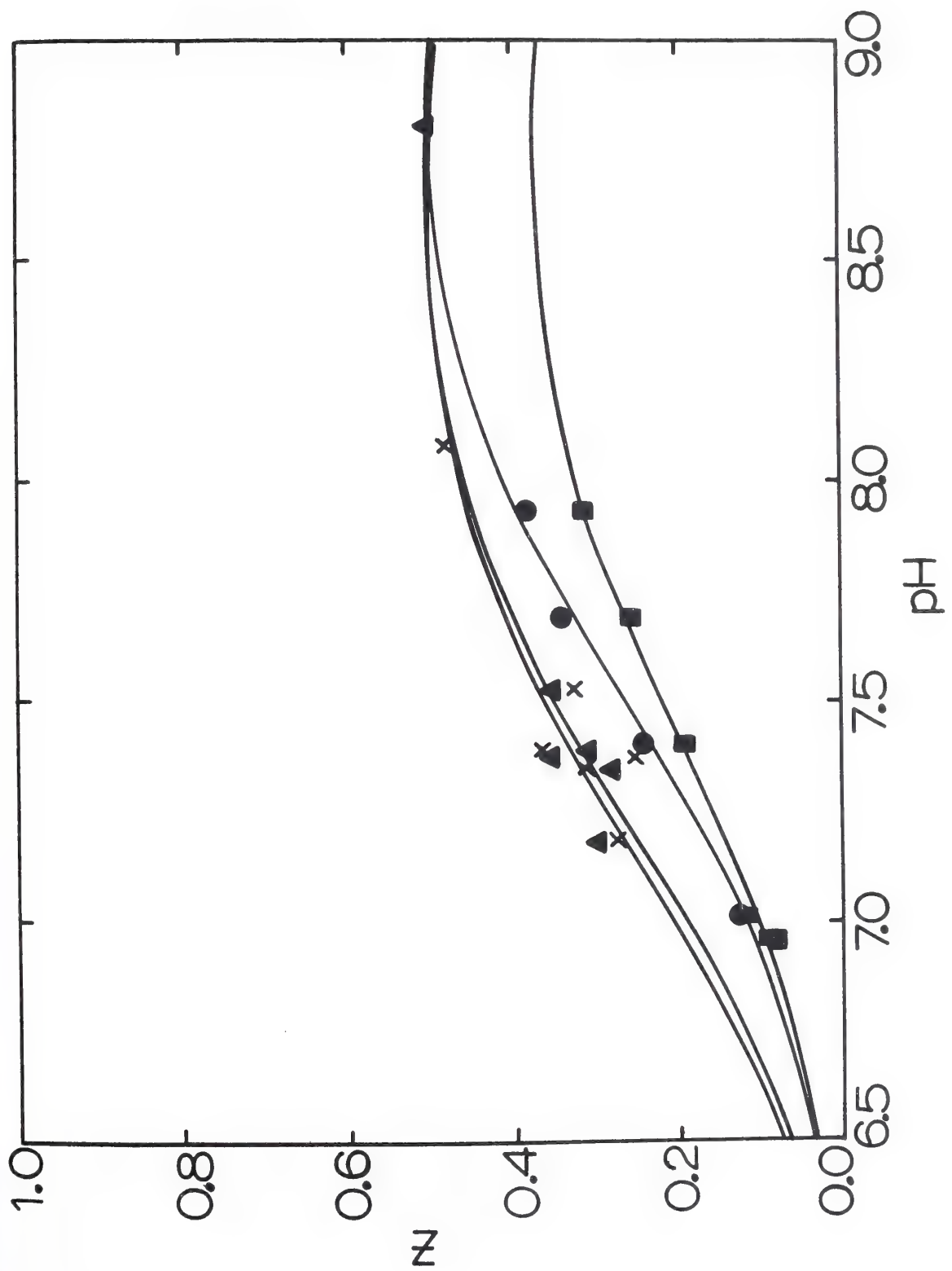
(■) 29.8 ppm resonance, in ~ 8 mM DPG.

(●) 29.2 ppm resonance, in ~ 8 mM DPG.

(▲) 29.8 ppm resonance, in ~ 5 mM DPG.

(X) 29.2 ppm resonance, in ~ 5 mM DPG.

See text for details.



and in 0.05 M NaCl (Table I) suggests only a minimal perturbation of this resonance upon the addition of the phosphate. Carbamino formation at such a site would be expected to show such behavior (25). Moreover, the addition of 2,3-DPG resulted in a significant alteration of the estimated equilibrium constants only for the 29.8 ppm resonance (Table I), lending further support to its assignment as the adduct bound to the β -chain NH_2 -terminus.

The effect of increased levels of 2,3-DPG, as evidenced in Figure 2 and Table I, is peculiar. Even if corrected for the presence of 2-7% of ferri Hb, a pronounced effect on both resonances would remain. At high DPG/Hb ratios, the stoichiometry of binding is known to exceed one molecule of 2,3-DPG per hemoglobin tetramer (14,15). The organic phosphates, being polyelectrolytes like the protein itself, are obviously capable of a multitude of non-specific binding interactions. The reduction in relative area of both resonances suggests that under the conditions of this experiment, 2,3-DPG interacts in some fashion with the α -chain NH_2 -terminal as well as the β -chain (19). The mode of such interaction most probably is electrostatic binding with the NH_2 -terminal and other neighboring groups (Figure 3). While the binding energy at this site is certainly much weaker than that characteristic of the high affinity site, it is possible that such binding near the α -chain NH_2 -terminal may not be without allosteric consequences. As pointed out in 1948 by Wyman (27), and reemphasized by Benesch and Benesch (11), the only binding which matters from a functional point of view is that which is "oxygen linked". The pK_Z of the α -chain NH_2 -terminal is "oxygen linked", so also is the proximity of 2 nearby cationic sites, the guanidino group of arginine 141 α and the ϵ -amino group of lysine 127 α (Figure 3). It

Table I

Carbamate Formation Data for Hemoglobin A₀ with 2,3-DPG

The assumed number of equivalent sites contributing to the observed resonance is listed in Column 3. The ionic strength variation reflects changes due to the progressive ionization of hydrated CO₂. The error limits assigned to pK_C and pK_Z represent two estimated standard deviations, based on the goodness of the data fit. No correspondence for the presence of ferri Hb were made. Temperature of the measurements was 29-32°. See text for details.

Sample	Carbamate Resonance ppm	No. sites per $\alpha\beta$ dimer	[NaCl] mM	Ionic Strength mM	[2,3-DPG] mM	[Hb] mM	\overline{TC} mM	pK _C ^a	pK _Z ^a	No. of Meas.
HbA ₀	29.8	1	50	259-327	8	10.06	53	5.05 ± .02	7.65 ± .04	5
	29.2	1	50	259-327	8	10.06	53	4.80 ± .04	7.87 ± .06	5
	29.8	1	50	213-252	5	11.97	53	4.84 ± .06	7.47 ± .10	6
	29.2	1	50	213-242	5	11.97	53	4.83 ± .08	7.55 ± .14	6
HbA ₀ CO	29.8	2	100	294-402	8	11.32	57	5.62 ± .10	7.20 ± .29	10

^a In the presence of 2,3-DPG, these values may only be empirically useful, since the model upon which they are based does not rigorously apply.

Figure 3. Structure of the C-terminal and N-terminal regions of the α -chain in horse hemoglobin, as a function of the ligand state of the heme. (Redrawn from Reference (39)).

(A) oxyhemoglobin

(B) deoxyhemoglobin

•

Figure 3A

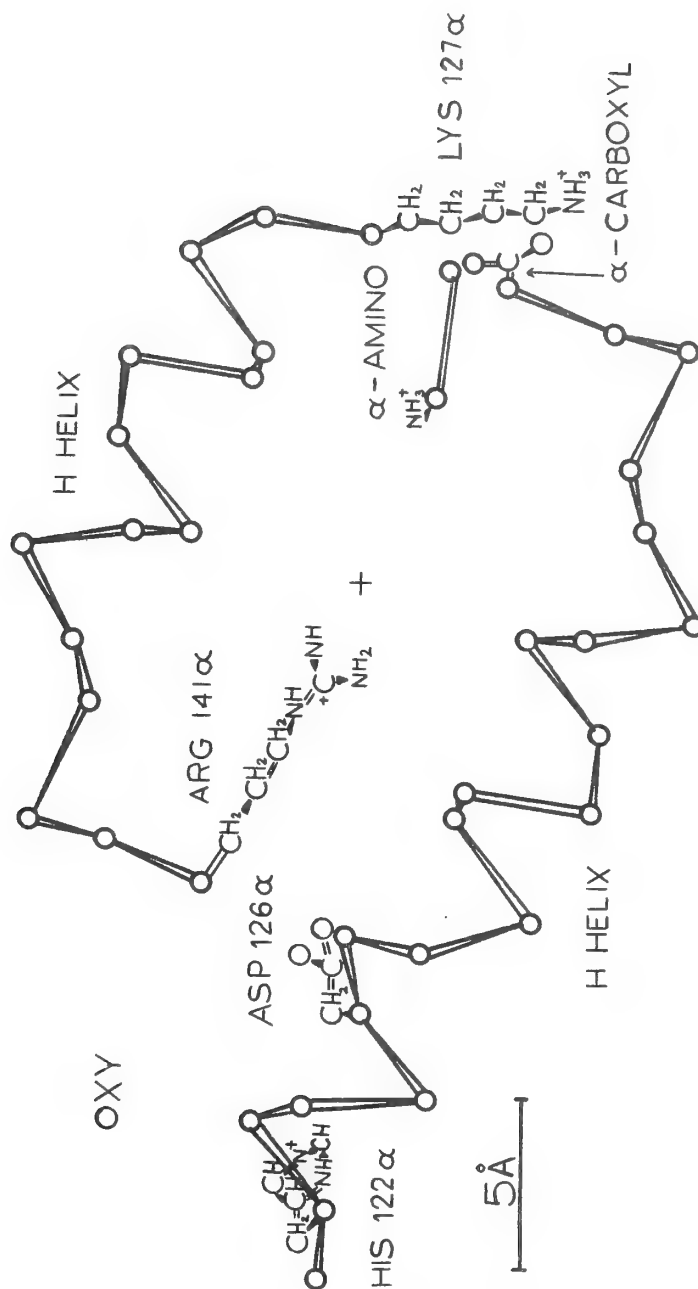
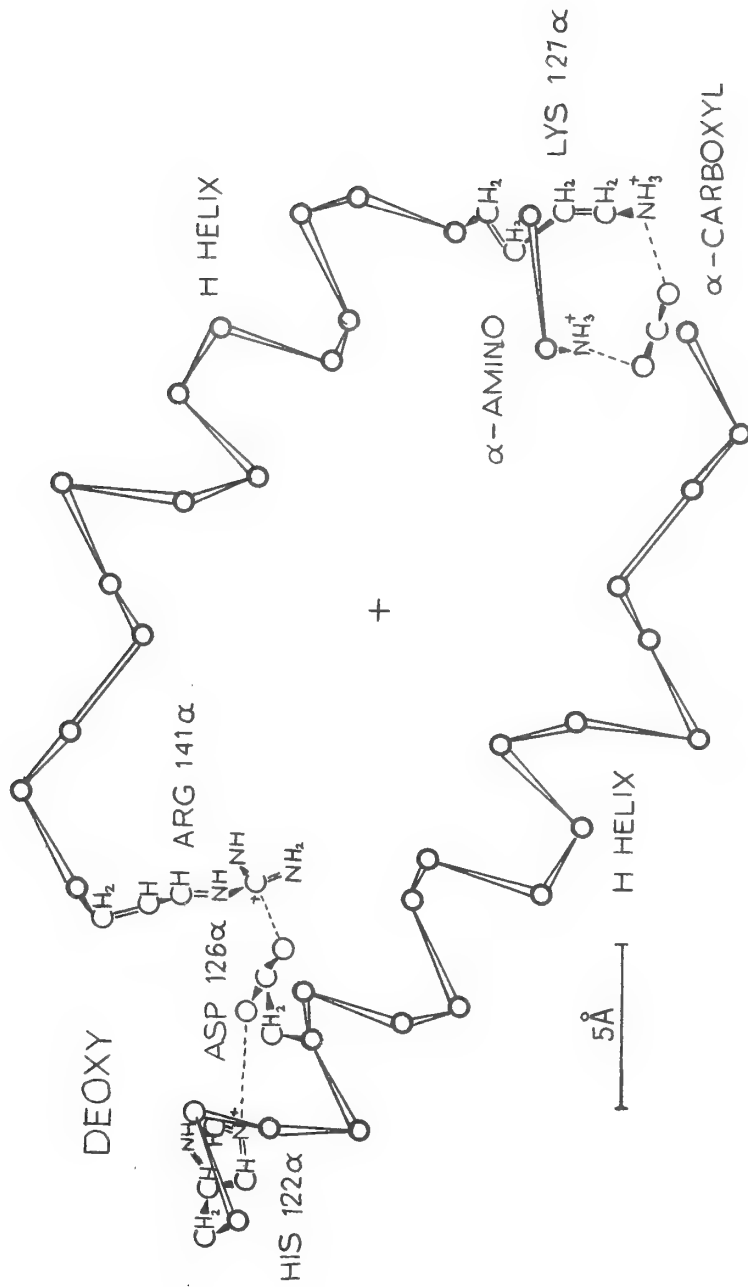


Figure 3B



is difficult to predict which state will be most favorable to 2,3-DPG binding, but it seems likely that the interaction energy at this site with 2,3-DPG should change significantly upon oxygenation.

In Figure 4 is shown a series of observations on carboxyhemoglobin in the presence of 8 ± 2 mM DPG and 0.1 M NaCl. The mean protein concentration was 11.32 mM and mean total carbonates 57 mM. The spectra of Figure 4 are nearly indistinguishable from those in Chapter IV for carboxyhemoglobin in the absence of 2,3-DPG. The careful observer, however, will note that the intensity of the lone carbamate resonance (29.8 ppm) is relatively reduced especially at low values of pH. Integration of the resonance peaks yielded the points plotted in Figure 5. The fitted curve was generated as before with the values of pK_C and pK_Z specified in Table I. The somewhat higher apparent pK_Z value in the presence of 2,3-DPG is probably referable to residual phosphate binding at the β -chain NH_2 -terminals, reducing the levels of carbamate formation at low pH and resulting in an apparent shift of the carbamate formation curve to higher pH values. Such shifts are interpreted in Equation 9 or 10, Chapter III, to mean primarily an increased value of pK_Z .

The association constant for 2,3-DPG with carboxyhemoglobin is small but finite (28). The best estimates have placed its value at approximately 1/40 to 1/50th that for deoxyhemoglobin. Thus the slightly reduced binding of CO_2 in carboxyhemoglobin is consistent with its partial exclusion from the β -chain NH_2 -terminus.

Such an analysis, however, conflicts with an observation reported in Chapter IV that the addition of IHP to carboxyhemoglobin failed to

Figure 4. ^{13}C NMR spectrum as a function of pH for a 11.32 mM carboxyhemoglobin solution equilibrated with approximately 57 mM carbonates, in the presence of approximately 8 mM 2,3-DPG and 0.1 M NaCl.

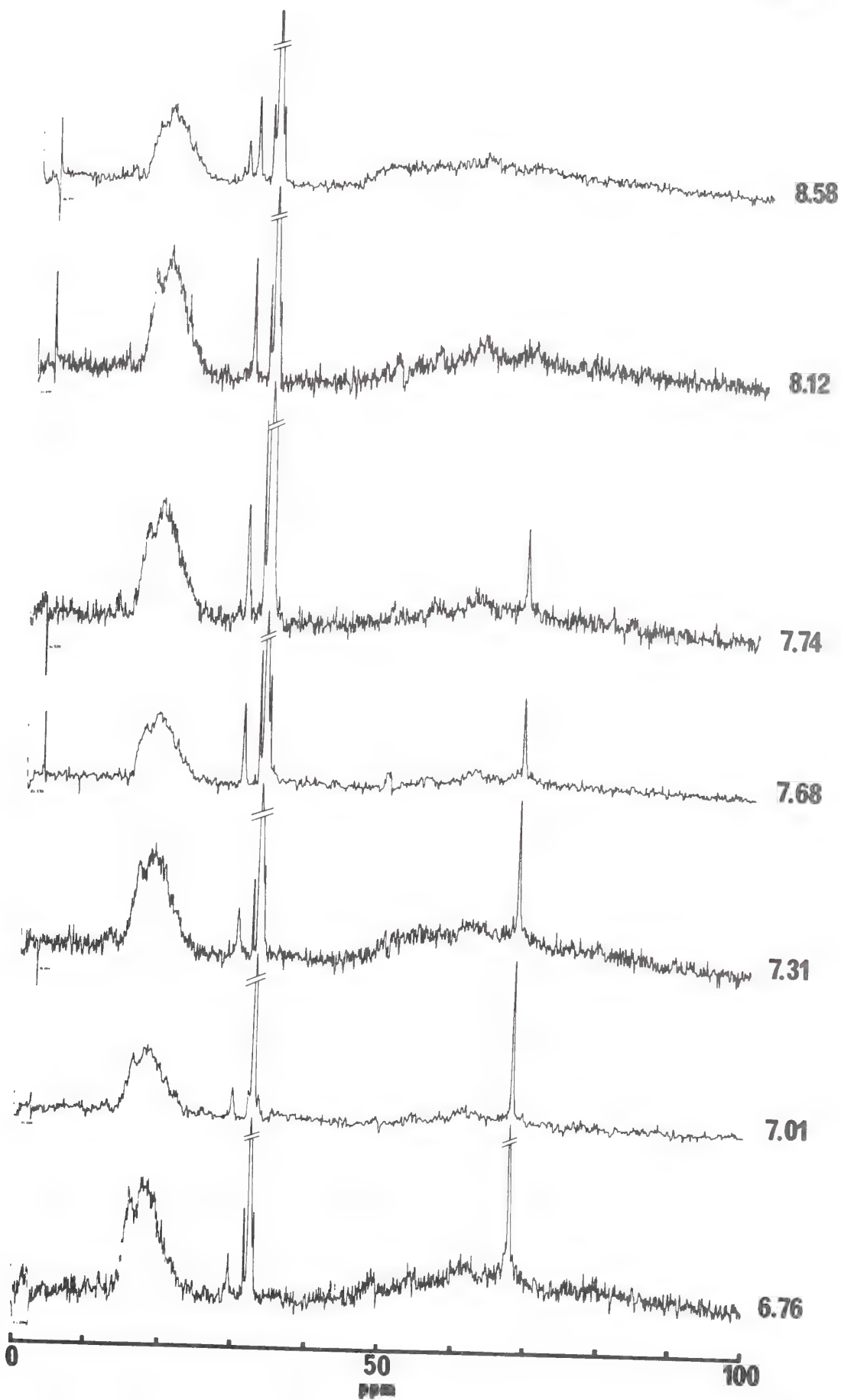
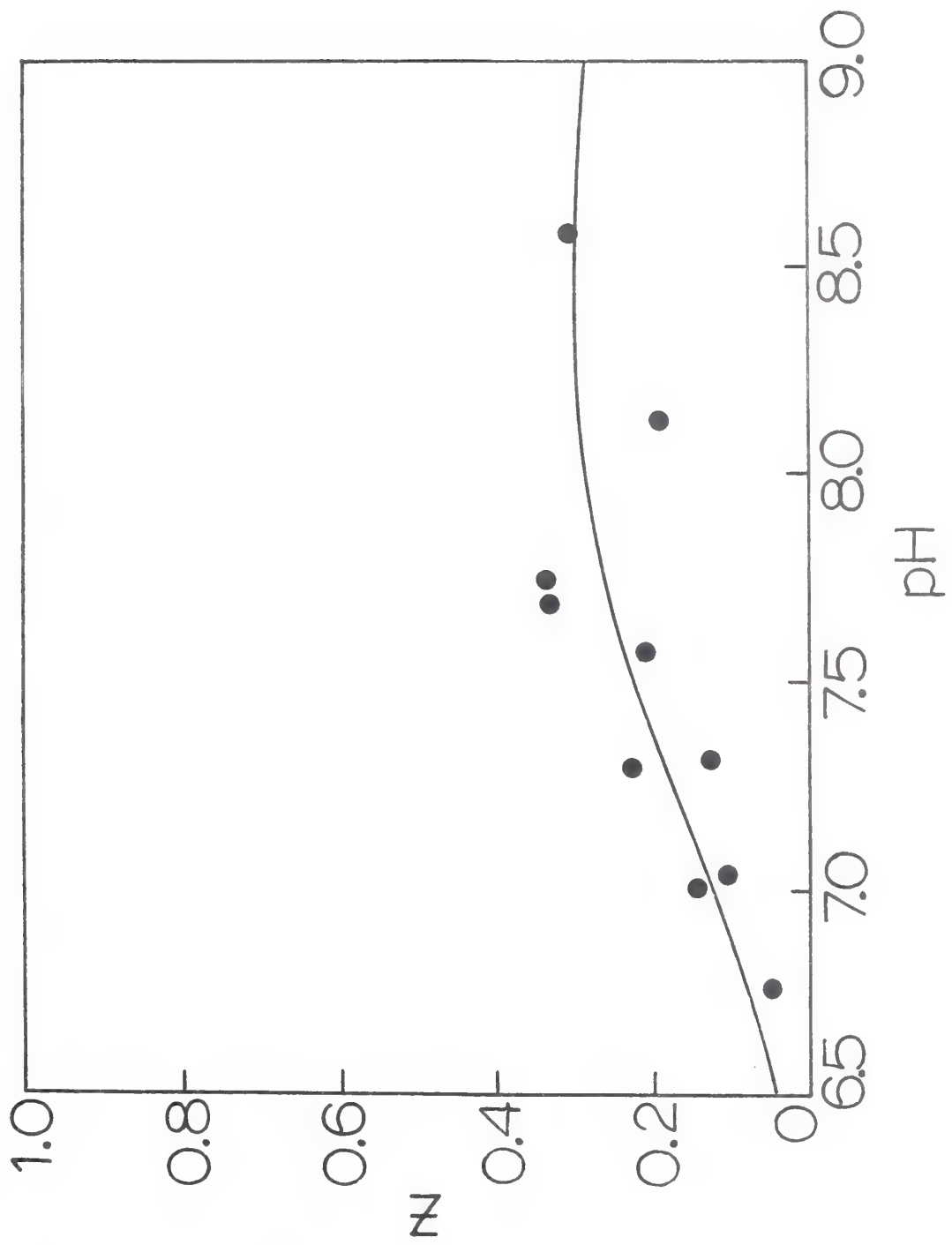


Figure 5. Mole fraction of carbamate formed (Z) as a function of pH for 11.32 mM carboxyhemoglobin in the presence of 8 mM 2,3-DPG. The parameters yielding the fitted curve are listed in Table I.



diminish significantly the carbamate resonance. More measurements are needed to verify the accuracy of this observation. If, however, it proves true, then the binding of IHP probably leads to a redistribution of the "R" to "T" equilibrium, to the gain of the "T" or high CO₂ affinity form (29-37). Thus, the enhanced CO₂ affinity of the alpha chains might offset the loss of β -chain carbamate due to IHP binding.

The total carbamates observed by the NMR method agree admirably with estimates by other workers (25) made on similar solutions. In Figure 6 the data of Brenna et al. (25), representing the total mole fraction of carbamino hemoglobin at pH 7.4 in the presence of variable amounts of ATP, has been replotted. ATP and DPG show similar association constants (38), and give indistinguishable results in these types of studies (39). The dashed lines represent the expected values of Z in approximately 8 mM DPG solutions, based on the values of pK_C and pK_Z (Table I) derived from the NMR experiments. The bottom dashed curve represents the resonance at 29.8 ppm, while the middle dashed curve corresponds to the 29.2 ppm resonance. The uppermost dashed curve represents the sum of the bottom pair, and should correspond to the total mole fraction carbamate. The solid curves are based on the pK_C and pK_Z estimates derived from the NMR experiments in approximately 5 mM 2,3-DPG. As before, the bottom pair of (solid) curves represent the extent of formation monitored by each resonance, while the top curve designates the total. The work of Brenna et al. was done at 37°, which would tend to diminish carbamate formation (39); their ionic strength was also a bit lower. These effects tend to compensate. Thus under comparable organic phosphate levels (2.5-5.4 mM in Reference 25) the agreement of methods is excellent.

Figure 6. Comparison of carbamino formation as measured by the NMR method, and published reports. The data points are from Brenna et al. (25). Dashed curve is expected carbamate binding at each site, 29.2 and 29.8 ppm for middle and lower dashed curves respectively in the presence of ~ 8 mM 2,3-DPG. Top dashed curve represents total of bottom two. Solid curves are based on the estimates derived from the experiments in ~ 5 mM 2,3-DPG. The bottom curve represents the 29.2 ppm resonance; top curve is again total observed carbamate binding in these solutions.

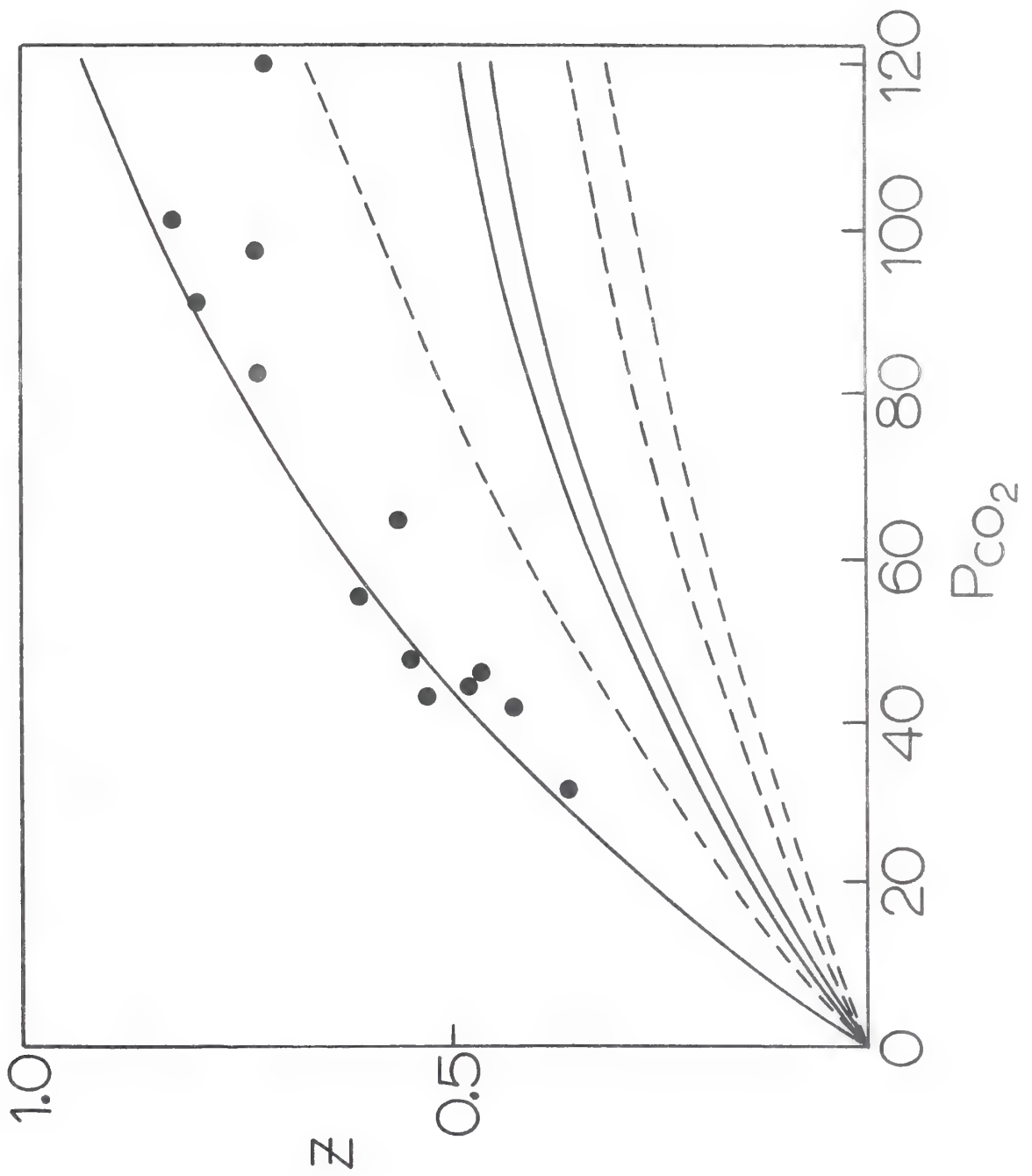
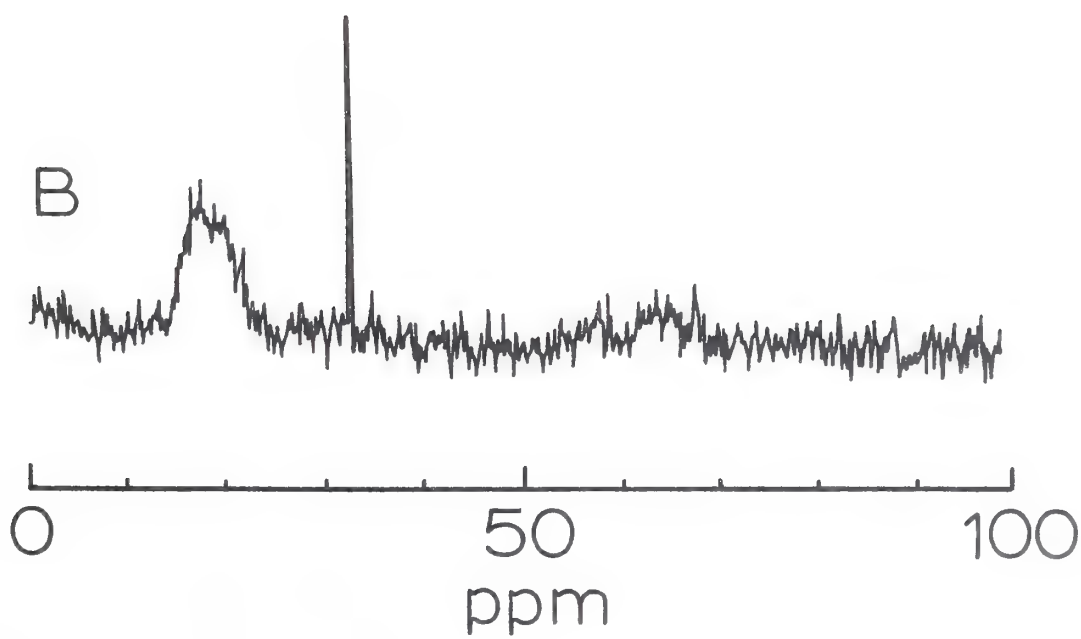
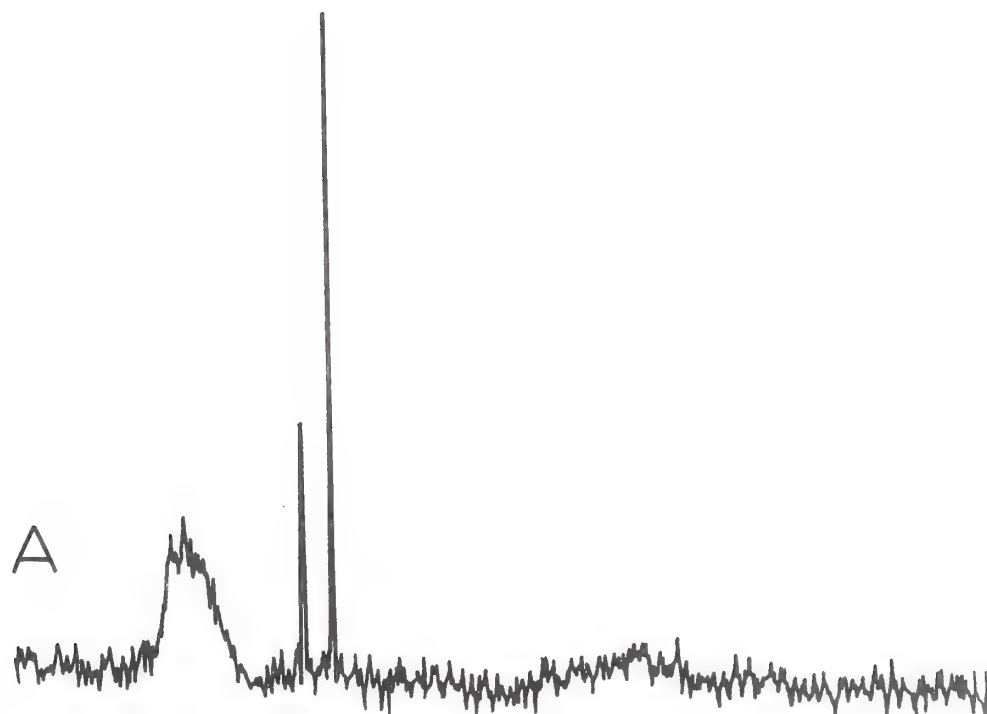


Figure 7. Effect of the addition of 2,3-DPG on carbamino resonances under conditions of low pH and low total carbonates.

(A) 9.9 mM deoxy Hb, 7.2 mM total carbonates, pH 7.20.

(B) 9.4 mM deoxy Hb, 9.9 mM total carbonates, pH 6.94.

This solution also contains 5 mM of 2,3-DPG.



Brenna et al. (25) interpreted their results on the assumption that carbamate formation at the β -chain NH_2 -terminals was nearly totally inhibited under the conditions of their experiments. Experiments by other workers indicate that such an assumption might be invalid (40), as Brenna et al. were careful to point out. On the basis of the NMR observations reported here and in Chapter IV, it seems clear that their assumption was indeed incorrect.

Further support of the contention that the β -chain NH_2 -terminal plays the most significant role in carbamate formation in human hemoglobin comes from the effect of organic phosphates on the resonance at 29.8 ppm under conditions of low carbonates. In Figure 7A is shown the 15.1 MHz ^{13}C NMR spectrum of 9.9 mM deoxyhemoglobin hemolyzate with 0.9 mM acetazolamide equilibrated with 7.2 mM total carbonates at pH 7.20. This is the same spectrum as shown in Figure 1A of Chapter IV. In Figure 7B, 9.4 mM hemoglobin hemolyzate with 0.9 mM acetazolamide is equilibrated with 9.9 mM total carbonates and 5 mM 2,3-DPG at pH 6.94. Under these conditions, the addition of the organic phosphate was sufficient to eliminate completely the only observable carbamino resonance. This resonance was at 29.9 ± 0.12 ppm, and corresponds to the β -chain NH_2 -terminus on the basis of the arguments presented above and in Chapter IV.

As in Chapter IV, the possibility of slow conformational exchange in the protein could also account for the results obtained in the presence of 2,3-DPG, without conflicting with the interpretation of Brenna et al. (25). DPG has, moreover, been reported to have a significant effect on the relative populations of the "R" and "T" forms in mixed hybrid hemoglobins and des-(146 β) hemoglobin (41,42). Although

of the two interpretations the more likely seems to be the specific assignment of one resonance per adduct, further experiments are needed to select unambiguously which interpretation is correct.

Observation of Carbamino Formation in Human Fetal Hemoglobin (Fo).

Human fetal hemoglobin (Fo) possesses alpha chains identical with those of adult hemoglobin Ao, but the β -chains are replaced by γ -chains (43). While the γ - and β -chains share a large degree of homology, the pattern of carbamino formation as monitored with the ^{13}C NMR is strikingly different. Typical observations at 15.1 MHz are shown in Figure 8 for deoxy fetal hemoglobin, and in Figure 9 for carboxy fetal hemoglobin. The conditions of the experiments shown in Figure 8 were 11.30 mM mean protein concentration, with 63 mM mean total carbonates. In Figure 9, 12.02 mM hemoglobin was equilibrated with 64 mM mean total carbonates. The NaCl concentration was 0.05 M in both studies.

In deoxy fetal hemoglobin, only a single narrow resonance was observed, until reaching pH values well above 8.0. The chemical shift of this large adduct was at 29.2 ppm, and did not shift by more than 0.1 ppm over the entire pH range studied. The additional adduct resonance apparent at high pH was at 28.4 ppm. Quantitative estimates of pK_C and pK_Z were not made in this study. However, a rough integration of the resonance at 29.2 ppm suggested that it quickly exceeded a Z value of 1, thereby proving its multicomponent nature. A very approximate estimation of the apparent pK_Z of this resonance would place its value near 8.0.

The contrast of deoxy fetal hemoglobin with carboxy fetal hemoglobin, Figure 9, is striking. Also unlike adult carboxyhemoglobin, the fetal counterpart exhibits no clearly resolved carbamate resonances

Figure 8. Deoxy fetal hemoglobin (Hb Fo) equilibrated with 63 mM mean total carbonates. Protein concentration was 11.30 mM.

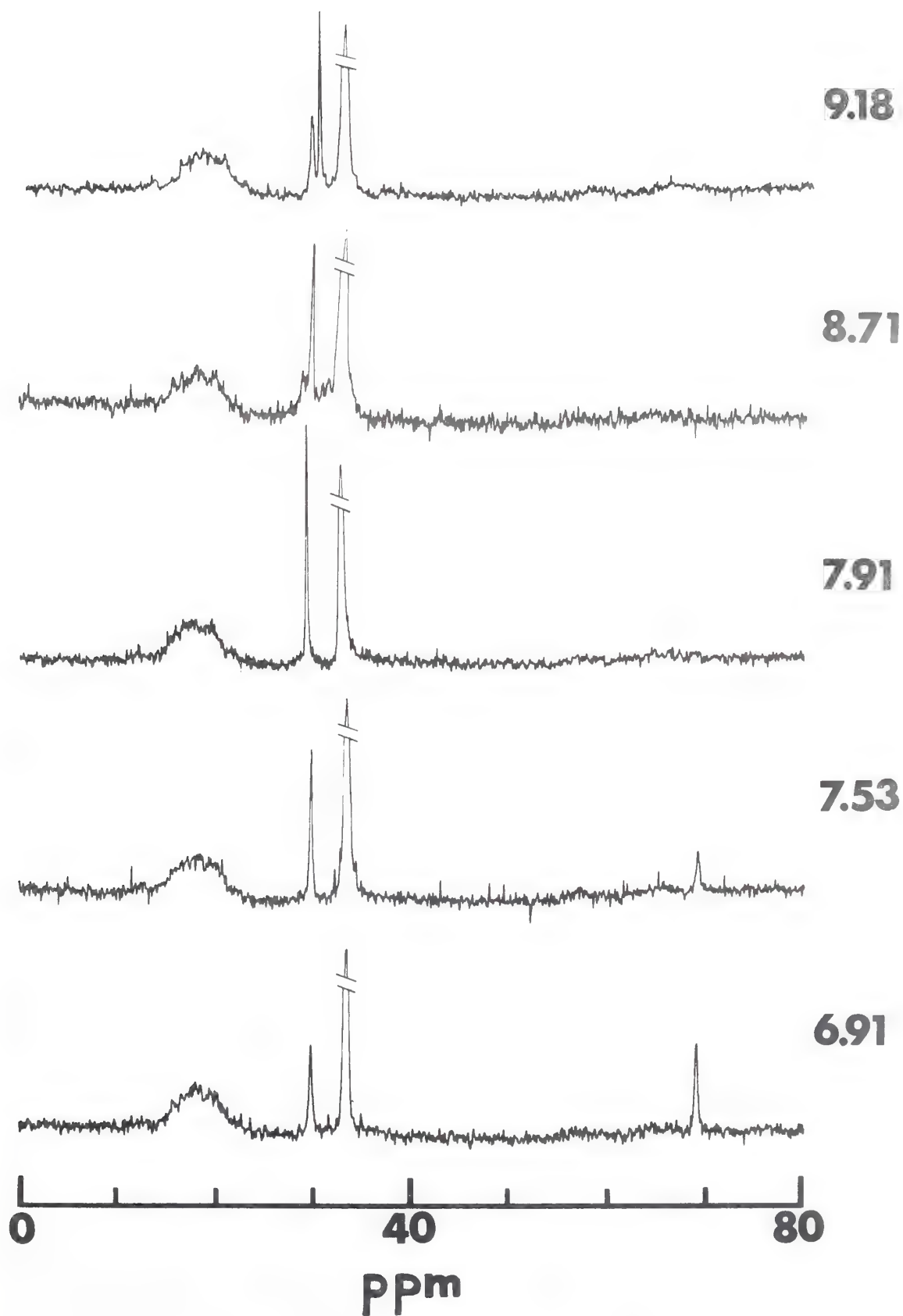
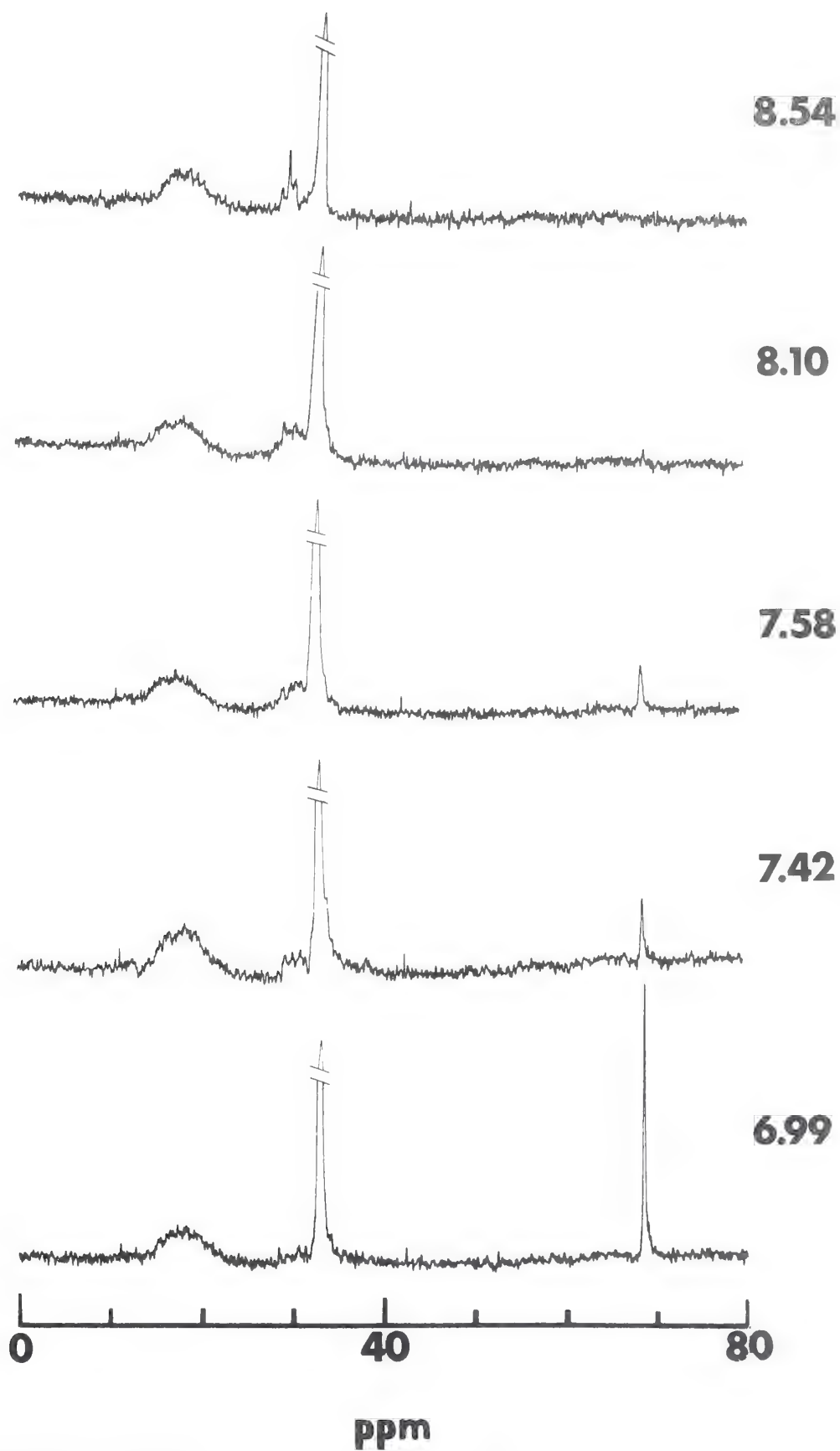


Figure 9. Carboxy fetal hemoglobin equilibrated with 64 mM carbonates. Mean protein concentration was 11.30 mM.



below pH values of approximately 8.5. The major resonance which finally becomes apparent at pH 8.54 is near 29.0 ppm, with one small shoulder upfield near 29.7 ppm, and another downfield at 28.3 ppm. No reliable estimates of the resonance integrals in these spectra could be made.

There exist 37 amino acid replacements in the γ -chain compared to the β -chains of hemoglobin (43). Eight of the first 13 residues are replaced, as well as the histidine 143, crucial to the DPG binding site (12). The NH_2 -terminal is a glycine; the proline at position 5 of the β -chain is replaced by a glutamic acid. A substantial reordering about the region of the β -chain NH_2 -terminus would thus not be unexpected. The NMR results reported above are qualitatively in accord with expectations. It seems likely that the resonance at 29.2 ppm represents the carbamate on the α -chain NH_2 -terminus as before. However, the carbamate resonance of the γ -chain NH_2 -terminal glycine probably also appears at 29.2 ppm. The resonance at 29.8 ppm in adult deoxyhemoglobin is completely absent, as would be expected if previous assignments were correct. The large amount of carbamate apparently being formed by solutions of deoxy fetal hemoglobin is also qualitatively in accord with the findings of Bauer and Schroder (44).

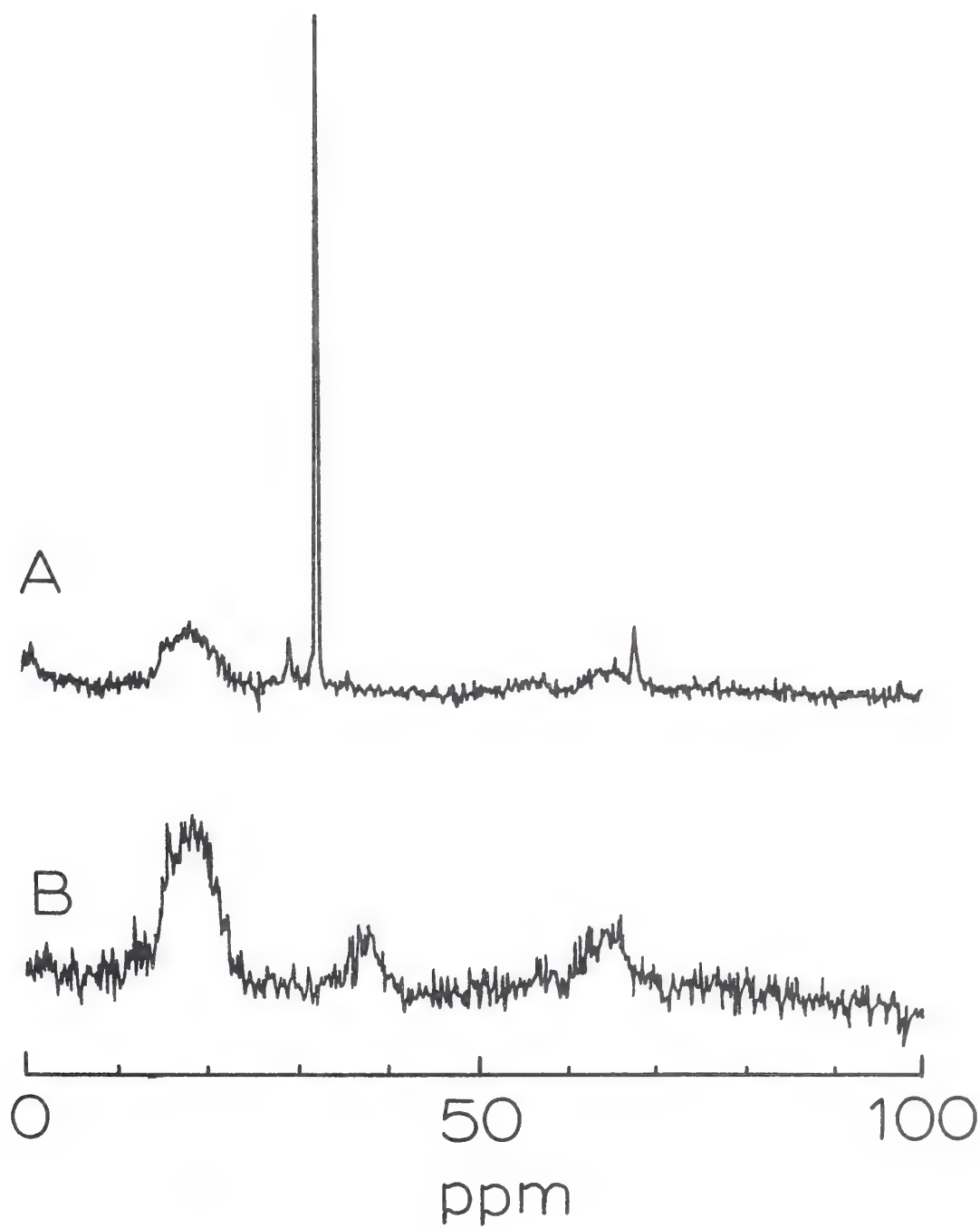
The most probable explanation of the behavior of the carbamate resonance(s) in carboxy fetal hemoglobin would attribute the broadness to chemical exchange with dissolved CO_2 (see Chapter IV), at rates appreciably greater than those characteristic of adult hemoglobin. However, the narrowness of the dissolved CO_2 resonance demands that if exchange at such rates is occurring between the carbamates and CO_2 , then the actual population of the carbamates must be minimal (Chapter IV). The absence of a narrow resonance representing carbamate on the

Figure 10. Human hemoglobin A₂($\alpha_2\delta_2$).

(A) deoxy Hb, 4.43 mM, 34 mM total carbonates, pH 7.08.

This solution also contained 0.1 mM acetazolamide to inhibit the carbonic anhydrase, responsible for the broadening of the bicarbonate resonance in (B).

(B) 7.04 mM carboxy Hb, 3 mM total carbonates at pH 7.16.



α -chain NH_2 -terminus is puzzling, since this site is presumably unchanged between fetal and adult hemoglobin. The possible catalytic role of salts, buffers, or paramagnetic impurities needs to be examined before a final solution can be proposed.

Observations of Carbamate Formation in Adult Human Hemoglobin A₂.

A single observation was made on deoxy and carboxyhemoglobin component A₂ ($\alpha_2\delta_2$) (Chapter II). The delta chain is 93% homologous with the β -chain, differing by only 10 residues (45). None of the differences involve residues about the NH_2 -terminal region. Histidine 143 is preserved. Thus, one expects the pattern of carbamate formation in this protein to be similar to that of HbA₀. Observations on HbA₂ are shown in Figure 10.

In Figure 10A, 4.43 mM deoxyhemoglobin ($\alpha_2\delta_2$) was equilibrated with 34 mM total carbonates at pH 7.08. The solution also contained 0.1 mM acetazolamide to inhibit the carbonic anhydrase responsible for the broadness of the bicarbonate-carbonate resonance in Figure 10B (see Appendix B). The hemoglobin concentration of the measurement shown in Figure 10B was 7.05 mM; total carbonates were 3 mM at pH 7.16. In the deoxy sample (Figure 10A) a single resonance is apparent at 29.9 ppm, while in the carboxy sample, albeit at lower carbonate levels, no resonance was apparent. The chemical shift of the adduct resonance in the deoxy sample was at 29.9 ppm, reminiscent of the adduct at 29.8 ppm in the HbA₀ under similar conditions.

Carbamate Formation in Hemoglobin S. Observations on sickle cell hemoglobin (HbS, β^6 (Glu→Val)) in the deoxy and carboxy states are shown in Figures 11A and B respectively. The conditions of the measurement shown in Figure 11A were 10.36 mM hemoglobin, equilibrated with

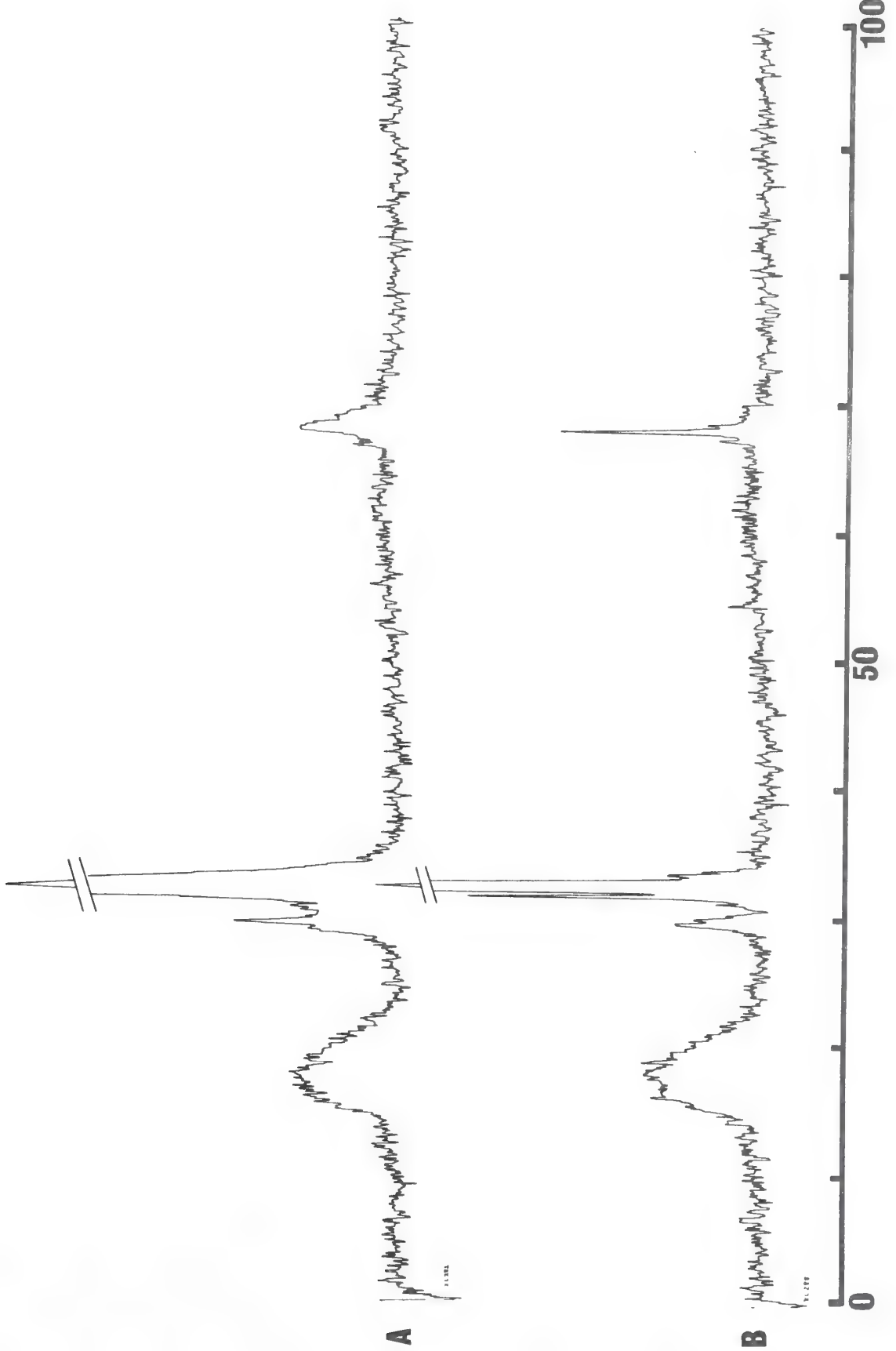
94 mM total carbonates at pH 8.28. In Figure 11B, 15.74 mM protein was equilibrated with 53 mM total carbonates at pH 7.65.

The broadness and overlap of the resonances in deoxy HbS (Figure 11A) probably result from a combination of factors, most significant of which include viscosity effects (46) and the elevated levels of carbonates. Deoxyhemoglobin S forms highly ordered aggregates of very high average molecular weight (47). Macroscopically, this is evidenced by gel formation. The sample used for the NMR measurement in Figure 11A was so gelled. Nevertheless, at least one clearly resolved carbamate resonance is discernible at 29.9 ppm, confirming the ability of the protein to combine with appreciable amounts of CO₂ even while simultaneously involved in the gel matrix. This result was expected, since CO₂ enhances the tendency of HbS to gel. It is not clear why the resonance expected at 29.2 ppm is absent. The process of gelation may block access to this site, or favor alternate salt linkages, diminishing K_c. Rapid exchange with solution CO₂, suggested by the very broad CO₂ resonance, is also possible. Further comment must await more detailed study.

The pattern of carbamate formation in carboxyhemoglobin S (Figure 11B) is highly reminiscent of that observed in carboxyhemoglobin A₀ at pH values less than about 7.3 (Chapter IV). Two adduct resonances were distinguishable at 29.8 and 30.6 ppm. The small difference in the behavior of carboxy HbS and carboxy HbA₀ is consistent with the suggestion made in Chapter IV that the resonance moving upfield at low pH in carboxy HbA₀ represented the β -chain NH₂-terminal adduct. Presumably in HbS the substitution of a valine for the glutamic acid residue at position 6 of the β -chain has perturbed in some manner the

Figure 11. ^{13}C NMR spectra of sickle cell hemoglobin (HbS) in the presence of $[^{13}\text{C}]$ carbamates.

- (A) Deoxy HbS, 10.36 mM, equilibrated with 94 mM total carbonates at pH 8.28.
- (B) (15.74 mM) Carboxy hemoglobin S equilibrated with 53 mM total carbonates at pH 7.65.

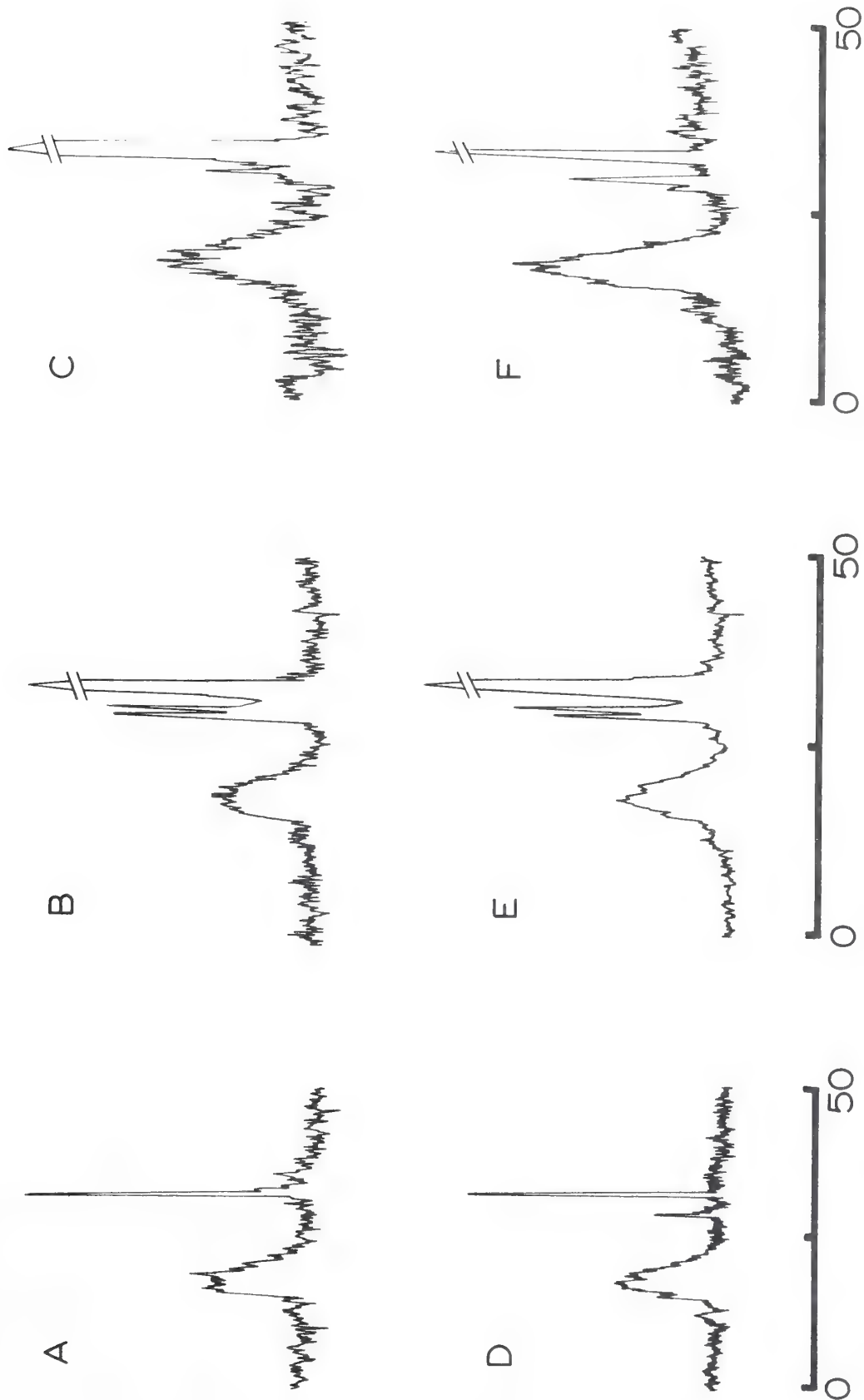


pH dependence of the environment of the carbamate (48,49). Other explanations are of course possible; more experiments are needed.

Carbamate Formation in Chicken Hemoglobin. The study of CO₂ binding to chicken hemoglobin was initially undertaken on the basis of reports that the α -chain NH₂-terminus of the A_I component was naturally acetylated (50). Subsequent work in this laboratory, however, in collaboration with Mr. R. J. Wittebort, has shown that the white leghorn chickens obtained through Dr. Zeller from the local farm cooperative did not possess an acetylated NH₂-terminus on either hemoglobin component A_I or A_{II}. However, the A_I component did possess another unusual and striking property. Upon deoxygenation in solutions of low ionic strength, the A_I chicken hemoglobin was found to become turbid and viscous, in marked similarity to the in vitro behavior of HbS. This aggregation was found to be completely reversible upon reoxygenation. A more thorough study of this interesting phenomena, made in collaboration with Mr. Wittebort (Appendix D), demonstrated that the aggregation probably was the result of micro-crystallization, and that it was markedly inhibited by the presence of CO₂ (or bicarbonate). For this reason, its NMR behavior was of some interest.

In Figure 12, observations on chicken HbA_I are compared with similar observations on the chicken HbA_{II} component, which was not found to behave unusually. Sequence analysis (51) (Appendix D) had shown that the β -chains of the two hemoglobins were probably identical, while the α -chains were markedly different. The NH₂-terminal of the HbA_I α -chain was found to be methionine; that of the HbA_{II} α -chain is known to be valine.

Figure 12. 15.1 MHz ^{13}C NMR spectra of chicken hemoglobins A_I (top), A_{II} (bottom) in 0.05 M NaCl under various conditions. (Except C, which was done at 25.2 MHz.) Temperature was 30°. A, HbA_I pH 7.00, 7 mM carbonates; B, HbA_I pH 8.66, 68 mM carbonates; C, HbA_I CO pH 8.12, 67 mM carbonates; D, HbA_{II} pH 7.28, 13 mM carbonates; E, HbA_{II} pH 8.40, 70 mM carbonates; F, HbA_{II} CO pH 7.47, 29 mM carbonates; Hemoglobin concentration was between 6 to 12 mM.



At neutral pH and low carbonate levels, HbA_I formed no detectable carbamino signals (Figure 12A). With increased pH and carbonate levels, there developed two strong resonances at 29.2 and 28.4 ppm (Figure 23B), presumably representing the N-terminal and ϵ -amino carbamino adducts, respectively. This behavior may be contrasted with that of hemoglobin component A_{II} under comparable conditions, which formed a single resonance at 29.3 ppm near neutral pH (Figure 12D), and two resonances, again at 29.2 and 28.4 ppm, at alkaline pH values and higher carbonate levels (Figure 12E). The small difference in CO₂ affinity between the two deoxygenated hemoglobins, most apparent in Figures 12A and 12D, is enhanced upon ligation of the heme. While the two adduct resonances present in HbA_{II} are found in HbA_{II}CO (Figure 12F), HbA_ICO exhibits only a relatively weak resonance at 29.2 ppm (Figure 12C). At much higher pH values, the resonance at 28.4 ppm, missing in Figure 12C, becomes quite large, reinforcing its assignment to ϵ -amino carbamino adducts. The conditions of each measurement are described in the figure legend.

The presence of CO₂ clearly favors the deoxy HbA_I conformation. In HbS, this leads to enhanced gelation (52). The inhibition of aggregation in HbA_I solutions may imply that bicarbonate ion, even at relatively low concentrations, is a potent inhibitor of the gelation, a property not shared by NaCl solutions at concentrations greater than even 0.1 M. Alternatively, the aggregation may actually involve a conformational transition of the protein to a form which is neither truly "R" nor "T", but rather some third configuration, stabilized by the formation of macromolecular aggregates. This possibility is consonant with the inhibition of the aggregation by IHP, a compound also expected

to stabilized the "deoxy" conformation (13). Appendix D reports further details on the nature of chicken hemoglobin A_I and its reversible ligand dependent aggregation.

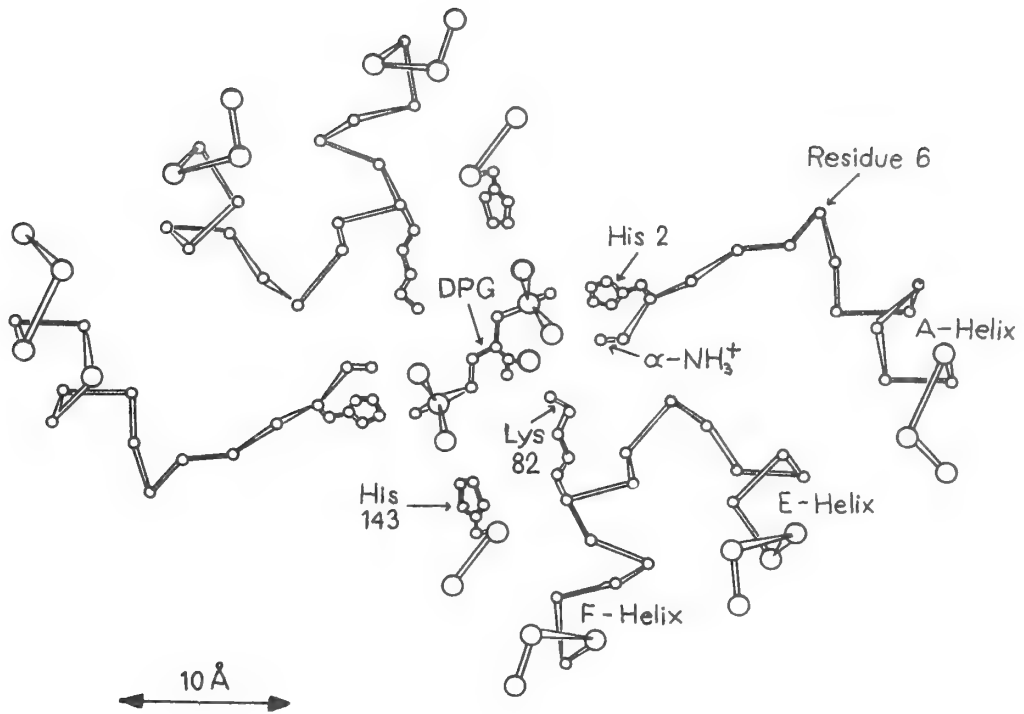
Conclusion

The sensitivity and discriminatory power of the NMR technique allows the detection of allosteric events in hemoglobin at the molecular level. As such, the effect of the competition of CO₂ with 2,3-DPG was monitored directly. The results imply that CO₂ can compete effectively with DPG for binding at the β -chain NH₂-terminus, and conversely, that a high concentration of 2,3-DPG is not without effect on the binding of CO₂ to the α -chain NH₂-terminus. The former result might not have been expected (25), based on the high affinity of deoxyhemoglobin for 2,3-DPG. An adequate mathematical description of the competing effects of CO₂ and 2,3-DPG thus remains to be established.

The complete elimination of the resonance at 28.3 to 28.4 ppm in deoxyhemoglobin by small amounts of 2,3-DPG suggests an additional site of direct competition. The pK_Z value determined in the absence of 2,3-DPG for this resonance was 8.8 (Chapter IV). Its chemical shift is characteristic of an ϵ -amino adduct. The changes in pK_C and pK_Z of this resonance upon conversion to the liganded form suggest that below pH 9, the resonance probably represents multiple adducts in carboxyhemoglobin, all with normal pK_Z values, but primarily a single adduct in deoxyhemoglobin. These findings implicate lysine 82 β (Figure 13) as the most likely site of carbamino formation subsequent to that at the NH₂-terminals.

The results with hemoglobins other than HbA₀ displayed a large variability in response to CO₂, suggestive that as in their interactions with 2,3-DPG (19), different hemoglobins may exhibit physiological non-equivalence.

Figure 13. Sketch showing the NH_2 - and C-terminal regions of the β -chains of human deoxyhemoglobin. Also depicted is the binding of 2,3-DPG at this site. (From Arnone (12)).



REFERENCES

1. Benesch, R. and Benesch, R. E. (1967) Biochem. Biophys. Res. Commun. 26, 162-167
2. Benesch, R. and Benesch, R. E. (1967) Fed. Proc., Fed. Amer. Soc. Exp. Biol. 26, 673
3. Chanutin, A. and Curnish, R. R. (1967) Arch. Biochem. Biophys. 121, 96-102
4. Brewer, G. J. ed. (1970) "Red Cell Metabolism and Function," Plenum, New York
5. Rørth, M. and Astrup, P. eds. (1972) "Oxygen Affinity of Hemoglobin and Red Cell Acid Base Status," Academic Press, New York
6. de Verdier, C. H., Garby, L., Hogman, C. F. and Akerblom, O. (1969) Forsvarsmedicin 5, 145
7. Benesch, R. and Benesch, R. E. (1969) Nature 221, 618-622
8. Benesch, R. and Benesch, R. E. (1970) Fed. Proc., Fed. Amer. Soc. Exp. Biol. 29, 1101-1104
9. Bunn, H. F. and Jandl, J. H. (1970) N. Eng. J. Med. 282, 1414-1421
10. Klocke, R. A. (1972) Chest 62, 79S
11. Benesch, R. E. and Benesch, R. (1974) Adv. Prot. Chem. 28, 211-237
12. Arnone, A. (1972) Nature 237, 146-149
13. Arnone, A. and Perutz, M. F. (1974) Nature 249, 34-36
14. Garby, L., Robert, M. and Zaar, B. (1969) Eur. J. Biochem. 10, 110-115
15. Chanutin, A. and Hermann, E. (1969) Arch. Biochem. Biophys. 131, 180-184
16. Benesch, R., Benesch, R. E. and Yu, C. I. (1968) Proc. Natl. Acad.

- Sci. 59, 526-532.
17. Garby, G. and de Verdier, C. H. (1972) in Oxygen Affinity of Hemoglobin and Red Cell Acid-Base Status: Alfred Benzon Symp. IV, Rørth, M. and Astrup, P., eds., Academic Press, New York, 236-242
 18. Benesch, R. E., Benesch, R. and Yu, C. I. (1969) Biochem. 8, 2567-2571
 19. Tomita, K. and Riggs, A. (1971) J. Biol. Chem. 246, 547-554
 20. Riggs, A. (1971) Proc. Natl. Acad. Sci. 68, 2062-2065
 21. Bauer, C. (1969) Life Sci. 8, 1041-1046
 22. Bauer, C. (1970) Resp. Physiol. 10, 10-19
 23. Pace, M., Rossi-Bernardi, L. and Roughton, F. J. W. (1970) Biochem. J. 119, 67P
 24. Rossi-Bernardi, L., Roughton, F. J. W., Pace, M. and Coven, E. (1972) in Oxygen Affinity of Hemoglobin and Red Cell Acid Base Status, Rørth, M. and Astrup, P., eds., Academic Press, New York, 224-235.
 25. Brenna, O., Luzzana, M., Pace, M., Perrella, M., Rossi, F., Rossi-Bernardi, L. and Roughton, F. J. W. (1972) Adv. in Exp. Med. and Biology, Brewer, G. J. ed., Plenum, New York, 28, 19-37.
 26. Gray, R. D. and Gibson, Q. H. (1971) J. Biol. Chem. 246, 7168-7174
 27. Wyman, J. (1948) Advan. Prot. Chem. 4, 407-531.
 28. Benesch, R. E., Benesch, R., Renthal, R. and Gratzer, W. B. (1971) Nature New Biol. 234, 174-175.
 29. Olson, J. S. and Gibson, Q. H. (1970) Biochem. Biophys. Res. Commun. 42, 9-15
 30. Olson, J. S. and Gibson, Q. H. (1971) J. Biol. Chem. 247, 5241-5253

31. Olson, J. S. and Gibson, Q. H. (1972) *J. Biol. Chem.* 247, 1713-1726
32. Lindstrom, T. R., Olson, J. S., Mock, N. H., Gibson, Q. H. and Ho, C. (1971) *Biochem. Biophys. Res. Commun.* 45, 22-26
33. Cassoly, R., Gibson, Q. H., Ogawa, S. and Shulman, R. G. (1971) *Biochem. Biophys. Res. Commun.* 44, 1015-1021
34. Lindstrom, T. R. and Ho, C. (1972) *Proc. Natl. Acad. Sci.* 69, 1707-1710
35. Ogawa, S. and Shulman, R. G. (1971) *Biochem. Biophys. Res. Commun.* 42, 9-15
36. Shulman, R. G., Ogawa, S. and Hopfield, J. J. (1971) *Cold Spring Harbor Symp. Quant. Biol.* 36, 337-341
37. Bonaventura, J., Bonaventura, C., Giardina, B., Antonini, E., Brunori, M. and Wyman, J. (1972) *Proc. Natl. Acad. Sci.* 69, 2174-2178
38. Bunn, H. F. and Briehl, R. W. (1970) *J. Clin. Invest.* 49, 1088-1095
39. Kilmartin, J. V. and Rossi-Bernardi, L. (1973) *Physiol. Rev.* 53, 836-890
40. Caldwell, P. R. B., Nagel, R. L. and Jaffe, E. R. (1971) *Biochem. Biophys. Res. Commun.* 44, 1504-1509
41. Moffat, K., Olson, J. S., Gibson, Q. H. and Kilmartin, J. V. (1973) *J. Biol. Chem.* 248, 6387-6393
42. Cassoly, R. and Gibson, Q. H. (1972) *J. Biol. Chem.* 247, 7332-7341
43. Schroeder, W. A. (1963) *Ann. Rev. Biochem.* 32, 301-320
44. Bauer, C. and Schroder, E. (1972) *J. Physiol.* 227, 457-471
45. Huisman, T. H. J. (1969) in *Biochemical Methods in Red Cell Genetics*, Yunis, J. J., ed., Academic Press, New York, 393-394

46. Carrington, A. and McLachlan, A. D. (1967) Introduction to Magnetic Resonance, Harper and Row, New York, Chap. 3
47. Murayama, M. (1973) CRC Crit. Rev. in Biochem., Sept., 461-499
48. Shire, S. J., Hanania, G. H. and Gurd, F. R. N. (1974) Biochem. 13, 2967-2974
49. Shire, S. J., Hanania, G. H. and Gurd, F. R. N. (1974) Biochem. 13, 2974-2979
50. Matsuda, G., Maita, T. and Nakagina, M. (1974) J. Biochem. (Tokyo) 56, 490-491
51. Matsuda, G., Maita, T., Mizuno, K. and Ota, H. (1973) Nature New Biol. 244, 244-245
52. Arnone, A. (1974) Nature 247, 143-145

CHAPTER VI

Carbamino Compounds and Homeostasis

Chapter VI

Carbamino Compounds and Homeostasis

It is certain that all bodies whatsoever, though they have no sense, yet they have perception; for when one body is applied to another, there is a kind of election to embrace that which is agreeable, and to exclude or expel that which is ingrate; and whether the body be alterant or altered, evermore a perception precedeth operation; for else all bodies would be like one to another.

Francis Bacon
(c. 1620)

The preceding chapters have described the generality of the carbamino reaction and the factors defining the extent of carbamate formation under a variety of conditions. In the present and final chapter, it is proposed that carbamino formation is capable of modulating the activity of numerous biologically active peptides and hormones, thereby providing a sensitive mechanism of local response to changes in CO_2 or pH. As is apparent by Equation 9, Chapter III, the carbamino reaction is only indirectly linked to bicarbonate, but is exquisitely sensitive to pH. The extent of formation for any given amine will thus be determined by K_c , K_z , pH and pCO_2 . K_c and K_z act so as to alter the emphasis of the carbamate response in the physiological range, increased K_z favoring diminished pH sensitivity. Thus by appropriate adjustments of K_c and K_z , systems responding with different weights but by the same mechanism may be envisioned.

The importance of CO_2 homeostasis need hardly be stressed. As Hastings (1) has pointed out, CO_2 tension is more carefully controlled by the body than is pH. However, because a biochemical reason was

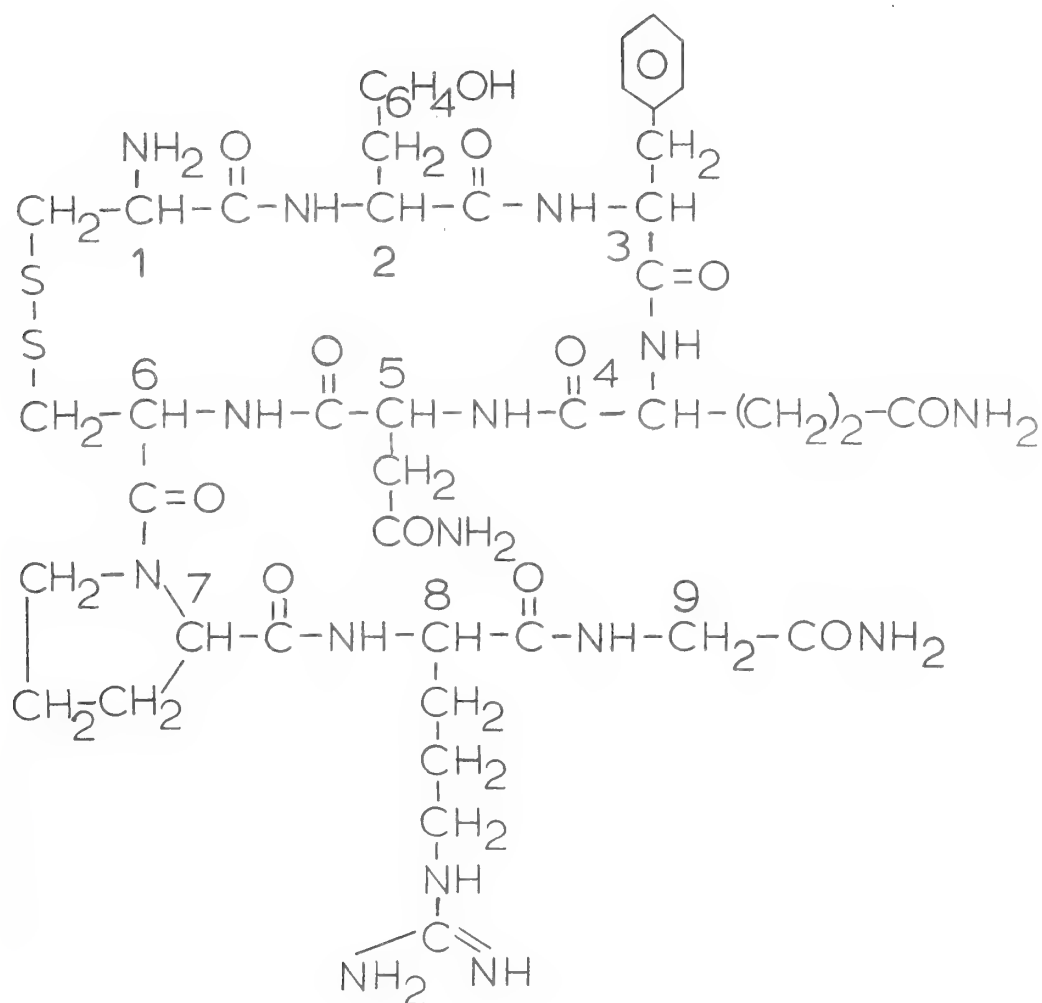
lacking, the CO_2 sensitivity of biological reactions has essentially been neglected (1). The experiments with the model compounds described in Chapter III, as well as with hemoglobin in Chapters IV and V, suggested a number of mechanisms by which the presence of the carbamate might be expressed. Moreover, the effect of the carbamate need not be limited to intramolecular responses. The possibility of the free amine and carbamate forms being related as agonist and antagonist with respect to a receptor site is distinctly tangible. The susceptibility of peptides and proteins to attack by aminopeptidases will probably be reduced upon formation of the carbamate. Partition coefficients between lipid and aqueous phases are also likely to be altered. Thus, carbamino formation could lead to activation or inactivation of the compound itself, affect synthesis or degradation, reduce its ability to penetrate lipid membranes, and even convert it into an antagonist.

Many potential avenues exist to explore the concept that control of CO_2 homeostasis through formation of carbamino compounds is central to general regulatory mechanisms. A particularly attractive first step is the examination of the reactivity with CO_2 of the vasoactive principles involved in cardiovascular and fluid adjustments. These principles are elaborated or activated in situations, both physiological and pathological, characterized by alterations in the local (or general) levels of CO_2 . Such situations include exercise, stagnation and ischemia. Among the compounds that might be considered are those involved in the renin-angiotensin system, kinins, vasopressins, histamine, serotonin, and various less well characterized compounds, such as myocardial depressant factor, vasoactive intestinal peptide, and the slow reacting

substance of anaphylaxis (2-8). Of these, members of the vasopressin and angiotensin series were selected for further study.

Vasopressin. Although in man the antidiuretic action of the vasopressins appears functionally dominant, the development of synthetic analogs has shown that the α -amino group is associated relatively with the vasopressor activity, and that its absence is compatible with full antidiuretic function (9). The primary structure of arginine vasopressin is shown in Figure 1 (10). Its NH_2 -terminal is a cystine, and it possesses no other amines reactive with CO_2 . Conversely, in lysine vasopressin position 8 is replaced by a lysine residue, which while potentially reactive with CO_2 , probably does not form carbamate in the physiological pH range.

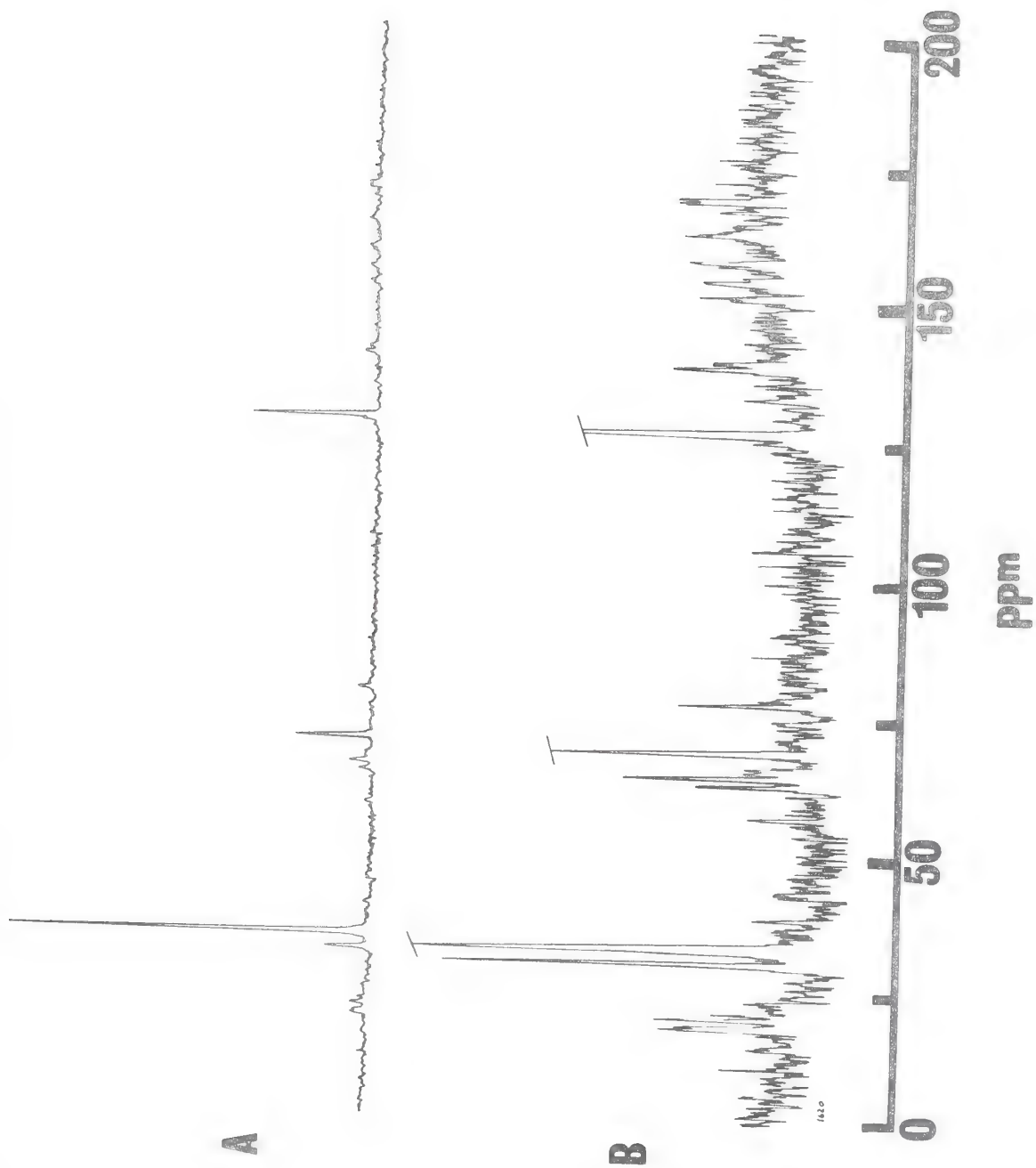
Figure 2 shows the spectrum of [8-L-homolysine]-vasopressin, a close analogue of lysine vasopressin, equilibrated with $^{13}\text{CO}_2$ at pH 6.62, total carbonates 52 mM, and 30° . The upper spectrum, A, at lower gain, shows the carbamino resonance at 30.0 ppm, the dominant bicarbonate-carbonate resonance at 32.6 ppm, and the CO_2 resonance at 68.3 ppm. The large resonance at 126.2 ppm represents the dioxane marker. The chemical shifts of the various resonances are in keeping with previous experience. That for the carbamino derivative is somewhat distinctive, in that precisely the same chemical shift has been observed only for the carbamino adduct of proline. The shift observed for the carbamino adduct of L-cysteine was 28.4 to 29.2 ppm (Chapter III). The lower spectrum, B, shows the natural abundance signals from the peptide itself. The signal to noise ratio is adequate to recognize the resonances by comparison with the measurements of Lyster and Freedman on lysine vasopressin (11). The chemical shifts generally fit with previous studies on small



cys-tyr-phe-gln-asn-cys-pro-arg-gly(NH₂)

Figure 1. Primary structure of Arginine vasopressin.

Figure 2. 15.1 MHz ^{13}C NMR spectrum of [8-homolysine] vasopressin equilibrated with 52mM total carbonates; mole fraction ^{13}C was 0.03, pH = 6.62. The top spectrum (A) clearly shows the carbamino, bicarbonate, and free CO_2 resonances, in that order with increasing chemical shifts, as well as the dioxane standard at 126.2 ppm. (B) The same spectrum at increased gain; many of the resonances of the peptide itself (at natural abundance) are now discernible (11).



peptides (12-15). Spectra were also obtained at pH 7.22 and pH 7.62.

The chemical shift of the carbamino carbon was invariant with pH.

The chemical shift of the carbamino adduct was also found to be at 30.0 ppm for a 5 mM solution of [4-valine]-arginine vasopressin at pH 8.24. The natural abundance contribution to the spectrum was not observable at this low concentration. With a similar solution of [1-deamino-4-valine]-arginine vasopressin at pH 7.44 no carbamino adduct was observed. These results confirm the assignment of the resonance at 30.0 ppm in the present study to the carbamino adduct of the NH₂-terminal, and also confirm that the reaction with the homolysine vasopressin was confined to the α -amino group under these conditions. The ϵ -amino adduct, if present, would be expected to show a chemical shift near 28.2 ppm, by analogy with the ϵ -amino adduct (Chapter III).

The carbamino signals for the 8-L-homolysine vasopressin obtained at each pH value were integrated digitally, and related to the integral values observed for the bicarbonate-carbonate and dissolved CO₂ resonances and the known concentrations of total carbonates. Equation 9, Chapter III, was adapted to deal directly with pairs of experiments to yield an expression, independent of total amine concentration, leading to values of K_c. More explicitly:

$$K_c = \frac{[CO_2]_1 \cdot CAM_2 \cdot (K_Z[H^+]_2 + [H^+]_2^2) - [CO_2]_2 \cdot CAM_1 \cdot (K_Z[H^+]_1 + [H^+]_1^2)}{[CO_2]_2 \cdot [CO_2]_1 \cdot K_Z \cdot (CAM_1 - CAM_2)} \quad (1)$$

where

$$[CO_2]_i = \frac{(TC_i - CAM_i) \cdot [H^+]_i^2}{K'_1 K'_2 + [H^+] \cdot (K'_1 + [H^+])} \quad (2)$$

CAM_i and TC_i represent the concentration of carbamate and total carbonates in solutions (i) respectively.

The value of pK_Z was estimated from the literature for the experimental conditions as 6.4 (16). A 40° pulse width was used for the measurements at a pulse repetition rate of 1 sec⁻¹. Small corrections were applied assuming spin-lattice relaxation times of 1 second for the carbamino resonance and 5 seconds for the other resonances. The estimated maximum value of pK_C was near 5.0.

Also of interest in these solutions was the lack of significant broadening of the carbamate resonance, considering the pH at which some of the measurements were made. If the linewidth of the internal dioxane marker is taken as representative of $\frac{1}{\pi T_2}$ in the absence of exchange, then by Equation 4 Chapter IV the dissociation rate of the carbamate from the vasopressin cannot be greater than approximately 5 sec⁻¹ at pH 6.67, in contrast to an expected rate of 25 to 50 sec⁻¹ for other primary amines at this pH (17).

[5-Ile]-Angiotensin II. Angiotensin II is one of the most powerful pressor agents known, with direct and indirect effects upon both the heart and peripheral vasculature. It is also the prime activator of the aldosterone system (18), and thus constitutes an intriguing link between electrolyte balance and vascular phenomena. Its high affinity for CO₂, described below, extends its range of interaction to include the potential for respiratory and metabolic sensing and control.

The primary structure of [5-Ile]-angiotensin II is shown in Figure 3. Also shown in Figure 3 is the sequence of its activation from angiotensinogen. While the present consideration concerns only

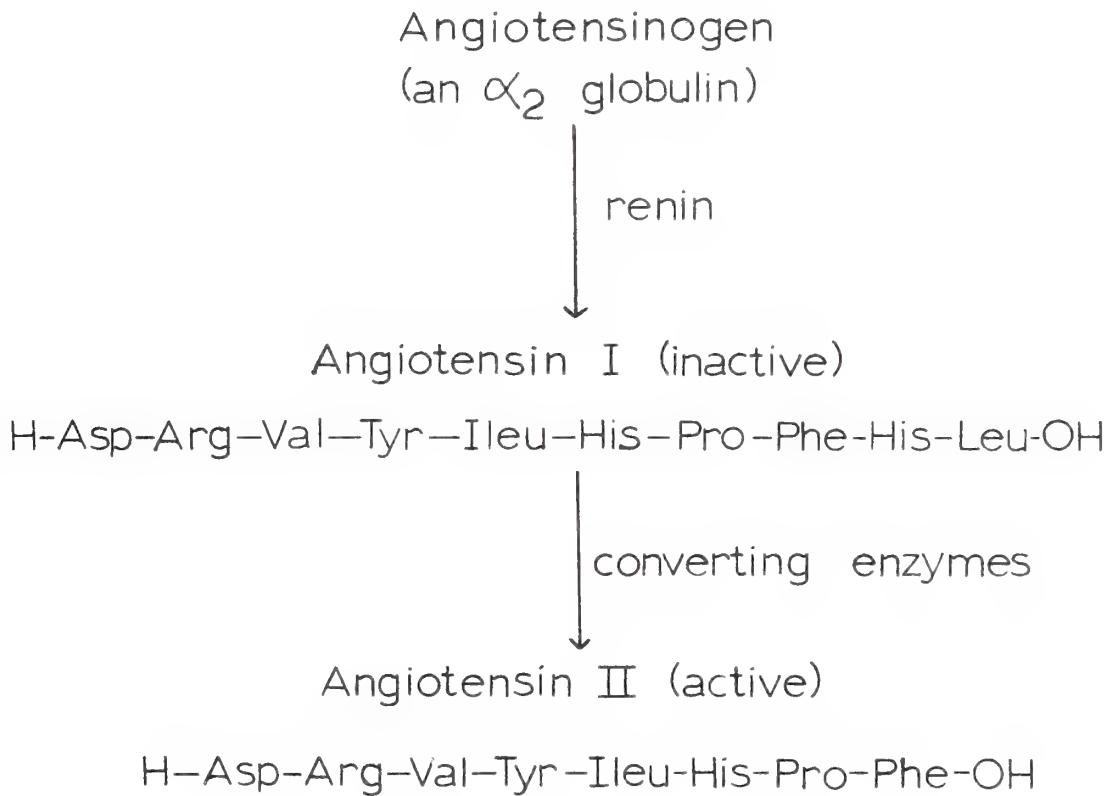


Figure 3. The primary structure and sequence of activation of Angiotensin II.

the active form, the possibility of in vivo control by CO_2 at any stage of its formation must not be overlooked.

In Figure 4 is shown the spectrum obtained with an approximately 20 mM solution of [5-Ile]-angiotensin II at pH 7.39 with 69 mM total carbonates at 30° . As before, similar measurements were made at pH values of 7.84 and 8.05. The carbamino adduct resonance was at 29.5 ppm, and did not vary with pH. The chemical shift of this adduct is upfield of that observed in free aspartic amino acid. The carbamino signals at the three pH values were integrated as before. The value of pK_C obtained was approximately 4.7, assuming a pK_Z of 7.6. This last value was estimated from the value for an asparagine analogue (19), and adjusted for the difference in pK_Z between aspartic acid and asparagine (20).

In Figure 5 is shown the spectrum of angiotensin II measured by means of a $180^\circ\text{-}\tau\text{-}90^\circ$ pulse sequence; τ was 1 sec. Under such conditions, the degree of recovery of the resonance to its normal upright appearance is a function of its spin-lattice relaxation time (T_1) (c.f. Chapter III, Chapter IV). While quantitative measurements of T_1 were not made, the single experiment shown in Figure 5 is sufficient to establish that the relaxation time of the bicarbonate-carbonate resonance near 32.6 ppm is less than the T_1 of the carbamate resonance, and is drastically shortened when compared with its value measured in the absence of other solutes (10 sec) (Chapter III and Appendix B). While contamination by paramagnetic compounds might account for this behavior, the result is reminiscent of that observed for certain of the pentapeptides in Chapter III. As such, it may constitute additional evidence for a direct bicarbonate interaction distinct from carbamino formation with certain polypeptides.

Figure 4. 15.1 MHz ^{13}C NMR spectrum of [5-Ile] angiotensin II equilibrated with 69mM total carbonates; mole fraction C^{13} was 0.86, pH 7.39. In (A), the pattern of enriched resonances is again clearly seen, as in Figure 2, while in (B) some of the natural abundance resonances of the peptide itself are discernible.

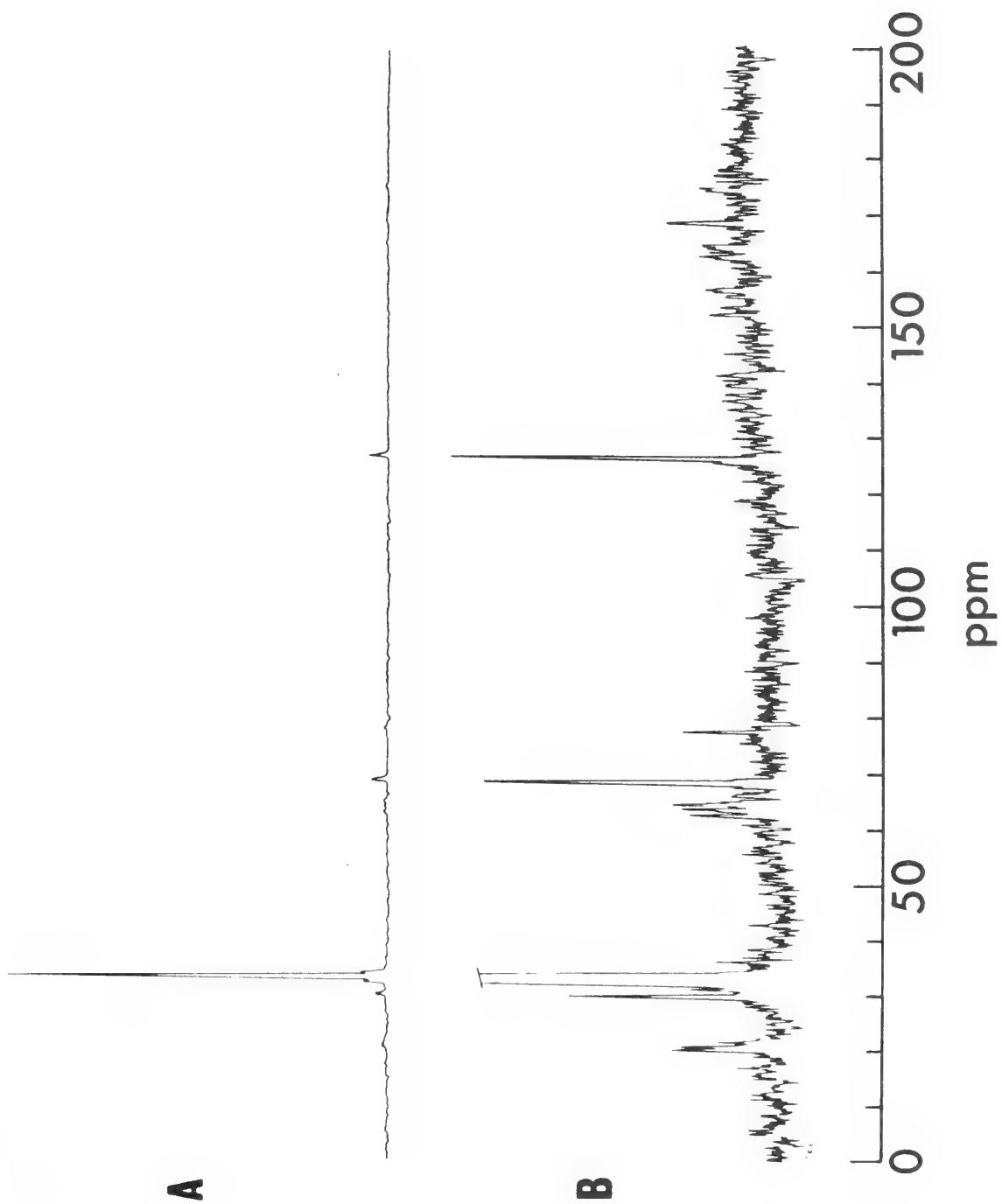
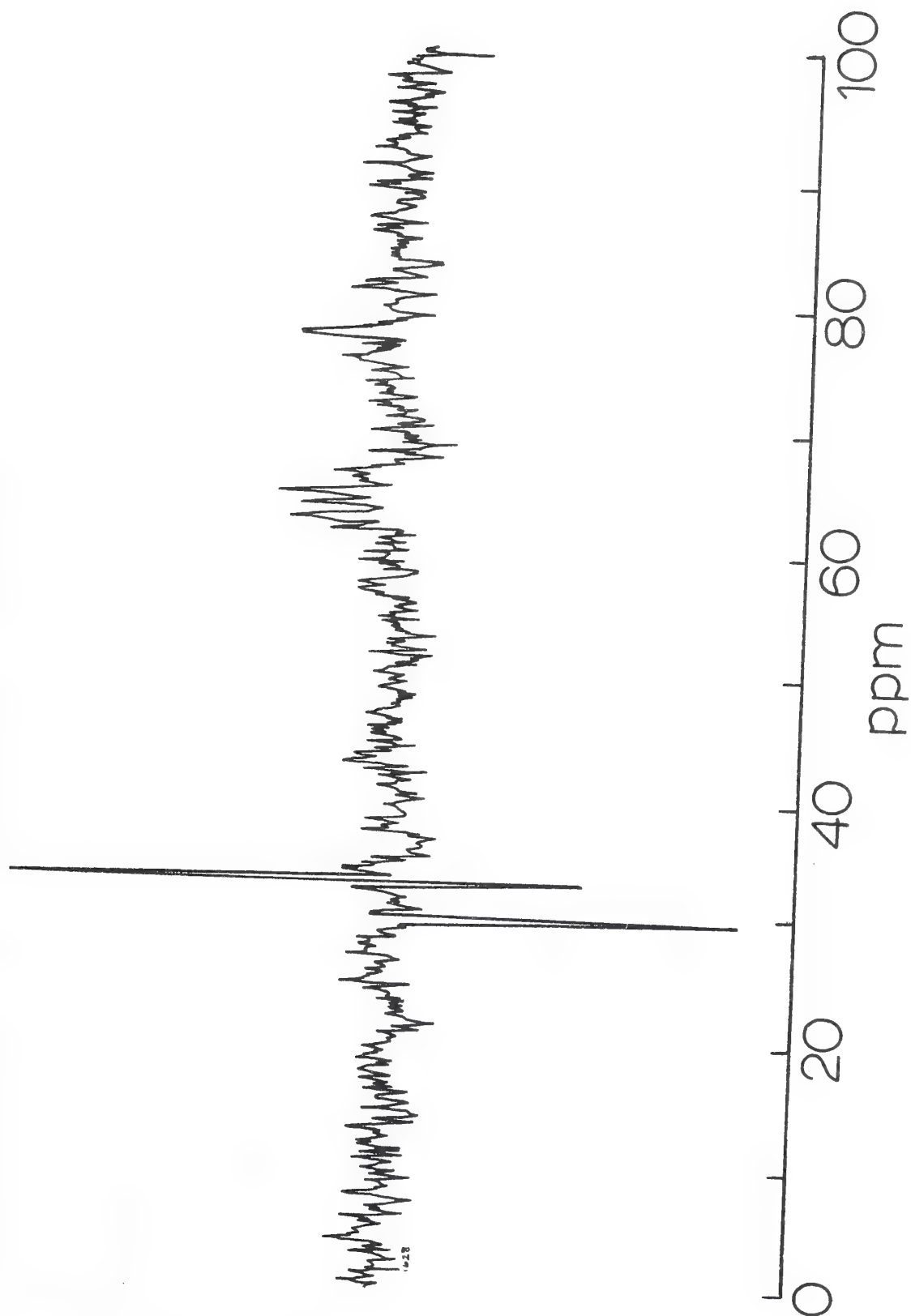


Figure 5. Partially relaxed $180-\tau-90^\circ$, 15.1 mHz ^{13}C NMR spectrum of Angiotensin II, at pH 7.66. Recycle time 5.00 sec; $\tau = 1.0 \text{ sec}$.



Discussion

Stability Ranges of Carbamino Derivatives. The approximate value of pK_c found for [8-homolysine]-vasopressin, 5.0, taken with the pK_z of 6.4, was used to compute the mole fraction, Z , of the peptide in the carbamino form (Equation 9, Chapter III). The results are shown in the form of Figure 6, calculated with Fortran program ISOBAR (Appendix C). The curves for various values of Z are identified on the right hand ordinate. The left hand ordinate shows bicarbonate concentration. The abscissa indicates pH values between 7.0 and 8.0. The curves that are concave upward represent a series of isobars for the pressure of CO_2 , varying between 10 and 150 mm Hg.

The graph in Figure 6 shows that for a normal arterial pCO_2 of 40 mm Hg, 24 mM bicarbonate, and pH 7.41, the mole fraction of the vasopressin in the form of the carbamino derivative is near 0.3. For a normal venous pCO_2 of 47 mm Hg, 28 mM bicarbonate, and pH 7.38, the mole fraction of the carbamino derivative rises somewhat but remains near 0.3.

The upper left region of Figure 6 corresponds to conditions of respiratory acidosis, and the lower right to respiratory alkalosis. The adjustments in both these directions from the normal are accompanied by changes in Z that are similar to those that will accompany metabolic acidosis (lower left) and metabolic alkalosis (upper right).

The corresponding figure for the angiotensin II system is shown in Figure 7. The values of pK_z and pK_c used here are 7.6 and 4.7 respectively. The main differences from Figure 6 are the consequences of a higher value for pK_z which displaces the curves for the carbamino mole

Figure 6. Relationship between pH, $p\text{CO}_2$, bicarbonate concentration, and mole fraction (Z) of [8-homolysine] vasopressin in the carbamino form, under conditions approximating the physiological range. Approximate normal arterial conditions (Θ); approximate mixed venous conditions (ϕ). See text for details.

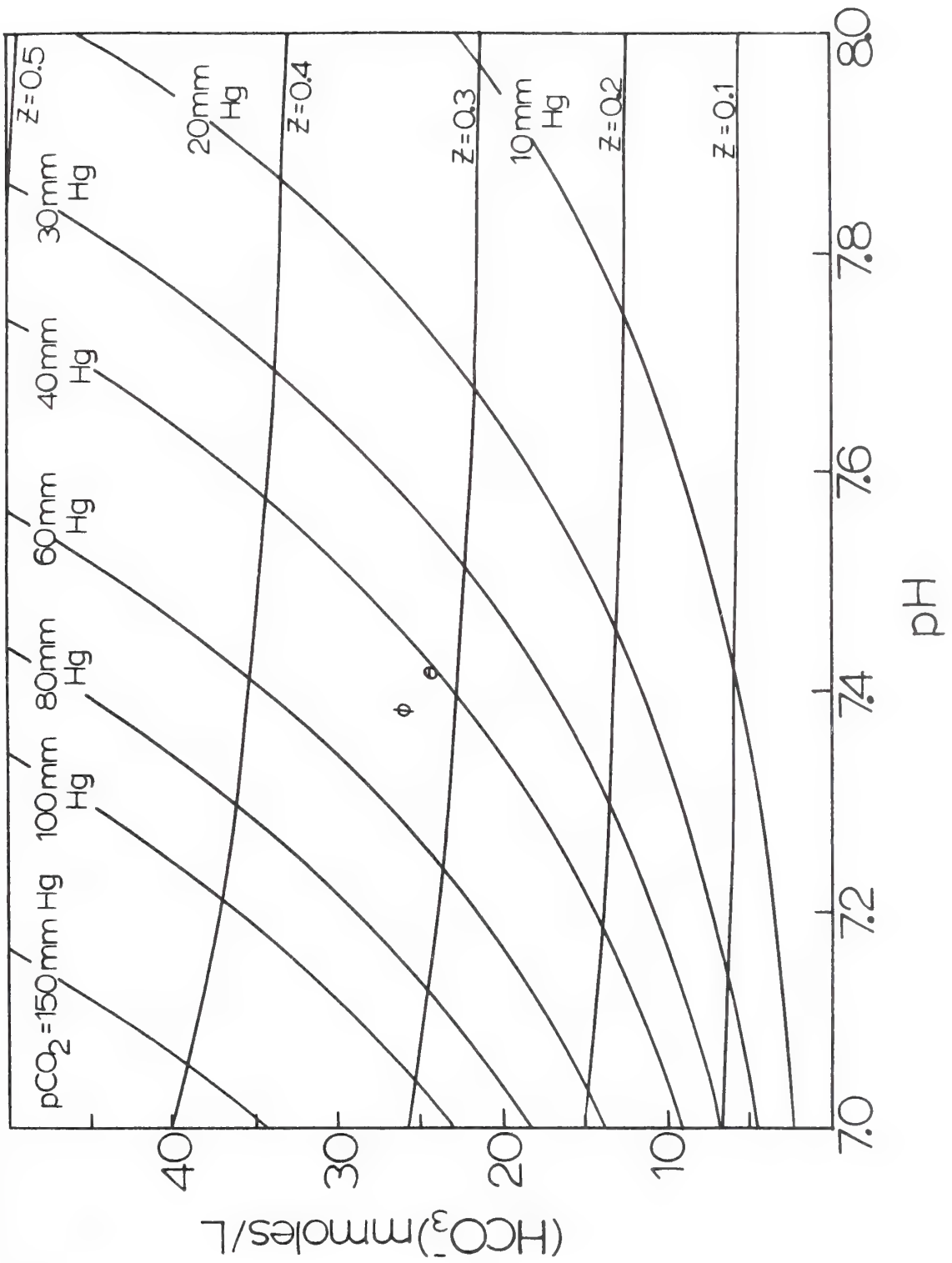
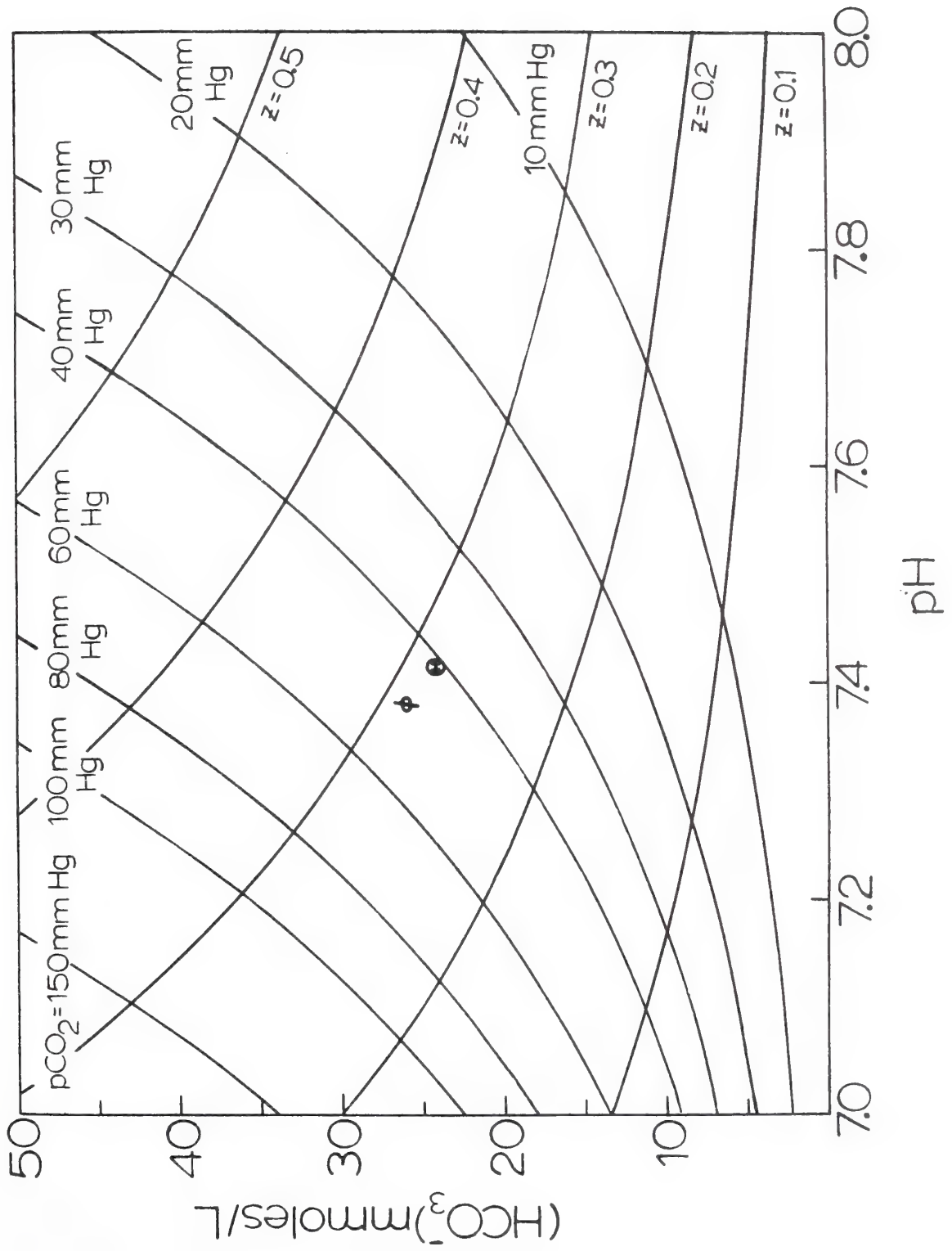


Figure 7. Relationship between pH, CO_2 , bicarbonate concentration, and mole fraction (Z) of [5-Ile] Angiotensin II in the carbamino form. (●) and (○) are representative of normal arterial and venous conditions, respectively. The enhanced steepness of the carbamino isobars (Z) is due primarily to the increased value of pK_Z for angiotensin relative to that of vasopressin. See text.



fraction, Z , to higher pH values, making it now a more sensitive function of both pH and $p\text{CO}_2$. The value of Z under the typical arterial and venous conditions is designated as before.

In comparison with vasopressin (Figure 6), the higher pK_Z of angiotensin II together with the lowered pK_C , yields an equilibrium which is now highly sensitive to the conditions of metabolic acidosis or alkalosis, but much less sensitive to the corresponding respiratory derangements. These two vasoactive compounds thus demonstrate in their interactions with CO_2 and hydrogen ions molecular mechanisms that respond with different emphasis within a common pattern, potentially a basis for separate but concurrent homeostatic mechanisms.

The relative slowness of carbamate decomposition, as evidenced by the linewidth measurements or as reported by Caplow (17), as well as the even slower uncatalyzed hydration of CO_2 (21), allows non-equilibrium states to gain significance. Thus, the carbamate potentially possesses a "memory" on the time scale of many molecular processes, allowing knowledge of localized $p\text{CO}_2$ or pH levels to be transmitted to a more distant site.

Such behavior may provide an explanation for the potentiation of pressor effects of angiotensin II in alkaline solution. Paladini and coworkers showed that increases of $66 \pm 11\%$ in pressor activity resulted from adjustment of the peptide sample to pH 11.7 before injection (22-24). These observations suggest that the carbamino form of the angiotensin is more active than the simple amine. Angiotensin II carbamate, formed immediately upon injection by the reaction of the basic NH_2 -terminus with the 40 mm Hg $p\text{CO}_2$ present in the blood, may be reaching receptors before it is relatively slowly converted back to the

descarbamino form. The time ranges of both the pressor response and the partial decarboxylation are probably measured in seconds (5, 17). The design of the experiment appears to rule out effects of such factors as sodium loading (25). Compounds characterized by higher values for pK_Z will show less tendency in the physiological range to form carbamino derivative, but the derivative formation will become increasingly sensitive to pH in contrast to pCO_2 . The level of the carbamino derivative, if sufficient to be functionally significant, would represent the concentration of a species that is readily altered by small pH changes as well as by pCO_2 changes, and yet persists for long periods on the time scale of molecular motions such as those involved in the processes of binding to a receptor site or producing a conformational change.

In principle it is not essential that a large proportion of the amine in question should be converted to the carbamino derivative, only that it should be functionally distinct and effective in this form. Histamine, with its higher pK_Z , is illustrative of a molecule that forms a carbamino derivative (Chapter III) with a sharp pH dependence of the (small) value of Z in the physiological range of pH and pCO_2 . The same argument would apply to some catecholamine neurotransmitters¹ that have been found to form carbamino compounds, and to the free amino acids (Chapter III). Among the latter are glycine, glutamic acid, and aspartic acid which are putative neurotransmitters.

Attention should be drawn to the ability of phenylhydrazine, with

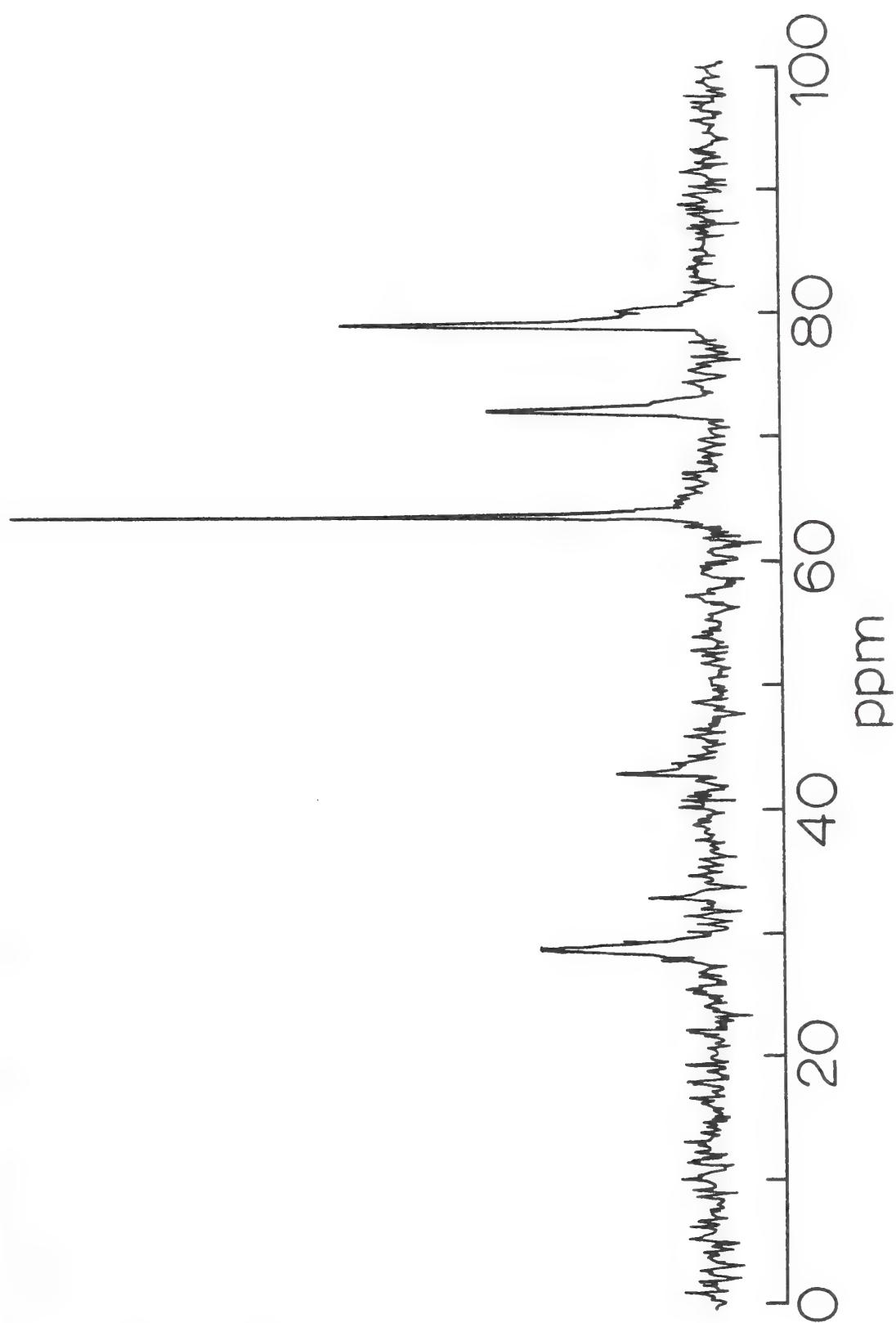
¹ Morrow, J. S., Gurd, R. S. and Gurd, F. R. N., unpublished observations.

a pK_z below the range for alkylamines (17) to form a carbamino derivative even below pH 6. A typical observation of phenylhydrazine carbamate is shown in Figure 7. The conditions of this measurement were approximately 50 mM phenylhydrazine equilibrated with 400 mm Hg $p^{13}CO_2$, at pH 6.56. The carbamino resonance, noteworthy for its greater width, is at 28.4 ppm. The enhanced linewidth arises from a more rapid rate of chemical exchange with dissolved CO_2 (17). The latter resonance is not apparent, due to low abundance and exchange broadening. A small bicarbonate resonance is apparent at 32.6 ppm. It is interesting that substituted hydrazines are among the therapeutic inhibitors of monamine oxidase (25).

Conclusion

The potential for interaction with CO_2 is a factor which must be considered in nearly any in vivo process involving free amino groups. Discounting unknown plasma factors which might prevent such an interaction, it is clear that an appreciable percentage of vasopressin and angiotensin II will exist in vivo as their carbamates. A host of other biologically active polypeptides including oxytocin and bradykinin would be expected to undergo similar transformations. Thus concurrent response through two or more systems based on the same fundamental carbamino mechanism could permit very fine physiological regulation.

Figure 7. 15.1 mHz ^{13}C NMR spectrum of ~ 50 mM phenylhydrazine in the presence of CO_2 , pH = 6.56. The increased linewidth of the carbamate resonance probably reflects a higher rate of exchange with CO_2 .



REFERENCES

1. Hastings, A. B. (1970) *Ann. Rev. Biochem.* 39, 1-24
2. Heinemann, H. O. (1973) *Fed. Proc.* 32, 1955
3. Said, S. I. (1973) *Fed. Proc.* 32, 1972
4. Said, S. I. (1972) in *Pathophysiology: Altered Regulatory Mechanisms in Disease*, Frohlich, F. D. ed., J. B. Lippincott Co., Philadelphia, 167
5. Douglass, W. W. (1970) in *The Pharmacological Basis of Therapeutics*, 4th ed., Goodman, L. S. and Gilman, A., eds., Macmillan, New York, 620-676
6. Sander, G. E. and Huggins, C. G. (1972) *Ann. Rev. Pharmacol.* 12, 227-264
7. Wilhelm, D. C. (1971) *Ann. Rev. Med.* 22, 63-73
8. Lefer, A. M. (1970) *Fed. Proc.* 29, 1836-1847
9. Manning, M., Balaspiri, L., Acosta, M. and Sawyer, W. H. (1973) *J. Med. Chem.* 16, 975-978
10. du Vigneaud, V., Gish, D. T. and Katsoyannis, P. G. (1954) *J. Am. Chem. Soc.* 76, 4751-4752
11. Lyster, J. R., Jr., and Freedman M. H. (1972) *J. Biol. Chem.* 247, 8183-8192
12. Keim, P., Vigna, R. A., Morrow, J. S., Marshall, R. C. and Gurd, F. R. N. (1973) *J. Biol. Chem.* 248, 7811-7818
13. Gurd, F. R. N., Keim, P., Glushko, V., Lawson, P. J., Marshall, R. C., Nigen, A. M. and Vigna, R. A. (1972) in *Chemistry and Biology of Peptides*, J. Meienhofer, ed., Ann Arbor Science Publishers, Inc., Ann Arbor, Michigan, 45-49

14. Keim, P. Vigna, R. A., Marshall, R. C. and Gurd, F. R. N. (1973) J. Biol. Chem. 248, 6104-6113
15. Keim, P., Vigna, R. A., Nigen, A. M., Morrow, J. S. and Gurd, F. R. N. (1974) J. Biol. Chem., in press
16. Campbell, B. J., Chu, F. S. and Hubbard, S. (1963) Biochem. 2, 764-769
17. Caplow, M. (1968) J. Amer. Chem. Soc. 90, 6795-6803
18. Sander, G. E. and Huggins, C. G. (1972) Ann. Rev. Pharmacol. 12, 227-264
19. Paiva, T. B., Paiva, A. C. M. and Scheraga, M. A. (1963) Biochem. 2, 1327-1334
20. Cohn, E. J. and Edsall, J. T. (1943) Proteins, Amino Acids and Peptides as Ions and Dipolar Ions, Reinhold Publishing Corp., New York, 84
21. Edsall, J. T. (1969) in CO₂: Chemical, Biochemical, and Physiological Aspects, Forster, R. E., Edsall, J. T., Otis, A. B. and Roughton, F. J. W., eds., NASA SP-188, Washington, D.C., 15-27
22. Paladini, A. C., Delius, A. E. and Frazee Fernandez, M. T. (1963) Biochem. Biophys. Acta 74, 168-170
23. Methot, A. L., Meyer, P., Biron, P., Lorain, M. F., Lagrue, G. and Milliez, P. (1964) Nature 203, 531-532
24. Craig, L. C., Harfenist, E. J. and Paladini, A. C. (1964) Biochem. 3, 764-769
25. Blair-west, J. R. and McKenzie, J. S. (1966) Experientia 22, 291-292
26. Creveling, C. R. and Daly, J. W. (1971) in Biogenic Amines and Physiological Membranes in Drug Therapy, Biel, J. M. and Abood, L. G., eds., Marial Dekker, Inc. New York, part B, 355

APPENDIX A

Methemoglobin Formation in the Presence of
Catalase, Glutathione, or Triethylenetetramine

Appendix A

Ferrihemoglobin formation in the presence of
Catalase, Glutathione, or Triethylenetetramine

Stripped oxyhemoglobin hemolyzate solutions initially free of ferrihemoglobin were maintained 5 days at room temperature in 0.05 M phosphate buffer at pH 7.0. Also included in the solutions were various amounts of either catalase (Calbiochem, 1.11.1.6, from beef liver), reduced glutathione (Sigma, Crystalline) or triethylenetetramine (TETA) (twice redistilled). The reported activity of the catalase (3100 μ /mg) was verified in assays based on the method of Maehly and Chance (1). The amounts of each material used are shown in Table I. The samples were spectrophotometrically analyzed for the presence of ferrihemoglobin by method of Benesch et al. (2) upon termination of the experiment. The results are reported in Table I. The hemoglobin concentration was 9.4 μ M in all experiments.

All samples containing glutathione formed considerable precipitate. The precipitate appeared yellowish in color, suggestive of the apoprotein; nearly complete absence of the Soret band absorbance confirmed these suspicions. As may be seen by inspection of Table I, only the presence of small amounts of TETA proved effective in retarding ferrihemoglobin formation. This is consonant with a recent report (3) attributing to trace copper contamination a catalytic role in the oxidation of hemoglobin. The stability constant for TETA-Copper complexes is greater than that for EDTA-Copper complexes (4), making it an attractive alternative for hemoglobin studies in which the anionic milieu needs to be carefully controlled.

Table I

Autooxidation of Human Hemoglobin Hemolyzates

Dilute HbO₂ solutions (9.4 μ M) were maintained at room temperature for 5 days. The effect of various agents on the extent of heme iron oxidation was measured. The HbO₂ samples were free of detectable ferrihemoglobin at the initiation of the experiments. The added agent is referred to as "X" in the second column.

Sample	Concentration of X mM	% ferrihemoglobin formed	percent Reduction
HbO ₂ control #1	0.0	31.1	0.0
HbO ₂ control #2	0.0	30.9	0.0
HbO ₂ + catalase	8×10^{-6}	32.1	- 3.5
HbO ₂ + catalase	4×10^{-5}	27.6	11.0
HbO ₂ + glutathione	4.6	54.5 ^a	-75.8
HbO ₂ + glutathione	18.2	39.6 ^a	-27.7
HbO ₂ + TETA	4.2	8.0	74.2
HbO ₂ + TETA	420	5.8	81.3
HbO ₂ + catalase + TETA	8×10^{-6} ; 4.2	10.3	66.8

^aMeasurements made after centrifugation to remove considerable precipitate. See text.

REFERENCES

1. Maehly, A. C. and Chance, B. (1954) in Methods of Biochemical Analysis, Glick, D., ed., Interscience Publishers Inc., New York, 1, 357
2. Benesch, R., Masdutt, G., and Benesch, R. E. (1965) Anal. Biochem. 12, 81-
3. Rifkin, J. M. (1974) Biochem. 13, 2475-2481
4. Perrin, D. D. (1964) Organic Complexing Reagents, Wiley and Sons, New York, 116

APPENDIX B

Interaction of $^{13}\text{CO}_2$ and Bicarbonate
with Carbonic Anhydrase

Appendix B

Interaction of $^{13}\text{CO}_2$ and Bicarbonate with Carbonic Anhydrase

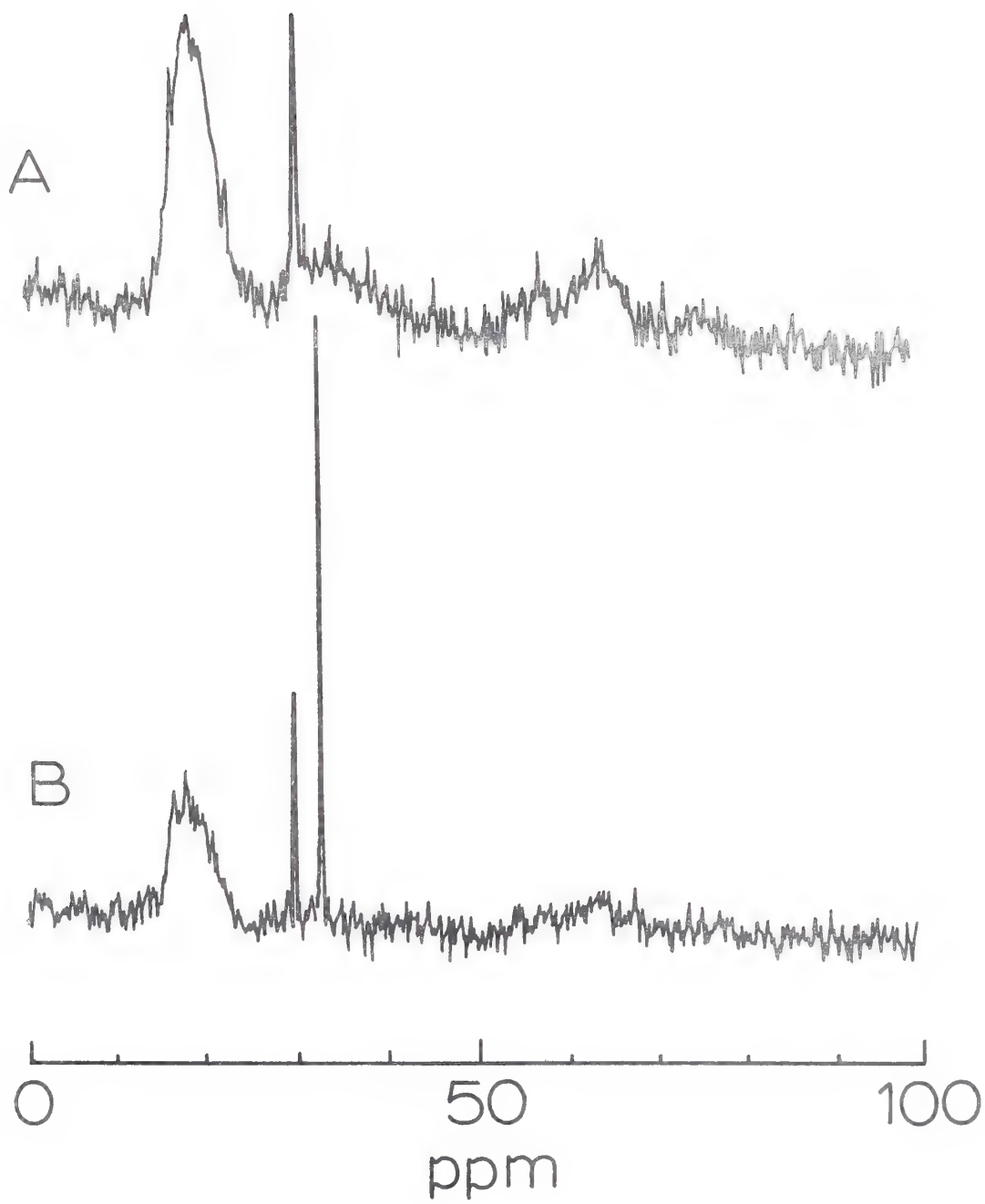
In initial studies with the hemoglobin hemolyzate preparations, a marked broadening of the bicarbonate and CO_2 resonances was apparent. The origin of this broadening was attributable to exchange effects between HCO_3^- and CO_2 , catalyzed by the red blood cell carbonic anhydrases present in any hemolyzate. As such, this broadening could be eliminated by the addition of acetazolamide (Diamox[®]), a potent inhibitor of carbonic anhydrase (1). In Figure 1 are shown examples of the effect on the observed NMR spectrum. In Figure 1A, 11.6 mM deoxy Hb hemolyzate was equilibrated with 8.4 mM total carbonates at pH 7.10. In Figure 1B, 9.9 mM deoxyhemoglobin hemolyzate was equilibrated with 7.2 mM total carbonates at pH 7.20. In addition, the sample in Figure 1B contained 0.9 mM acetazolamide. The difference between the spectra is striking. The addition of the carbonic anhydrase dramatically narrowed the resonance near 33-34 ppm in 1A, and shifted it downfield to 32.7 ppm. Preparations purified by DEAE Sephadex chromatography, and in which the carbonic anhydrase is absent, do not show this effect. The reintroduction of carbonic anhydrase (bovine, Worthington) will reproduce the line broadening.

These effects may be ascribed to differences in the exchange rate between HCO_3^- and CO_2 , when the catalyzed reaction is compared with the uncatalyzed rate. The uncatalyzed hydration rate of CO_2 , Equation 4,

Chapter III, is slow, on the order of $3.5 \times 10^{-2} \text{ sec}^{-1}$ (2). In the presence of carbonic anhydrase, the hydration rate potentially can rise to $\sim 10^6 \text{ sec}^{-1}$ (3). The amplification of the exchange rate by eight orders of magnitude is more than sufficient to move the observed resonances from slow exchange to fast exchange (see Equation 3, Chapter IV). In actuality, one would expect an exchange narrowed resonance at 10^6 sec^{-1} . The observed broadness thus suggests that under the conditions of these experiments, the rate of hydration (or dehydration) is considerably sub-maximal.

Also of interest was the relaxation behavior of the bicarbonate resonance in such solutions. As previously alluded to (Chapter III), the relaxation of bicarbonate proved to be highly variable. In a hemoglobin solution with increased levels of carbonates but no acetazolamide, the T_1 value of the bicarbonate resonance was 340 mses. Upon the addition of 0.9 mM acetazolamide, this value rose to 3.3 sec.

Figure 1. ^{13}C NMR spectra of deoxyhemoglobin hemolyzate equilibrated with $^{13}\text{CO}_2$ in the presence and absence of acetazolamide.
(A) Hb, pH 7.10; (B) Hb, 0.9 mM acetazolamide, pH 7.20.



REFERENCES

1. Mudge, G. H. (1965) in The Pharmacological Basis of Therapeutics, 4th edition, Goodman, L. S. and Gillman, A., eds., Collier-Macmillan, Co., 855
2. Edsall, J. T. (1969) in CO₂: Chemical, Biochemical, and Physiological Aspects, Forster, R. E., Edsall, J. T., Otis, A. B., and Roughton, F. J. W., eds., NASA SP-188, 15-27
3. Lindskog, S., Henderson, L. E., Kannan, K. K., Wyman, P. O. and Strandberg, B. (1971) The Enzymes, 3rd Ed., 5, 587

APPENDIX C

Computer Programs

Appendix C

Computer Programs

The computer proved to be a necessary and vital tool for the analysis of the experimental data, especially when a fit to such complex equations as those in Chapter III was required. While a variety of programs were conceived and developed during the course of this investigation, only the five which were the most useful, and which were necessary for the data analysis reported in this thesis, are reported here. The program used for the fitting of the titration curves, as determined from chemical shift measurements (Chapters III and IV), and the program used for the T_1 calculations (Chapters III, IV, and Appendix B) were well proven "in house" programs available in this laboratory. These are not reported here, although credit should be given to Dr. Robert Marshall for developing these programs and to Mr. R. Bogart for improving them and making them conveniently available.

The following list provides a short description of each program.

CAL3 (or CAL4) -- Computes least squares fit to (z) versus pH data, on basis of Equation 10, Chapter III.

ISOBAR -- Computes Z on basis of pK_C and pK_Z for many pCO_2 and pH levels. Output is a graph as in Figure 6, Chapter VI.

ABX Analysis -- A Fortran II program, computes coupling constants and chemical shifts for 12 line ABX spectrum.

NMRFIT3 -- Calculates least squares fit to selected regions of experimental NMR spectrum, based on the general NMR line shape

program of Binsch (1).

CONVERT -- Converts unformatted binary paper tape output from Nicolet 1080 computer to decimal integers on cards.

The programs are all written in Fortran IV, with the exception of ABX Analysis, which is Fortran II. All will work on a medium sized computer, with the exception of NMRFIT3, which requires 100,000₈ words of memory space.

In general, all FORMAT statements are listed at the end of each segment I/O operations; most I/O procedures are limited to the source program in each case.

CAL3 (or CAL4)

CAL3 (4) computes a least squares fit to experimentally determined values of the carbamate mole fraction (Z) as a function of pH, at constant total carbonates. The function upon which the fit is based is Equation 10, Chapter III. The mean carbonate level of the experimental data is used in this calculation; each experimentally determined Z value is adjusted to correspond to this carbonate level if desired, by Equation 7, Chapter IV. Standard values of the first and second ionization constants, pK_1^O and pK_2^O , of carbonic acid (Equation 1,3, Chapter III) are read as input, and adjusted to the ionic strength of each experiment by the Davies equation (2). Various plotting and output options are available in the program. The gradient-expansion algorithm used for the fitting procedure (3) was from Bevington (4), and yielded rapid convergence in most cases. In such cases where convergence did not occur, a simple grid search (subroutine KSTART) could be called for, yielding an approximate solution without the danger of divergence.

Ordering of Data Deck for CAL3 (CAL4)

<u>Card No.</u>	<u>FORMAT</u>	<u>DATA</u>
1.	(6A10,2F5.1)	<p>a) Columns 1-60: Identification information up to 60 columns.</p> <p>b) Columns 61-65: Number of unit concentrations of protein necessary to provide 1 unit concentration of a given amino group; e.g., if concentration is expressed on a per heme basis, <u>2.0</u> unit concentrations are necessary to provide 1 unit concentration of free NH_2-terminal alpha chain. Default value = 1.0.</p> <p>c) Columns 66-70: Terminate Flag. If non-zero number, program will exit.</p>
2.	(2F10.5)	Desired <u>maximum</u> and <u>minimum</u> values of pH on plot. 10 columns each; e.g. 10.0, 6.5.
3.	I2	L, the number of values in input table of protein charge vs. pH. Only needed if a calculation of the net charge on the protein is desired. Otherwise set = 1 in column 2.
4. (\rightarrow L+4)	(2F20.5)	Array of pH and charge values of protein, needed for Lagrangian Interpolation. The number of cards must be equal to "L" specified on card 3. Normally, L on card 3 is 01, and a blank card is inserted for card 4.
5.	(I2,6F10.5,I2)	<p>a) Columns 1,2: number of measurements of Z for a given resonance; e.g. 07.</p> <p>b) Columns 3-12: Concentration of NaCl, in molarity; e.g. 0.050.</p> <p>c) Columns 13-22: Standard pK_1^0 values for hydration of CO_2 to HCO_3^-. Usually 6.329.</p> <p>d) Columns 23-32: Standard pK_2^0 value for $\text{HCO}_3^- \rightarrow \text{CO}_3^{=}$. Usually 10.229.</p> <p>e) Columns 33-42: Position of resonance peak being analyzed; e.g. 29.8.</p> <p>f) Columns 43-52: Concentration of 2,3-DPG, in molarity; e.g. 0.005.</p>

Card No.FORMATDATA

- g) Columns 53-62: Initial estimate of pK_z ; e.g. 7.0.
- h) Columns 63-64: Basis of error analysis. If non-zero, each data point will be weighted proportional to its assigned σ . If 00, all points will be weighted equally, and estimation of errors will be on basis of the estimated variance of the fit; e.g. 00.
6. (5F10.5)
- a) Columns 1-10: If number > 00 is read, fit will be based on experimental Z values with no correction for varying carbonate levels.
- b) Columns 11-20: A number > 1.0, but < 10.0, will yield fit, and plot input data, but will not draw a curve through points. A number > 10.0 will cause data points only to be plotted, without attempting a fit.
- c) Columns 21-30: A number > 0.0 will yield a grid search only. This is necessary only when analytical fit will not converge.
- d) Columns 31-40: The number of equivalent amines per resonance, for cases where the resonance represents more than one site. Default value is 1.0.
- e) Columns 41-50: If a scaling of the data to a carbonate level other than the mean, enter the desired level here; e.g. 0.055.
7. (5F10.5)
- a) Columns 1-10: pH value of experimental measurements.
- b) Columns 11-20: Experimental Z value.
- c) Columns 21-30: Carbonate level of experimental measurement in molar.
- d) Columns 31-40: σ of experimental measurement. Only need be specified if weighted fit is desired (see card 5).
- e) Columns 41-50: Protein concentration of actual experimental measurement, in molar.

CARD 7 is repeated for each experimental measurement for the conditions specified in CARD 5. If more than one curve is desired per graph, the series of cards 5, 6, and 7 is repeated for each curve. To close plot, follow data set with blank card. The entire data set may then be repeated any number of times. Use a non-zero punch in columns 66-70, following a blank card (see card 1) to end.

The output of CAL3 is a listing of the input data, the corrected Z values, the apparent pK_1 and pK_2 values, and the mean values (with σ) of total carbonates and protein concentration. Also returned is the estimated values of K_C and K_Z , and pK_C and pK_Z , along with estimates of their standard deviations. Also returned is a CAL comp plot of the data and fitted curve. Execution time varies, but is usually less than 10 sec per fit. A listing of CAL4 appears below.


```

PROGRAM CAL4 (INPUT,OUTPUT,PLBT,TAPE60=INPUT,TAPE61=OUTPUT,TAPE1=P
1LBT)
DIMENSION Z(50), XU(20), A(3), KBN(4), TC(20), XK1(20), XK2(20),
1SN(20), YK1(20), YK2(20), U(20), PKE(2), SDPK(2), SIGMAA(5), PRBT(
220), CHG(20), Z(500), PH(500), H(500), NAME(6)
COMMON TCM,PRBTM,L,BCHG(50),BPH(50),PK1,PK2,S,DPG,SUB,AK,H2NN0
REAL NAME
ANTI(A)=1./EXP(2.302585*A)

```

```

C
C MODE = 1 FOR WEIGHTING PROPORTIONAL TO SN, 0 FOR NO WGT FACTOR
C

```

```

GO TO 2

```

```

1 CALL PLBTX

```

```

2 READ 23, NAME, SUB, EXI

```

```

C
C SUB**PRBT/SUB = TOTAL AMINE AVAILABLE FOR CAM, FOR MB=1, HB=2.
C

```

```

IF (EXI.GT.0.) CALL EXIT

```

```

IF (SUB.LT..1) SUB=1.0

```

```

READ 25, XMAX,XMIN

```

```

READ 24, L

```

```

READ 25, (BPH(I),BCHG(I)),I=1,L)

```

```

C
C THE PH EXTREMES OF PROTEIN CHARGE ARRAY MUST ENCOMPASS THE EXTREMES OF
C THE DATA AND THE PLAT. IF ONE WISHES TO NEGLECT THE IONIC STRENGTH
C EFFECTS OF THE PROTEIN, SET L=1, FOLLOWED BY A BLANK CARD.
C

```

```

J=1

```

```

KBN(1)=5

```

```

KBN(2)=6H(F5.2)

```

```

KBN(3)=5

```

```

KBN(4)=6H(F5.2)

```

```

CALL PLBTI (KBN,XMAX,XMIN,1.0,0.0)

```

```

CALL TITLE (60,NAME)

```

```

CALL XLABL (31,31H

```

```

CALL YLABL (25,25H

```

PH)

Z)

```

3 READ 27, N,S,PK1,PK2,PPM,DPG,AK,MODE

```

```

IF (N=1) 1,1,4

```

```

4 DO 5 I=1,500

```

```

    PH(I)=0.

```

```

    Z(I)=0.

```

```

5    H(I)=0.

```

```

    READ 28, SHIFT,DRAW,AFIT,H2NN0,TCS

```

```

IF SHIFT IS GT ZERO, NO CORRECTION OF Z TO MEAN TC LEVELS WILL BE MADE

```

```

IF DRAW IS GT 1.0, DATA POINTS ONLY WILL BE PLOTTED.

```

```

IF DRAW IS GT 10.0, DATA POINTS ONLY, NO FIT

```

```

IF AFIT GT ZERO, ROUGH GRID SEARCH ONLY IS DONE.

```

```

AFIT GT ZERO WILL NOT DIVERGE.

```

```

H2NN0 IS THE NUMBER OF EQUIVALENT AMMINES/RESONANCE (/UNIT CONCENTRATI

```


C IF H2NN9 IS BLANK, IT IS ASSUMED EQUAL TO ONE.
 C IF TCS IS GT ZERO, MEAN CARBONATES WILL BE SET = TO TCS.
 C DATA WILL BE SCALED ACCORDINGLY

```

IF (H2NN9.LE.0.0) H2NN9=1.0
SIGMAA(1)=0.0
SIGMAA(2)=0.0
READ 28, (PH(I),Z(I),TC(I),SN(I),PRBT(I),I=1,N)
DO 6 I=1,N
  H(I)=ANTI(PH(I))
  CALL CHARGE (PRBT(I),BPH,BCHG,PH(I),CHG(I),L)
  CALL CBRK (TC(I),PH(I),PK1,PK2,YK1(I),YK2(I),U(I),S,CHG(I),PRBT(
1  I))
  XK1(I)=ANTI(YK1(I))
6  XK2(I)=ANTI(YK2(I))
TCM=0.
PRBTM=0.
XK1M=0.
XK2M=0.
DO 7 I=1,N
  TCM=TCM+TC(I)
  PRBTM=PRBTM+PRBT(I)
  XK1M=XK1M+XK1(I)
7  XK2M=XK2M+XK2(I)
YN=FLOAT(N)
TCM=TCM/YN
IF (TCS.GT.0.0) TCM=TCS
PRBTM=PRBTM/YN
XK1M=XK1M/YN
PK1M=.1.*ALOG10(XK1M)
XK2M=XK2M/YN
PK2M=.1.*ALOG10(XK2M)
SDC=0.
SDP=0.
SD1=0.
SD2=0.
DO 8 I=1,N
  SDC=SDC+(TC(I)-TCM)**2
  SDP=SDP+(PRBT(I)-PRBTM)**2
  SD1=SD1+(XK1(I)-XK1M)**2
8  SD2=SD2+(XK2(I)-XK2M)**2
SDC=SQRT(SDC/(YN-1.))
SDP=SQRT(SDP/(YN-1.))
SD1=SQRT(SD1/(YN-1.))
SD2=SQRT(SD2/(YN-1.))
SD1=SD1/(2.303*XK1M)
SD2=SD2/(2.303*XK2M)
A(1)=ANTI(4.95)
A(2)=ANTI(AK)
IF (SHIFT.GT.0.) GO TO 9

```



```

CALL ZSHIFT (Z,Z0,TCM,TC,N)
9 CALL KSTART (Z,N,MODE,A,H,SN,CHISQR)
  IF (DRAW.GT.10.0) GO TO 15
  IF (AFIT.GT.0.0) GO TO 13
  CHIDIF=1.E-15
  INTERV=0
  FLAMDA=1.0E-15
10 CALL CURFIT (H,Z,SN,N,2,MODE,A,SIGMAA,CHISQR,PR0B,FLAMDA)
  INTERV=INTERV+1
  PRINT 29, CHISQR
  IF (INTERV=1) 11,11,12
11 CHISQ1=CHISQR
  GO TO 10
12 PCHI=(ABS(CHISQ1-CHISQR)/CHISQ1)*100.
  CHISQ1=CHISQR
  IF (PCHI-CHIDIF) 13,13,10
13 DO 14 I=1,2
    PKE(I)=-1.*ALEG10(A(I))
14   SDPK(I)=SIGMAA(I)/(2.303*A(I))
  GO TO 16
15 PRINT 30, NAME
  GO TO 17
16 PRINT 32, NAME
  PRINT 31, H2NNS
  IF (AFIT.EQ.0.0) GO TO 17
  PRINT 33
17 PRINT 34, PPM,S,DPG
  IF (TCS.GT.0.0) GO TO 18
  PRINT 35, TCM,SDC
  GO TO 19
18 PRINT 36, TCM,SDC
19 PRINT 37, PK1,PK2
  PRINT 38, PR0TM,SDP
  PRINT 39
  PRINT 40
  PRINT 41, (PH(I),Z0(I),Z(I),SN(I),U(I),TC(I),YK1(I),YK2(I),PR0T(I),
1,CHG(I),I=1,N)
  PRINT 39
  IF (MODE.NE.0) GO TO 20
  PRINT 42, CHISQR
  GO TO 22
20 IF (MODE.GT.0) GO TO 21
  PRINT 43
21 PRINT 44, CHISQR,PR0B
22 PRINT 45, A(1),SIGMAA(1),PKE(1),SDPK(1)
  PRINT 46, A(2),SIGMAA(2),PKE(2),SDPK(2)
  J=J+1
  CALL PLOTS (J,PH,Z,N)
  IF (DRAW.GT.1.0) GO TO 3
  PH(1)=XMIN

```



```

IFIT=250
XFIT=FL6AT(IFIT)
ZPH=(XMAX-XMIN)/XFIT
DO 23 I=1,IFIT
  H(I)=ANTI(PH(I))
  Z(I)=FUNTCN(H(I),A)
23  PH(I+1)=PH(I)+ZPH
  CALL PLOTS (1H,PH,Z,-IFIT)
  GO TO 3

```

C

```

24  FORMAT (I2)
25  FORMAT (2F10.5)
26  FORMAT (6A10,2F5.1)
27  FORMAT (I2,6F10.5,I2)
28  FORMAT (5F10.5)
29  FORMAT (E16.8)
30  FORMAT (1H1,14H DATA ONLY FOR,6A10)
31  FORMAT (31H EQUIVALENT ADDUCTS/RESONANCE =,,F8.1)
32  FORMAT (1H1,18HCARBAMINE DATA FOR,6A10)
33  FORMAT (17H GRID SEARCH ONLY)
34  FORMAT (6H PEAK=,F10.3,13H PPM, (NACL)=,F10.4,14H MOLAR, (DPG)=,F1
10.4,12H MOLAR
35  FORMAT (23H MEAN TOTAL CARBONATES=,F10.4,13H MOLAR, S.D.=,F10.5)
36  FORMAT (23H TOTAL CARBONATES SET =,F10.4,13H MOLAR, S.D.=,F10.5)
37  FORMAT (9H ST PK1=,,F10.4,13H STD PK2 =,F10.4,25H FOR CA
1RBONIC ACID)
38  FORMAT (29H MEAN PROTEIN CONCENTRATION =,F10.5,13H MOLAR, S.D.=,F1
10.5/)
39  FORMAT (90(1H*))
40  FORMAT (/5X,2HPPH,9X,1HZ,8X,2HZ*,9X,2HSD,9X,1HU,9X,2HTC,8X,3HPK1,7
1X,3HPK2,7X,4HPRBT,7X,3HCHG/)
41  FORMAT (4F10.3,2F10.5,4F10.4)
42  FORMAT (/51H DATA VARIANCE NOT SPECIFIED, ESTIMATED VARIANCE =,F
110.5)
43  FORMAT (/45H STATISTICAL WEIGHTING OF DATA, SIGMA**2 = Y.)
44  FORMAT (/41H LEAST SQUARES FIT TO DATA, CHI SQUARED =,F10.4,41H P
1RBB EXCEEDING CHI**2 WITH RANDOM DATA =,F10.5)
45  FORMAT (1X,4HKC =,E13.8,5H, SD=,E13.8,7H, PKC =,F10.5,5H, SD=,F10.
15)
46  FORMAT (1X,4HKZ =,E13.8,5H, SD=,E13.8,7H, PKZ =,F10.5,5H, SD=,F10.
15)
  END

```



```

FUNCTION FUNTCN (XI,A)
DIMENSION A(2)
COMMON TCM,PRBTM,L,BCHG(50),BPH(50),PK1,PK2,S,DPG,SUB,AK,H2NN0
EQUIVALENCE (D,TCM)
ANTI(CD)=1./EXP(2.302585*CD)
PH=-1.*ALOG10(XI)
P=PRBTM/SUB
CALL CORK (TCM,PH,PK1,PK2,PKA1,PKA2,U,S,FCHG,PRBTM)
XK1=ANTI(PKA1)
XK2=ANTI(PKA2)
C=A(1)*A(2)*XI*P
B=-1.*(XK1*XK2*A(2)/C+XI*(A(2)*A(1)*(D+P)+A(2)*XK1+XK1*XK2)/C+(XI*
1*2)*(A(2)+XK1)/C+XI**3/C)
FUNTCN=((-B+SQRT(B**2-4.*D/P))/2.)*H2NN0
C
C
C
A(1) = KC, A(2) = KZ
RETURN
END

```



```
SUBROUTINE ZSHIFT (Z,Z0,TCM,TC,N)
DIMENSION Z(500), Z0(500), TC(500)
DO 2 I=1,N
  Z0(I)=Z(I)
  SUM2=0.
  SUM1=.0
  K=1
1  SUM1=SUM1+(-1.0)**K*Z(I)**K*(Z(I)-1.0)*((TCM-TC(I))/TC(I))**K
  IF (ABS(SUM1-SUM2).LT.0.0001) GO TO 2
  SUM2=SUM1
  K=K+1
  GO TO 1
2  Z(I)=Z(I)+SUM1
RETURN
END
```


SUBROUTINE CHARGE (PRD,BPH,BCHG,PH,CHG,L)

DIMENSION BPH(50), BCHG(50)

CHG=0.

DO 3 I=1,L

PRD=BCHG(I)

DO 2 K=1,L

IF (I-K) 1,2,1

1 PRD=PRD*(PH-BPH(K))/(BPH(I)-BPH(K))

2 CONTINUE

3 CHG=CHG+PRD

RETURN

END


```

SUBROUTINE KSTART (Z,N,MODE,A,H,SN,CHISQ1)
DIMENSION YF(500), A(2), H(500), Z(500), SN(20)
COUNT=0.0
XK=1.
CHIMIN=1000.
1 SAVE=A(2)
NF=N-2
ND=0
NK=0
IF (NF.LE.0) NF=1
STEP=.05
DO 2 J=1,N
2 YF(J)=FUNTCN(H(J),A)
CHISQ1=FCHISQ(Z,N,NF,MODE,YF,SN)
3 A(2)=A(2)*EXP(2.303*STEP)
K=1
GO TO 5
4 A(2)=A(2)/EXP(2.303*STEP)
K=-1
5 DO 6 J=1,N
6 YF(J)=FUNTCN(H(J),A)
CHISQ2=FCHISQ(Z,N,NF,MODE,YF,SN)
NK=NK+1
PCHI=(ABS(CHISQ1-CHISQ2)/CHISQ1)*100.
DCHI=CHISQ1-CHISQ2
CHISQ1=CHISQ2
IF (NK-1000) 8,8,7
7 A(2)=SAVE
GO TO 14
8 IF (DCHI) 10,14,9
9 ND=ND+1
IF (PCHI-1.) 14,14,13
10 IF (ND-1) 12,12,11
11 A(2)=A(2)/EXP(FL9AT(K)*STEP)
GO TO 14
12 IF (K) 3,14,4
13 IF (K) 4,14,3
14 PCHIM=(ABS(CHISQ1-CHIMIN)/CHIMIN)*100.
DCHIM=(CHIMIN-CHISQ1)
IF (PCHIM-1.) 18,18,15
15 CHIMIN=CHISQ1
COUNT=COUNT+1.
IF (DCHIM) 16,16,17
16 XK=XK*(-1.)
17 A(1)=A(1)*EXP(2.303*XK*STEP)
IF (COUNT.GT.100.) GO TO 18
GO TO 1
18 PRINT 19, A(1),A(2)
RETURN

19 FORMAT (2E16.8)
END

```



```

SUBROUTINE CBRK (TCA,PH,PK1,PK2,PKA1,PKA2,US,S,CHG,PRBT)
  SQRTU(A)=SQRT(A)/(1.+SQRT(A)).*2*A
  X(A)=2.*PH-PK1-PK2+4.*0.5146*SQRTU(A)
  B(A)=PH-PK1+.5146*SQRTU(A)
  TEXP(Z)=EXP(2.303*Z)
  C(A)=1.+TEXP(B(A))+TEXP(X(A))
  D(A)=2.*.5146*(1./(SQRT(A)+A)-1./(1.+SQRT(A)).*2*.4)
  C93(A)=TCA*TEXP(X(A))/C(A)
  E(A)=PH-PK2+3.*.5146*SQRTU(A)
  DC93(A)=2.303*TEXP(X(A))*TCA*(D(A)/C(A)*(1.+TEXP(X(A))/C(A))-TEXP(
1 B(A)).*25*D(A)/C(A).**2)
  CALL ADION (PH,PRBT,S2)
  US=TCA+S+S2
  F=0.
1 DF=-1.+DC93(US)*(3.+1./TEXP(E(US))).*75*2.30258*C93(US)*D(US)/(TEX
1 P(E(US)))
  US=US+F/DF
  F=C93(US)*(3.+1./TEXP(E(US)))+S*US+S2
  IF (ABS(F/DF).*.00001) 2,2,1
2 PKA1=PH-B(US)
  PKA2=PH-E(US)
  RETURN
  END

```


SUBROUTINE ADIGN (PH,PR0T,S2)

DPG SUBROUTINE

COMMON TCM,PR0TM,L,BCHG(50),BPH(50),PK1,PK2,S,DPG,SUB,AK

ANTI(B)=1./EXP(2.302585*B)

PKZ=6.95

H=ANTI(PH)

ZK=ANTI(PKZ)

RAT=ZK/H

D3=DPG*(1./((1.+RAT+RAT**2)))

D4=RAT*D3

D5=RAT*D4

S2=D5*30.+D4*20.+D3*12.

RETURN

END

SUBROUTINE CURFIT (X,Y,SN,NPTS,NTERMS,MODE,A,SIGMAA,CHISQR,PRBB,FL
1AMDA)
REAL ARRAY

SUBROUTINE CURFIT
PURPOSE

MAKE A LEAST-SQUARES FIT TO A NON-LINEAR FUNCTION
WITH A LINEARIZATION OF THE FITTING FUNCTION

X = ARRAY OF DATA POINTS FOR INDEPENDENT VARIABLE

Y = ARRAY OF DATA POINTS FOR DEPENDENT VARIABLE

NPTS = NUMBER OF DATA POINTS

NTERMS = NUMBER OF PARAMETERS

MODE = METHOD OF WEIGHTING = NOT USED

A = ARRAY OF PARAMETERS

DELTA A = ARRAY OF INCREMENTS FOR PARAMETERS A

SIGMA A = ARRAY OF STANDARD DEVIATIONS FOR PARAMETERS A

FLAMDA = PROPORTION OF GRADIENT SEARCH INCLUDED

YFIT = ARRAY OF CALCULATED Y VALUES

CHISQR = REDUCED CHI SQUARE FOR FIT

REFERENCE

BEVINGTON, P. R., DATA REDUCTION AND ERROR ANALYSIS FOR THE

PHYSICAL SCIENCES, MAGRAW-HILL, NEW YORK, (1969).

PAGE 238.

DIMENSION X(100), Y(100), A(10), DELTAA(10), SIGMAA(10), YFIT(100),
1. WEIGHT(100), ALPHA(10,10), BETA(10), DERIV(10), ARRAY(10,10), D(210), SN(100)

DO 2 I=1,10

DO 1 J=1,10

ALPHA(I,J)=0.0

1 ARRAY(I,J)=ALPHA(I,J)

2 DELTAA(I)=1.E-15

NFREE=NPTS-NTERMS

IF (NFREE) 3,3,4

3 NFREE=1

4 DO 10 I=1,NPTS

IF (MODE) 5,8,9

5 IF (Y(I)) 7,8,6

6 WEIGHT(I)=1./Y(I)

GO TO 10

7 WEIGHT(I)=1./(-Y(I))

GO TO 10

8 WEIGHT(I)=1.

GO TO 10

9 WEIGHT(I)=1./SN(I)**2

10 CONTINUE

DO 11 J=1,NTERMS

BETA(J)=0.

DO 11 K=1,J

11 ALPHA(J,K)=0.


```

D0 13 I=1,NPTS
CALL FDERIV (X(I),A,DELTA,NTERMS,DERIV)
D0 12 J=1,NTERMS
  BETA(J)=BETA(J)+WEIGHT(I)*(Y(I)-FUNTCN(X(I),A))*DERIV(J)
  D0 12 K=1,J
    ALPHA(J,K)=ALPHA(J,K)+WEIGHT(I)*DERIV(J)*DERIV(K)
12 13 CONTINUE
D0 14 J=1,NTERMS
  D0 14 K=1,J
14 14 ALPHA(K,J)=ALPHA(J,K)
D0 15 I=1,NPTS
15 YFIT(I)=FUNTCN(X(I),A)
CHISQ1=FCHISQ(Y,NPTS,NFREE,MODE,YFIT,SN)
16 D0 18 J=1,NTERMS
  D0 17 K=1,NTERMS
17 17 ARRAY(J,K)=ALPHA(J,K)/SQRT(ALPHA(J,J)*ALPHA(K,K))
18 18 ARRAY(J,J)=1.+FLAMDA
CALL MATINV (ARRAY,NTERMS,DET)
D0 19 J=1,NTERMS
  B(J)=A(J)
  D0 19 K=1,NTERMS
19 19 B(J)=B(J)+BETA(K)*ARRAY(J,K)/SQRT(ALPHA(J,J)*ALPHA(K,K))
D0 20 I=1,NPTS
20 YFIT(I)=FUNTCN(X(I),B)
CHISQR=FCHISQ(Y,NPTS,NFREE,MODE,YFIT,SN)
IF (CHISQ1-CHISQR) 21,22,22
21 FLAMDA=10.*FLAMDA
GO TO 16
22 D0 24 J=1,NTERMS
  A(J)=B(J)
  IF (MODE.NE.0) GO TO 23
  SIGMAA(J)=SQRT(CHISQR/ALPHA(J,J))
  GO TO 24
23 SIGMAA(J)=SQRT(1./ALPHA(J,J))
24 CONTINUE
FLAMDA=FLAMDA/10.
PR0B=PCHISQ(CHISQR,NFREE)
RETURN
END

```


SUBROUTINE FDERIV (XI,A,DELTAA,NTERMS,DERIV)
 DIMENSION A(10), DELTAA(10), DERIV(10)

SUBROUTINE FDERIV(NON ANALYTICAL)

PURPOSE

EVALUATE DERIVATIVES OF FUNCTION FOR LEAST-SQUARES SEARCH
 FOR ARBITRARY FUNCTION GIVEN BY FUNCTN

X = ARRAY OF DATA POINTS FOR INDEPENDENT VARIABLE

I = INDEX OF DATA POINTS

A = ARRAY OF PARAMETERS

DELTAA = ARRAY OF PARAMETER INCREMENTS

NTERMS = NUMBER OF PARAMETERS

DERIV = DERIVATIVES OF FUNCTION

REFERENCE

BEVINGTON, P. R., DATA REDUCTION AND ERROR ANALYSIS FOR THE
 PHYSICAL SCIENCES, MAGRAW-HILL, NEW YORK, (1969).

PAGE 242.

1 DO 2 J=1,NTERMS

AJ=A(J)

DELTA=DELTAA(J)

A(J)=AJ+DELTA

YFIT=FUNCTN(XI,A)

A(J)=AJ-DELTA

DERIV(J)=(YFIT-FUNCTN(XI,A))/(2.*DELTA)

2 A(J)=AJ

IK=0

DO 4 J=1,NTERMS

IF (DERIV(J)) 4,3,4

3 IK=10

DELTAA(J)=DELTAA(J)*10.

4 CONTINUE

IF (IK) 5,5,1

5 CONTINUE

RETURN

END

FUNCTION PCHISQ (CHISQR,NFREE)

FUNCTION PCHISQ

PURPOSE

EVALUATE PROBABILITY FOR EXCEEDING CHI SQUARE

USAGE

RESULT = PCHISQ(CHISQR,NFREE)

DESCRIPTION OF PARAMETERS

CHISQR = COMPARISON VALUE OF REDUCED CHI SQUARE

NFREE = NUMBER OF DEGREES OF FREEDOM

SUBROUTINES AND FUNCTION PROGRAMS REQUIRED

GAMMA(X)

CALCULATES GAMMA FUNCTION

REFERENCE

BEVINGTON, P. R., DATA REDUCTION AND ERROR ANALYSIS FOR THE
PHYSICAL SCIENCES, MAGRAW-HILL, NEW YORK, (1969).

PAGE 192.

COMMENTS

CALCULATION IS APPROXIMATE FOR NFREE ODD AND CHI SQUARE
GREATER THAN 50

1 IF (NFREE) 2,2,3

2 PCHISQ=0.

GO TO 11

3 FREE=FLOAT(NFREE;

Z=CHISQR*FREE/2.

NEVEN=2*(NFREE/2)

IF (NFREE=NEVEN) 4,4,6

NUMBER OF DEGREES OF FREEDOM IS EVEN

4 IMAX=NFREE/2

TERM=1.

SUM=0.

DO 5 I=1,IMAX

FI=FLOAT(I)

SUM=SUM+TERM

5 TERM=TERM*Z/FI

PCHISQ=SUM*EXP(-Z)

GO TO 11

NUMBER OF DEGREES OF FREEDOM IS ODD

6 IF (Z=25.) 8,8,7

7 Z=CHISQR*(FREE-1.)/2.

GO TO 4

8 PWR=FREE/2.

TERM=1.

SUM=TERM/PWR

DO 9 I=1,1000


```
FI=FLBAT(I)
TERM=TERM*Z/FI
SUM=SUM+TERM/(PWR+FI)
IF (ABS(TERM/SUM) < .00001) 10,10,9
9  CONTINUE
10 PCHSQ=1.+(Z**PWR)*SUM/GAMMA(PWR)
11 RETURN
END
```


FUNCTION GAMMA (X)

FUNCTION GAMMA(X)

PURPOSE

CALCULATE THE GAMMA FUNCTION FOR INTEGERS AND HALF-INTEGERS

REFERENCE

BEVINGTON, P. R., DATA REDUCTION AND ERROR ANALYSIS FOR THE
PHYSICAL SCIENCES, MAGRAW-HILL, NEW YORK, (1969).

PAGE 126

DESCRIPTION OF PARAMETERS

X = INTEGER OR HALF-INTEGER

SUBROUTINES OR SUBPROGRAMS REQUIRED

FACTOR(N)

CALCULATES N FACTORIAL FOR INTEGERS

INTEGERIZE ARGUMENT

1 N=INT(X+.25)

XN=FLOAT(N)

IF (X-XN+.75) 3,3,2

ARGUMENT IS INTEGER

2 GAMMA=FACTOR(N)

GO TO 10

ARGUMENT IS HALF-INTEGER

3 PRD=1.77245385

IF (N) 7,7,4

4 IF (N=10) 5,5,8

5 DO 6 I=1,N

FI=FLOAT(I)

6 PRD=PRD*(FI+.5)

7 GAMMA=PRD

GO TO 10

8 SUM=0.

DO 9 I=11,N

FI=FLOAT(I)

9 SUM=SUM+ALOG(FI+.5)

GAMMA=PRD*.639383.8623*EXP(SUM)

10 RETURN

END

FUNCTION FACTOR (N)

FUNCTION FACTOR(N)

PURPOSE

CALCULATE FACTORIAL FUNCTION FOR INTEGERS

REFERENCE

BEVINGTON, P. R., DATA REDUCTION AND ERROR ANALYSIS FOR THE
PHYSICAL SCIENCES, MAGRAW-HILL, NEW YORK, (1969).
PAGE 32.

1 FACTOR=1.

IF (N=1) 7,7,2

2 IF (N=10) 3,3,5

N IS LESS THAN 11

3 DO 4 I=2,N

FI=FLOAT(I)

4 FACTOR=FACTOR*FI

GO TO 7

N GREATER THAN 10

5 SUM=0.

DO 6 I=11,N

FI=FLOAT(I)

6 SUM=SUM+ALOG(FI)

FACTOR=3628800.*EXP(SUM)

7 RETURN

END

FUNCTION FCHISQ (Y,NPTS,NFREE,MODE,YFIT,SN)

FUNCTION FCHISQ

PURPOSE

EVALUATE REDUCED CHI SQUARE FOR FIT TO DATA

FCHISQ=SUM((Y-YFIT)**2/SIGM**2/NFREE

BEVINGTON, P. R., DATA REDUCTION AND ERROR ANALYSIS FOR THE
PHYSICAL SCIENCES, MAGRAW-HILL, NEW YORK, (1969).

PAGE 194.

DIMENSION Y(100), YFIT(100), WEIGHT(99), SN(100)

1 CHISQ=0.

IF (NFREE) 2,2,3

2 FCHISQ=0.

GO TO 10

3 DO 9 I=1,NPTS

IF (MODE) 4,7,8

4 IF (Y(I)) 6,7,5

5 WEIGHT(I)=1./Y(I)

GO TO 9

6 WEIGHT(I)=1./(-Y(I))

GO TO 9

7 WEIGHT(I)=1.

GO TO 9

8 WEIGHT(I)=1./SN(I)**2

9 CHISQ=CHISQ+WEIGHT(I)*(Y(I)-YFIT(I))**2

FREE=FLOAT(NFREE)

FCHISQ=CHISQ/FREE

10 RETURN

END

SUBROUTINE MATINV (ARRAY,NORDER,DET)
REAL ARRAY,AMAX,SAVE

MATRIX INVERSION AND DETERMINATE
REFERENCE

BEVINGTON, P. R., DATA REDUCTION AND ERROR ANALYSIS FOR THE
PHYSICAL SCIENCES, MAGRAW-HILL, NEW YORK, (1969).
PAGE 302.

DIMENSION ARRAY(10,10), IK(10), JK(10)

```

1 DET=1.
  DO 20 K=1,NORDER
    AMAX=0.
2    DO 4 I=K,NORDER
      DO 4 J=K,NORDER
        IF (ABS(AMAX)-ABS(ARRAY(I,J))) 3,3,4
3      AMAX=ARRAY(I,J)
      IK(K)=I
      JK(K)=J
4    CONTINUE
    IF (AMAX) 6,5,6
5    DET=0.
    GO TO 27
6    I=IK(K)
    IF (I=K) 2,9,7
7    DO 8 J=1,NORDER
      SAVE=ARRAY(K,J)
      ARRAY(K,J)=ARRAY(I,J)
8    ARRAY(I,J)=-SAVE
9    J=JK(K)
    IF (J=K) 2,12,10
10   DO 11 I=1,NORDER
      SAVE=ARRAY(I,K)
      ARRAY(I,K)=ARRAY(I,J)
11   ARRAY(I,J)=-SAVE
12   DO 14 I=1,NORDER
      IF (I=K) 13,14,13
13   ARRAY(I,K)=-ARRAY(I,K)/AMAX
14   CONTINUE
      DO 17 I=1,NORDER
        DO 17 J=1,NORDER
          IF (I=K) 15,17,15
15         IF (J=K) 16,17,16
16         ARRAY(I,J)=ARRAY(I,J)+ARRAY(I,K)*ARRAY(K,J)
17         CONTINUE
      DO 19 J=1,NORDER
        IF (J=K) 18,19,18
18         ARRAY(K,J)=ARRAY(K,J)/AMAX
19         CONTINUE
      ARRAY(K,K)=1./AMAX

```


SUBROUTINE CALCOM (P1,P2,P3,P4,P5)

SUBROUTINE CALCOMPL IS A COLLECTION OF SUBROUTINES DESIGNED TO SIMULATE ... UMPLBT ... ON THE CALCOMP PLOTTER. THE PLOT IS CONTAINED IN AN 8.5 BY 11.0 INCH BOUNDARY (INCLUDING ALL TITLES ETC.). THE PLOT ITSELF IS CONTAINED IN A 6.0 BY 8.0 INCH BOX, WITH TIC MARKS ALL SIDES. THE ENTIRE FORMAT OF CALCOMPL IS SUITABLE FOR BINDING REPRODUCING WITHOUT ALTERATION. CODED BY G. P. ECKLEY, PHYSICS DE MSIDIFIED BY RICHARD A. BOGARDT JR.

CONTROL OPTIONS

KON(1)=THE NUMBER OF X-AXIS DIVISIONS IF IT IS POSITIVE. IF KON(1) IS NEGATIVE, A LOGARITHMIC PLOT WILL BE MADE ALONG THE X-AXIS.
 KON(2)=THE X-AXIS FORMAT. IT IS SPECIFIED AS KON(2)=6H(F5.N).
 KON(3)=THE NUMBER OF Y-AXIS DIVISIONS IF IT IS POSITIVE. IF KON(3) IS NEGATIVE, A LOGARITHMIC PLOT WILL BE MADE ALONG THE Y-AXIS.
 KON(4)=THE Y-AXIS FORMAT. IT IS SPECIFIED AS KON(4)=6H(F5.N).
 IF A LOGARITHMIC SCALE IS CHOSEN, THE FORMAT CORRESPONDING TO THAT AXIS IS IGNORED, HENCE IT NEED NOT BE SPECIFIED.

CALLING SEQUENCE FOR EXECUTION

CALL PLOTI(KON,XMAX,XMIN,YMAX,YMIN)

CALL PLOTS(ISYM,X-ARRAY,Y-ARRAY,N9,POINTS)

CALL PLOTX

PLOTI INITIALIZES THE PLOT, PLOTS STORES THE PLOT, PLOTX EXECUTES THE PLOT. PLOTS MAY BE CALLED AS MANY TIMES AS NEEDED IN ORDER TO OBTAIN SIMULTANEOUS PLOTS, OR IF ONLY ONE POINT AT A TIME IS BEING PLOTTED. THE PEN IS CONTROLLED FROM PLOTS AS FOLLOWS

CALL PLOTS(J,X,Y,-N) SYMBOLS PLOTTED WITH CONNECTING LINES.
 CALL PLOTS(J,X,Y,N) SYMBOLS PLOTTED WITH NO CONNECTING LINE
 J IS CONTROL NUMBER FOR SYMBOL.

CALL PLOTS(1H,X,Y,-N) CONNECTING LINES DRAWN WITH NO SYMBOLS
 LABELING INFORMATION INITIALLY ALL LABELS ARE BLANK. IF ANY LABEL CALLS ARE MADE, THEY REMAIN IN EFFECT UNTIL THE NEXT CALL FOR THE SAME LABEL. THE EXCEPTION IS THE COMMENT OPTION WHICH MUST BE EXECUTED AFTER CALLING PLOTI AND BEFORE CALLING PLOTX. THE X AND LOCATIONS SPECIFIED FOR SUBROUTINE COMNT MUST BE LESS THAN 8.00 AN 6.00 INCHES RESPECTIVELY. SUBROUTINE COMNT IS CALLED AS

CALL COMNT(NCH,COMMENT,X,Y)

WHERE X AND Y ARE THE LOCATIONS OF THE FIRST CHARACTER TO BE PLOTT THE OTHER LABEL SUBROUTINES ARE ... TITLE, XLABL, YLABL. ALL OF WHICH MAY BE CALLED AT ANY TIME AND IN ANY ORDER AS

NCH MUST BE LESS THAN OR EQUAL TO 60 CHAREACTERS FOR LABELS ALONG THE X-AXIS. NCH MUST BE LESS THAN OR EQUAL TO 50 CHARACTERS ALONG THE Y-AXIS. NCH MUST BE LESS THAN OR EQUAL TO 62 CHARACTERS FOR LABELS ALONG THE X-AXIS. NCH MUST BE LESS THAN OR EQUAL TO 46 CHARACTERS ALONG THE Y-AXIS. THE MAXIMUM NUMBER OF CHARACTERS USED BY SUBROUTINE COMNT IS COMPUTED AS NCH(MAX)=(8-X)/.128, Y LESS THAN 5.8 INC THE LOGICAL UNIT USED BY CALCOMPL IS UNIT NUMBER 1. AN EQUIP CARD MUST BE INCLUDED WITH THE PROGRAM EQUIP,1=**,PL

EQUIVALENCE (FLT,INT), (C9N,KON), (NDX,KON(1)), (NXFORM,KON(2)), (


```

1NDY,KBN(3)), (NYFORM,KBN(4)), (PI,IP)
  DIMENSION P1(60), P2(600), P3(600), P4(60), ALGC(20), KBN(4), CBN
1(4), ALGX(20), ALGY(20), TITL(6), XLAB(6), YLAB(6), LOGLAB(50)

```

```

  IF A CALL IS MADE DIRECTLY TO SUBROUTINE CALCOMPL, THE PROGRAM WILL

```

```

DATA ALGC/.301,.4771,.6021,.699,.7782,.8451,.9031,.9542/
DATA LOGLAB/10HLOGARITHMI,10H SCALE 10H EXP0,10H NENT 0F 1
10/

```

```

DATA (TITL(J),J=1,6)/6(1H )/, (XLAB(J),J=1,6)/6(1H )/
DATA NFIRST/0/,ALOG10/.434294481903252/, (YLAB(J),J=1,5)/5(1H )/
RETURN

```

```

ENTRY PLBT1
ENTRY PLBT2

```

```

NFIRST=3

```

```

CALL IDENT (1,8HCALCOMPL)

```

```

DO 1 J=1,4

```

```

1 CBN(J)=P1(J)

```

```

  XMX=P2

```

```

  XMN=P3

```

```

  YMX=P4

```

```

  YMN=P5

```

```

  IF (NDX) 2,3,3

```

```

2 XMX=FIX(ALG(XMX)*ALOG10)

```

```

  XMN=ALG(XMN)*ALOG10

```

```

  XMN=FIX(XMN)

```

```

  NDX=XMX-XMN

```

```

  NXFORM=6H(F5.0)

```

```

  LOGX=2

```

```

  GO TO 4

```

```

3 LOGX=1

```

```

4 IF (NDY) 5,6,6

```

```

5 YMX=FIX(ALG(YMX)*ALOG10)

```

```

  YMN=ALG(YMN)*ALOG10

```

```

  YMN=FIX(YMN)

```

```

  NDY=YMX-YMN

```

```

  LOGY=2

```

```

  NYFORM=6H(F5.0)

```

```

  GO TO 7

```

```

6 LOGY=1

```

```

7 DLX=-8.0/(XMX-XMN)

```

```

  DLY=6.0/(YMX-YMN)

```

```

  ADX=-DLX*XMN+9.5

```

```

  ADY=-DLY*YMN+1.25

```

```

  DTX=8.0/FLBAT(NDX)

```

```

  GO TO (10,8), LOGX

```

```

8 DO 9 J=1,8

```

```

9 ALGX(J)=DTX*ALGC(J)

```

```

10 DTY=6.0/FLBAT(NDY)

```



```

      GO TO (13,11), LOGY
11 DO 12 J=1,8
12   ALBGY(J)=DTY*ALBGC(J)

C
C   DRAW BORDER
C
13 CALL PLBT (+0.02,+0.02,3)
   CALL PLBT (8.48,+0.02,2)
   CALL PLBT (8.48,10.98,2)
   CALL PLBT (+0.02,10.98,2)
   CALL PLBT (+0.02,+0.02,2)

C
C   DRAW PLBT BOX
C
   CALL PLBT (1.25,1.50,3)
   JMP=2
   YINCH=1.25
14 GO TO (17,15), LOGY
15 DO 16 J=1,8
   FLT=ALBGY(J)+YINCH
   CALL PLBT (FLT,1.5,2)
   CALL PLBT (FLT,1.55,2)
16   CALL PLBT (FLT,1.5,2)
17 IF (JMP.GT.NDY) GO TO 18
   YINCH=YINCH+DTY
   CALL PLBT (YINCH,1.5,2)
   CALL PLBT (YINCH,1.6,2)
   CALL PLBT (YINCH,1.5,2)
   JMP=JMP+1
   GO TO 14
18 CALL PLBT (7.25,1.5,2)
   JMP=2
   XINCH=1.5
19 XINCH=XINCH+DTX
   GO TO (22,20), LOGX
20 DO 21 J=1,8
   FLT=XINCH-ALBGX(9-J)
   CALL PLBT (7.25,FLT,2)
   CALL PLBT (7.20,FLT,2)
21   CALL PLBT (7.25,FLT,2)
22 IF (JMP.GT.NDX) GO TO 23
   CALL PLBT (7.25,XINCH,2)
   CALL PLBT (7.15,XINCH,2)
   CALL PLBT (7.25,XINCH,2)
   JMP=JMP+1
   GO TO 19
23 CALL PLBT (7.25,9.5,2)
   JMP=2
   YINCH=7.25
24 YINCH=YINCH+DTY

```



```

      GO TO (27,25), LOGY
25 DO 26 J=1,8
      FLT=YINCH+ALOGY(9,J)
      CALL PL0T (FLT,9.5,2)
      CALL PL0T (FLT,9.45,2)
26   CALL PL0T (FLT,9.5,2)
27 IF (JMP.GT.NDY) GO TO 28
      CALL PL0T (YINCH,9.5,2)
      CALL PL0T (YINCH,9.4,2)
      CALL PL0T (YINCH,9.5,2)
      JMP=JMP+1
      GO TO 24
28 CALL PL0T (1.25,9.5,2)
      JMP=2
      XINCH=9.5
29 GO TO (32,30), LOGX
30 DO 31 J=1,8
      FLT=XINCH-ALOGX(J)
      CALL PL0T (1.25,FLT,2)
      CALL PL0T (1.3,FLT,2)
31   CALL PL0T (1.25,FLT,2)
32 IF (JMP.GT.NDX) GO TO 33
      XINCH=XINCH+DTX
      CALL PL0T (1.25,XINCH,2)
      CALL PL0T (1.35,XINCH,2)
      CALL PL0T (1.25,XINCH,2)
      JMP=JMP+1
      GO TO 29
33 CALL PL0T (1.25,1.5,2)
      GO TO (35,34), LOGX
34 CALL SYMB0L (.8,8.06,.15,LOGLAB,270.,40)
35 DX=(XMX-XMN)/FL0AT(NDX)
      XINCH=2.0
36 X=FL0AT(NDX)*DX+XMN
      ENCODE (5,NXF0RM,INT) X
      CALL SYMB0L (1.05,XINCH,.15,INT,270.,5)
      XINCH=XINCH+DTX
      NDX=NDX+1
      IF (NDX.GE.0) GO TO 36
      DY=(YMX-YNM)/FL0AT(NDY)
      JMP=0
      YINCH=1.25
37 X=FL0AT(JMP)*DY+YMN
      ENCODE (5,NYF0RM,INT) X
      CALL SYMB0L (YINCH,10.16,.15,INT,270.,5)
      YINCH=YINCH+DTY
      JMP=JMP+1
      IF (JMP.LE.NDY) GO TO 37
      GO TO (39,38), LOGY
38 CALL SYMB0L (1.69,10.05,.15,LOGLAB,0,40)

```


39 RETURN

SUBROUTINE PLOTS(SYMBOL,X-ARRAY,Y-ARRAY,NO-POINTS)

ENTRY PLOTS

ENTRY PLOT3

P1=P1

CON=P1

FLT=P4

JMP=2

IF (INT) 40,53,41

40 INT=INT

JPEN=2

GO TO 42

41 JPEN=3

42 DO 52 J=1,INT

GO TO (44,43), LOGX

43 IF (P2(J).LE.0) GO TO 52

XINCH=ALOG(P2(J))*ALOG10*DLX+ADX

GO TO 45

44 XINCH=P2(J)*DLX+ADX

45 GO TO (47,46), LOGY

46 IF (P3(J).LE.0) GO TO 52

YINCH=ALOG(P3(J))*ALOG10*DLY+ADY

GO TO 48

47 YINCH=P3(J)*DLY+ADY

48 IF (XINCH.GT.9.5.OR.XINCH.LT.1.5) GO TO 52

IF (YINCH.GT.7.25.OR.YINCH.LT.1.25) GO TO 52

GO TO (50,49), JMP

49 JMP=1

CALL PLOT (YINCH,XINCH,3)

GO TO 51

50 CALL PLOT (YINCH,XINCH,JPEN)

51 IF (NDX.EQ.1H) GO TO 52

PRINT 61, IP

CALL SYMBOL (YINCH,XINCH,0.1,IP,270.0,0.1)

CALL PLOT (YINCH,XINCH,3)

52 CONTINUE

53 RETURN

SUBROUTINE COMNT(NCH,COMMENT,X,Y)

ENTRY COMNT

FLT=P1

DX=P3

DY=P4

IF (DY.GT.5.8.OR.DY.LT.0) GO TO 54

JMP=(8.-DX)/.128

IF (INT.GT.JMP) INT=JMP

IF (INT.LE.0.OR.DX.LT.0) GO TO 54


```

DX=9.5*DX
DY=1.25*DY
CALL SYMB9L (DY,DX,.15,P2,270.,INT)

```

```

54 RETURN

```

```

SUBROUTINE TITLE(NCH,TITLE)

```

```

ENTRY TITLE

```

```

FLT=P1

```

```

IF (INT.LE.0) GO TO 56

```

```

INT=(INT+9)/10

```

```

IF (INT.GT.6) INT=6

```

```

DO 55 J=1,INT

```

```

55   TITL(J)=P2(J)

```

```

56 RETURN

```

```

SUBROUTINE XLABL(NCH,X-LABEL)

```

```

ENTRY XLABL

```

```

FLT=P1

```

```

IF (INT.LE.0) GO TO 58

```

```

INT=(INT+9)/10

```

```

IF (INT.GT.6) INT=6

```

```

DO 57 J=1,INT

```

```

57   XLAB(J)=P2(J)

```

```

58 CONTINUE

```

```

RETURN

```

```

SUBROUTINE PLOT4(NCH,Y-LABEL)

```

```

ENTRY PLOT4

```

```

JMP=3

```

```

GO TO 59

```

```

SUBROUTINE YLABL(NCH,Y-LABEL)

```

```

ENTRY YLABL

```

```

JMP=0

```

```

59 FLT=P1

```

```

INT=(INT+9)/10

```

```

IF (INT.GT.5) INT=5

```

```

DO 60 J=1,INT

```

```

60   YLAB(J)=P2(J)

```

```

IF (JMP.EQ.0) RETURN

```

```

SUBROUTINE PLOTX

```

```

ENTRY PLOTX

```

```

CALL SYMB9L (.55,9.5,0.15,XLAB,270.,60)

```

```

CALL SYMB9L (1.25,10.3,0.15,YLAB,0.,50)

```

```

CALL SYMB9L (7.3,9.5,0.15,TITL,270.,60)

```

```

CALL CLOSEPF

```

```

RETURN

```

```

61 FORMAT (20X,I4)

```

```

END

```


ISOBAR

Fortran program ISOBAR uses pK_c and pK_z to calculate the expected Z values (mole fraction carbamate/amine) as a function of pH, pCO_2 , and total carbonates. Output is in the form of a Cal comp plot, as shown in Figure 6, Chapter VI. The calculation of Z is based on Equation 9, Chapter III. An internal value for the solubility coefficient of CO_2 is included, i.e. $[CO_2] = 10^{-4.33} \cdot pCO_2$. The negative logarithm of this value is specified as PALPHA in the program; if other values of the solubility coefficient are desired, PALPHA should be appropriately changed.

Ordering of Data Deck for ISOBAR

<u>Card No.</u>	<u>FORMAT</u>	<u>DATA</u>
1	6A10	Columns 1-60: Identification.
2	(2F10.4)	a) Columns 1-10: pK_c b) Columns 11-20: pK_z


```
PROGRAM ISGBAR (INPUT,OUTPUT,PLST,TAPE60=INPUT,TAPE61=OUTPUT,TAPE1
1=PLST)
```

```
DIMENSION PH(500), CARB(500), KON(4), NAME(6)
```

```
FUN1(A,B)=(XK1*ALPHA*B/A)*1000.
```

```
ANTI(A)=1./EXP(2.30258*A)
```

```
NEGLECTS CONTRIBUTION OF CO3 TO EQUILIBRIUM
```

```
1 READ 8, NAME
```

```
READ 9, PKC, PKZ
```

```
IF (PKC.LT.2.) CALL EXIT
```

```
KON(1)=5
```

```
KON(2)=6H(F5.1)
```

```
KON(3)=10
```

```
KON(4)=6H(F5.0)
```

```
YMAX=50.
```

```
YMIN=0.
```

```
XMAX=8.
```

```
XMIN=7.
```

```
PK1=6.317
```

```
PK2=9.89
```

```
PALPHA=4.33
```

```
CALL PLOTI (KON,XMAX,XMIN,YMAX,YMIN)
```

```
CALL TITLE (60,NAME)
```

```
CALL XLABL (31,31H
```

PH)

```
CALL YLABL (31,31H
```

(HCO3)MMOLES/L)

```
XK1=ANTI(PK1)
```

```
XK2=ANTI(PK2)
```

```
XKZ=ANTI(PKZ)
```

```
XKC=ANTI(PKC)
```

```
ALPHA=ANTI(PALPHA)
```

```
PCO2=10.
```

```
ZPH=(XMAX-XMIN)/250.
```

```
2 PH(1)=7.
```

```
DO 3 J=1,250
```

```
HC=ANTI(PH(J))
```

```
CARB(J)=FUN1(HC,PCO2)
```

```
3 PH(J+1)=PH(J)+ZPH
```

```
CALL PLOTS (1H,PH,CARB,-250)
```

```
PCO2=PCO2+10.
```

```
IF (PCO2.GT.140.) GO TO 4
```

```
IF (PCO2.GT.101.) PCO2=150.
```

```
GO TO 2
```

```
4 Z=1
```

```
5 PH(1)=7.
```

```
DO 6 J=1,250
```

```
HC=ANTI(PH(J))
```

```
PCO2=Z*(HC*XKZ+HC**2)/(ALPHA*XKC*XKZ*(1.-Z))
```

```
CARB(J)=FUN1(HC,PCO2)
```

```
6 PH(J+1)=PH(J)+ZPH
```



```
CALL PLOTS (1H ,PH,CARB,-250)
```

```
Z=Z+.1
```

```
IF (Z.GT.0.9) GO TO 7
```

```
GO TO 5
```

```
7 CALL PLOTX
```

```
PRINT 10, NAME
```

```
PRINT 11
```

```
PRINT 12, PKC,PKZ,PK1,PK2,PALPHA
```

```
GO TO 1
```

C

```
8 FORMAT (6A10)
```

```
9 FORMAT (2F10.4)
```

```
10 FORMAT (1H1,2X,6A10)
```

```
11 FORMAT (5X,3HPKC,6X,3HPKZ,7X,3HPK1,6X,3HPK2,6X,6HPALPHA/)
```

```
12 FORMAT (5F10.4)
```

```
END
```


SUBROUTINE CALCOM (P1,P2,P3,P4,P5)

SUBROUTINE CALCOMPL IS A COLLECTION OF SUBROUTINES DESIGNED TO SIMULATE ... UMPLT ... ON THE CALCOMP PLOTTER. THE PLOT IS CONTAINED IN AN 8.5 BY 11.0 INCH BOUNDARY (INCLUDING ALL TITLES ETC.). THE PLOT ITSELF IS CONTAINED IN A 6.0 BY 8.0 INCH BOX, WITH TIC MARKS ALL SIDES. THE ENTIRE FORMAT OF CALCOMPL IS SUITABLE FOR BINDING REPRODUCING WITHOUT ALTERATION. CODED BY G. P. ECKLEY, PHYSICS DE MODIFIED BY RICHARD A. BOGARDT JR.

CONTROL OPTIONS

KON(1)=THE NUMBER OF X-AXIS DIVISIONS IF IT IS POSITIVE. IF KON(1) IS NEGATIVE, A LOGARITHMIC PLOT WILL BE MADE ALONG THE X-AXIS.

KON(2)=THE X-AXIS FORMAT. IT IS SPECIFIED AS KON(2)=6H(F5.N).

KON(3)=THE NUMBER OF Y-AXIS DIVISIONS IF IT IS POSITIVE. IF KON(3) IS NEGATIVE, A LOGARITHMIC PLOT WILL BE MADE ALONG THE Y-AXIS.

KON(4)=THE Y-AXIS FORMAT. IT IS SPECIFIED AS KON(4)=6H(F5.N).

IF A LOGARITHMIC SCALE IS CHOSEN, THE FORMAT CORRESPONDING TO THAT AXIS IS IGNORED, HENCE IT NEED NOT BE SPECIFIED.

CALLING SEQUENCE FOR EXECUTION

CALL PLOTI(KON,XMAX,XMIN,YMAX,YMIN)

CALL PLOTS(ISYM ,X-ARRAY,Y-ARRAY,N0.,POINTS)

CALL PLOTX

PLOTI INITIALIZES THE PLOT, PLOTS STORES THE PLOT, PLOTX EXECUTES THE PLOT. PLOTS MAY BE CALLED AS MANY TIMES AS NEEDED IN ORDER TO OBTAIN SIMULTANEOUS PLOTS, OR IF ONLY ONE POINT AT A TIME IS BEING PLOTTED. THE PEN IS CONTROLLED FROM PLOTS AS FOLLOWS

CALL PLOTS(J ,X,Y,-N) SYMBOLS PLOTTED WITH CONNECTING LINES.

CALL PLOTS(J ,X,Y,N) SYMBOLS PLOTTED WITH NO CONNECTING LINE
J IS CONTROL NUMBER FOR SYMBOL.

CALL PLOTS(1H ,X,Y,-N) CONNECTING LINES DRAWN WITH NO SYMBOLS
LABELING INFORMATION INITIALLY ALL LABELS ARE BLANK. IF ANY

LABEL CALLS ARE MADE, THEY REMAIN IN EFFECT UNTIL THE NEXT CALL FOR THE SAME LABEL. THE EXCEPTION IS THE COMMENT OPTION WHICH MUST BE EXECUTED AFTER CALLING PLOTI AND BEFORE CALLING PLOTX. THE X AND LOCATIONS SPECIFIED FOR SUBROUTINE COMNT MUST BE LESS THAN 8.00 AN 6.00 INCHES RESPECTIVELY. SUBROUTINE COMNT IS CALLED AS

CALL COMNT(NCH,COMMENT,X,Y)

WHERE X AND Y ARE THE LOCATIONS OF THE FIRST CHARACTER TO BE PLOTT THE OTHER LABEL SUBROUTINES ARE ... TITLE, XLABL, YLABL. ALL OF WHICH MAY BE CALLED AT ANY TIME AND IN ANY ORDER AS

NCH MUST BE LESS THAN OR EQUAL TO 60 CHAREACTERS FOR LABELS ALONG

THE X-AXIS. NCH MUST BE LESS THAN OR EQUAL TO 50 CHARACTERS ALONG

NCH MUST BE LESS THAN OR EQUAL TO 62 CHARACTERS FOR LABELS ALONG

THE X-AXIS. NCH MUST BE LESS THAN OR EQUAL TO 46 CHARACTERS ALONG

THE Y-AXIS. THE MAXIMUM NUMBER OF CHARACTERS USED BY SUBROUTINE

COMNT IS COMPUTED AS NCH(MAX)=(8-X)/.128, Y LESS THAN 5.8 INC

THE LOGICAL UNIT USED BY CALCOMPL IS UNIT NUMBER 1. AN EQUIP CARD

MUST BE INCLUDED WITH THE PROGRAM EQUIP,1=**,PL

EQUIVALENCE (FLT,INT), (CON,KON), (NDX,KON(1)), (NXFORM,KON(2)), (


```

INDY,KBN(3)), (NYFORM,KBN(4)), (PI,IP)
DIMENSION P1(60), P2(600), P3(600), P4(60), ALGC(20), KBN(4), CON
1(4), ALGX(20), ALGY(20), TITL(6), XLAB(6), YLAB(6), LOGLAB(50)

```

IF A CALL IS MADE DIRECTLY TO SUBROUTINE CALCOMPL, THE PROGRAM WILL

```

DATA ALGC/.301,.4771,.6021,.699,.7782,.8451,.9031,.9542/
DATA LOGLAB/10HLSGARITHMI,10HC SCALE ,10H EXPONENT OF 1
10/

```

```

DATA (TITL(J),J=1,6)/6(1H )/(XLAB(J),J=1,6)/6(1H )/
DATA NFIRST/0/,ALG10/.434294481903252/(YLAB(J),J=1,5)/5(1H )/
RETURN

```

```

ENTRY PLOT1
ENTRY PLOT2

```

```

NFIRST=3

```

```

CALL IDENT (1,8HCALCOMPL)

```

```

DO 1 J=1,4

```

```

1 CON(J)=P1(J)

```

```

XMX=P2

```

```

XMN=P3

```

```

YMX=P4

```

```

YMN=P5

```

```

IF (NDX) 2,3,3

```

```

2 XMX=IFIX(ALG(XMX)*ALG10)

```

```

XMN=ALG(XMN)*ALG10

```

```

XMN=IFIX(XMN)

```

```

NDX=XMX-XMN

```

```

NXFORM=6H(F5.0)

```

```

LOGX=2

```

```

GO TO 4

```

```

3 LOGX=1

```

```

4 IF (NDY) 5,6,6

```

```

5 YMX=IFIX(ALG(YMX)*ALG10)

```

```

YMN=ALG(YMN)*ALG10

```

```

YMN=IFIX(YMN)

```

```

NDY=YMX-YMN

```

```

LOGY=2

```

```

NYFORM=6H(F5.0)

```

```

GO TO 7

```

```

6 LOGY=1

```

```

7 DLX=-8.0/(XMX-XMN)

```

```

DLY=6.0/(YMX-YMN)

```

```

ADX=-DLX*XMN+9.5

```

```

ADY=-DLY*YMN+1.25

```

```

DTX=8.0/FLBAT(NDX)

```

```

GO TO (10,8), LOGX

```

```

8 DO 9 J=1,8

```

```

9 ALGX(J)=DTX*ALGC(J)

```

```

10 DTY=6.0/FLBAT(NDY)

```



```

      GO TO (13,11), LOGY
11 DO 12 J=1,8
12   ALOGY(J)=DTY*ALOGC(J)
C
C   DRAW BORDER
13 CALL PLOT (+0.02,+0.02,3)
   CALL PLOT (8.48,+0.02,2)
   CALL PLOT (8.48,10.98,2)
   CALL PLOT (+0.02,10.98,2)
   CALL PLOT (+0.02,+0.02,2)
C
C   DRAW PLOT BOX
   CALL PLOT (1.25,1.50,3)
   JMP=2
   YINCH=1.25
14 GO TO (17,15), LOGY
15 DO 16 J=1,8
   FLT=ALOGY(J)+YINCH
   CALL PLOT (FLT,1.5,2)
   CALL PLOT (FLT,1.55,2)
16   CALL PLOT (FLT,1.5,2)
17 IF (JMP.GT.NDY) GO TO 18
   YINCH=YINCH+DTY
   CALL PLOT (YINCH,1.5,2)
   CALL PLOT (YINCH,1.6,2)
   CALL PLOT (YINCH,1.5,2)
   JMP=JMP+1
   GO TO 14
18 CALL PLOT (7.25,1.5,2)
   JMP=2
   XINCH=1.5
19 XINCH=XINCH+DTX
   GO TO (22,20), LOGX
20 DO 21 J=1,8
   FLT=XINCH-ALOGX(9-J)
   CALL PLOT (7.25,FLT,2)
   CALL PLOT (7.20,FLT,2)
21   CALL PLOT (7.25,FLT,2)
22 IF (JMP.GT.NDX) GO TO 23
   CALL PLOT (7.25,XINCH,2)
   CALL PLOT (7.15,XINCH,2)
   CALL PLOT (7.25,XINCH,2)
   JMP=JMP+1
   GO TO 19
23 CALL PLOT (7.25,9.5,2)
   JMP=2
   YINCH=7.25
24 YINCH=YINCH+DTY

```



```

      GO TO (27,25), LBGY
25 DO 26 J=1,8
      FLT=YINCH+ALBGY(9,J)
      CALL PLBT (FLT,9.5,2)
      CALL PLBT (FLT,9.45,2)
26   CALL PLBT (FLT,9.5,2)
27 IF (JMP.GT.NDY) GO TO 28
      CALL PLBT (YINCH,9.5,2)
      CALL PLBT (YINCH,9.4,2)
      CALL PLBT (YINCH,9.5,2)
      JMP=JMP+1
      GO TO 24
28 CALL PLBT (1.25,9.5,2)
      JMP=2
      XINCH=9.5
29 GO TO (32,30), LBGX
30 DO 31 J=1,8
      FLT=XINCH-ALBGX(J)
      CALL PLBT (1.25,FLT,2)
      CALL PLBT (1.3,FLT,2)
31   CALL PLBT (1.25,FLT,2)
32 IF (JMP.GT.NDX) GO TO 33
      XINCH=XINCH-DTX
      CALL PLBT (1.25,XINCH,2)
      CALL PLBT (1.35,XINCH,2)
      CALL PLBT (1.25,XINCH,2)
      JMP=JMP+1
      GO TO 29
33 CALL PLBT (1.25,1.5,2)
      GO TO (35,34), LBGX
34 CALL SYMBL (.8,8.06,.15,L9GLAB,270.,40)
35 DX=(XMX-XMN)/FLBAT(NDX)
      XINCH=2.0
36 X=FLBAT(NDX)*DX+XMN
      ENCODE (5,NXFORM,INT) X
      CALL SYMBL (1.05,XINCH,.15,INT,270.,5)
      XINCH=XINCH+DTX
      NDX=NDX+1
      IF (NDX.GE.0) GO TO 36
      DY=(YMX-YNM)/FLBAT(NDY)
      JMP=0
      YINCH=1.25
37 X=FLBAT(JMP)*DY+YMN
      ENCODE (5,NYFORM,INT) X
      CALL SYMBL (YINCH,10.16,.15,INT,270.,5)
      YINCH=YINCH+DTY
      JMP=JMP+1
      IF (JMP.LE.NDY) GO TO 37
      GO TO (39,38), LBGY
38 CALL SYMBL (1.69,10.05,.15,L9GLAB,0,40)

```


39 RETURN

SUBROUTINE PLOTS(SYMBOL,X-ARRAY,Y-ARRAY,N0.,POINTS)

ENTRY PLOTS

ENTRY PLOT3

PI=P1

CON=P1

FLT=P4

JMP=2

IF (INT) 40,53,41

40 INT=INT

JPEN=2

GO TO 42

41 JPEN=3

42 DO 52 J=1,INT

GO TO (44,43), LOGX

43 IF (P2(J).LE.0) GO TO 52

XINCH=ALOG(P2(J))*ALOG10*DLX+ADX

GO TO 45

44 XINCH=P2(J)*DLX+ADX

45 GO TO (47,46), LOGY

46 IF (P3(J).LE.0) GO TO 52

YINCH=ALOG(P3(J))*ALOG10*DLY+ADY

GO TO 48

47 YINCH=P3(J)*DLY+ADY

48 IF (XINCH.GT.9.5.8R.XINCH.LT.1.5) GO TO 52

IF (YINCH.GT.7.25.8R.YINCH.LT.1.25) GO TO 52

GO TO (50,49), JMP

49 JMP=1

CALL PLOT (YINCH,XINCH,3)

GO TO 51

50 CALL PLOT (YINCH,XINCH,JPEN)

51 IF (NDX.EQ.1H) GO TO 52

PRINT 61, IP

CALL SYMBOL (YINCH,XINCH,0.1,IP,270.0,-1)

CALL PLOT (YINCH,XINCH,3)

52 CONTINUE

53 RETURN

SUBROUTINE COMNT(NCH,COMMENT,X,Y)

ENTRY COMNT

FLT=P1

DX=P3

DY=P4

IF (DY.GT.5.8.8R.DY.LT.0) GO TO 54

JMP=(8.-DX)/.128

IF (INT.GT.JMP) INT=JMP

IF (INT.LE.0.8R.DX.LT.0) GO TO 54


```

DX=9.5*DX
DY=1.25*DY
CALL SYMB0L (DY,DX,.15,P2,270.,INT)

```

```

54 RETURN

```

```

C
C SUBROUTINE TITLE(NCH,TITLE)
C

```

```

ENTRY TITLE
FLT=P1

```

```

IF (INT.LE.0) GO TO 56

```

```

INT=(INT+9)/10

```

```

IF (INT.GT.6) INT=6

```

```

DO 55 J=1,INT

```

```

55 TITL(J)=P2(J)

```

```

56 RETURN

```

```

C
C SUBROUTINE XLABL(NCH,X-LABEL)
C

```

```

ENTRY XLABL

```

```

FLT=P1

```

```

IF (INT.LE.0) GO TO 58

```

```

INT=(INT+9)/10

```

```

IF (INT.GT.6) INT=6

```

```

DO 57 J=1,INT

```

```

57 XLAB(J)=P2(J)

```

```

58 CONTINUE

```

```

RETURN

```

```

C
C SUBROUTINE PLOT4(NCH,Y-LABEL)
C

```

```

ENTRY PLOT4

```

```

JMP=3

```

```

GO TO 59

```

```

C
C SUBROUTINE YLABL(NCH,Y-LABEL)
C

```

```

ENTRY YLABL

```

```

JMP=0

```

```

59 FLT=P1

```

```

INT=(INT+9)/10

```

```

IF (INT.GT.5) INT=5

```

```

DO 60 J=1,INT

```

```

60 YLAB(J)=P2(J)

```

```

IF (JMP.EQ.0) RETURN

```

```

C
C SUBROUTINE PLOTX
C

```

```

ENTRY PLOTX

```

```

CALL SYMB0L (.55,9.5,0.15,XLAB,270.,60)

```

```

CALL SYMB0L (1.25,10.3,0.15,YLAB,0.,50)

```



```
CALL SYMBOL (7.3,9.5,0.15,TITLE,270.,60)  
CALL CLOSEPF  
RETURN
```

C

```
61 FORMAT (20X,I4)  
END
```


ABX ANALYSIS

Fortran II program ABX Analysis was designed to run on the local Xerox data systems Sigma 2 computer. Input consists of the frequencies of the 12 lines in a typical ABX spectrum (5). The assignment at the transitions must correspond to the numbering scheme shown on p. 106 of Bovey (5). Also read are trans and gauche vicinal coupling constants. The computer returns with the calculated values of ν_A , ν_B , and ν_X , as well as J_{AX} , J_{BX} , and J_{AB} . Estimates of rotamer populations are also made. The calculations are based on the assumptions (not always valid) that J_{AX} and J_{BX} are positive, and that $J_{AX} < J_{BX}$. The sign of J_{AB} is indefinite.

Ordering of Card Deck for ABX Analysis

<u>Card No.</u>	<u>FORMAT</u>	<u>DATA</u>
1.	15A4	Columns 1-60: Identification.
2.	8F10.0	a) Columns 1-10: Trans coupling constant in hertz. b) Columns 11-29: Gauche coupling constant in hertz.
3.	F10.4	Columns 1-10: pH of measurement. This is for labeling purposes only, and may be substituted with blank card.
4. and 5.	8F10.4	Frequency in hertz of resonances 1 to 12 according to Bovey, p. 106 (5). 10 columns per resonance.


```

REAL J(3),JTBT
DIMENSION W(15),SAVE(25,13),XNU(3),TITLE(15),DIF(12),SD(10),CS(3)
C NUMBERING OF TRANSITIONS CORRESPONDS TO BOVEY,P106.
42 N = 1
  READ(60,109)(TITLE(I),I=1,15)
  READ(60,1) TJ,GJ
109 FORMAT(15A4)
99 READ(60,2) PH
  IF (PH=.1)100,100,98
98 READ(60,1)(W(I),I=1,12)
  2 FORMAT(F10.4)
  1 FORMAT(8F10.0)
  DIF(1) = W(3)-W(1)
  DIF(2) = W(4)-W(2)
  DIF(3) = W(7)-W(5)
  DIF(4) = W(8)-W(6)
  DIF(5) = W(2)-W(1)
  DIF(6) = W(4)-W(3)
  DIF(7) = W(11)-W(9)
  DIF(8) = W(12)-W(10)
  DIF(9) = W(10)-W(11)
  DIF(10) = W(8)-W(4)-W(5)+W(1)
  J(1) = (DIF(1)+DIF(2)+DIF(3)+DIF(4))/4.
  DO 11 I=1,10
11 SD(I) = 0.0
  DO 10 I=1,4
10 SD(I) = SD(I) + (DIF(I)-J(1))*2
  SD(1) = SQRT(SD(1))/3.
C J(1) IS ABS VALUE OF JAB
  JTBT = ABS(W(9)-W(12))
  TOTNU = 0.0
  DO 12 I=1,8
12 TOTNU = TOTNU + W(I)
  TOTNU = TOTNU/4.
  DELTA1 = SQRT((W(1)-W(7))*(W(3)-W(5)))
C DELTA1 = DELTA- (BOVEY)
  DELTA2 = SQRT((W(2)-W(8))*(W(4)-W(6)))
C ONLY SINGLE SOLUTION IS TRIED, APPROPRIATE FOR CYS
C ASSUMES JAX AND JBX ARE POSITIVE, AND JBX .GT. JAX
  J(2) = (JTBT-ABS(DELTA1-DELTA2))*0.5
C J(2) = JAX, J(3) = JBX
  J(3) = JTBT-J(2)
  XNU(1) = .5*((DELTA1+DELTA2)/2.+TOTNU)
C XNU(1) = VA, XNU(2) = VB, XNU(3) = VX
  XNU(2) = TOTNU-XNU(1)
  XNU(3) = (W(9)+W(10)+W(11)+W(12))/4.
C TJ AND GJ ARE THE TRANS AND GAUCHE VICINAL COUPLING CONSTANTS
  H = (JTBT - TJ-GJ)/(GJ-TJ)
  T = (GJ*J(2)-TJ*J(3)-H* GJ*(GJ-TJ))/(GJ**2-TJ**2)
  G = (J(3)-TJ*T-GJ*H)/GJ
  TM = H+G+T
  G = G/TM
  H = H/TM
  T = T/TM
  WRITE(61,3)(TITLE(I),I=1,15)
  3 FORMAT(1H1,26H ABX SPECTRAL ANALYSIS FOR,15A4/)
  WRITE(61,4)
  4 FORMAT(45H ASSUMES 12 LINE SPECTRUM AS BN P106 OF BOVEY/)
  WRITE(61,5)(I,W(I),I=1,12)
  5 FORMAT(11H RESONANCE(,I2,4H) = ,F9.2,3H HZ)
  WRITE(61,6) PH,GJ,TJ

```



```

6  FORMAT(1H0,5H PH =,F10.3,11H GALCHE J =,F6.2,10H TRANS J =,F6.2/)
   WRITE(61,7)
   WRITE(61,8) PH,(XNU(I),I=1,3),(J(I),I=1,3)
7  FORMAT(5X,2HPPH,8X,2HVA,8X,2HVB,8X,2HVX,7X,3HJAB,7X,3HJAX,7X,3HJBX)
8  FORMAT(7F10.3/)
   WRITE(61,2) SD(1)
   WRITE(61,9) T,G,H
9  FORMAT(4H T =,F7.3,4H G =,F7.3,4H H =,F7.3)
   DO 13 I=1,3
13  CS(I) = XNU(I)/220.22
   SAVE(N,1) = PH
   DO 14 I=1,3
   SAVE(N,I+1) = XNU(I)
   SAVE(N,I+4) = CS(I)
14  SAVE(N,I+7) = J(I)
   SAVE(N,11) = T
   SAVE(N,12) = G
   SAVE(N,13) = H
   N = N+1
   GO TO 99
100 WRITE(61,15)(TITLE(I),I=1,15)
15  FORMAT(1H1,20H SUMMARY OF DATA FOR,15A4/)
   WRITE(61,16)
16  FORMAT(120(1H*))
   WRITE(61,17)
17  FORMAT(6X,2HPPH,8X,2HVA,8X,2HVB,8X,2HVX,6X,4HAPPM,6X,4HBPPM,6X,4HXP
   $PM,7X,3HJAB,7X,3HJAX,7X,3HJBX,6X, 1HT,4X,1HG,4X,1HH/)
   N=N+1
   DO 21 I=1,N
21  WRITE(61,18)(SAVE(I,L),L=1,13)
18  FORMAT(10F10.3,3F5.2)
   WRITE(61,16)
   GO TO 42
END

```


NMRFIT3

Fortran program NMRFIT3 performs a lineshape and position analysis on digitized spectral data, yielding estimates of site populations and exchange rates. In its present form, it is specific for three site exchange, with the added restriction that exchange between two of the sites is set and not varied by the program. Usually, this exchange rate is set = 0.0, to represent carbamate interchange. The algorithms upon which the program is based are general, so that the program could be expanded to include n sites as well as spin-spin couplings. However, in such situations, the number of parameters grows exponentially, and meaningful fits become impossible. If inclusion of spin-spin couplings are desired for inter-molecular exchanges, further terms would have to be included, as described in the literature (6).

The digitized data input for NMRFIT3 is obtained by converting the paper tape representation of a transformed and phase corrected spectrum to decimal integers on cards, a task accomplished by program CONVERT. Execution time is typically 200 sec. per spectrum.

Data Card Ordering for NMRFIT3

<u>Card No.</u>	<u>FORMAT</u>	<u>DATA</u>
1.	(I2,4E10.3,4I1)	a) Columns 1,2: If 1, a trace map of the minimization process used by Subroutine STEPIT (7) will be printed. b) Columns 2-52: In blocks of 10: step sizes for each fitted variable, below which the fit will be assumed to have converged. See ref. 7.

<u>Card No.</u>	<u>FORMAT</u>	<u>DATA</u>
		c) Columns 53-56: A one in any columns holds that particular variable fixed at its initial value. Presently the program fits 4 parameters.
2.	(I3,6A10)	a) Columns 1-3: Number of NMR spectra. If default value, program will exit. b) Columns 4-64: Identification.
3.	(5I5, 5X, 3F10.0)	a) Columns 1-5: Total number of data points to be read; e.g. 04096. b) Columns 6-10: Channel number of beginning of region to be fitted. c) Columns 11-15: Channel number of end of fitted region. d) Columns 16-20: Channel number of beginning of region within (b and c) above to be excluded from fit. e) Columns 21-25: Channel number of end of excluded region. f) Columns 31-40: Spectral width in hertz. g) Columns 41-50: Dwell time per data channel in Msec. Dwell = Aquisition time/number data channels. h) Columns 51-60: The exponential filter time constant, in sec.
4.	(2I5)	a) Columns 1-5: Channel number at the start of a region containing no peaks which is representative of the mean baseline of the whole spectrum. b) Columns 6-10: Channel number at the end of above region.
5.	(2I5, 2F10.0)	a) Columns 1-5: Channel number at start of protein carboxyl resonances. b) Columns 6-10: Channel number at end of protein carboxyl resonances.

- c) Columns 11-20: Percentage of ^{13}C in the carbamate resonances.
- d) Columns 21-30: Total number of carbons in protein carbonyl region, e.g. in hemoglobin A₀, 328.0 (per $\alpha\beta$ dimer).
6. (I5) Columns 1-5: Spectrum number.
- 7 \rightarrow X. (3X, 11I 7) Data cards punched by CONVERT are read. Represents intensity at every channel.
- X + 1 (11, F10.0) a) Column 1: Number of chemical configurations. At present, this value is internally reset to 3, since the program is in its present form specific for this case.
- b) Columns 2-12: T_2 , representative of natural linewidth (without broadening due to exponential filtering). Units are sec.
- X + 2 (6F10.0) a) Columns 1-10: Fractional population of site 1.
- b) Columns 11-20: Fractional population of site 2.
- c) Columns 21-30: Fractional population of site 3.
- X + 3 (F10.0) Columns 1-10: Rate constants (sec^{-1}) for exchange site (1,2), site (1,3), and site (2,3). Only the exchange rate between sites 1,3 and 2,3 will be fitted. The 1,2 exchange will be held fixed.
- X + 4
- X + 5


```

PROGRAM NMRFIT (INPUT,OUTPUT,PL9T,TAPE60=INPUT,TAPE61=OUTPUT,TAPE3
1=PL9T)
EXTERNAL DYFIT
COMPLEX CR(24,24),CL(24,24),EIG(24),Q(10),D(10),TQ(10),TD(10),DQ(1
10,4),DD(10,4)
COMMON /STEPIT/ NV,NTRACE,MATRIX,CHISQR,MASK(20),A(20),AMAX(20),AM
1IN(20),DELTA(20),DELMIN(20),ERR(20,20)
COMMON /NFT/ IFIT1,IFIT2,IZR1,IZR2,WI(4100),STEP,YFIT(4100),T2,NCH
COMMON /PAR/ W(6,4),AJ(6,3,4)
COMMON /HAM/ H(6,8,8)
COMMON /INDEX/ IRBW(28),JCOL(28),IT(8,8)
COMMON /VEC/ V(10),PBV(10)
COMMON /SUB/ NB(5),LL(5),FZ(8,4)
COMMON /CFIT/ TQ,TD,DQ,DD,DERIV(10),NTBT
COMMON /VECT/ Q,D
COMMON /EIVEC/ CR,CL,EIG
COMMON /PLTPAR/ SCALE,HEIGHT
COMMON /PERMT/ IE(6,4),PT(6,8,8),MU
COMMON N,NP,MAX,MAXM,NE,NM,NEM,NEN,NSHIF
DIMENSION TEXT(6),ZF(6),PBP(6),SIGMAA(20),SD(6,6),SSD(6),RCS
1(6,6),RC(6,6),INP(11)
DATA NMAX/24/,NRS/1/
MU=0
N=1
READ 24, NTRACE,(DELMIN(I),I=1,4),(MASK(I),I=1,4)
1 IREP=0
READ 25, NUM,TEXT
IF (NUM.EQ.0) CALL EXIT

C
C INITIAL PARAMETERS FOR STEPIT FOLLOW
C STEPIT (SUBROUTINE) IS BY J.P. CHANDLER
C STEPIT IS AVAILABLE FROM QCPE, IU CHEM DEPT.
C

NV=4
MATRIX=105
DO 2 I=1,20
  AMAX(I)=0.0
2  AMIN(I)=0.0
DELTA(1)=.15
DELTA(2)=.15
DELTA(3)=4.
DELTA(4)=1.
READ 26, NCH,IFIT1,IFIT2,IZR1,IZR2,SW,DWEL,TC

C
C NCH IS NUMBER DATA CHANNELS IN SPECTRAL WINDOW
C IFIT1 AND IFIT2 ARE CHANNEL LIMITS OF DESIRED FIT
C IZR1 AND IZR2 ARE CHANNELS BETWEEN WHICH ALL DATA WILL BE ZEROED
C DWEL IS TIME/CHANNEL IN MICROSECONDS,BASED UPON FULL SPECTRAL WINDOW.
C IF NCH IS LESS THAN THAT ACTUALLY MEASURED, DWEL MUST BE ADJUSTED, SUCH
C THAT NCH*DWEL = AT.

```


C IBASE1 AND IBASE2 ARE CHANNELS BETWEEN WHICH A REPRESENTATIVE BASELINE
C IS FOUND, MUST CONTAIN NO RESONANCES
C

READ 27, IBASE1, IBASE2
READ 28, IC01, IC02, C13, TC0

C IC01 AND IC02 ARE CHANNEL LIMITS OF CARBOXYL INTEGRATION
C C13 IS PERCENT C13 IN THE CARBOXYLATES, TC0 IS TOTAL NUMBER OF C0 GROUPS
C IN THE PROTEIN CARBOXYL REGION.
C EG, TC0 IS 328 PER AB DIMER IN HUMAN HBA0.
C

READ 29, NUM

NC=11

DO 4 J=1, NCH

IF (NC.LT.11) GO TO 3

READ 30, (INP(I), I=1, 11)

NC=0

3 NC=NC+1

4 WI(J)=FLOAT(INP(NC))

C MEAN BASELINE IS SET TO ZERO
C
C

YC=0.0

YD=FLOAT(IBASE2-IBASE1)+1.

DO 5 I=IBASE1, IBASE2

5 YC=YC+WI(I)/YD

DO 6 I=1, NCH

WI(I)=WI(I)-YC

6 YFIT(I)=WI(I)

C AREA TO BE FITTED IS DEFINED, AND HIGHEST PEAK THEREIN NORMALIZED.
C
C

DO 7 I=IZR1, IZR2

7 WI(I)=0.0

YMAX=WI(IFIT1)

NM=IFIT1+1

DO 8 I=N, IFIT2

IF (YMAX.GT.WI(I)) GO TO 8

YMAX=WI(I)

8 CONTINUE

HEIGHT=4.724

FACTOR=HEIGHT/YMAX

DO 9 I=1, NCH

YFIT(I)=YFIT(I)*FACTOR+5.5

IF (YFIT(I).GT.10.5) YFIT(I)=10.5

9 WI(I)=WI(I)*FACTOR

C PROTEIN CARBOXYL PEAK INTEGRATED
C
C

CBSUM=0.0


```

      DO 10 I=IC01,IC02
10    C0SUM=C0SUM+W1(I)

```

```

      INPUT DATA PLOTTED

```

```

      SCALE=50.0
      XMAX=SCALE/2.54
      CALL IDENT (3)
      STEP=SW/NCH
      DENS=NCH/XMAX
      XX=1./DENS
      X=0.0
      CALL PLOT (X,YFIT(1),3)
      DO 11 I=2,NCH
        X=X+XX

```

```

11    CALL PLOT (X,YFIT(I),2)
      TITX=NCH*0.85*XX
      XNUM=NUM
      CALL SYMBOL (TITX,9.5,0.16,2HXL,0.0,2)
      CALL NUMBER (TITX+.23,9.5,.16,XNUM,0.0,.1)
      READ 31, NE,T2

```

```

      T2 IS NATURAL LINEWIDTH

```

```

      T2!=T2
      AT=FLOAT(NCH)*DWEL*1.0E-06
      T2=AT*T2/(AT-TC*T2)
      NE=3
      READ 32, (W(I,1),I=1,NE)

```

```

      AT PRESENT, PROGRAM IS SPECIFIC FOR 1 NUCLEUS, 3 CONFIGURATIONS

```

```

      NP=N+1
      MAX=2**N
      MAXM=MAX-1
      NEM=NE-1
      NEN=NE
      READ 32, (P0P(I),I=1,NE)
      DO 12 I=1,NEM
        IP=I+1
        SSD(I)=0.0
        DO 12 J=IP,NE
          READ 33, RC(I,J)
          RCS(I,J)=RC(I,J)
          SD(I,J)=0.0

```

```

12    CONTINUE
      IF (IREP.EQ.N) GO TO 13
      CALL BASIS (IREP)
13    CALL HAMILT
      A(1)=P0P(1)/P0P(3)

```



```

A(2)=PBP(2)/PBP(3)
A(3)=RC(1,3)
A(4)=RC(2,3)
CALL STEFIT (DYFIT)
CALL ERRBR (SIGMAA)
DO 14 L=1,NCH
  WI(L)=YFIT(L)
14  CONTINUE

```

C TOTAL CARBONATE AREA (EXCLUDES HCO₃) IS CALCULATED FROM FITTED SPECTRUM

```

CASUM=0.0
DO 15 I=1,NCH
15  CASUM=CASUM+WI(I)

```

C FITTED DATA PLOTTED

```

DO 16 I=1,NCH
16  WI(I)=WI(I)+0.5
  X=0.0
  CALL PLOT (X,WI(I),3)
DO 17 I=2,NCH
  X=X+X
17  CALL PLOT (X,WI(I),2)
  CALL CLOSEPF
  PRINT 34, NUM,TEXT
  PRINT 35
  PRINT 36, IFIT1,IFIT2,IZR1,IZR2
  PRINT 37, NCH
  PRINT 38, SW,AT,T2I,T2
  PRINT 39
  ISTOP=0
DO 18 I=1,NEM
  IP=I+1
  DO 18 J=IP,NE
18  RC(I,J)=RCS(I,J)
19  PRINT 40
  PRINT 41, (I,W(I,1),I=1,NE)
  PRINT 42
DO 20 I=1,NEM
  IP=I+1
  DO 20 J=IP,NE
20  PRINT 43, I,J,RC(I,J),SD(I,J)
  PRINT 44
  PRINT 45, (I,PBP(I),SSD(I),I=1,NE)
  IF (ISTOP.EQ.1) GO TO 22
  PRINT 47
  DPBP=1.+A(2)+A(1)
  PBP(1)=A(1)/DPBP
  PBP(2)=A(2)/DPBP

```



```

PBP(3)=1.-PBP(1)-PBP(2)
RC(1,3)=A(3)
RC(2,3)=A(4)
SSD(1)=SIGMAA(1)*(1./DPBP+A(1)/DPBP**2)+A(1)*SIGMAA(2)/DPBP**2
SSD(2)=SIGMAA(2)*(1./DPBP+A(2)/DPBP**2)+A(2)*SIGMAA(1)/DPBP**2
SSD(3)=SSD(1)+SSD(2)
SD(1,3)=SIGMAA(3)
SD(2,3)=SIGMAA(4)
WCNG=FLOAT(NSHIF)*STEP
DO 21 I=1,NE
21  W(I,1)=W(I,1)+WCNG
    ISTOP=1
GO TO 19
22  PRINT 46
    PRINT 48, CHISQR
    PRINT 49
    PRINT 50, (J,Q(J),D(J),J=1,NTOT)
    PRINT 51, NUM
    PRINT 52, C0SUM,TC0
    PRINT 53, CASUM,C13
    C0SUM=TC0/(C0SUM*C13/1.1)
DO 23 I=1,NE
23  ZF(I)=PBP(I)*CASUM*C0SUM
    PRINT 54, (I,ZF(I),I=1,NE)
GO TO 1

C
24  FORMAT (12,4E10.3,4I1)
25  FORMAT (13,6A10)
26  FORMAT (5I5,5X,3F10.0)
27  FORMAT (2I5)
28  FORMAT (2I5,2F10.0)
29  FORMAT (I5)
30  FORMAT (3X,11I7)
31  FORMAT (11,F10.0)
32  FORMAT (6F10.0)
33  FORMAT (F10.0)
34  FORMAT (14I1,16H SPECTRUM NO. XL,I3,2X,6A10/)
35  FORMAT (90H LEAST SQUARES FIT TO OBSERVED NMR SPECTRUM BASED ON TH
1REE SITE EXCHANGE OF SINGLE NUCLEUS)
36  FORMAT (32H REGION FITTED FROM CHANNEL NO. ,I5,4H TO ,I5,22H DELET
1ING CHANNEL NO. ,I5,4H TO ,I5)
37  FORMAT (48H TOTAL NUMBER CHANNELS IN OBSERVED SPECTRUM WAS ,I5)
38  FORMAT (1X,17HSPECTRAL WIDTH = ,F8.3,4H HZ,,5X,18HACQUISITION TIME
1 = ,F6.4,12H SEC., T2 = ,F8.4,17H SEC., AND T2* = ,F8.4/)
39  FORMAT (18H INPUT PARAMETERS ,70(1H*)//)
40  FORMAT (16H CHEMICAL SHIFTS/)
41  FORMAT (10X,5H SITE(,I1,4H) = ,F8.3,2HHZ)
42  FORMAT (/1X,25H RATE CONSTANTS IN (1/SEC)/)
43  FORMAT (10X,2HK(,I1,1H,,I1,4H) = ,F14.6,5X,5HSD = ,F16.8)
44  FORMAT (12H POPULATIONS)

```



```
45 FORMAT (10X,4HPBP(,11,4H) = ,F6.3,5X,5HSD = ,F6.4)
46 FORMAT (88(1H*)//)
47 FORMAT (//,18H FITTED PARAMETERS,70(1H*)//)
48 FORMAT (33H DATA VARIANCE IN REGION FITTED =,F10.4/)
49 FORMAT (1X///17X,16HCONTRACTED SHAPE,10X,19HCONTRACTED SPECTRAL/24
  1X,6HVECTOR,21X,6HVECTOR//)
50 FORMAT (15,5X,4E14.6)
51 FORMAT (1H1,57H CARBAMINE FORMATION DATA BASED ON FITTED SPECTRUM
  1N0. XL,13,/)
52 FORMAT (30H TOTAL PROTEIN CARBONYL AREA =,E14.6,4H FOR,F5.0,8H CAR
  1BONS)
53 FORMAT (30H TOTAL FITTED CARBONATE AREA =,E14.6,3H AT,F5.1,12H PER
  1CENT-C13/)
54 FORMAT (3H Z(,11,3H) =,F6.3/)
  END
```



```

SUBROUTINE ERRBR (SIGMAA)
  COMPLEX CR(24,24),CL(24,24),EIG(24),Q(10),D(10),TQ(10),TD(10),DQ(1
10,4),DD(10,4)
  COMMON /STEPIT/ NTERMS,NTRACE,MATRIX,CHISQR,MASK(20),A(20),AMAX(20
1),AMIN(20),DELTA(20),DELMIN(20),ALPHA(20,20)
  COMMON /NFT/ IFIT1,IFIT2,IZR1,IZR2,WI(4100),STEP,YFIT(4100),T2,NCH
  COMMON /CFIT/ TQ,TD,DQ,DD,DERIV(10),NTBT
  COMMON /SUB/ NB(5),LL(5),FZ(8,4)
  COMMON /PAR/ W(6,4),AJ(6,3,4)
  COMMON /HAM/ H(6,8,8)
  COMMON /INDEX/ IRBW(28),JCBL(28),IT(8,8)
  COMMON /VEC/ V(10),PBV(10)
  COMMON /VECT/ Q,D
  COMMON /EIVEC/ CR,CL,EIG
  COMMON /PLTPAR/ SCALE,HEIGHT
  COMMON /PERMT/ IE(6,4),PT(6,8,8),MU
  COMMON N,NP,MAX,MAXM,NE,NM,NEM,NEN,NSHIF
  DIMENSION POP(6),RC(6,6),SIGMAA(20)
  CALL CALIN (A,NT,NTR,T2,K)
  DO 1 I=1,K
    TD(I)=D(I)
    TQ(I)=Q(I)
1  CONTINUE
  CALL CDERIV (A,NTERMS,T2,K)
  J=1
  DO 3 I=1,K
    IF (ABS(REAL(TQ(I)))*LE+1.E-03) GO TO 3
    TQ(J)=TQ(I)
    TD(J)=TD(I)
    DO 2 L=1,NTERMS
      DD(J,L)=DD(I,L)
      DQ(J,L)=DQ(I,L)
2  J=J+1
3  CONTINUE
  JS=J-1
  NTBT=JS
  CALL FUNCTN (TQ,TD,JS,FACTOR)
  CALL WIGGLE (FACTOR,NFREE,CHISQR,NSHIF)
  DO 6 I=IFIT1,IFIT2
    IF (I.LT.IZR1) GO TO 4
    IF (I.GT.IZR2) GO TO 4
    GO TO 6
4  CONTINUE
    B=YFIT(I)
    CALL FDERIV (I,NTERMS,JS,FACTOR,NSHIF)
    DO 5 J=1,NTERMS
      ALPHA(J,J)=ALPHA(J,J)+DERIV(J)*DERIV(J)
      YFIT(I)=B
5  CONTINUE
6  FREE=FLSAT(IFIT2-IFIT1-IZR2+IZR1-NTERMS)

```



```
CHISQR=CHISQR/FREE  
DO 7 J=1, NTERMS  
7  SIGMAA(J)=SQRT(CHISQR/ALPHA(J,J))  
RETURN  
END
```



```

SUBROUTINE FDERIV (I, NTERMS, NTBT, FACTOR, NSHIF)
COMPLEX V, IM
COMPLEX TQ(10), TD(10), DQ(10,4), DD(10,4)
COMMON /NFT/ IFIT1, IFIT2, IZR1, IZR2, W1(4100), STEP, YFIT(4100), T2, NCH
COMMON /CFIT/ TQ, TD, DQ, DD, DERIV(10)
FR=FLOAT(I*NSHIF)*STEP
PI=3.14159
IM=CMPLX(0.,1.)
V=2.*PI*IM*FR
DO 2 J=1, NTERMS
  DERIV(J)=0.
  DO 1 L=1, NTBT
    1  DERIV(J)=DERIV(J)+REAL(DQ(L,J)/(TD(L)+V)+TQ(L)*DD(L,J)/(TD(L)+
    1  V)**2)
    2  DERIV(J)=DERIV(J)*FACTOR
RETURN
END

```



```

SUBROUTINE CDERIV (A, NTERMS, T2, K)
  COMPLEX CR(24,24), CL(24,24), EIG(24), Q(10), D(10), TQ(10), TD(10), T2D(
110), T2Q(10), DQ(10,4), DD(10,4)
  DIMENSION DELTAA(10), A(10), PBP(6)
  COMMON /VEC/ V(10), PBV(10)
  COMMON /PERMT/ IE(6,4), PT(6,8,8), MU
  COMMON /HAM/ H(6,8,8)
  COMMON /CFIT/ TQ, TD, DQ, DD, DERIV(10)
  COMMON /EIVC/ CR, CL, EIG
  COMMON /VECT/ Q, D
  COMMON N, NP, MAX, MAXM, NE, NM, NEM, NEN
  COMMON /SUB/ N9(5), LL(5), FZ(8,4)
  COMMON /INDEX/ IRBW(28), JCP4(28), IT(8,8)
  DELTAA(1)=1.E=6
  DELTAA(2)=DELTAA(1)
  DELTAA(3)=1.E=5
  DELTAA(4)=DELTAA(3)
  DO 3 J=1, NTERMS
    AJ=A(J)
    DELTA=DELTAA(J)
    A(J)=A(J)+DELTA
    CALL CALIN (A, NT, NTR, T2, K)
    DO 1 I=1, K
      T2D(I)=D(I)
1      T2Q(I)=Q(I)
      A(J)=AJ-DELTA
      CALL CALIN (A, NT, NTR, T2, K)
      DO 2 I=1, K
        DQ(I,J)=(T2Q(I)-Q(I))/(2.*DELTA)
        DD(I,J)=(T2D(I)-D(I))/(2.*DELTA)
2      CONTINUE
3      A(J)=AJ
  RETURN
  END

```



```

SUBROUTINE DYFIT
COMMON /STEPIT/ NV,NTRACE,MATRIX,CHISQR,MASK(20),A(20),AMAX(20),AM
1IN(20),DELTA(20),DELMIN(20),ERR(20,20)
COMMON /CR/ CR(24,24),CL(24,24),EIG(24),Q(10),D(10),TQ(10),TD(10),DQ(1
10,4),DD(10,4)
COMMON /NFT/ IFIT1,IFIT2,IZR1,IZR2,WI(4100),STEP,YFIT(4100),T2,NCH
COMMON /CFIT/ TQ,TD,DQ,DD,DERIV(10),NTOT
COMMON /SUB/ NB(5),LL(5),FZ(8,4)
COMMON /PAR/ W(6,4),AJ(6,3,4)
COMMON /HAM/ H(6,8,8)
COMMON /INDEX/ IRBW(28),JCBL(28),IT(8,8)
COMMON /VEC/ V(10),PBV(10)
COMMON /VECT/ Q,D
COMMON /EIVC/ CR,CL,EIG
COMMON /PLTPAR/ SCALE,HEIGHT
COMMON /PERMT/ IE(6,4),PT(6,8,8),MU
COMMON N,NP,MAX,MAXM,NE,NM,NEM,NEN,NSHIF
DIMENSION POP(6),RC(6,6)
CALL CALIN (A,NT,NTR,T2,K)
DO 1 I=1,K
  TD(I)=D(I)
  TQ(I)=Q(I)
1 CONTINUE
J=1
DO 2 I=1,K
  IF (ABS(REAL(TQ(I)))*LE*1.E+03) GO TO 2
  TQ(J)=TQ(I)
  TD(J)=TD(I)
  J=J+1
2 CONTINUE
JS=J-1
CALL FUNCTN (TQ,TD,JS,FACTOR)
CALL WIGGLE (FACTOR,NFREE,CHISQR,NSHIF)
RETURN
END

```



```
FUNCTION CRVSCL (I)
COMMON /NFT/ IFIT1,IFIT2,IZR1,IZR2,WI(4100),STEP,YFIT(4100),T2,NCH
F=0.0
P=0.0
DO 2 L=IFIT1,IFIT2
  IF (L.LT.IZR1) GO TO 1
  IF (L.GT.IZR2) GO TO 1
  GO TO 2
1  F=F+YFIT(L)**2
  P=P+YFIT(L)*WI(L)
2  CONTINUE
CRVSCL=P/F
RETURN
END
```



```
SUBROUTINE FUNCTN (TQ,TD,NTBT,FACTOR)
COMPLEX TQ(10),TD(10)
COMPLEX V,G,IM
COMMON /NFT/ IFIT1,IFIT2,IZR1,IZR2,WI(4100),STEP,Y(4100),T2,NCH
COMMON /PLTPAR/ SCALE,HEIGHT
IM=CMPLX(0.,1.)
PI=3.14159
FR=0.0
DO 2 L=1,NCH
  FR=FR+STEP
  G=CMPLX(0.,0.)
  V=2.*PI*IM*FR
  DO 1 K=1,NTBT
    G=G+TQ(K)/(TD(K)*V)
  1  Y(L)=REAL(G)
2  CONTINUE
  YMAX=Y(1)
  YMIN=Y(1)
  DO 4 I=2,NCH
    IF (YMAX.GT.Y(I)) GO TO 3
    YMAX=Y(I)
  3  IF (YMIN.LT.Y(I)) GO TO 4
    YMIN=Y(I)
  4  CONTINUE
  DO 5 I=1,NCH
    Y(I)=(Y(I)-YMIN)
  5  CONTINUE
  FACTOR=CRVSCL(0)
  DO 6 I=1,NCH
    Y(I)=Y(I)*FACTOR
  6  RETURN
END
```



```

SUBROUTINE CALIN (A,NT,NTR,T2,K)
COMPLEX CR(24,24),CL(24,24),EIG(24),Q(10),D(10)
COMPLEX AA(24,24)
DIMENSION A(10), PBP(6), RC(6,6)
COMMON N,NP,MAX,MAXM,NE,NEM,NEN
COMMON /SUB/ N9(5),LL(5),FZ(8,4)
COMMON /INDEX/ IRBW(28),JCBL(28),IT(8,8)
COMMON /VEC/ V(10),PBV(10)
COMMON /PERMT/ IE(6,4),PT(6,8,8),MU
COMMON /HAM/ H(6,8,8)
COMMON /EIVC/ CR,CL,EIG
COMMON /VECT/ G,D
EQUIVALENCE (CR(1),AA(1))
NCOUNT=0
CALL TERMS (A,PBP,RC,NREPT,NCOUNT)
IF (NCOUNT.GT.5) CALL EXIT
K=1
NB=0
DO 1 II=1,N
  NTR=N9(II)*N9(II+1)
  NT=NTR*NE
  CALL PROJECT (PBP)
  CALL TRMAT (AA,NTR,NT,NB,RC,T2)
  CALL ALLMAT (AA,NT,CL,EIG)
  CALL CONVEC (K,NT)
1  NB=NB+NTR
  K=K-1
  KM=K-1
DO 2 I=1,KM
  IP1=I+1
  DO 2 J=IP1,K
    IF (AIMAG(D(I))*LE*AIMAG(D(I))) GO TO 2
    TEMP=Q(I)
    Q(I)=Q(J)
    Q(J)=TEMP
    TEMP=D(I)
    D(I)=D(J)
    D(J)=TEMP
2  CONTINUE
RETURN
END

```



```
SUBROUTINE TERMS (A,P0P,RC,NREPT,NCOUNT)
DIMENSION P0P(6), RC(6,6), A(10)
COMMON N,NP,MAX,MAXM,NE,NM,NEM,NEN
NCOUNT=0
```

```
A(1) = P0P(1)/P0P(2)   ,,, A(2)/ = P0P(2)/P0P(3)
```

```
DP0P=1.+A(2)+A(1)
```

```
P0P(1)=A(1)/DP0P
```

```
P0P(2)=A(2)/DP0P
```

```
P0P(3)=1.0-P0P(1)-P0P(2)
```

```
RC(1,3)=A(3)
```

```
RC(2,3)=A(4)
```

```
RC(1,2)=0.0
```

```
DO 1 I=1,NEM
```

```
  IP=I+1
```

```
  DO 1 J=IP,NE
```

```
1  RC(J,I)=RC(I,J)*P0P(I)/P0P(J)
```

```
RETURN
```

```
END
```



```
SUBROUTINE WIGGLE (FACTOR,NFREE,CHISQ,N)
COMMON /NFT/ IFIT1,IFIT2,IZR1,IZR2,WI(4100),STEP,YFIT(4100),T2,NCH
CHISQ1=FCHISQ(NFREE)
NR=0
N=0
FAC1=1.
FAC2=1.
SFAC=FACTOR
1 SFAC=SFAC*FAC1
DO 2 I=IFIT1,IFIT2
2 YFIT(I)=YFIT(I+1)
N=N+1
FAC1=CRVSCL(0)
DO 3 I=1,NCH
3 YFIT(I)=YFIT(I)*FAC1
CHISQ2=FCHISQ(NFREE)
IF (CHISQ2.GT.CHISQ1) GO TO 4
CHISQ1=CHISQ2
GO TO 1
4 B=YFIT(IFIT1+1)
SFAC=SFAC*FAC2
DO 5 I=IFIT1,IFIT2
A=B
B=YFIT(I)
5 YFIT(I)=A
NR=NR+1
N=N+1
FAC2=CRVSCL(0)
DO 6 I=1,NCH
6 YFIT(I)=YFIT(I)*FAC2
IF (NR.LE.1) GO TO 4
CHISQ2=FCHISQ(NFREE)
IF (CHISQ2.GT.CHISQ1) GO TO 7
CHISQ1=CHISQ2
GO TO 4
7 DO 8 I=IFIT1,IFIT2
8 YFIT(I)=YFIT(I+1)
DO 9 I=1,NCH
9 YFIT(I)=YFIT(I)*1./FAC2
N=N+1
CHISQ=CHISQ1
FACTOR=SFAC
RETURN
END
```



```
FUNCTION FCHISQ (NFREE)
COMMON /NFT/ IFIT1,IFIT2,IZR1,IZR2,Y(4100),STEP,YFIT(4100),T2,NCH
CHISQ=0.
DO 3 I=IFIT1,IFIT2
  IF (I=IZR1) 2,1,1
  IF (I=IZR2) 3,3,2
1  CHISQ=CHISQ+(Y(I)-YFIT(I))**2
2  CONTINUE
3  FCHISQ=CHISQ
RETURN
END
```


SUBROUTINE BASIS (IREP)

SPIN BASIS FUNCTIONS ARE GENERATED, ORDERED, AND THEIR
IZ COMPONENTS ACCUMULATED. DIMENSIONS AND INDEX VECTORS
FOR HAMILTONIAN SUBMATRICES ARE COMPUTED.

COMMON /SUB/ NB(5),LL(5),FZ(8,4)
COMMON N,NP,MAX,MAXM
DIMENSION NBIN(8)

IREP=N
NB(1)=1
LL(1)=1
DO 1 J=1,N
JP=J+1
JD=NP-J
NB(JP)=(NB(J)+JD)/J
1 LL(JP)=LL(J)+NB(J)
NBIN(1)=0
DO 3 J=1,MAXM
ISUM=1
DO 2 M=1,N
M2=2**M
IZ=(2*J)/M2-2*(J/M2)
2 ISUM=ISUM+IZ
K=LL(ISUM)
NBIN(K)=J
3 LL(ISUM)=LL(ISUM)+1
DO 4 J=2,NP
4 LL(J)=LL(J)-NB(J)
DO 5 K=1,MAX
NN=NBIN(K)
DO 5 M=1,N
M2=2**M
FZ(K,M)=2*(NN/M2)-(2*NN)/M2
5 FZ(K,M)=FZ(K,M)+0.5
RETURN
END

SUBROUTINE HAMILT

THIS SUBROUTINE ASSEMBLES THE HAMILTONIAN MATRICES

```

COMMON /HAM/ H(6,8,8)
COMMON /SUB/ N9(5),LL(5),FZ(8,4)
COMMON /PAR/ W(6,4),AJ(6,3,4)
COMMON N,NP,MAX,MAXM,NE,NM,NEM,NEN

```

```

DO 1 I=1,NEN
  DO 1 J=1,MAX
    DO 1 K=1,MAX
      1 H(I,J,K)=0
    DO 11 I=1,NEN
      DO 11 IA=1,NP
        MM=N9(IA)
        DO 10 J=1,MM
          DO 10 K=J,MM
            JJ=LL(IA)+J-1
            KK=LL(IA)+K-1
            IF (J.EQ.K) GO TO 7
            KINV=0
            DO 6 M=1,N
              P=FZ(JJ,M)*FZ(KK,M)
              IF (P) 2,6,6
              2 KINV=KINV+1
              IF (KINV=1) 6,3,4
              3 MA=M
              GO TO 6
              4 IF (KINV=2) 6,5,10
              5 MB=M
              6 CONTINUE
              H(I,JJ,KK)=AJ(I,MA,MB)*0.5
              H(I,KK,JJ)=H(I,JJ,KK)
              GO TO 10
              7 DO 8 M=1,N
                8 H(I,JJ,JJ)=H(I,JJ,JJ)-FZ(JJ,M)*W(I,M)
                IF (N.EQ.1) GO TO 10
                DO 9 M=1,NM
                  MP=M+1
                  DO 9 NN=MP,N
                    9 H(I,JJ,JJ)=H(I,JJ,JJ)+FZ(JJ,M)*FZ(JJ,NN)*AJ(I,M,NN)
                10 CONTINUE
              11 CONTINUE
            RETURN
          END

```


SUBROUTINE PROJECT (POP)

THIS SUBROUTINE GENERATES VARIOUS AUXILIARY INDEX ARRAYS,
NEEDED FOR THE PROJECTION OF THE DENSITY VECTOR INTO THE
PROPER LIOUVILLE SUBSPACE, AND COMPUTES THE POPULATION
VECTOR

```
COMMON /INDEX/ IRBW(28),JCBL(28),IT(8,8)
COMMON /VEC/ V(10),POV(10)
COMMON /SUB/ NO(5),LL(5),FZ(8,4)
COMMON /PERMT/ IE(6,4),PT(6,8,8),MU
COMMON N,NP,MAX,MAXM,NE,NM,NEM
DIMENSION POP(6)
```

```
DO 1 I=1,MAX
  DO 1 J=1,MAX
1  IT(I,J)=0
  L=0
  DO 2 I=1,N
    K=0
    IA=LL(I)
    JA=LL(I+1)
    IEE=IA+NO(I)=1
    JE=JA+NO(I+1)=1
    DO 2 II=IA,IEE
      DO 2 J=JA,JE
        L=L+1
        IRBW(L)=I
        JCBL(L)=J
        K=K+1
2  IT(II,J)=K
    L=0
    DO 12 II=1,N
      MM=NO(II)*NO(II+1)
      MA=LL(II)
      ME=MA+NO(II)=1
      MX=LL(II+1)
      MY=MX+NO(II+1)=1
      DO 7 I=MA,ME
        DO 7 J=MX,MY
          KINV=0
          DO 4 M=1,N
            P=FZ(I,M)*FZ(J,M)
            IF (P) 3,4,4
          3  KINV=KINV+1
          IF (KINV.GT.1) GO TO 5
          4  CONTINUE
          L=L+1
          V(L)=1.
          GO TO 6
```



```
5      L=L+1
      V(L)=0.
      POV(L)=0.
      GO TO 7
6      POV(L)=POP(1)
7      CONTINUE
      IF (NE.EQ.1) GO TO 12
      IF (MU.EQ.1) GO TO 12
      DO 11 JJ=1,NEM
          JM=JJ-1
          LA=L+1+MM*JM
          LE=L+MM*JJ
          DO 11 LX=LA,LE
              LY=LX-MM
              IF (POV(LY)) 9,9,8
8          POV(LX)=POP(JJ+1)
          GO TO 10
9          POV(LX)=0.
10         V(LX)=V(LY)
11         CONTINUE
      L=LE
12     CONTINUE
      RETURN
      END
```


SUBROUTINE TRAMAT (A,NTR,NT,NB,RC,T2)

THIS SUBROUTINE COMPUTES THE COMMUTATOR (RHO,H) AND
ASSEMBLES THE TRANSITION SUBMATRICES

COMPLEX A(24,24)
COMPLEX IM
COMMON /INDEX/ IROW(28),JCBL(28),IT(8,8)
COMMON N,NP,MAX,MAXM,NE,NM,NEM
COMMON /HAM/ H(6,8,8)
COMMON /PERMT/ IE(6,4),PT(6,8,8),MU
DIMENSION RC(6,6)

DATA NMAX/48/

IM=CMPLX(0.,1.)

PI=3.14159

DO 1 I=1,NT

DO 1 J=1,NT

1 A(I,J)=CMPLX(0.,0.)

INC=0

DO 8 KK=1,NE

DO 7 I=1,NTR

IC=I+INC

IF (MU.EQ.1) GO TO 3

DO 2 IR=1,NE

IF (IR.EQ.KK) GO TO 2

A(IC,IC)=A(IC,IC)-RC(KK,IR)

CONTINUE

2

3

II=I+NB

K=IROW(II)

L=JCBL(II)

DO 5 M=1,MAX

IF (H(KK,M,L)) 4,5,4

4

J=IT(K,M)+INC

A(IC,J)=A(IC,J)+H(KK,M,L)*2.*IM*PI

5

CONTINUE

DO 7 M=1,MAX

IF (H(KK,K,M)) 6,7,6

6

J=IT(M,L)+INC

A(IC,J)=A(IC,J)-H(KK,K,M)*2.*IM*PI

7

CONTINUE

IF (MU.EQ.1) GO TO 9

INC=INC+NTR

8

CONTINUE

GO TO 18

9

DO 16 NPR=1,NEM

DO 15 I=1,NT

II=NB+I

K=IROW(II)

L=JCBL(II)


```

      DO 11 J=1,MAX
        IF (PT(NPR,J,K)) 10,11,10
10      USAVE=J
        GO TO 12
11      CONTINUE
12      DO 13 J=1,MAX
        IF (PT(NPR,J,L)) 14,13,14
13      CONTINUE
14      J=IT(USAVE,J)
15      A(I,J)=A(I,J)+RC(1,2)
16      CONTINUE
      DO 17 I=1,NT
        DO 17 J=2,NE
17      A(I,I)=A(I,I)+RC(1,2)
18      DO 19 I=1,NT
19      A(I,I)=A(I,I)+1./T2
        IF (MU.EQ.1) GO TO 23
        NA=1
        IF (NE.EQ.1) GO TO 23
        DO 22 IR=1,NEM
          NTRR=NTR*IR
          DO 21 I2=NA,NTRR
            I2P=I2+NTR
            I3=IR
            DO 20 I4=I2P,NT,NTR
              I3=I3+1
              A(I2,I4)=RC(I3,IR)
              A(I4,I2)=RC(IR,I3)
20          CONTINUE
21          CONTINUE
          NA=NA+NTR
22      CONTINUE
23      CONTINUE
      RETURN
      END

```


SUBROUTINE CONVEC (K,NT)

THIS SUBROUTINE GENERATES THE SHAPE VECTOR
AND RADIOFREQUENCY INDEPENDENT PART OF THE
SPECTRAL VECTOR

COMPLEX CR(24,24),CL(24,24),EIG(24),Q(10),D(10)

COMPLEX CRS,CLS

COMMON /EIVC/ CR,CL,EIG

COMMON /VECT/ Q,D

COMMON /VEC/ V(10),PEV(10)

DATA NMAX/24/

K1=1

KK=K+1

1 Q(K)=CMPLX(0.,0.)

CRS=CMPLX(0.,0.)

DO 2 LA=1,NT

LAK=LA+KK

2 CRS=CRS+V(LAK)*CR(LA,K1)

CLS=CMPLX(0.,0.)

DO 3 NU=1,NT

NUK=NU+KK

3 CLS=CLS+PEV(NUK)*CL(K1,NU)

Q(K)=CRS+CLS

D(K)=EIG(K1)

K=K+1

K1=K1+1

IF (K1.LE.NT) GO TO 1

RETURN

END

SUBROUTINE STEPIT (FUNK)

COPYRIGHT 1965 -- J. P. CHANDLER, PHYSICS DEPT., INDIANA UNIVERSITY,
 STEPIT 5.3 MARCH 1968
 AVAILABLE FROM.... QUANTUM CHEMISTRY PROGRAM EXCHANGE
 I.U. CHEMISTRY DEPT., BLOOMINGTON, INDIANA.

COMMON /STEPIT/ NV,NTRACE,MATRIX,CHISQ,MASK(20),X(20),XMAX(20),XMI
 1N(20),DELTA(20),DELMIN(20),ERR(20,20)
 COMMON /FRBD9/ NFMAX,NFLAT,JVARY
 REAL LOGF,MAX1F,MIN1F
 INTEGER XABSF,XMAXOF
 DIMENSION VEC(20), TRIAL(20), XSAVE(20), CHI(20), DX(20), SECBND(2
 1,2)
 DIMENSION OLDVEC(20), SALV8(20), X9SC(20,15), CHI9SC(15), JFLAT(20
 1)

DATA NFMAX/1000000/,NFLAT/1/

ABSF(X)=ABS(X)

SQRTF(X)=SQRT(X)

XABSF(I)=IABS(I)

XMAXOF(I,J)=MAXO(I,J)

LOGF(X)=ALOG(X)

FLGATF(I)=FLGAT(I)

SIGNF(X,Y)=SIGN(X,Y)

MAX1F(X,Y)=AMAX1(X,Y)

MIN1F(X,Y)=AMIN1(X,Y)

NVMAX=20

MSQUE=15

KW=61

RATIO=10.0

COLIN=0.99

NCOMP=5

ACK=2.0

SIGNIF=2.E8

SIGNIF=1.E10

HUGE=1.E307

JVARY=0

CALL SSWTCH (6,J)

IF (J.EQ.2) GO TO 2

WRITE (KW,153)

1 CALL SSWTCH (6,J)

IF (J.EQ.1) GO TO 1

2 IF (NV) 20,20,3

3 NACTIV=0

DO 13 I=1,NV

IF (MASK(I)) 13,4,13

4 IF (SIGNIF*ABS(DELTA(I))-ABS(X(I))) 5,5,8

5 IF (X(I)) 7,6,7


```

6  DELTAX(I)=0.01
   GO TO 8
7  DELTAX(I)=0.01*X(I)
8  IF (DELMIN(I)) 10,9,10
9  DELMIN(I)=DELTAX(I)/SIGNIF
10 IF (XMAX(I)-XMIN(I)) 11,11,12
11 XMAX(I)=HUGE
   XMIN(I)=-HUGE
12 NACTIV=NACTIV+1
   X(I)=AMAX1(XMIN(I),AMIN1(XMAX(I),X(I)))
13 CONTINUE
   COMPAR=0.0
   IF (NACTIV=1) 14,17,16
14 DO 15 J=1,NV
15   MASK(J)=0
   GO TO 3
16 A=NACTIV
   SUB=2.0/(A+1.0)
   P=2.0*(1.0/SQRT(A))/((1.0-0.5**SUB)=1.0)
   COMPAR=AMIN1(.999,ABS(((1.0-(1.0-COLIN)**SUB)*(1.0+P*(1.-COLIN))))))
17 IF (NTRACE) 19,18,18
18 WRITE (KW,154)
   WRITE (KW,155) (MASK(J),J=1,NV)
   WRITE (KW,156) (X(J),J=1,NV)
   WRITE (KW,157) (XMAX(J),J=1,NV)
   WRITE (KW,158) (XMIN(J),J=1,NV)
   WRITE (KW,159) (DELTAX(J),J=1,NV)
   WRITE (KW,160) (DELMIN(J),J=1,NV)
19 CALL FUNK
   NF=1
   JBCK=1
20 IF (NTRACE) 22,21,21
21 WRITE (KW,161) NV,NACTIV,MATRIX,NCOMP,RATIO,ACK,COLIN,COMPAR,CHISQ
22 IF (NV) 148,148,23
23 IF (NTRACE) 25,25,24
24 WRITE (KW,162)
C
25 DO 26 I=1,NV
   DX(I)=DELTAX(I)
   VEC(I)=0.
   DO 26 J=1,NV
26   ERR(I,J)=0.
   CHIOLD=CHISQ
   NOSC=0
C
27 NCIRC=0
   NZIP=0
C
C  MAIN DO LOOP FOR CYCLING THROUGH THE VARIABLES.
C  FIRST TRIAL STEP WITH EACH VARIABLE IS SEPARATE.

```


C

```

28 NACK=0
   DO 116 I=1,NV
      OLDVEC(I)=VEC(I)
      VEC(I)=0.0
      TRIAL(I)=0.0
      IF (MASK(I)) 29,30,29
29  VEC(I)=0.0
      JFLAT(I)=1
      GO TO 116
30  NACK=NACK+1
      SAVE=X(I)
      IF (SIGNIF*ABS(DX(I))=ABS(X(I))) 47,47,31
31  X(I)=SAVE+DX(I)
      JVARY=0
      IF (JBCK) 33,33,32
32  JBCK=0
      JVARY=I
      NFLAG=1
33  IF (X(I)-XMIN(I)) 35,34,34
34  IF (X(I)-XMAX(I)) 36,36,35
35  NFLAG=NFLAG+3
      GO TO 38
36  CALL FUNK
      NF=NF+1
      JVARY=I
      CHIME=CHISQ
      IF (CHISQ=CHIOLD) 51,37,38
37  NFLAG=NFLAG+1
38  X(I)=SAVE-DX(I)
      IF (X(I)-XMIN(I)) 48,39,39
39  IF (X(I)-XMAX(I)) 40,40,48
40  CALL FUNK
      NF=NF+1
      JVARY=I
      IF (CHISQ=CHIOLD) 50,41,42
41  NFLAG=NFLAG+1
42  IF (NFLAG=3) 43,47,48
43  IF ((CHISQ-CHIME)*(CHIME-2.*CHIOLD+CHISQ)) 44,48,44
44  TRIAL(I)=.5*DX(I)*(CHISQ-CHIME)/(CHIME-2.*CHIOLD+CHISQ)
      VEC(I)=TRIAL(I)/ABS(DX(I))
      JFLAT(I)=0
      X(I)=SAVE+TRIAL(I)
      CALL FUNK
      NF=NF+1
      IF (CHISQ=CHIOLD) 45,46,46
45  CHIOLD=CHISQ
      JBCK=1
      GO TO 49
46  TRIAL(I)=0.0

```



```

      VEC(I)=0.0
      GO TO 48
47  VEC(I)=-0.0
      JFLAT(I)=1
48  X(I)=SAVE
49  NCIRC=NCIRC+1
      IF (NCIRC-NACTIV) 58,122,122
50  DX(I)=-DX(I)

C
C  A LOWER VALUE HAS BEEN FOUND.  HENCE THIS VARIABLE WILL CHANGE.
C
51  NCIRC=0
      DEL=DX(I)
52  CHIME=CHIOLD
      CHISQ=CHISQ
      VEC(I)=VEC(I)+DEL/ABS(DX(I))
      JFLAT(I)=0
      TRIAL(I)=TRIAL(I)+DEL
      DEL=ACK*DEL
      SAVE=X(I)
      X(I)=SAVE+DEL
      IF (X(I)=XMIN(I)) 57,53,53
53  IF (X(I)=XMAX(I)) 54,54,57
54  CALL FUNK
      NF=NF+1
      IF (CHISQ=CHIOLD) 52,55,55
55  CINDER=(0.5/ACK)*(ACK**2*CHIME-(ACK**2*1.0)*CHIOLD-CHISQ)/(ACK*0
1  HIME=(ACK+1.0)*CHIOLD+CHISQ)
      X(I)=SAVE+CINDER*DEL
      CALL FUNK
      NF=NF+1
      IF (CHISQ=CHIOLD) 56,57,57
56  CHIOLD=CHISQ
      TRIAL(I)=TRIAL(I)+CINDER*DEL
      VEC(I)=VEC(I)+CINDER*DEL/ABS(DX(I))
      GO TO 58
57  X(I)=SAVE
58  IF (NZIP=1) 115,59,59
59  IF (ABS(VEC(I))-ACK) 63,60,60
60  DX(I)=ACK*ABS(DX(I))
      VEC(I)=VEC(I)/ACK
      OLDVEC(I)=OLDVEC(I)/ACK
      DO 61 J=1,MBSQUE
61  ERR(I,J)=ERR(I,J)/ACK
      IF (NTRACE) 63,63,62
62  WRITE (KW,163) I,DX(I)
63  SUM0=0.0
      SUMV=0.0
      DO 64 J=1,NV
          SUM0=SUM0+OLDVEC(J)**2

```



```

64     SUMV=SUMV+VEC(J)**2
      IF (SUM0*SUMV) 115,115,65
65     SUM0=SQRT(SUM0)
      SUMV=SQRT(SUMV)
      COSINE=0.0
      DO 66 J=1,NV
66     COSINE=COSINE+(OLDVEC(J)/SUM0)*(VEC(J)/SUMV)
      IF (NZIP=1) 115,67,68
67     IF (NACK=NACTIV) 115,70,70
68     IF (NACK=NACTIV) 70,69,69
69     IF (NZIP=NCOMP) 70,71,71
70     IF (COSINE=COMPAR) 115,71,71

```

SIMON SAYS, TAKE AS MANY GIANT STEPS AS POSSIBLE...

```

71     IF (NTRACE) 73,73,72
72     WRITE (KW,164) CHI0LD,(VEC(J),J=1,I)
73     NGIANT=0
      NTRY=0
      NRETRY=0
      KL=1
      N0SC=N0SC+1
      IF (N0SC=M0SQUE) 76,76,74
74     N0SC=M0SQUE
      DO 75 K=2,M0SQUE
        CHI0SC(K-1)=CHI0SC(K)
        DO 75 J=1,NV
          X0SC(J,K-1)=X0SC(J,K)
75     ERR(J,K-1)=ERR(J,K)
76     DO 77 J=1,NV
          X0SC(J,N0SC)=X(J)
77     ERR(J,N0SC)=VEC(J)/SUMV
      CHI0SC(N0SC)=CHI0LD
      IF (N0SC=3) 83,78,78

```

SEARCH FOR A PREVIOUS SUCCESSFUL GIANT STEP IN A DIRECTION MORE NEARLY PARALLEL TO THE DIRECTION OF THE PROPOSED STEP THAN WAS THE IMMEDIATELY PREVIOUS ONE.

```

78     C0XC0M=0.0
      DO 79 J=1,NV
79     C0XC0M=C0XC0M+ERR(J,N0SC)*ERR(J,N0SC-1)
      NAH=N0SC-2
80     NTRY=0
      DO 82 K=KL,NAH
        NRETRY=NAH-K
        COSINE=0.0
        DO 81 J=1,NV
81     COSINE=COSINE+ERR(J,N0SC)*ERR(J,K)
        IF (COSINE=C0XC0M) 82,82,84

```



```

82     CONTINUE
83     CHIBAK=CHI(I)
      GO TO 88
84     NTRY=1
      KL=K+1
      IF (NTRACE) 86,86,85
85     NT=NBSC=K
      WRITE (KW,165) NT
86     DO 87 J=1,NV
          SALV0(J)=TRIAL(J)
87     TRIAL(J)=(X(J)-XBSC(J,K))/ACK
      CHIBAK=CHI0LD+(CHI0SC(K)-CHI0LD)/ACK
C
88     DO 90 J=1,NV
          XSAVE(J)=X(J)
          TRIAL(J)=ACK*TRIAL(J)
          IF (MASK(J)) 90,89,90
89     X(J)=AMAX1(AMIN1(X(J)+TRIAL(J),XMAX(J)),XMIN(J))
90     CONTINUE
      JBCK=0
      JVARY=0
      CALL FUNK
      NF=NF+1
      IF (CHISQ-CHI0LD) 91,93,93
91     CHIBAK=CHI0LD
      CHI0LD=CHISQ
      NGIANT=NGIANT+1
      IF (NTRACE) 88,88,92
92     WRITE (KW,166) CHISQ,(X(J),J=1,NV)
      GO TO 88
C
93     IF (NRETRY) 95,95,94
94     IF (NGIANT) 100,100,95
95     CINDER=(0.5/ACK)*(ACK**2*CHIBAK-(ACK**2+1.0)*CHI0LD-CHISQ)/(ACK*
1     CHIBAK-(ACK+1.0)*CHI0LD+CHISQ)
      DO 97 J=1,NV
          IF (MASK(J)) 97,96,97
96     X(J)=AMAX1(AMIN1(XSAVE(J)+CINDER*TRIAL(J),XMAX(J)),XMIN(J))
97     CONTINUE
      JBCK=0
      JVARY=0
      CALL FUNK
      NF=NF+1
      IF (CHISQ-CHI0LD) 110,98,98
98     IF (NGIANT) 102,99,102
99     IF (NTRY) 100,102,100
100    DO 101 J=1,NV
          TRIAL(J)=SALV0(J)
101    X(J)=XSAVE(J)
      GO TO 104

```



```

102  DO 103 J=1,NV
      TRIAL(J)=TRIAL(J)/ACK
103    X(J)=XSAVE(J)
104  IF (NTRACE) 106,106,105
105  WRITE (KW,167) CHIOLD,NGIANT
      WRITE (KW,168) (X(J),J=1,NV)
      WRITE (KW,169)
106  IF (NGIANT) 107,107,112
107  IF (NRETRY) 108,108,80
108  IF (NTRY) 109,114,109
109  NTRY=0
      GO TO 83

```

C

```

110  CHIOLD=CHISO
      JACK=1
      IF (NTRACE) 112,112,111
111  STEPS=FLOAT(NGIANT)+CINDER
      WRITE (KW,170) CHIOLD,STEPS
      WRITE (KW,168) (X(J),J=1,NV)
      WRITE (KW,169)
112  IF (NTRY) 113,27,113
113  NOSC=0
      GO TO 27
114  NOSC=MAX0(NOSC-1,0)
115  CHI(I)=CHIOLD
116  CONTINUE

```

C

```

C  ANOTHER CYCLE THROUGH THE VARIABLES HAS BEEN COMPLETED.
C  PRINT ANOTHER LINE OF TRACES.
C

```

```

      IF (NTRACE) 118,118,117
117  WRITE (KW,164) CHIOLD,(VEC(J),J=1,NV)
118  CALL SSWTCH (6,J)
      IF (J.EQ.1) GO TO 124
      IF (NZIP) 121,119,121
119  IF (NTRACE) 121,121,120
120  WRITE (KW,168) (X(J),J=1,NV)
      WRITE (KW,171)
121  NZIP=NZIP+1
      GO TO 28

```

C

```

C  A MINIMUM HAS BEEN FOUND. PRINT THE REMAINING TRACES.
C

```

```

122  IF (NTRACE) 124,124,123
123  WRITE (KW,164) CHIOLD,(VEC(J),J=1,I)
124  IF (NTRACE) 126,126,125
125  WRITE (KW,168) (X(J),J=1,NV)
      WRITE (KW,169)
126  CALL SSWTCH (6,J)
      IF (J.EQ.1) GO TO 142

```


C
C
C

DECREASE THE SIZE OF THE STEPS FOR ALL VARIABLES.

```

NBSC=0
NGATE=1
DO 129 J=1,NV
  IF (MASK(J)) 129,127,129
127  IF (ABS(DX(J))-ABS(DELMIN(J))) 129,129,128
128  NGATE=0
129  DX(J)=DX(J)/RATIO
  IF (NGATE) 132,132,130
130  IF (NTRACE) 143,131,131
131  WRITE (KW,172)
  GO TO 143
132  IF (NFLAT) 137,137,133
133  DO 135 J=1,NV
  IF (MASK(J)) 135,134,135
134  IF (JFLAT(J)) 137,137,135
135  CONTINUE
  IF (NTRACE) 143,136,136
136  WRITE (KW,173)
  GO TO 143
137  IF (NF=NFMAX) 139,139,138
138  WRITE (KW,174)
  GO TO 143
139  IF (NTRACE) 141,141,140
140  WRITE (KW,175) (DX(J),J=1,NV)
  WRITE (KW,176)
141  CALL SSWTCH (6,J)
  IF (J.EQ.1) GO TO 124
  GO TO 27
142  WRITE (KW,177) (DX(J),J=1,NV)
143  CHISQ=CHIOLD
  IF (NTRACE) 145,144,144
144  WRITE (KW,178) NF
145  CALL SSWTCH (6,J)
  IF (J.EQ.1) GO TO 149
  IF (IABS(MATRIX-100)-50) 146,146,149
146  IF (NACTIV=NV) 149,147,149
C
147  CONTINUE
148  WRITE (KW,178) NF
149  CALL DVCHK (J)
  IF (J.EQ.2) GO TO 150
  WRITE (KW,179)
150  JVARY=0
  IF (NTRACE) 152,151,151
151  WRITE (KW,180) (X(J),J=1,NV)
  WRITE (KW,181) CHISQ
152  RETURN

```


C

```

153 FORMAT (24H TURN OFF SENSE SWITCH 6)
154 FORMAT (92H ENTER SUBROUTINE STEPIT.  COPYRIGHT 1965 J. P. CHANDLE
1R, PHYSICS DEPT., INDIANA UNIVERSITY.//19H INITIAL VALUES..../)
155 FORMAT (/10H MASK      = ,10(16,6X)/(4X,10I12))
156 FORMAT (/10H X        = ,10E12.4/(10X,10E12.4))
157 FORMAT (/10H XMAX     = ,10E12.4/(10X,10E12.4))
158 FORMAT (/10H XMIN     = ,10E12.4/(10X,10E12.4))
159 FORMAT (/10H DELTAX   = ,10E12.4/(10X,10E12.4))
160 FORMAT (/10H DELMIN   = ,10E12.4/(10X,10E12.4))
161 FORMAT (/1H ,I3,11H VARIABLES,,I3,8H ACTIVE,,10X,8H MATRIX =,I4,10
1X,7HNCOMP =,I2//8H RATIO =,F5.1,10X,5HACK =,F5.1,10X,7HCOLIN =,F6.
23,10X,8HCOMPAR =,F6.3//8H CHISQ =,E15.8//23H BEGIN MINIMIZATION.
3...))
162 FORMAT (//60(1X,1H*)//10X,37HTRACE MAP OF THE MINIMIZATION PROCESS
1//)
163 FORMAT (10H STEP SIZE,I3,14H INCREASED TO ,E12.5)
164 FORMAT (8H CHISQ =,E15.8,5X,14HNO. OF STEPS =,10F9.2/(42X,10F9.2))
165 FORMAT (/1X,8H*****5X,34H POSSIBLE OSCILLATION WITH PERIOD ,I2
1,10H DETECTED.)
166 FORMAT (8H CHISQ =,E15.8/9H X(I)..../(10(1X,E12.5)))
167 FORMAT (/8H CHISQ =,E15.8,7H AFTER,I3,13H GIANT STEPS.)
168 FORMAT (9H X(I)..../(10(1X,E12.5)))
169 FORMAT (/)
170 FORMAT (/8H CHISQ =,E15.8,7H AFTER,F6.1,13H GIANT STEPS.)
171 FORMAT (1H )
172 FORMAT (///65H TERMINATED WHEN THE STEP SIZES BECAME AS SMALL AS T
1HE DELMIN(J).)
173 FORMAT (///72H TERMINATED WHEN THE FUNCTION VALUES AT ALL TRIAL PO
1INTS WERE IDENTICAL.)
174 FORMAT (///78H TERMINATED WHEN THE NUMBER OF CALLS TO THE CHISQ SU
1BROUTINE EXCEEDED NFMAX = ,I7)
175 FORMAT (60(1X,1H*)//26H STEP SIZES REDUCED TO..../(10(1X,E12.5)))
176 FORMAT (//)
177 FORMAT (///42H SUBROUTINE STEPIT TERMINATED BY OPERATOR.///29H CUR
1RENT STEP SIZE VALUES..../(10(1X,E12.5)))
178 FORMAT (///1X,I5,23H FUNCTION COMPUTATIONS )
179 FORMAT (///17H DIVIDE CHECK ON.)
180 FORMAT (///10X,24HFINAL VALUES OF X(I)..../(7(1X,E16.9)))
181 FORMAT (///24H FINAL VALUE OF CHISQ = ,E15.8//)
END

```


SUBROUTINE ALLMAT (A,M,CL,LAMBDA)

C
C
C
C
C

ALLMAT DIAGONALIZES THE NT BY NT DIMENSIONAL A MATRIX. THE EIGENVECTORS ARE OVERWRITTEN ON THE ORIGINAL A MATRIX. THE INVERSE OF THE EIGENVECTOR MATRIX IS CALCULATED AS THE CL MATRIX. THE EIGENVALUES ARE CONTAINED IN THE ONE DIMENSIONAL LAMBDA ARRAY.

DIMENSION INT(24)
COMPLEX A(24,24),H(24,24),HL(24,24),LAMBDA(24),VECT(24),MULT(24),SHIFT(6),TEMP,SIN,COS,TEMP1,TEMP2,CR(24,24),CL(24,24),EIG(24),TRACE
2,SUMEIG,CSORT
INTEGER R,RP1,RP2
LOGICAL INTN(55),TWICE
COMMON /EIVEC/ CR,H,EIG
COMMON /TEM/ HL

C
C
C
C
C

PROG. AUTHORS JOHN RINZEL,R.E.FUNDERLIC,UNION CARBIDE CORP.
NUCLEAR DIVISION,CENTRAL DATA PROCESSING FACILITY,
OAK RIDGE TENNESSEE

DATA NMAX/48/
N=M
TRACE=0.0
DO 1 I=1,N
1 TRACE=TRACE+A(I,I)
NCAL=N
IF (N.NE.1) GO TO 2
LAMBDA(1)=A(1,1)
A(1,1)=1.
GO TO 59
2 ICOUNT=0
SHIFT=0.
IF (N.NE.2) GO TO 5
3 TEMP=(A(1,1)+A(2,2)+CSORT((A(1,1)+A(2,2))*2+4.*(A(2,2)*A(1,1)-A(2,1)*A(1,2))))/2.
IF (REAL(TEMP).NE.0.0.OR.AIMAG(TEMP).NE.0.0) GO TO 4
LAMBDA(M)=SHIFT
LAMBDA(M-1)=A(1,1)+A(2,2)+SHIFT
GO TO 37
4 LAMBDA(M)=TEMP+SHIFT
LAMBDA(M-1)=(A(2,2)*A(1,1)-A(2,1)*A(1,2))/(LAMBDA(M)-SHIFT)+SHIFT
GO TO 37

C
C
C

REDUCE MATRIX A TO HESSENBERG FORM

5 NM2=N-2
DO 16 R=1,NM2
RP1=R+1
RP2=R+2


```

ABIG=0.
INT(R)=RP1
DO 6 I=RP1,N
    ABSSQ=REAL(A(I,R))**2+AIMAG(A(I,R))**2
    IF (ABSSQ.LE,ABIG) GO TO 6
    INT(R)=I
    ABIG=ABSSQ
6    CONTINUE
    INTER=INT(R)
    IF (ABIG.EQ.0.) GO TO 16
    IF (INTER.EQ.RP1) GO TO 9
    DO 7 I=R,N
        TEMP=A(RP1,I)
        A(RP1,I)=A(INTER,I)
7    A(INTER,I)=TEMP
    DO 8 I=1,N
        TEMP=A(I,RP1)
        A(I,RP1)=A(I,INTER)
8    A(I,INTER)=TEMP
9    DO 10 I=RP2,N
        MULT(I)=A(I,R)/A(RP1,R)
10   A(I,R)=MULT(I)
    DO 12 I=1,RP1
        TEMP=0.
        DO 11 J=RP2,N
            TEMP=TEMP+A(I,J)*MULT(J)
11   TEMP=TEMP+A(I,RP1)+TEMP
12   DO 14 I=RP2,N
            TEMP=0.
            DO 13 J=RP2,N
                TEMP=TEMP+A(I,J)*MULT(J)
13   A(I,RP1)=A(I,RP1)+TEMP*MULT(I)*A(RP1,RP1)
14   DO 15 I=RP2,N
            DO 15 J=RP2,N
                A(I,J)=A(I,J)-MULT(I)*A(RP1,J)
15   CONTINUE
16

```

C
C
C

CALCULATE EPSILON

```

EPS=0.
DO 17 I=1,N
17  EPS=EPS+CABS(A(1,I))
    DO 19 I=2,N
        SUM=0.
        IM1=I-1
        DO 18 J=IM1,N
            SUM=SUM+CABS(A(I,J))
18  IF (SUM.GT.EPS) EPS=SUM
19  EPS=SQRT(FL64T(N))*EPS*1.E-12
    IF (EPS.EQ.0.) EPS=1.E-12

```



```

      DO 20 I=1,N
        DO 20 J=1,N
20      H(I,J)=A(I,J)
21      IF (N.EQ.1) GO TO 22
        LAMBDA(M)=A(1,1)+SHIFT
        GO TO 37
22      IF (N.EQ.2) GO TO 3
23      MN1=M+N+1
        IF (REAL(A(N,N)).NE.0..OR.AIMAG(A(N,N)).NE.0.)
1      IIF (ABS(REAL(A(N,N-1)/A(N,N))+ABS(AIMAG(A(N,N-1)/A(N,N)))-1.E-9)
224,24,23
        IF (ABS(REAL(A(N,N-1)))+ABS(AIMAG(A(N,N-1)))*GE.EPS) GO TO 24
        LAMBDA(MN1)=A(N,N)+SHIFT
        ICOUNT=0
        N=N-1
        GO TO 22
C
C      DETERMINE SHIFT
C
24      SHIFT(2)=(A(N-1,N-1)+A(N,N)+CSQRT(((A(N-1,N-1)+A(N,N))*2+4*(A(N,N)
1      )*(A(N-1,N-1)-A(N,N-1)*A(N-1,N))))/2.
        IF (REAL(SHIFT(2)).NE.0..OR.AIMAG(SHIFT(2)).NE.0.) GO TO 25
        SHIFT(3)=A(N-1,N-1)+A(N,N)
        GO TO 26
25      SHIFT(3)=(A(N,N)*A(N-1,N-1)-A(N,N-1)*A(N-1,N))/SHIFT(2)
26      IF (CABS(SHIFT(2)-A(N,N)).LT.CABS(SHIFT(3)-A(N,N))) GO TO 27
        INDEX=3
        GO TO 28
27      INDEX=2
28      IF (CABS(A(N-1,N-2))*GE.EPS) GO TO 29
        LAMBDA(MN1)=SHIFT(2)+SHIFT
        LAMBDA(MN1+1)=SHIFT(3)+SHIFT
        ICOUNT=0
        N=N-2
        GO TO 21
29      SHIFT=SHIFT+SHIFT(INDEX)
        DO 30 I=1,N
30      A(I,I)=A(I,I)-SHIFT(INDEX)
C
C      PERFORM GIVEN ROTATIONS, OR ITERATES
C
        IF (ICOUNT.LE.10) GO TO 31
        NCAL=M=N
        GO TO 37
31      NM1=N-1
        TEMP1=A(1,1)
        TEMP2=A(2,1)
        DO 36 R=1,NM1
          RP1=R+1
          RH0=SQRT(REAL(TEMP1)**2+AIMAG(TEMP1)**2+REAL(TEMP2)**2+AIMAG(TEM
1      P2)**2)
          IF (RH0.EQ.0) GO TO 33

```



```

COS=TEMP1/RH0
SIN=TEMP2/RH0
INDEX=MAX0(R-1,1)
DO 32 I=INDEX,N
    TEMP=CONJG(COS)*A(R,I)+CONJG(SIN)*A(RP1,I)
    A(RP1,I)=-SIN*A(R,I)+COS*A(RP1,I)
32    A(R,I)=TEMP
33    TEMP1=A(RP1,RP1)
    TEMP2=A(R+2,R+1)
    IF (RH0.EQ.0) GO TO 36
    DO 34 I=1,R
        TEMP=COS*A(I,R)+SIN*A(I,RP1)
        A(I,RP1)=-CONJG(SIN)*A(I,R)+CONJG(COS)*A(I,RP1)
34    A(I,R)=TEMP
    INDEX=MIN0(R+2,N)
    DO 35 I=RP1,INDEX
        A(I,R)=SIN*A(I,RP1)
35    A(I,RP1)=CONJG(COS)*A(I,RP1)
36    CONTINUE
    ICOUNT=ICOUNT+1
    GO TO 23

```

C
C
C

CALCULATE VECTORS

```

37 IF (NCAL.EQ.0) GO TO 59
    N=M
    NM1=N-1
    IF (N.NE.2) GO TO 38
    EPS=AMAX1(CABS(LAMBDA(1)),CABS(LAMBDA(2)))*1.E-8
    IF (EPS.EQ.0.) EPS=1.E-12
    H(1,1)=A(1,1)
    H(1,2)=A(1,2)
    H(2,1)=A(2,1)
    H(2,2)=A(2,2)
38 DO 56 L=1,NCAL
    DO 40 I=1,N
        DO 39 J=1,N
39    HL(I,J)=H(I,J)
40    HL(I,I)=HL(I,I)-LAMBDA(L)
    DO 44 I=1,NM1
        MULT(I)=0.
        INTI(I)=.FALSE.
        IP1=I+1
        IF (CABS(HL(IP1,I)).LE.CABS(HL(I,I))) GO TO 42
        INTI(I)=.TRUE.
        DO 41 J=I,N
            TEMP=HL(IP1,J)
            HL(IP1,J)=HL(I,J)
41    HL(I,J)=TEMP
42    IF (REAL(HL(I,I)).EQ.0..AND..AIMAG(HL(I,I)).EQ.0.) GO TO 44

```



```

      MULT(I)=-HL(I+1,I)/HL(I,I)
      DO 43 J=I+1,N
43      HL(I+1,J)=HL(I+1,J)+MULT(I)*HL(I,J)
44      CONTINUE
      DO 45 I=1,N
45      VECT(I)=1.
      TWICE=.FALSE.
46      IF (REAL(HL(N,N)).EQ.0..AND.AIMAG(HL(N,N)).EQ.0.) HL(N,N)=EPS
      VECT(N)=VECT(N)/HL(N,N)
      DO 48 I=1,NM1
      K=N-I
      DO 47 J=K,NM1
47      VECT(K)=VECT(K)-HL(K,J+1)*VECT(J+1)
      IF (REAL(HL(K,K)).EQ.0..AND.AIMAG(HL(K,K)).EQ.0.) HL(K,K)=EPS
48      VECT(K)=VECT(K)/HL(K,K)
      SSS=0.
      DO 49 I=1,N
49      SSS=SSS+(REAL(VECT(I)))**2+(AIMAG(VECT(I)))**2
      SSS=SQRT(SSS)
      DO 50 I=1,N
50      VECT(I)=VECT(I)/SSS
      IF (TWICE) GO TO 52
      DO 51 I=1,NM1
      IF (.NOT.INTH(I)) GO TO 51
      TEMP=VECT(I)
      VECT(I)=VECT(I+1)
      VECT(I+1)=TEMP
51      VECT(I+1)=VECT(I+1)+MULT(I)*VECT(I)
      TWICE=.TRUE.
      GO TO 46
52      IF (N.EQ.2) GO TO 55
      NM2=N-2
      DO 54 I=1,NM2
      N1I=N-1-I
      NI1=N-I+1
      DO 53 J=NI1,N
53      VECT(J)=H(J,N1I)*VECT(N1I+1)+VECT(J)
      INDEX=INT(N1I)
      TEMP=VECT(N1I+1)
      VECT(N1I+1)=VECT(INDEX)
54      VECT(INDEX)=TEMP
55      DO 56 I=1,N
56      A(I,L)=VECT(I)
      CALL NVRT (A,CL,N)
      IF (NCAL.EQ.N) GO TO 57
      GO TO 59
57      SUMEIG=0.0
      DO 58 I=1,NCAL
58      SUMEIG=SUMEIG+LAMBDA(I)
59      RETURN

```

C

END

SUBROUTINE NVRT (Q,QNV,N)

NVRT INVERTS THE EIGENVECTOR MATRIX GENERATED BY ALLMAT

COMPLEX Q(24,24),QQNV(24,24),TEMP(24,24),QNV(24,24),P(24)
COMPLEX TFR
COMMON /TEM/ TEMP

DATA NMAX/24/

DO 1 I=1,N

DO 1 J=1,N

TEMP(I,J)=Q(I,J)

1 QQNV(I,J)=CMPLX(0.,0.)

DO 2 I=1,N

2 QQNV(I,I)=CMPLX(1.,0.)

K=1

3 I=K

L=K

4 S=CABS(TEMP(I,K))

T=CABS(TEMP(L,K))

IF (S=T) 6,6,5

5 L=I

6 IF (I=N) 7,8,7

7 I=I+1

GO TO 4

8 IF (L=K) 9,14,9

9 J=K

10 TFR=TEMP(K,J)

TEMP(K,J)=TEMP(L,J)

TEMP(L,J)=TFR

IF (J=N) 11,12,11

11 J=J+1

GO TO 10

12 DO 13 IN=1,N

TFR=QQNV(K,IN)

QQNV(K,IN)=QQNV(L,IN)

13 QQNV(L,IN)=TFR

14 I=K+1

15 TFR=TEMP(I,K)/TEMP(K,K)

TEMP(I,K)=CMPLX(0.,0.)

J=K+1

16 TEMP(I,J)=TEMP(I,J)+TFR*TEMP(K,J)

IF (J=N) 17,18,17

17 J=J+1

GO TO 16

18 DO 19 IN=1,N

19 QQNV(I,IN)=QQNV(I,IN)+TFR*QQNV(K,IN)

IF (I=N) 20,21,20

20 I=I+1

GO TO 15


```
21 IF (K=N+1) 22,23,22
22 K=K+1
   GO TO 3
23 DO 24 IN=1,N
24   QNV(N,IN)=QQNV(N,IN)/TEMP(N,N)
   I=N+1
25 J=I+1
   DO 26 IN=1,N
26   P(IN)=CMPLX(0.,0.)
27 DO 28 IN=1,N
28   P(IN)=P(IN)+TEMP(I,J)*QNV(J,IN)
   IF (J=N) 29,30,29
29 J=J+1
   GO TO 27
30 DO 31 IN=1,N
31   QNV(I,IN)=(QQNV(I,IN)+P(IN))/TEMP(I,I)
   IF (I=1) 32,33,32
32 I=I+1
   GO TO 25
33 RETURN
   END
```


CONVERT

Fortran program CONVERT was kindly supplied by Mr. Chris Hasenkampf. It is reproduced here since it is an essential part of NMRFIT3. The input consists only of the unformatted 2's complement binary paper tape as punched by the Nicolet 1080 computer. Output is a plot of the data, a listing of the decimal representations, and punched cards, format (I3, 11I7), of these decimal integers. A 4096 data channel spectrum requires 373 cards.


```

PROGRAM CONVERT(INPUT,OUTPUT,PLOT,PUNCH,PTESR,TAPE1=PTESR,TAPE2=PL
10T)
COMMON LL(13000),IN(2000),KK(4400)
DIMENSION X(4200),Y(4200)
C VERSION FOR CONVERTING XL-100 TAPES TO CARDS.
CALL IDENT(2)
8 FORMAT(1H ,15X,2H*=,I5)
  BUFFER IN(1,1)(IN(1),IN(2000))
  IF(UNIT(1))20,80,80
2) CONTINUE
  L=LENGTH(1)
  PRINT 11,L
11 FORMAT(1H1,2H=,I7)
  IF(L.GE.2200) PRINT 17
17 FORMAT(1H1,64HWARNING TOO MANY LEADING ZEROES HAVE BEEN READ STORA
1GE EXCEEDED.)
  K=0
  DO 30 J=1,L
  M=0
  DO 10 I=1,7
  K=K+1
  M=J+M
10 LL(K)=LC(IN(J),M).AND.3770
30 CONTINUE
  DO 33 I=1,100
  IA=(I-1)*5+1
  IB=I*5
33 PRINT 3+, (LL(J),J=IA,IB)
14 FORMAT(1H ,5(1020,3X))
  PRINT 7
  KA=0
  DO 12 I=1,K
  IF(LL(I).NE.128)GO TO 13
C THIS LOOKS FOR THE PUNCH IN COL 7
  KA=KA+1
12 CONTINUE
13 CONTINUE
  KA=KA+3
C THIS SKIPS OVER THE CHANNEL NUMBER DATA.
  K=K-KA
  DO 14 I=1,K
14 LL(I)=LL(I+KA)
  KI=0
  DO 2 I=1,500
  LJ=(K-I)+1
  IF((LL(LJ).NE.128).AND.(LL(LJ).NE.0).AND.(LL(LJ).NE.255))GO TO 3
  KI=KI+1
2 CONTINUE
3 CONTINUE
  K=K-(KI+3)
7 FORMAT(1H1)
  J=0
  PRINT 9,K
  DO 1 I=1,K,3
  J=J+1

```



```

1 KK(J)=LC(LL(I),14)+LC(LL(I+1),7)+LL(I+2)
36 FORMAT(1H,5(6X,I6))
C TAKE CARE OF NEGATIVE NUMBERS
PRINT 7
DO 21 I=1,J
IT=KK(I).AND.20000003
IF(IT.HI.524288)GO TO 22
IS=.NOT.KK(I)
IY=IS.AND.37777778
KK(I)=-(IY+1)
22 CONTINUE
21 CONTINUE
PRINT 7
DO 4 I=1,J
4 LL(I)=KK(I)
K=J-1
37 FORMAT(1H,12(2X,I7))
PRINT 37,(LL(I),I=1,K)
IJ=0
DO 81 I=1,K,11
IJ=IJ+1
II=I+10
81 PUNCH 82,IJ,(LL(IJ)+JJ=I,II)
82 FORMAT(I3,11I7)
PRINT 8,K
N=0
DO 40 I=1,K
N=N+1
X(I)=N
40 Y(I)=LL(I)
PRINT 8,N
CALL AXISCL(X,0.0,N,1,1HX,-1,1.0,1.0,10.0,0,0,0.20)
CALL AXISCL(Y,90.0,N,1,1HY,1,1.0,1.0,7.0,0,0,0.20)
CALL JDLIN(X,Y,N,1,1.0,1.0,0.0,0.0)
CALL CLOSEPF
80 STOP
END

```


REFERENCES

1. Binisch, G. and Kleier, D. A., Computation of Complex Exchange-Broadened NMR Spectra, Computer Program DNMR, available from Quantum Chemistry Program Exchange, Indiana University, Bloomington, Indiana 47401
2. Butler, J. N. (1964) Ionic Equilibrium, A Mathematical Approach, Addison-Wesley Pub. Co., Reading, Mass., 437
3. Marquardt, D. W. (1963) Soc. Ind. Appl. Math. 11, 431-441
4. Bevington, P. R. (1969) Data Reduction and Error Analysis for the Physical Sciences, McGraw-Hill, New York
5. Bovey, F. R. (1969) Nuclear Magnetic Resonance Spectroscopy, Academic Press, New York, 105-113
6. Binsch, G. (1969) J. Amer. Chem. Soc. 91, 1304-1309
7. Chandler, J. P. (1965) Subroutine Stepit, QCPE #66, available from Quantum Chemistry Program Exchange, Indiana University, Bloomington, Indiana 47401

APPENDIX D
Ligand Dependent Aggregation
of Chicken Hemoglobin

Appendix D
Ligand-Dependent Aggregation
of Chicken Hemoglobin A_I

As reported in Chapter V, hemoglobin A_I from white leghorn chickens has been found to undergo ligand-dependent aggregation in vitro (1) in a pattern similar to that of human hemoglobin S (2-6). In collaboration with Mr. R. J. Wittebort, the two major chicken hemoglobin chromatographic components, designated A_I and A_{II} (Chap. II) have been compared with respect to (1) reversible effects of ligand binding on aggregation under various conditions, (2) amino acid composition and N-terminal sequences of the subunits, and (3) ligand-dependent microstructure.

Chicken hemoglobins A_I and A_{II} were prepared as described in Chapter II.

Upon deoxygenation in a tonometer (8) unbuffered solutions of HbA_I but not HbA_{II} became turbid and opalescent. The uppermost curve in Figure 1 for the deoxy HbA_I in 0.05 M NaCl at pH 7.5 shows the strong decrease in transmission at 700 nm and deviation from Beer's law accompanying the aggregation. The lowest curve (0) shows the small absorbance of the solution of the HbA_IO₂ regained after air had been readmitted into the tonometer. The corresponding curves (▲) and (Δ) refer to the deoxy- and oxy-forms of HbA_I at the same pH and salt concentration, but following treatment (9) of the HbA_IO₂ with a tenfold molar excess of recrystallized NaNCO at 37° and pH 6.9 for two hours. Loss of reactive N-terminal groups was measured by automated Edman degradation on a Beckman model 890C Sequencer. Homocitrulline derived from lysine residues was measured (10). The results shown in Figure 1

apply to a preparation containing on the average per tetramer 1.4 modified termini each of α - and β -chains, designated as $\alpha_2^c\beta_2^c$. Less than 2 lysine residues on the average were modified per tetramer. The results in Figure 2 show that with this cyanate modified preparation the onset of aggregation was at higher concentration and the development appeared weakly inhibited. The time required after deoxygenation to achieve a constant level of turbidity, typically of the order of 30 minutes with the unmodified HbA_I was now greater than 90 minutes. The aggregation was less readily reversed on readmission of O₂.

The effect of various buffers on the aggregation was observed qualitatively. Higher ionic strength generally decreased aggregation. For example, it was almost completely inhibited in 0.1 M phosphate at pH 7.5, Figure 1. The tendency to aggregate was restored by dialysis into 0.05 M NaCl. At comparable concentrations, inhibition of aggregation relative to NaCl was observed for phosphate, Tris-HCl, and bicarbonate buffers. Stoichiometric addition of inositol hexaphosphate showed the same effect. An analogous effect of Tris buffer on HbS gelation has been reported (11) HbA_{II} was soluble over the range of conditions examined.

Many points of primary structural difference between HbA_I and HbA_{II} appear to reside in the α -chain. the composition of the α -chain (Table I) differs markedly from that of the α -chain of HbA_{II}, whereas that of the β -chain is not readily distinguished from the reported composition of HbA_{II} (12,13,16,17). The previously reported differences between the proteins (14,17) in glutamic acid, lysine and histidine contents are ascribable to the differences in the α -chains. Automated Edman degradation confirmed for 21 residues of the β -chain of HbA_I the N-terminal sequence reported

by Matsuda et al. (13) for the β -chain of HbA_{II}. The N-terminal sequence of the HbA_I α -chain was found to be H₂N-met-leu-thr-ala-glu-asg extending a previous report by Moss and Thompson (17). The HbA_I isolated here appears to differ from that described earlier (19) in which an acetylated N-terminal group was reported.

Deoxygenation of HbA_I under conditions that lead to aggregation (Figure 1) produces suspensions that appear to contain molecular order under the polarizing microscope and that scintillate when stirred. Under conditions of preparation for electron microscopy, R. J. Wittebort has found that crystalline arrays are formed (Figure 2). The nature of the aggregates under various conditions is under study to define the points of similarity and contrast with the properties of human HbS (2-6,9,20).

Table I

Amino Acid Composition of A_I α and β Subunits

The purified subunits were hydrolysed for 24, 48 and 72 h in 6 N HCl at 110°. Cysteine was determined as cysteic acid (18). The α and β subunits were assumed to have 141 and 142 non-tryptophane residues respectively as in HbA_{II}.

Amino Acid	α Mol %	α Mol per 141 amino acids	β Mol %	β Mol per 142 amino acids
Lysine	7.42	10.4	7.12	10.0
Histidine	3.89	5.5	4.84	6.9
Arginine	3.17	4.5	4.34	6.2
Aspartic	9.29	13.1	9.05	12.8
Threonine	4.97	7.0	4.91	7.0
Serine	6.41	9.0	5.13	7.3
Glutamic	11.30	15.9	8.62	12.2
Proline	3.74	5.3	3.85	5.5
Glycine	6.26	8.8	5.70	8.1
Alanine	12.74	18.0	10.61	15.1
Cysteine	0.86	1.2	2.07	2.9
Valine	7.63	10.8	8.26	11.7
Methionine	2.45	3.5	1.07	1.5
Isoleucine	1.58	2.2	4.27	6.1
Leucine	10.08	14.2	12.82	18.2
Tyrosine	3.38	4.8	1.64	2.3
Phenylalanine	4.82	6.8	5.70	8.1

Figure 1

Concentration-dependent absorbance at 700 nm of chicken A_I hemoglobin under various conditions, at pH $7.50 \pm .07$, 25° , and 2 mm path-length cell. ● Hb, 0.05 M NaCl; ▲ Hb ($\alpha_2^c\beta_2^c$) 0.5 M NaCl; Δ HbO₂ ($\alpha_2^c\beta_2^c$), 0.05 M NaCl; ○ HbO₂, 0.05 M NaCl; ■ Hb, 0.1 M phosphate buffer. Concentrations, expressed as heme content, were determined as the cyanoferric derivative, assuming a millimolar extinction coefficient of 11.1. In all cases, the oxy-determinations were made following the deoxy measurements.

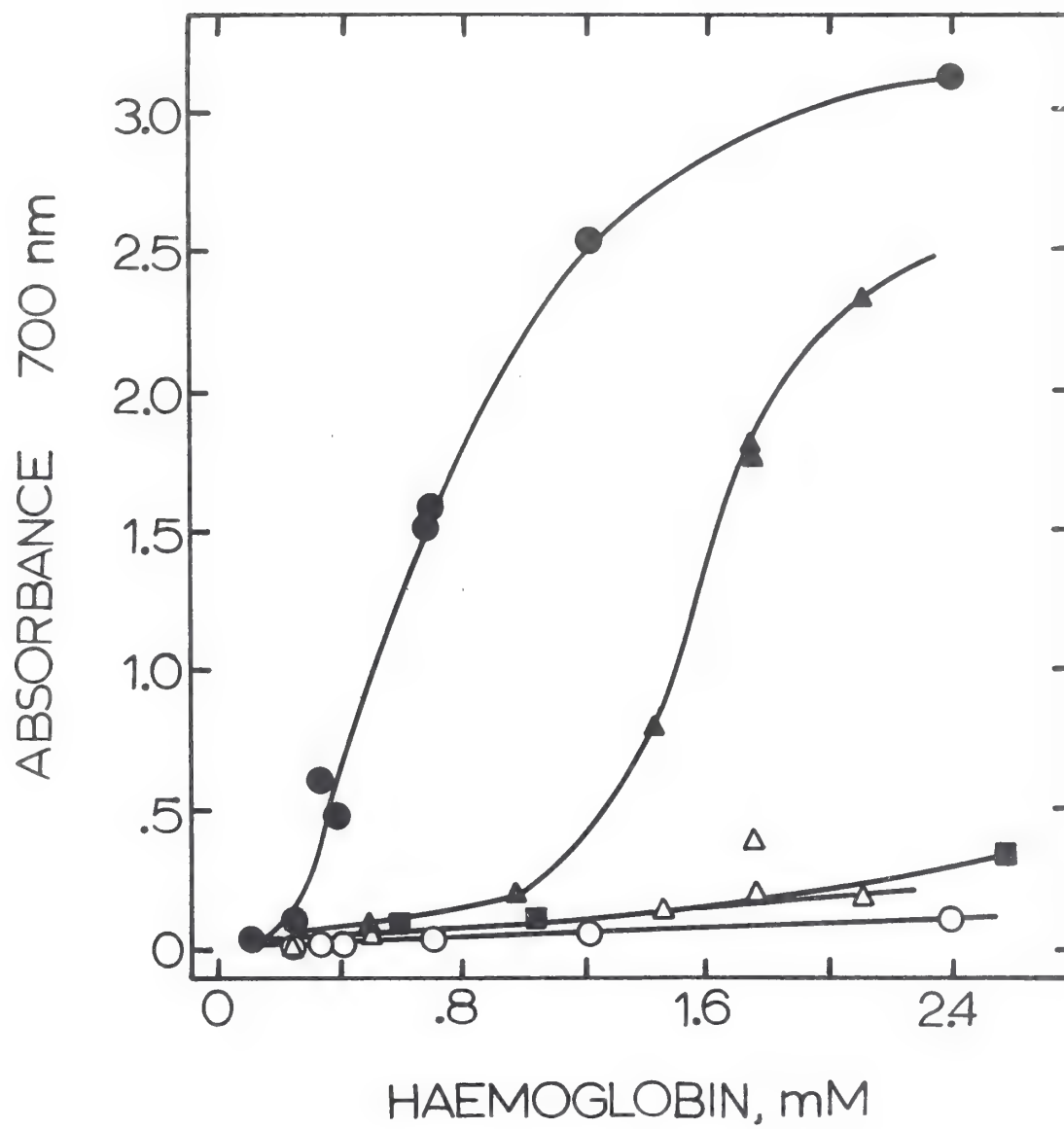
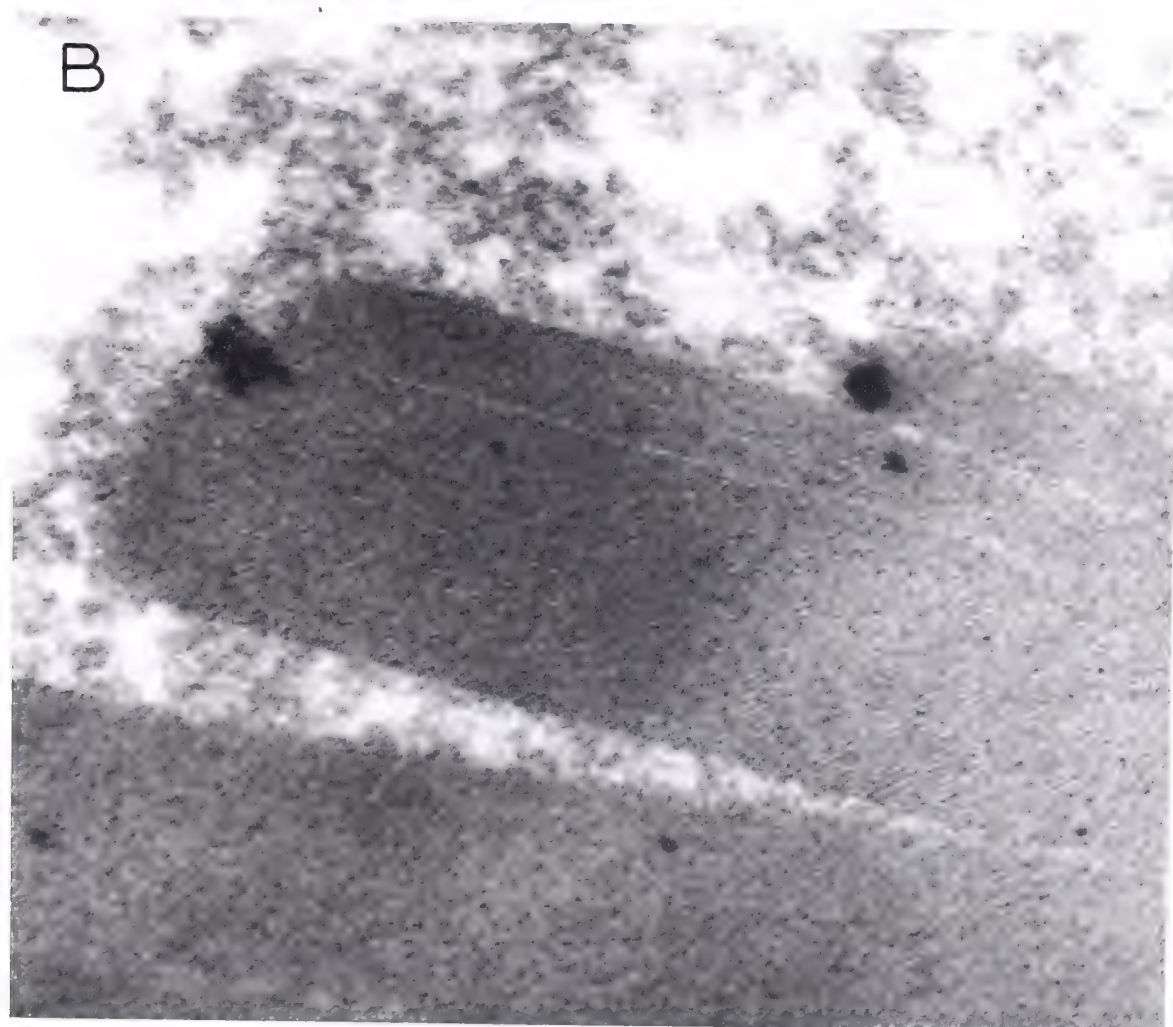
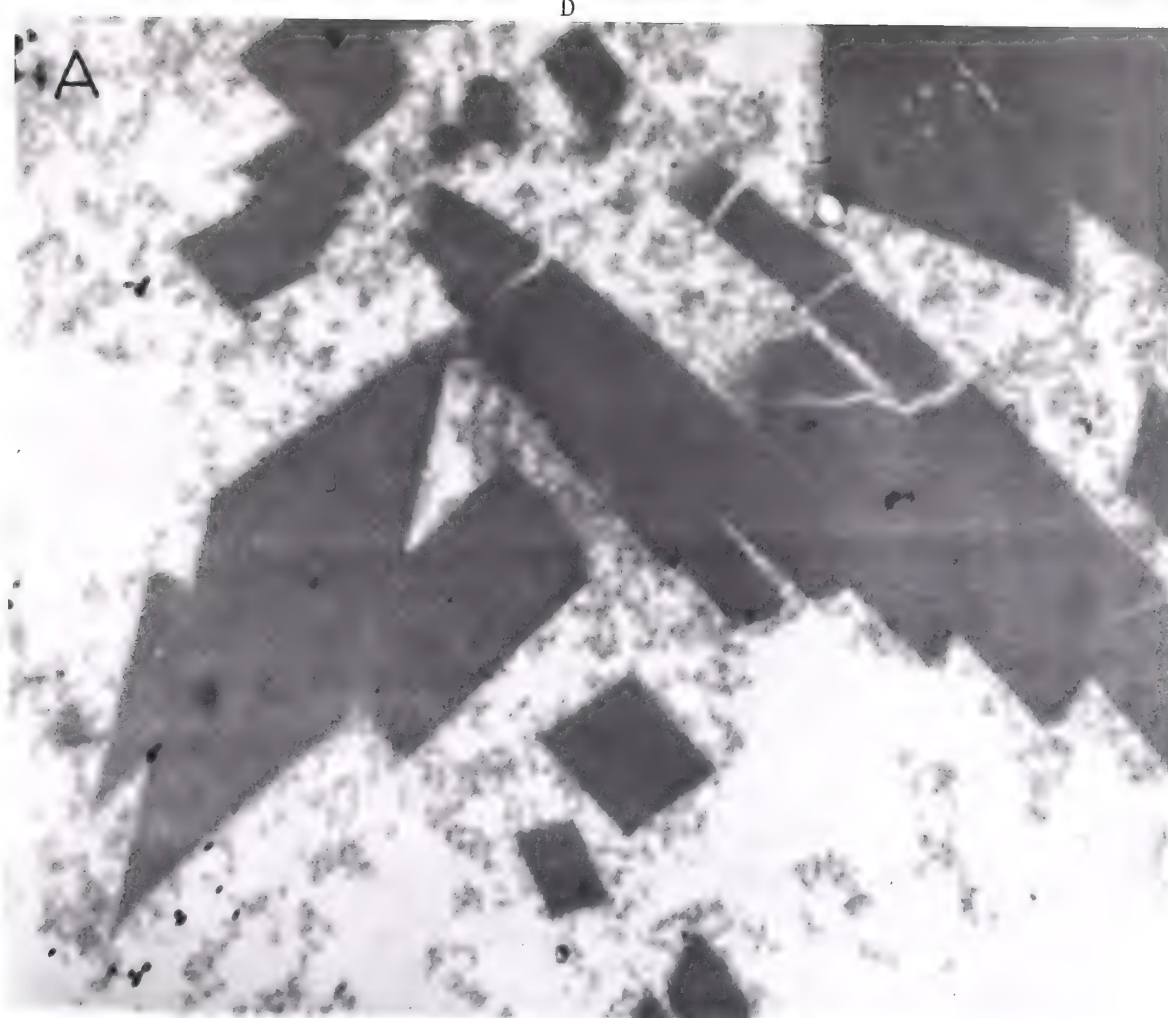


Figure 2

Electron micrographs of deoxy HbA_I X13,000 (a) and X100,000 (b). Deoxyhemoglobin was fixed in 1% glutaraldehyde for 12 hr. at 4°, post fixed 1 hr. in 1% OsO₄ and embedded in Epon(21). Thin sections were stained with lead citrate. The rhomboid array seen in (b) has spacings of 90 to 100 Å in both dimensions. The electron micrographs were prepared by Mr. R. J. Wittebort, with the assistance of Mr. Gary Minkler.



REFERENCES

1. Morrow, J. S., Wittebort, R. J. and Gurd, F. R. N. (1974) *Nature*, submitted for publication
2. Pauling, L., Itano, H. A., Singer, S. J. and Wells, I. C. (1949) *Science* 110, 543-548
3. Perutz, M. R., Liquori, A. M. and Eirich, F. (1951) *Nature* 167, 929-931
4. Allison, A. C. (1957) *Biochem. J.* 65, 212-219
5. Finch, J. T., Perutz, M. F., Bertles, J. F. and Dobler, J. (1973) *Proc. Natl. Acad. Sci.* 70, 718-722
6. Murayama, M. (1973) *C.R.C. Critical Rev. Biochem.* 1(4), 461-499
7. Matsuda, G. and Takei, H. (1964) *J. Biochem., Tokyo* 54, 156-160
8. Keyes, M., Mizukami, H. and Lumry, R. (1967) *Anal. Biochem.* 18, 126-142
9. Cerami, A. and Manning, J. M. (1971) *Proc. Natl. Acad. Sci.* 68, 1180-1183
10. Stark, G. R. and Smyth, D. G. (1963) *J. Biol. Chem.* 238, 214-226
11. Freedman, M. L., Weissman, G., Gorman, B. D. and Cunningham-Rundles, W. (1973) *Biochem. Pharmacol.* 22, 667-674
12. Matsuda, G., Takei, H., Wu, K. C. and Shiozawa, T. (1971) *Intl. J. Protein Res.* 3, 149
13. Matsuda, G., Maita, T., Mizuno, K. and Ota, H. (1973) *Nature New Biol.* 244, 244
14. van der Helm, J. H. and Huisman, T. H. J. (1958) *Science* 127, 762
15. Moss, B. A. and Thompson, E. O. P. (1969) *Aust. J. Biol. Sci.*, 22, 1455-1471

16. Saha, A. (1964) *Biochim. Biophys. Acta* 93, 573-584
17. Moss, B. A. and Thompson, E. O. P. (1969) *Biochim. Biophys. Acta* 188, 348
18. Hirs, C. H. W. (1967) in *Methods in Enzymology* 11, Hirs, C. H. W. ed., Academic Press, Chap. 6
19. Matsuda, G., Maita, T. and Makajima, H. (1964) *J. Biochem., Tokyo* 56, 490
20. Arnone, A. (1974) *Nature*, 247, 143
21. Luft, J. H. (1961) *J. Biophys. and Biochem. Cyt.* 9, 409

VITA

JON STANLEY MORROW

Place and Date of Birth

Fort Wayne, Indiana July 4, 1947

Education

Northside High School, Fort Wayne, Indiana 1961-1965

Indiana University at Fort Wayne, Fort Wayne, Indiana
1965-1966Indiana University, Bloomington, Indiana 1966-1969
B.S. ChemistryIndiana University, Bloomington, Indiana 1969-1974
Ph.D. ChemistrySocieties

Sigma Pi Sigma

Alpha Chi Sigma

Positions

Associate Instructor, Indiana University 1969-1974

Fellowships

N.I.H. Biochemistry Trainee

Publications

1. Nigen, A. M., Keim, P., Marshall, R. C., Morrow, J. S. and Gurd, F. R. N. (1972) J. Biol. Chem. 247, 4100-4102
2. Garner, W. H., Keim, P., Marshall, R. C., Morrow, J. S., Visscher, R. B. and Gurd, F. R. N. (1973) Fed. Proc. 32, 501

3. Morrow, J. S., Keim, P., Visscher, R. B., Marshall, R. C., and Gurd, F. R. N. (1973) Proc. Nat. Acad. Sci., 70, 1414-1418
4. Keim, P., Garner, M., Garner, W., Gurd, F. R. N., Marshall, R. C., Morrow, J. S., Vigna, R. A., and Visscher, R. B. (1973) Am. Chem. Soc. Abs., 166th Meeting
5. Gurd, F. R. N., Garner, W., Keim, P., Marshall, R. C., Morrow, J. S. and Visscher, R. B. (1973) 9th Interntl. Congress of Biochem. Abs.
6. Gurd, F. R. N., Morrow, J. S., Keim, P., Visscher, R. B. and Marshall, R. C. (1973) Am. Chem. Soc. Abs., 166th Meeting
7. Nigen, A. M., Keim, P., Marshall, R. C., Morrow, J. S., Vigna, R. A. and Gurd, F. R. N. (1973) J. Biol. Chem. 248, 3724-3732
8. Keim, P., Vigna, R. A., Morrow, J. S., Marshall, R. C. and Gurd, F. R. N. (1973) J. Biol. Chem. 248, 7811-7818
9. Keim, P., Vigna, R. A., Nigen, A. M., Morrow, J. S. and Gurd, F. R. N. (1974) J. Biol. Chem. 249, 4149-4156
10. Morrow, J. S. and Gurd, F. R. N. (1974) Amer. Chem. Soc. Abs.
11. Morrow, J. S., Keim, P. and Gurd, F. R. N. (1974) J. Biol. Chem., in press
12. Gurd, F. R. N., Morrow, J. S., Keim, P., Visscher, R. B. and Marshall, R. C. (1974) in Protein-metal Interactions, Friedman, M. ed., Plenum Publishing Corp., New York, in press
13. Morrow, J. S., Gurd, R. S. and Gurd, F. R. N. (1974) Rehevot Symposium on Peptides, Goodman, M. ed., in press
14. Morrow, J. S., Wittebort, R. J. and Gurd, F. R. N. (1974) Nature, submitted

YALE MEDICAL LIBRARY

Manuscript Theses

Unpublished theses submitted for the Master's and Doctor's degrees and deposited in the Yale Medical Library are to be used only with due regard to the rights of the authors. Bibliographical references may be noted, but passages must not be copied without permission of the authors, and without proper credit being given in subsequent written or published work.

This thesis by _____ has been
used by the following persons, whose signatures attest their acceptance of the
above restrictions.

NAME AND ADDRESS

DATE

H. M. ZACHARIS, Nuclear Med. 333 Cedar St.

11/12/80

